The Impact of Simulated Motion Blur on Breast Cancer Detection Performance in Full Field Digital Mammography (FFDM)

Ahmed Khalid Abdullah

School of Health Sciences,

UNIVERSITY OF SALFORD, SALFORD, UK

Submitted in Partial Fulfilment of the Requirements of the Degree of Doctor of Philosophy, May 2018

(Medical physics)

Contents

Contents ..... **I**

List of Tables ..... **VIII**

List of Figures ..... **XII**

List of Publications ..... **XIX**

List of Development Skills ..... **XXI**

Training Sessions Attended ..... **XXII**

Acknowledgement ..... **XXIV**

Dedications ..... **XXV**

Abbreviations ..... **XXVI**

Abstract ..... **XXVIII**

Chapter One: Introduction and Thesis Outline **1**

1.1 Introduction 1

1.2 Aim 2

1.3 Objectives 2

1.4 Research Questions 2

1.5 Rational of the thesis 2

1.6 The Contribution of this Thesis: 3

1.7 Thesis Structure 4

Chapter Two: Literature Review **7**

2.1 Overview of the Chapter 7

2.2 Breast Anatomy 7

2.3 Breast Cancer 11
2.3.1 Factors Affecting Breast Cancer 12
2.4 Mammography 13
2.4.1 Characteristics of Malignant Microcalcifications within Mammography Images 16
2.4.2 Breast Masses 18
2.5 Factors Affecting Diagnostic Efficiency 20
2.5.1 Mammographic Breast Density (MBD) Assessment 22
2.5.2 Effect of Mammographic Breast Density on Lesion Detection Performance 23
2.5.3 Effect of Image Quality on Lesion Detection Performance 25
2.5.4 Mammography Image Interpretation 29
2.6 Full-field Digital Mammography 30
2.6.1 Components of FFDM Systems 31
2.6.2 Automatic Exposure Control (AEC) 33
2.6.3 Paddles 33
2.7 Motion Blur in Mammography Images 34
2.7.1 Causes and Effects of Image Blurring 36
2.7.2 Paddle Movement Effects 37
2.7.3 Thixotropic Behavior and Breast Tissue Characteristics 39
2.8 Physics of Mammography System 40
2.8.1 X-ray Spectrum 40
2.8.2 X-rays Incident on the Detector 44

2.8.3 Digitization 44

2.8.4 Pixel Size in Mammography 45

Chapter Three: Medical Images Assessment Methods 46

3.1 Chapter Overview 46

3.2 The Relationship between Visual Performance and Medical Image Interpretation 47

3.3 Human Visual Function 49

3.3.1 Visual Acuity 51

3.3.2 Contrast Sensitivity 51

3.3.3 Visual Function Assessment 52

3.4 Receiver Operating Characteristics (ROC) Methods 53

3.5 Free-Response Receiver Operating Characteristics (FROC) Method 57

3.5.1 Constructing Curves from FROC Data 58

3.5.2 FROC Data Analysis 59

3.5.3 Jackknife Analysis of FROC Data (JAFROC) 60

3.6 Perceptual Measures 61

3.7 The Physical Measures of Mammographic Images 62

3.7.1 Measuring Conspicuity Index 62

3.7.2 Factors Affecting Conspicuity 64

Chapter Four: Methodology 66

4.1 Chapter Overview 66

4.2 Step 1: Image Selection 69

4.3 Step 2: Image Assessment 69

4.4 Step 3: Applying & Validating Simulated Motion Blur 70

4.4.2 Validation Method for Simulated Motion Blur Software 76

4.5 Step 4: Observer Performance Study 77

4.6 Step 5: Statistical Analysis 82

4.6.1 Data Analysis for Single Observer Free-response Method 83

4.6.2 Data Analysis for Combined Observer Data Method 83

4.7 Step 6: Lesion Conspicuity (Masses) 85

4.8 Step 7: Dispersion Index 88

4.9 Step 8: Missed Lesion Calculation Method 93

4.10 Ethical Issues 94

4.10.1 Ethical Approval in Observers' Studies 94

4.11 Chapter Summary 96

Chapter Five: Results 97

5.1 Chapter Overview 97

5.2 Section One: Results of the Free-response Study 98

5.2.1 Overview of wJAFROC Analysis 98

5.2.2 Microcalcifications 98

5.2.3 Masses 103

5.3 Section Two: Results of the Combining Two Observers' Data 108

5.3.1 The Combining Two Observers' Data of Microcalcifications 109

5.3.2 Combining Two Observers' Data of Masses 111

5.4 Section Three: A Comparison between the Results of Single Observer and the Combining Two Observers' Data 113

5.4.1 Microcalcification....113

5.4.2 Masses....115

Chapter Six: Results of Physical Measures....118

6.1 Chapter Overview....118

6.2 Part I: Physical Measures of Breast Masses....119

6.2.1 Normality Test of Masses Data....121

6.2.2 Conspicuity Index (χ)....122

6.2.3 Edge Angle....124

6.2.4 The Grey Level Change (ΔGL):....126

6.2.5 Signal to Noise Ratio (SNR):....128

6.3 Part II: Physical Measures of Microcalcifications....130

6.3.1 Normality Tests of Microcalcifications Data....130

6.3.2 Dispersion Index (DI) of Microcalcifications....131

6.3.3 Contrast of Microcalcifications....133

6.3.4 Dispersion Index and Contrast of Microcalcifications....135

6.3.5 Signal to Noise Ratio (SNR) of Microcalcifications Images:....136

6.4 The Relationship between Physical Measures and Detectability of Microcalcifications....138

6.5 Missed Lesion Analysis....146

Chapter Seven: Discussion....150

7.1. Overview....150

7.2 Free-response Performance Study (single observer)....150

7.2.1 Microcalcifications 153

7.2.2 Masses Cases 155

7.2.3 Reflection – comparison of laboratory and clinical studies 157

7.3 The Combined two Observers' Data 158

7.3.1 Microcalcifications Combined two Observers' Data 159

7.3.2 Masses Combined Two Observers' Data 160

7.4 Physical Measures: 161

7.4.1 Physical Measures of Microcalcifications 161

7.4.2 Physical Measures of Malignant Masses 163

7.5 The Impact of Motion Blur on Mammographic Features of Microcalcifications 166

7.6 The Impact of Motion Blur on Mammographic Image Features of Breast Masses: 175

7.6.1 Examples of Masses Affected by Simulated Motion Blur 180

7.6.2 Masses Not Affected by Simulated Motion Blur 186

7.7 Limitations of this Thesis: 189

7.8 Chapter Summary: 191

Chapter 8: Conclusion, Recommendations and Future work 192

8.2 Statement of Novelty 193

8.7 Recommendations and Future work 194

Appendices: 196

Appendix A: Ethics Application HSCR 15-107 196

Appendix B: Ethics Application HSCR 15-110 197

Appendix C : Organisation Management Consent/ Agreement Letter 198

Appendix D: Participant Invitation Letter.....200

Appendix E: Participant Information Sheet 201

Appendix F: Poster to Invite the Participants.....205

Appendix G: Tables of the Collected Data 206

Appendix H: ROCView Instructions 214

Appendix I:.....218

Table (I-1) The results of observation session for one observer represent true positive cases (images contain malignant masses without image blurring). 218

Table (I-2) The results of observation session for one observer represent true positive cases (images contain malignant masses with image blurring 0.7 mm). 220

Table (I-3) The results of observation session for one observer represent true positive cases (images contain malignant masses with image blurring 1.5 mm). 222

Table (I-4) The results of observation session for one observer represent false positive cases (images contain malignant masses with image blurring). 224

Appendix J: The Results of Combined Two Observers Data 226

Appendix K: Conspicuity Index.....228

Appendix M: Dispersion Index Tables 231

References.....237

List of Tables

Chapter Two

Table 2.1 Main types of benign and malignant breast lesions 18

Chapter Three

Table 3.1 Summary of development and comparison between ROC methods. 55

Chapter Four

Table 4.1 Demonstrates the sample size of the images and the number of the observers with the normal distribution of the population of breast density for this study. 78

Table 4.2 Shows the single and combined two observers' data assessments and the rating score for each case 84

Table 4.3 Illustrates the physical measures of breast lesion with three levels of simulated motion blur using conspicuity software 88

Table 4.4 Demonstrates the physical measures of breast lesion with three levels of simulated motion blur using ImageJ software 92

Table 4.5 demonstrates the missed lesion calculation method 93

Chapter Five

Table 5.1 Demonstrates a summary of the wJAFROC FOM with confidence interval (95% CI), sensitivity and specificity analysis for microcalcifications case. 99

Table 5.2 Demonstrates the wJAFROC FOM with confidence interval (95% CI), sensitivity and specificity analysis for each observer for the image with no motion blur and two levels of simulated motion blur of microcalcifications. 100

Table 5.3 Shows a comparison of the p-values difference between treatment pairs of average wJAFROC FOMs (95%) of single observer for microcalcification images. 100

Table 5.4 A summary of the wJAFROC analysis for masses. Shows the observer averaged wJAFROC FOM and 95% confidence intervals (CIs), Sensitivity % (HrSe) and Specificity % (HrSp). 103

Table 5.5 Demonstrates a comparison of the p-value difference between two treatment pairs of average wJAFROC FOMs (95%) and the p-value difference between two sensitivity and specificity for single observer of masses cases. 104

Table 5.6 The wJAFROC FOM with confidence interval (95% CI), sensitivity and specificity analysis for each observer at 0 mm, 0.7 mm, and 1.5 mm of simulated motion blur for masses. 106

Table 5.7 A summary of the wJAFROC analysis of microcalcification. Shows the observer averaged wJAFROC FOM and 95% confidence intervals (CIs), Sensitivity % (HrSe) and Specificity % (HrSp) of combining two observers' data. 109

Table 5.8 A summary of the wJAFROC analysis of masses. Shows the observer averaged wJAFROC FOM and 95% confidence intervals (CIs), Sensitivity % (HrSe) and Specificity % (HrSp) of combined two observers' data. 111

Table 5.9 Demonstrates the comparison between wJAFROC FOMs, sensitivity and specificity of single and combined two observers' data with three levels of simulated blur. 113

Table 5.10 Demonstrates a comparison of the p-value difference between treatment pairs of average wJAFROC FOMs (95%) and the p-value difference between two sensitivity and specificity for single observer and combined two observers' data of microcalcifications. 114

Table 5.11 Demonstrates a comparison between wJAFROC FOMs and sensitivity and specificity for single observer and combined two observers' data of masse. 115

Table 5.12 Demonstrates a comparison of the p-value difference between two treatment pairs of average wJAFROC FOMs (95%) of masses. 116

Table 5.13 The wJAFROC FOM and 95% confidence intervals (CI) for single and combined observers for masses and microcalcifications. 117

Chapter Six

Table 6.1 Physical measurements of breast masses within mammographic images using conspicuity software. 120

Table 6.2 Values of Kolmogorov-Smirnov test and Shapiro-Wilk normality test for the physical measures data of breast masses 121

Table 6.3 The results of conspicuity index of 23 masses cases for images with no motion blur and two levels of simulated motion blur. 123

Table 6.4 Demonstrates the results of edge angle measures for 23 masses cases of images with no motion blur and two levels of simulated motion blur..... 125

Table 6.5 Demonstrates the grey level measures of 23 masses cases for images with no blur and two levels of simulated motion blur. 127

Table 6.6 Demonstrates SNR measures of 23 masses cases for images with no motion blur and two levels of simulated motion blur. 129

Table 6.7 Values of Kolmogorov-Smirnov test and Shapiro-Wilk normality test for the physical measures data of breast masses 130

Table 6.8 Demonstrates dispersion index of microcalcifications between images without motion blur (0.0 mm), and images with simulated motion blur (0.7 mm & 1.5 mm)..... 132

Table 6.9 Demonstrates the P-values of Wilcoxon Signed Ranks Test of physical measures of microcalcifications between images with no motion blur (0.0 mm), and images with simulated motion blur (0.7 mm & 1.5 mm)..... 133

Table 6.10 Demonstrates contrast of microcalcifications for images without motion blur (0.0 mm), and images with simulated motion blur (0.7 & 1.5 mm)..... 134

Table 6.11 Demonstrates measures DI x contrast of microcalcifications for images without motion blur (0.0 mm), and images with simulated motion blur (0.7 & 1.5 mm). 135

Table 6.12 demonstrates SNR of microcalcification for images with no blur and two levels of simulated motion blur..... 137

Table 6.13 The physical measures of microcalcifications in image with no simulated motion blur (0.0 mm), and images with simulated motion blur (0.7 & 1.5 mm). 138

Table 6.14 The detectability of malignant masses by the observers in images without motion blur (0.0 mm), and images with simulated motion blur (0.7mm & 1.5 mm). 146

Table 6.15 The detectability of malignant microcalcifications by the observers in images without motion blur (0.0 mm), and images with simulated motion blur (0.7mm & 1.5 mm). 148

Chapter Seven

Table 7.1 The types of clustered microcalcifications and the impact of motion blur on each type. .. 168

Table 7.2 Summary of the impact of motion blur on detection performance on each type of breast masses. 175

List of Figures

Chapter One

Figure 1.1 A flowchart demonstrating the structure of this PhD thesis 6

Chapter Two

Figure 2.1 Structures of the adult woman breast: (A1) schematic breast anatomy and (B1) the corresponding mammographic features (Hogg et al., 2015). 9
Figure 2.2 Demonstrates a simplified drawing of the structure of a Terminal Ductal Lobular Unit (TDLU). 10
Figure 2.3 Mammographic Projections (Imaginis Corporation, 2014). 14
Figure 2.4 Normal mammography- Cranio-Caudal Projection (A&B) and Medio-Lateral Oblique Projection (C&D). 15
Figure 2.5 Malignant microcalcifications in different shapes, sizes and distributions pattern. 17
Figure 2.6 shapes and Margins of Breast Lesions (The radiology Assestant, 201 19
Figure 2.7 Mammographic images demonstrating benign and malignant masses 19
Figure 2.8 Malignant microcalcification and mass with different lesion characteristics. 21
Figure 2.9 Variations in breast density according to BI-RADS classification system 23
Figure 2.10 Demonstrate same breast image with different spatial and contrast resolution. 28
Figure 2.11 Full- field digital mammography equipment (Ossati 2015; Hologic Inc., 2014). 32
Figure 2.12 Molybdenum / Molybdenum spectrum (Sprawls, 1995) 41
Figure 2.13 Molybdenum / Rhodium spectrum (Sprawls, 1995). 42
Figure 2.14 The interaction of X-ray through Compton scatter (Haidekker, 2013) 43
Figure 2.15 The pathways of transmitted X-ray A: through normal tissue of breast B: during interest structure (Yaffe, 2010). 44

Chapter Three

Figure 3.1 Relationship between visual performance, image interpretation and image quality assessment methods. 47

Figure 3.2 Three categories of perceptual mistakes in observing mammograms (Zuley, 2010; Ossati, 2015) 49

Figure 3.3 Anatomical structures of the human eye (Van De Graaff, 2001) 50

Figure 3.4 The use of FROC methods to localise breast lesions..... 59

Chapter Four

Figure 4.1 Key Steps within Study Methodology..... 68

Figure 4.2 Example of FFDM images with two levels of simulated blur and without simulated blur 71

Figure 4.3 Digital convolution: the mask is put on the original image, mask components are multiplied pixel values, and the outcomes added to form an output pixel (Tobergte & Curtis 2013). 73

Figure 4.4 (A) Demonstrates wireframe image of two-dimensional Gaussian (Ma et al. 2015). (B) Demonstrates Gaussian profile (one-dimensional) (Tobergte & Curtis 2013)..... 75

Figure 4.5 Shows different convolution masks; (i) averaging mask (3x3); (ii) averaging mask (5x5); (iii) weighted-average mask (3x3) (Tobergte & Curtis 2013)..... 75

Figure 4. 6 Confidence scale variant..... 81

Figure 4.7 A mammographic image containing malignant clustered microcalcification and the mark placed in the centre of the clusters using ROCView software. 82

Figure 4.8 The conspicuity software demonstrates the measurement of a breast mass.. 87

Figure 4.9 Line profiles are drawn 180° surrounding the region of interest. 87

Figure 4.10 The Imagej software demonstrates the measurement of breast microcalcification. Shows the first stage for selecting the region of interest..... 90

Figure 4.11 (A) Demonstrates the step 2 of measurement of breast microcalcification using Imagej software. (B) demonstrates the regions of interest data sets are stored as TSV files in the same directory as the analysed images for three levels of simulated motion blur..... 91

Figure 4.12 demonstrates the same region of interest for clustered microcalcification for the three levels of simulated motion blur. 92

Chapter Five

Figure 5.1 Demonstrates the distribution of FOM difference and 95% CIs for all FOM treatment pairs in the analysis of microcalcifications (this is the same data as indicated in Table 5.3). .. 101

Figure 5.2 Demonstrates the wAFROC curve of microcalcification cases with three levels of motion blur. The highest performance is represented in level 0.0 mm (blue line) and the performance decreased with increase motion blur 0.7 mm (red line) 101

Figure 5.3 demonstrates the highest-rating inferred ROC curve of microcalcification for the image with no motion blur and two levels of simulated motion blur..... 102

Figure 5.4 The observers averaged FOM of microcalcifications for the image without motion blur and two levels of simulated motion blur. 102

Figure 5.5 Demonstrates the distribution of FOM difference and 95% CIs for all FOM treatment pairs in the analysis of masses (this is the same data as indicated in Table 5.5)..... 104

Figure 5.6 Demonstrates the wAFROC curve of masses in image with no blur (0.0 mm) and two levels of simulated motion blur (0.7 & 1.5 mm). 105

Figure 5.7 Demonstrates the observers averaged FOM of masses at 0.0 mm, 0.7 mm, and 1.5 mm of simulated motion blur..... 106

Figure 5.8 The wJAFROC FOM and 95% confidence intervals for microcalcifications and masses at 0.0 mm, 0.7 mm, and 1.5 mm of simulated motion blur. 107

Figure 5.9 Demonstrates averaged FOM of the combining two observers' data of microcalcifications at 0 mm, 0.7 mm, and 1.5 mm of simulated motion blur. 110

Figure 5.10 Demonstrates wAFROC curve of combined two observers' data of microcalcifications cases at 0.0 mm, 0.7 mm, and 1.5 mm of simulated motion blur..... 110

Figure 5.11 Demonstrates averaged FOM of the combining two observers' data in images with no motion blur and two levels of simulated motion blur of masses 112

Figure 5.12 Demonstrates wAFROC curve of combined two observers' data of masses with three levels 0.0 mm, 0.7 and 1.5 mm..... 112

Figure 5.13 The comparison between wJAFROC FOMs for single observer and combined two observers' data in microcalcification. 113

Figure 5.14 The difference between the wAFROC curve of single observer and combined two observers' data of microcalcifications. 114

Figure 5.15 The comparison between wJAFROC FOMs for single observer and combined two observers' data of masses. 115

Figure 5.16 The difference between wAFROC curve of single and combined two observers' data of masses. 116

Chapter Six

Figure 6.1 Demonstrates the relationship between the magnitudes of simulated motion blur and conspicuity index of breast masses. 123

Figure 6.2 demonstrates the relationship between the magnitudes of simulated motion blur and edge angle of masses. 125

Figure 6.3 Relationship between the magnitude of simulated motion blur and the grey level of breast masses. 127

Figure 6.4 Relationship between the magnitude of simulated motion blur and the signal to noise ratio (SNR) of breast masses. 129

Figure 6.5 The relationship between the magnitude of simulated motion blur and Dispersion Index. 132

Figure 6.6 The relationship between the magnitude of simulated motion blur and contrast of malignant microcalcifications. 134

Figure 6.7 The relationship between the magnitude of simulated motion blur and DI x contrast of microcalcifications. 136

Figure 6.8 The relationship between the magnitude of simulated motion blur and SNR of microcalcifications. 137

Figure 6.9 Shows the relationship between dispersion index of microcalcifications and their detectability in images without motion blur. 140

Figure 6.10 Demonstrates the relationship between the contrast of microcalcifications and their detectability in images without simulated motion blur. 140

Figure 6.11 Demonstrates the relationship between the DI x contrast of microcalcifications and their detectability in images without simulated motion blur. 141

Figure 6.12 Demonstrates there is no relationship between dispersion index of microcalcifications and the detectability of the lesion in images with blurring (0.7mm). 142

Figure 6.13 Demonstrates there is no relationship between the contrast of microcalcifications and the detectability of the lesion in images with blurring (0.7mm). 142

Figure 6.14 Demonstrates there is no relationship between DI x contrast of microcalcifications and the detectability of the lesion in images with blurring (0.7mm)..... 143

Figure 6.15 Shows the relationship between dispersion index of microcalcifications and their detectability in images with (1.5 mm) motion blur. 144

Figure 6.16 Demonstrates that there is no relationship between Dispersion index of microcalcifications and the detectability of the lesion in images with blurring (1.5 mm). 144

Figure 6.17 Demonstrates there is no relationship between DI x contrast of microcalcifications and the detectability of the lesion in images in images with blurring (1.5 mm). 145

Chapter Seven

Figure 7.1 Magnified area of right cranio-caudal projection. Demonstrates a cluster of microcalcifications have irregular shapes..... 154

Figure 7.2 Magnified views of images without simulated motion blur (0.0mm) and blurred mammography images (0.7mm & 1.5mm). The images illustrate a cluster of malignant microcalcifications, which were affected by simulated motion blur. 155

Figure 7.3 Magnified mammographic images contain clustered microcalcification. The DI in the image without motion blur (0.0mm) was 0.608 per cm2, while the DI for images with motion blur (0.7 and 1.5mm) were 0.405 and 0.262 per cm2 respectively. 162

Figure 7.4 A group of malignant microcalcifications, which were affected by motion blur. 169

Figure 7.5 A group of malignant microcalcifications, which are not affected by motion blur. 169

Figure 7.6 (A) Right CC projection demonstrates (B) Magnified areas of FFDM images at 0 mm, 0.7 mm, and 1.5 mm of simulated motion blur. 170

Figure 7.7 (A) left CC projection demonstrates (B) Magnified areas of FFDM images at 0 mm, 0.7 mm, and 1.5 mm of simulated motion blur. 171

Figure 7.8 (A) Screening mammography image of right CC Projection. Magnified areas of a cluster of microcalcifications. 172

Figure 7.9 Screening mammography image of right cranio-caudal projection. 173

Figure 7.10 (A) a magnified mediolateral Projection demonstrates a small irregular mass with pleomorphic clustered microcalcifications. (B) Magnified cranio-caudal Projection demonstrates a small irregular mass with pleomorphic clustered microcalcifications. 174

Figure 7.11 Demonstrates mammography images containing breast masses with different lesion appearance due to location, size and tissue background. 177

Figure 7.12 Demonstrates a group of malignant of breast masses, which are not affected by motion blur 178

Figure 7.13 Demonstrates a group of malignant of breast masses, which are not affected by motion blur 179

Figure 7.14 (A) mammography images with left MLO Projection, contains different magnitudes of motion blur (0.7 & 1.5 mm) and image without motion blur (0.0mm). (B) Magnified views show small malignant mass (signposted by red arrows). 180

Figure 7.15 Left CC Projection, this mammography image shows a spiculated mass (arrow) that has an irregular shape with indefinite edges. 181

Figure 7.16 Left Cranio-Caudal Projection mammography image contains a stellate mass (arrow) that has an irregular outline (Lesion size 2.2 cm2)..... 182

Figure 7.17 Mammography image left Medio-lateral oblique Projection shows indistinct breast mass (arrow) that has an irregular outline. 183

Figure 7.18 Mammography image with left Cranio-Caudal Projection demonstrates a stellate mass (arrow) that has an irregular outline. 184

Figure 7.19 Mammography image with left mediolateral oblique Projection contains breast mass (arrow) that has an irregular outline (fuzzy edges)..... 185

Figure 7.20 Mammography images of left CC projection contain focal breast mass (arrow) with the dense central area. 186

Figure 7. 21 Screening mammography image of right Medio-lateral Oblique projection. 187

Figure 7.22 Screening mammography image of left CC projection. 187

Figure 7.23 Left MLO projection, mammography images show malignant breast mass, with an oval or round shape and definite edges. 188

List of Publications

No.	Title	Status
1	The impact of simulated motion blur on lesion detection performance in full field digital mammography. Br. J. Radiol., vol. 90, no. 1075, p. 20160871, Jul. 2017. A. K. Abdullah, J. Kelly, J. D. Thompson, C. E. Mercer, R. Aspin, and P. Hogg.	Journal paper Published in BJR
2	The impact of image blurring on lesion detection performance in full field digital mammography. A. K. Abdullah, J. Thompson, C. E. Mercer, J. Kelly, R. Aspin, and P. Hogg.	Conference paper published in ECR congress 2017
3	The impact of image blurring on lesion detection performance in full field digital mammography. A. K. Abdullah, J. Thompson, C. E. Mercer, J. Kelly, R. Aspin, and P. Hogg.	Poster presented in UKRC congress 2017
4	The impact of image blurring on lesion detection performance in full field digital mammography. A. K. Abdullah, J. Thompson, C. E. Mercer, J. Kelly, R. Aspin, and P. Hogg.	Conference paper was presented in SPARC/ University of Salford
5	Impact of the anode heel effect on image quality and effective dose for AP pelvis: A pilot study. Book Chapter 'Optimising image quality for medical imaging' 19-08-2016. Buissink, C., Bowdler, M., Abdullah, A., Al-Murshedi, S., Custódio, S., Huhn, A., & Urdahl, T. and Hogg, P.	Book Chapter OPTIMAX 2016
6	The impact of simulated motion blur on lesion detection performance in full field digital mammography. A. K. Abdullah, J. Thompson, C. E. Mercer, J. Kelly, R. Aspin, and P. Hogg.	Poster presented in Showcase event/ University of Salford
7	A comparison between single data and a combination of two readers' data on mammography images with simulated motion blur. A. K. Abdullah, , J. D. Thompson, C. E. Mercer, J. Kelly, R. Aspin, and P. Hogg. doi: 10.1594/ecr2018/C-1048	E-poster presented in ECR congress 2018
8	Malignant breast masses-conspicuity analysis in motion- simulated mammograms. Abdullah, A. K., Thompson, J. D., Mercer, C. E., Kelly, J., R. Aspin and Hogg, P. (2018) doi:10.1594/ecr2018/C-1043.	E-poster presented in ECR congress 2018

9	A comparison of the performance of a 2.4 MP colour monitor and a 5.0 MP monochrome monitor in visualising low contrast detail using the CDRAD phantom. S. Al-Murshedi, P. Hogg, Abdullah, A. and A. England (2017)	E-poster Poster presented in ECR congress 2018
10	The impact of simulated motion blur on the physical characteristics of malignant breast masses in full field digital mammography. A. K. Abdullah, J. Thompson, C. E. Mercer, J. Kelly, R. Aspin, and P. Hogg.	Poster accepted in Symposium Mammographican 2018
11	The impact of simulated double reporting on the detection performance of masses and microcalcifications in FFDM images containing different magnitudes of image blurring. A. K. Abdullah, J. Thompson, C. E. Mercer, J. Kelly, R. Aspin, and P. Hogg.	Poster accepted in Symposium Mammographican 2018

List of Development Skills

No.	Type of Skill	
1	Applying simulated motion using image blurring software	
2	Operation and set-up the ROCView software for ROC assessment	
3	Data analysis using JAFROC software	
4	How to utilise Conspicuity software for physical measures and data manipulation.	
5	How to utilise ImageJ software for advanced image processing and manipulation.	
6	How to use Endnote software for references coding	
7	How to use SPSS software for different and advanced statistics.	
8	How to use Excel, Word, PowerPoint and publisher at an advanced level	
9	How to operate and set-up the bespoke software for 2-AFC assessment	
10	How to write journal papers (review & empirical), and design poster for conference presentation	
11	How to critically analyse literature	
12	How to use TLD system for the direct measurement of dose.	
13	How to operate the Unfors dosimeter for dose measurements and QC protocols	

Training Sessions Attended

	Date	Title of training course/module/conference	Key learning point
1	02-10-2014	Introduction to the module / Research methods	
2	06-10-2014	Electronic Resources	
3	09-10-2014	Developing research questions and approaches to research	
4	15-10-2014	Time management	
5	16-10-2014	Researching for evidence and information	
6	23-10-2014	Over view of critiquing research papers	
7	28-10-2014	Completing a learning agreement and PhD progression points	
8	29-10-2014	Introduction to Nvivo	
9	30-10-2010	Quantitative designs	
10	06-11-2014	Qualitative designs / Research methods	Methods of data collection
11	11-11-2014	The interview: its place in social scientific research strategies	
12	12-11-2014	Doing a literature Review	
13	12-11-2014	Inspiration: Mind Mapping Software Training	
14	13-11-2014	Analysis, presentation, and interpretation of quantitative research	Fundamentals of statistical analysis
15	18-11-2014	Endnote 7	
16	20-11-2014	Analysis, presentation, interpretation, and rigour in qualitative research	Fundamentals of thematic and content analytic approaches
17	24-11-2014	Open Access publishing	
18	27-11-2014	Advance statistic data analysis	
19	04-12-2014	Ethical issues in research	
20	05-12-2014	Excel Basic	
21	11-12-2014	Excel Charts	
22	11-12-2014	Dissemination and publication of research/ Implementation strategies	
23	12-12-2014	Excel Formulas Functions	

24	18-12-2014	Research in the real world	
25	02-02-2015	Seminar diagnostic medical image	
26	12-02-2015	Working in the UK during and after PhD	
27	16-02-2015	Turbo churching your writing	
28	17-02-2015	How to publish in IEEE	
29	19-02-2015	Word scope workshop for writing	
30	02-03-2015	LEAP Higher Language Review	Session 1
31	06-03-2015	LEAP Higher Language Review	Session 2
32	09-03-2015	LEAP Higher Language Review	Session 3
33	17-03-2015	LEAP Higher Language Review	Session 6
34	19-11-2015	Word scope workshop for writing	
35	24-11-2015	Learning English for Academic Purposes-LEAP Unit 3	Critical writing skills
36	30-11-2015	Learning English for Academic Purposes-LEAP Unit 3	Critical writing skills
37	10-12-2015	Learning English for Academic Purposes-LEAP Unit 3	Critical writing skills
38	13-01-2016	Quantitative research method	SPSS
39	14-01-2016	Quantitative research method	SPSS
40	15-01-2016	Quantitative research method	SPSS
41	10-02-2016	Controversial issues in breast cancer diagnosis using full field digital mammography	Seminar
42	26-02-2016	PhD students session	Critical reading and writing
43	1-03-2016	LEAP Higher writing session	Critical writing
44	7-03-2016	Theory and content as methodology	
45	4-05-2016	LEAP higher session for academic writing	Critical writing skills
46	10-05-2016	LEAP higher session for academic writing	Critical writing skills
47	17-05-2016	LEAP higher session for academic writing	Critical writing skills

Acknowledgement

First and foremost, I would like to start with ‘In The Name of Allah Most Gracious Most Merciful’ I am grateful to God for the good health and wellbeing that were essential to the completion of this thesis.

I would like to express my deepest appreciation to my supervisors Professor Peter Hogg and Dr John D. Thompson my Co-supervisors Dr Claire Mercer, Mrs Judith Kelly and Dr Rob Aspin. Without their guidance and persistent help, this thesis would not exist. In addition, they imparted a lot of knowledge necessary in becoming a good researcher. Stressing the importance of always thinking critically and being patient.

I am also grateful to Mrs Katy Szczepura a lecturer in the school of health sciences. I am extremely thankful and indebted to her for sharing her expertise and sincere, valuable guidance, which helped me to complete this thesis. I would like to thank Professor David Manning, who gave valuable suggestions and interesting feedback. I would also like offer a special thank you to all the practitioners who participated as observer in this study.

I also thank my Father and my Mother for their endless support, encouragement and attention. I am also grateful to my beloved wife Nabaa Sameer Al-Dulaimi for her support, kindness and patience as she accompanied me along this journey. I would like to thanks my Aunt Radhiyah Kamil to here support and encouragement.

I would like to acknowledge The Ministry of Higher Education in Iraq/ Iraqi Cultural Attaché-London for their financial support in which they have covered the tuition fees and living expenses that were needed for the completion of this thesis. I also would like to acknowledge the University of Diyala for their allowing me to take a study leave to do my PhD in the UK. Finally, I would like to express my upmost gratitude to all who, whether directly or indirectly, have aided me in this thesis.

Dedications

I dedicate this thesis to my Father **Khalid Abdullah**, my Mother **Kareema Hamdan** and my wife **Nabaa Sameer Al-Dulaimi**; I never forget their prayers and their love, which motivate me forward. Their words and feelings keep me working hard to finish this thesis. I also dedicate this thesis to my lovely children **Hagr, Ans, Abdullah** and **Humam**.

Abbreviations

AUC	Area under the Curve
AFROC	Alternative Free-response Receiver Operating Characteristic
BI-RADS	Breast Imaging-Reporting and Data System
CC	Cranio-Caudal
CR	Computed Radiography
CT	Computed Tomography
X	Conspicuity Index
DCIS	Ductal Carcinoma in Situ
DICOM	Digital Imaging and Communications in Medicine
DR	Digital Radiography
DI	Dispersion Index
FFMM	Full Field Digital Mammography
FROC	Free-response Receiver Operating Characteristics
FOM	Figure of Merit
HVS	Human Visual System
IDC	Invasive Ductal Carcinoma
IQA	Image Quality Assessment
JAFROC	Jackknife Free-response Receiver Operating Characteristics
kV	kilo-Voltage
LLF	Lesion Localisation Fraction
LROC	Localisation Receiver Operating Characteristic

mA	milliampere
MLO	Medio-Lateral Oblique
mm	millimetre
NLF	Non-lesion Localisation Fraction
NHSBSP	National Health Services Breast Screening Programme
ROC	Receiver Operating Characteristics
UK	United Kingdom
wJAFROC	weighted Jackknife Alternative Free-response Receiver Operating Characteristic
ΔGL	Change in grey level

Abstract

Objective: Full-field Digital Mammography (FFDM) is employed in breast screening for the early detection of breast cancer. High quality, artefact free, diagnostic images are crucial to the accuracy of this process. Unwanted motion during the image acquisition phase and subsequent image blurring is an unfortunate occurrence in some FFDM images. The research detailed in this thesis seeks to understand the impact of motion blur on cancer detection performance in FFDM images using novel software to perform simulation of motion, an observer study to measure the lesion detection performance and physical measures to assess the impact of simulated motion blur on image characteristics of the lesions.

Method: Seven observers (15±5 years' reporting experience) evaluated 248 cases (62 containing malignant masses, 62 containing malignant microcalcifications and 124 normal cases) for three conditions: no motion blur (0.0 mm) and two magnitudes of simulated motion blur (0.7 mm and 1.5 mm). Abnormal cases were biopsy proven. A free-response observer study was conducted to compare lesion detection performance for the three conditions. Equally weighted jackknife alternative free-response receiver operating characteristic (wJAFROC) was used as the figure of merit. A secondary analysis of data was deemed important to simulate 'double reporting'. In this secondary analysis, six of the observers are combined with the seventh observer to evaluate the impact of combined free-response data for lesion detection and to assess if combined two observers data could reduce the impact of simulated motion blur on detection performance. To compliment this, the physical characteristics of the lesions were obtained under the three conditions in order to assess any change in characteristics of the lesions when blur is present in the image. The impact of simulated motion blur on physical characteristics of malignant masses was assessed using a conspicuity index; for microcalcifications, a new novel metric, known as dispersion index, was used.

Results: wJAFROC analysis found a statistically significant difference in lesion detection performance for both masses (F (2,22) = 6.01, P=0.0084) and microcalcifications (F(2,49) = 23.14, P<0.0001). For both lesion types, the figure of merit reduced as the magnitude of simulated motion blur increased. Statistical differences were found between some of the pairs investigated for the detection of masses (0.0mm v 0.7mm, and 0.0mm v 1.5mm) and all pairs

for microcalcifications (0.0 mm v 0.7 mm, 0.0 mm v 1.5 mm, and 0.7 mm v 1.5 mm). No difference was detected between 0.7 mm and 1.5 mm for masses.

For combined two observers' data of masses, there was no statistically significant difference between single and combined free-response data for masses ($F(1,6) = 4.04$, $p=0.1001$, -0.031 (-0.070, 0.008) [treatment difference (95% CI)]. For combined data of microcalcifications, there was a statistically significant difference between single and combined free-response data ($F(1,6) = 12.28$, $p=0.0122$, -0.056 (-0.095, -0.017) [treatment difference (95% CI)]. Regarding the physical measures of masses, conspicuity index increases as the magnitude of simulated motion blur increases. Statistically significant differences were demonstrated for 0.0–0.7 mm $t(22)=-6.158$ ($p<0.000$); 0.0–1.5 mm $t(22)=-6.273$ ($p<0.000$); and 0.7–1.5 mm ($t(22)=-6.231$ ($p<0.000$). Lesion edge angle decreases as the magnitude of simulated motion blur increases. Statistically significant differences were demonstrated for 0.0–0.7 mm $t(22)=3.232$ ($p<0.004$); for 0.0–1.5 mm $t(22)=6.592$ ($p<0.000$); and 0.7–1.5mm $t(22)=2.234$ ($p<0.036$). For the grey level change there was no statistically significant difference as simulated motion blur increases to 0.7 and then to 1.5mm. For image noise there was a statistically significant difference, where noise reduced as simulated motion blur increased: 0.0–0.7 mm $t(22)=22.95$ ($p<0.000$); 0.0–1.5mm $t(22)=24.66$ ($p<0.000$); 0.7–1.5 mm $t(22)=18.11$ ($p<0.000$). For microcalcifications, simulated motion blur had a negative impact on the 'dispersion index'.

Conclusion: Mathematical simulations of motion blur resulted in a statistically significant reduction in lesion detection performance. This reduction in performance could have implications for clinical practice. Simulated motion blur has a negative impact on the edge angle of breast masses and a negative impact on the image characteristics of microcalcifications. These changes in the image lesion characteristics appear to have a negative effect on the visual identification of breast cancer.

Chapter One: Introduction and Thesis Outline

1.1 Introduction

Full-field Digital Mammography (FFDM) is the current standard imaging technique for the early detection of breast cancer. High quality, artefact free, diagnostic images are crucial to the accuracy of this process. Unwanted motion during the image acquisition phase and subsequent image blurring are unfortunate consequences in some FFDM images (Rosen, Baker and Soo, 2002). It is thought that this could lead to a reduction in diagnostic performance. The cause of motion blur can be patient-based (e.g. breast and/or chest wall motion), or technology-based (e.g. paddle movement) (Geiser et al., 2011). This can lead to distortion of the image in one or more directions. Chest wall motion could be due to respiration, and by its nature, fairly predictable, but it is reasonable to hypothesise that breast motion could be more complex, and could be the outcome of a combination of paddle movement, thixotropic behaviour and blood being forced away from the breast due to the applied compression force (see section 2.7.3). Thixotropic behaviour represents a time-dependent reduction of viscosity and modulus induced by deformation when mechanical loading changes breast volume and results in the motion of fixed structures (glandular and adipose tissues) (Geerligs, Peter, Ackermans, Oomens and Baaijens, 2010).

Anecdotal evidence within the National Health Service Breast Screening Programme (NHSBSP) suggests that image blurring requires images to be repeated, thus increasing patient radiation dose, anxiety, and service costs. The paucity of literature on this topic suggests that this technical issue continues to be under-reported. Recent research (Ma, Aspin, Kelly, Millington, and Hogg, 2015) suggests that motion blur can be visible to practitioners at sub-millimetre levels, but presently we do not know the impact of motion blur on breast cancer detection. At the current level of understanding it can only be assumed that motion blur will have a negative impact on cancer detection. Consequently, this thesis seeks to understand whether motion blur does indeed have an impact on cancer detection performance in FFDM. The methodological approach applied in this work uses novel software to perform a pixel shift simulation of motion to introduce simulated motion blur to clinical FFDM images. These images are the foundation of an observer performance assessment to realise the impact of simulated motion blur on cancer detection.

1.2 Aim

The aim of this thesis is to assess the impact of simulated motion blur on lesion detection performance in FFDM using the free-response receiver operating characteristic (FROC) method. The research will evaluate the impact on lesion detection performance on two different magnitudes of simulated motion blur. The selection of two different magnitudes of motion blur was to determine whether performance would become incrementally worse with greater magnitudes of motion blur.

1.3 Objectives

1. Characterise non-simulated blurring in FFDM images and determine the magnitude of computer generated blurring required to simulate this. A validation study of the non-simulated blur will be conducted to see if experienced FFDM observers could differentiate between real blur and simulated blur.
2. Determine the impact of simulated motion blur on lesion detection performance.
3. Determine the impact of simulated motion blur on physical characteristics of:
    a. malignant masses using Conspicuity Index, and,
    b. microcalcifications using a novel metric, described as the 'dispersion index'.

1.4 Research Questions

What is the impact of different magnitudes of simulated motion blur on:

- Lesion detection performance in FFDM images
- Physical characteristics of lesion images

1.5 Rational of the thesis

Motion blur in FFDM images has the potential to obscure breast lesions; as a result, clinically significant abnormalities could go undetected which may have a negative impact on patient care. Anecdotal evidence suggests that many practitioners in mammography have realised the potential impact of motion blur in digital mammography but they do not know how much of an impact this can have on breast cancer diagnosis, or indeed, whether they are even detecting the smaller magnitudes of motion. If motion blur is detected, this could lead to repeated images or increased recall rates, both of which will increase radiation dose to the patient. If motion

blur is not recognised, this could lead to missed diagnosis, late detection or symptomatic presentation as an interval cancer. On the other hand, motion blur also has the potential to increase the number of lesion mimics (false positives), which may lead to unnecessary biopsy, with the consequence of an unnecessary invasive procedure and increased anxiety for the patient. Presently, no study exists to determine the impact of simulated motion blur on observer performance. Therefore, this thesis aims to evaluate the impact of motion blur on breast cancer detection performance in FFDM using novel image blurring software.

1.6 The Contribution of this Thesis:

This thesis demonstrates for the first time, that motion blur has a negative and statistically significant impact on the detection performance of malignant masses and microcalcifications in FFDM images. In view of this, caution should be exercised when making decisions about the acceptability of images that appear to contain blur as false-negative decisions could be reached. This thesis recommends further research is required to highlight the impact of this problem. This thesis also provides a number of recommendations to breast specialist clinicians, particularly radiographers and radiologists. Firstly, it has recommended that radiographers be aware about motion blur during quality assessment of images in the mammography imaging room. Secondly, clinicians during image reading, should be aware of the impact of motion blur on cancer detection, in relation to the potential for false positives and false negatives.

1.7 Thesis Structure

This thesis is composed of eight distinct chapters, summarised in **Figure (1.1).**

Chapter One– Introduction and Thesis Outline: comprises a brief introduction, aim, objectives and thesis rational.

Chapter Two– Literature Review: This chapter provides a review of areas of interest that are of critical relevance to this thesis. In respect of one of the key objectives of this thesis, it is important that the anatomy of the breast is explored and understood in detail. In addition to this it was important to develop a working understanding of the presentation of breast cancer and the characteristics of breast tissue, as displayed in mammographic images. Since it has been hypothesized that image blurring may originate from the equipment used to generate the mammographic images it was also valuable to understand the detailed operation and technical aspects of these systems. This work is heavily influenced by the observers' ability to detect cancer in images, so it is vitally important that the factors affecting diagnostic performance in mammography are understood.

Chapter Three– Medical Image Assessment Methods: The relationship between visual performance and medical image interpretation is explored here, with a focus on the human visual system due to the fact that medical image interpretation is based on visual performance of an observer and visual appearance of the image. Image perception was evaluated to help understand the challenges presented to clinicians who evaluate FFDM images. The methods to evaluate observer performance were reviewed in detail and this helped inform the choice of optimal method to apply for the thesis research question. In addition to the perceptual evaluation by the observers, it was valuable to understand what is happening to the characteristics of the breast tissue and lesions, as presented in the images. Understanding how lesion characteristics change when simulated motion blur is applied and the methods available for physically evaluating these characteristics was another critical step in the literary analysis, as this help inform the design of the methods.

Chapter Four– Methodology: In this section the methodological choices are explained and justified for the following components of the research: (i) the design of the free-response study, (ii) the method to apply simulated motion blur to the FFDM images, and (iii) the methods used

to measure the physical characteristics of the lesions. This section describes eight logical steps using five different software applications; each having a specific function in the thesis.

Chapter Five– The Results of the Free-response Study: This chapter presents the results of the observer performance study. The main outcomes focus on the detection of malignant masses and microcalcifications under three conditions: (i) no motion blur, (ii) 0.7 mm of simulated motion blur, and (iii) 1.5 mm of simulated motion blur. In addition to this, a decision was made to investigate the impact of dual reader evaluations on detection performance in the presence of simulated motion blur. This was done following a method to combine the free-response data of two observers. The aim was to mimic the double reporting scheme used in screening mammography.

Chapter Six– The Results of Physical Measures: In this chapter the physical characteristics of the lesions are described and compared at different magnitudes of simulated motion blur. Generating this data also enabled an analysis of 'missed lesions' to try and establish whether simulated motion blur had a greater impact, thus causing a greater reduction in detection, on lesions of different characteristics.

Chapter Seven– Discussion: This chapter evaluates the results of the free-response study and the physical measures. This chapter is set out in the same manner as the results chapter, where the data from each section is discussed separately. The impact of motion blur on the detection performance of breast masses and microcalcifications are discussed. The missed lesion calculation method and the impact of motion blur on lesion characteristics image are discussed.

Chapter Eight: Conclusion, Recommendations and Future work:

This chapter summarises the results of the thesis in a concise manner. The final conclusions that were obtained from free-response study, and then an overall conclusion regarding the impact of motion blur on physical characteristics of malignant masses and microcalcifications is presented. A statement of novelty and recommendations for future work is presented.

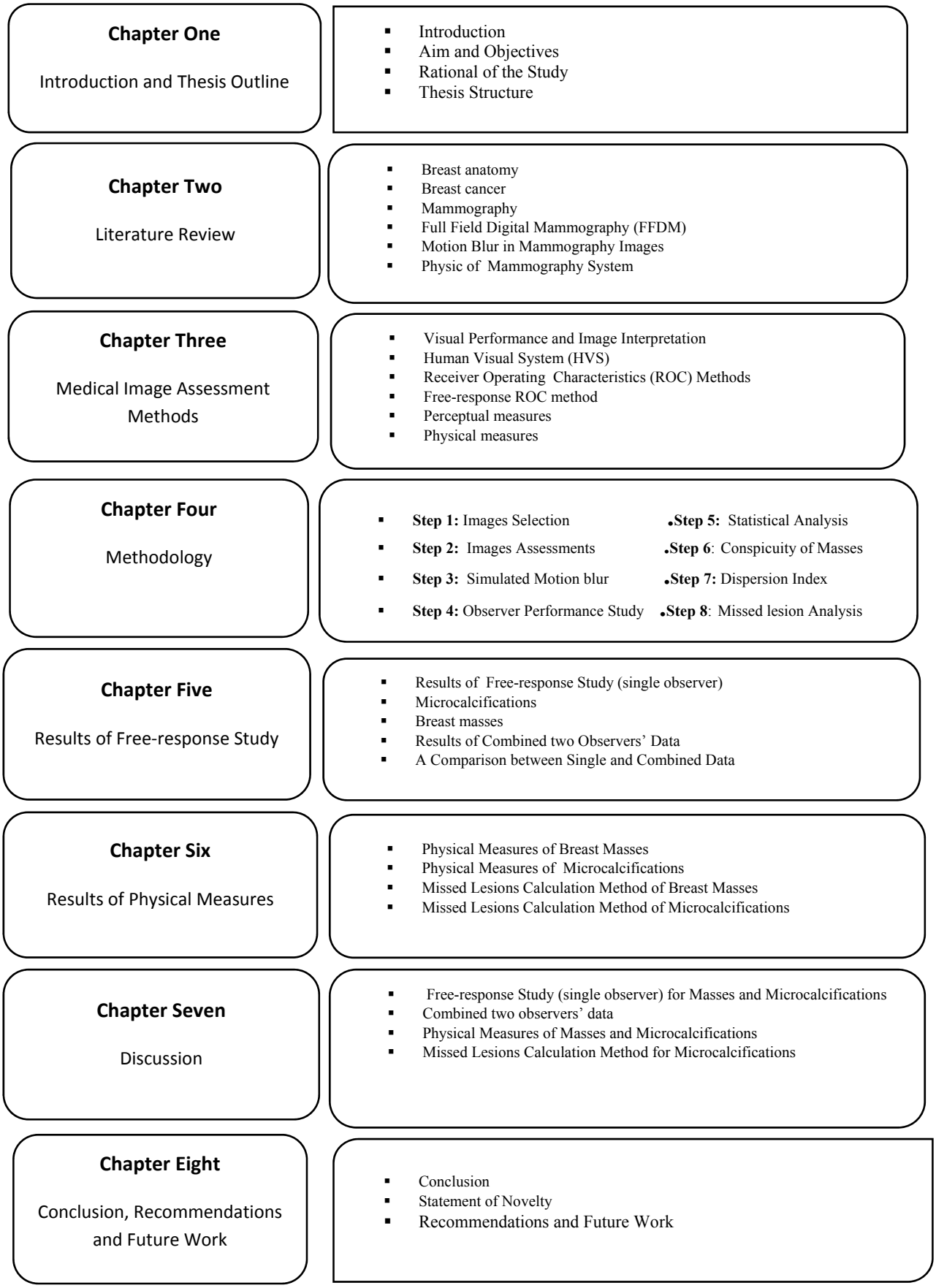

Figure 1.1 A flowchart demonstrating the structure of this PhD thesis

Chapter Two: Literature Review

2.1 Overview of the Chapter

This literature review provides a critical analysis of previous studies, which investigated the cause and effect of motion blur in FFDM images. A literature search was undertaken, and was followed by assessment of study elements. This assessment offers justification for the method described in chapter four, in addition to the rationale for the research study described in chapter one. The literature search was implemented utilising Medline, Google scholar and Solar databases at the University of Salford, with different sets of the keywords such as motion blur, full field digital mammography, lesion detection performance, breast cancer. There were no limits applied for publishing dates.

This chapter is organized into seven main sections. The first section (2.2) will focus on breast anatomy. The second section (2.3) will focus on breast cancer and factors effecting the risk of breast cancer. The third section (2.4) will focus on mammography and the characteristics of breast tissue in mammography images. The fourth section of this literature review will focus on the factors affecting diagnostic efficiency of breast cancer detection in mammographic images such as breast density, image quality and the effect of shape and margin of breast lesion on detection performance. In the fifth section (2.6), the focus will centre on the components of FFDM system. The sixth section (2.7) will focus on motion blur in mammography images and the contributory factors. The reviewed studies in this section were sub-divided for structure. The first (2.7.1) investigated the causes of motion blur in FFDM images according to extra and intra patient movement focusing into the causes of motion blur related to both patient and system parts; paddle movements, inadequate compression and pain related to paddle compression. The second (2.7.2) reviews the papers that investigated the visual detection of motion blur on FFDM using different types of monitors. The third (2.7.3) relates to the thixotropic behaviours of breast tissue. The seventh section focuses on the physics of mammography systems, X-ray production and X-ray incident on the detectors.

2.2 Breast Anatomy

The breast is tear-shaped and supported by the front of the chest wall. It is located over the pectoral muscles and attached to the upper border of the chest wall by fibrous ligaments known as Cooper's ligaments. The composition of the breast is a mass of soft tissue consisting of fatty,

fibrous and glandular tissue (Hogg et al., 2015). The development of the breast begins during puberty when the female body undergoes changes to prepare for reproduction. Puberty often starts around the ages of 10 or 11 year when the breast responds to hormonal changes in the body. The production of two hormones, progesterone and oestrogen, signal the development of the glandular tissue of breast (Pathmanathan, 2006).

The anatomical structures of the female breast are represented in **Figure 2.1.** The interior part of the female breast consists of three major tissue types: glandular or parenchymal tissue, fatty and fibrous tissue. The glandular tissues are typically divided into 15-20 lobes, wherein the production of milk occurs. The lobes are divided into smaller sections known as lobules and separated by fibrous walls (Darlington, 2015). The nipple is connected to the lobules by a network of small ducts (intralobular ducts). The ducts often start as tiny ductules at the lobules; after that they combine near the nipple to become larger sized ducts (Van De Graaff, 2001). The connective or fibrous tissue in the breast contains and supports both the ducts and lobules. The ducts and lobes (glandular tissue) can be grouped with fibrous tissue, together forming the fibro-glandular tissue. The fibro-glandular tissue is covered on the outside by a layer of fat or adipose tissue (Van De Graaff, 2001). The variation between adipose to glandular tissue proportion is due to age and individual characteristics. However, the features of the female breast are like a unique map for every individual; the breast structure alters over time according to age, hormonal changes, and menopausal status (Ossati, 2015). It is because of this that the interpretation of mammographic images is considered a complex task.

Breast parenchyma comprises of three kinds of tissues–adipose and subcutaneous tissue, functional glandular tissue, and skin. The macroscopic anatomy of the breast, divides the component female breast into two main parts. The first part known as glandular component (milk production) and the second part comprising muscles, fascia (connective tissue) and fat, which are concerned with support and make up the breast (Darlington, 2015). The variations in breast structure can be illustrated by differences in breast density on mammography. Commonly, younger aged females tend to increase dense glandular tissue. Likewise, the breast density in older age females tend to have less density through the changing of fatty tissue instead of glandular tissue. Lactation and pregnancy are among some of the compounding factors that are indicative of being important in raising the density of breast tissue (McDonald, 2015).

The microscopic anatomy of the breast was firstly described by Welling in (Wellings et al., 1975). He identified the terminal ductal lobular units (TDLU) as the functional unit of the breast, consisting of acini (built up from 10 to 100 sac-like units), an extralobular duct and an intralobular terminal duct. The TDLU is important physiologically due to its responsibility for milk production during the period of lactation. **Figure 2.2** illustrates a simplified drawing of the structure of a Terminal Ductal Lobular Unit (TDLU). During pregnancy and lactation, increases in oestrogen, prolactin and progesterone produce enlargement of the acini, an evolution in myoepithelial cells and hyperplasia of the lactogenic epithelium to prepare for milk producing. During lactation, the breast passes through many of changes and deferent degrees of involution, and its appearance might seem to consist of a smaller amount glandular tissue than before the pregnancy period. This process continues for about three months before returning to a new baseline.

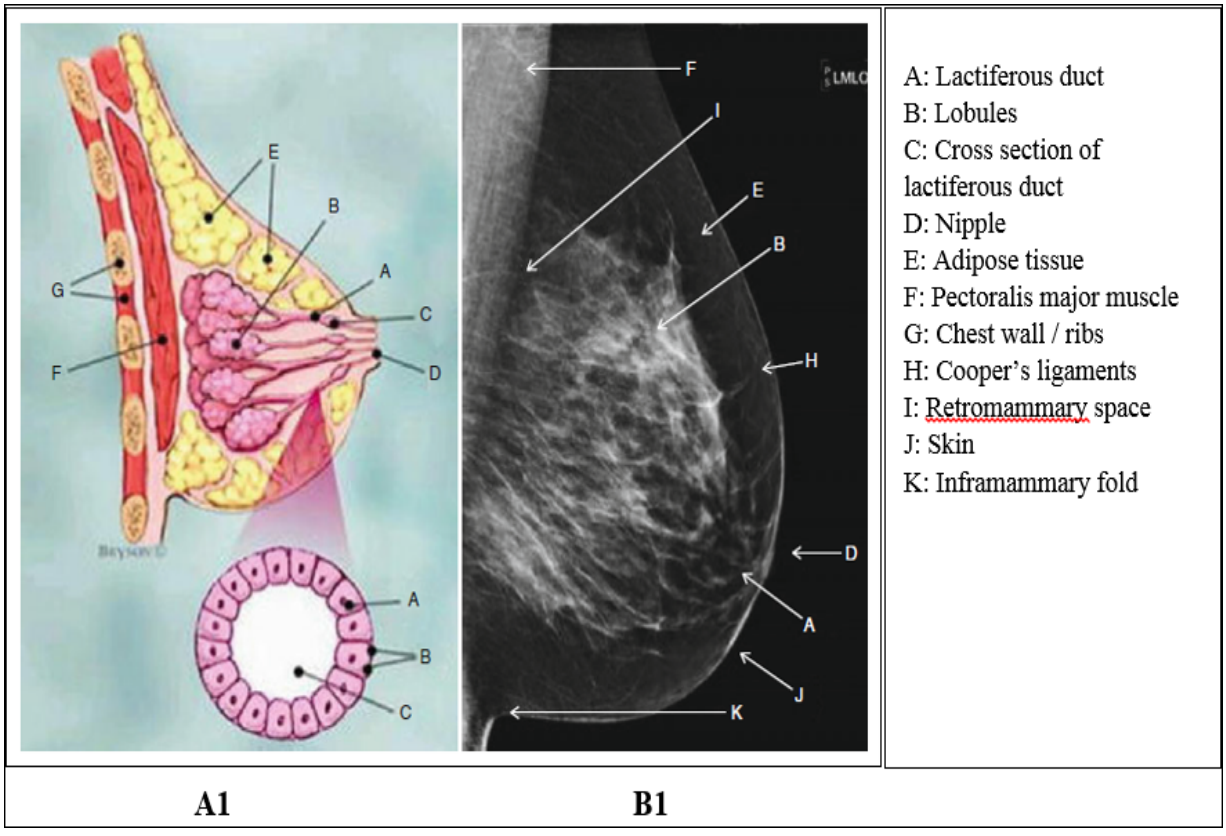

Figure 2.1 Structures of the adult woman breast: (A1) schematic breast anatomy and (B1) the corresponding mammographic features (Hogg et al., 2015).

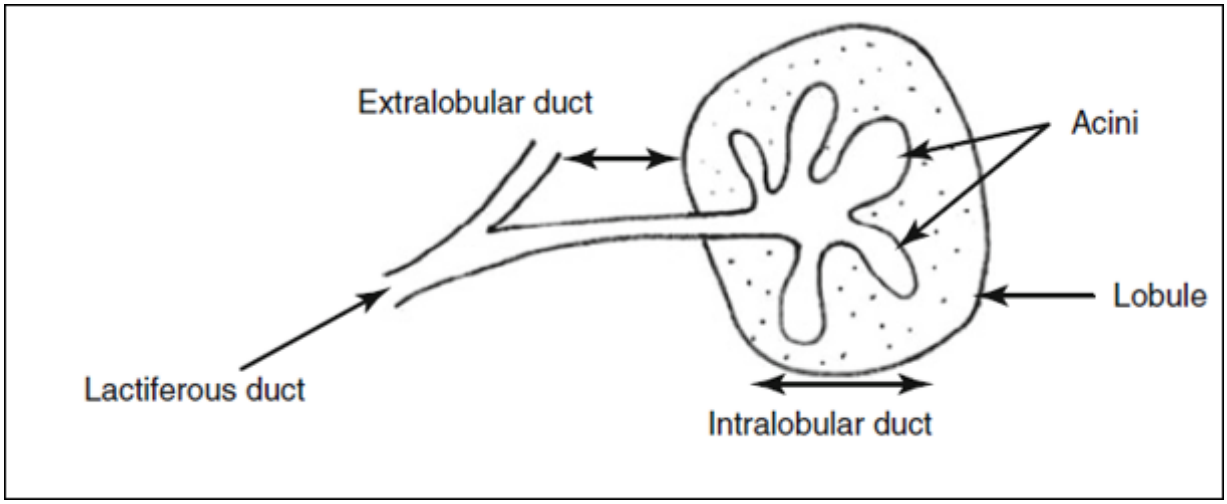

Figure 2.2 Demonstrates a simplified drawing of the structure of a Terminal Ductal Lobular Unit (TDLU).

Breast size is fundamentally identified via the amount of adipose tissue (fat cells) in the breast. The adipose tissue reaches from the collarbone to the armpit and to the middle of the ribcage (Whitman and Haygood, 2012). Commonly, smaller breasts have a smaller amount of adipose tissue compared to their glandular tissue, while the larger size of breasts have a higher amount of adipose tissue compared to their glandular tissue (Spear et al., 2004). The shape and size of the breast varies according to several factors: diet, age, race, the situation menopausal of women and parity (Williams, 1995). Physical techniques can be used to identify breast volume or size through either casting the breast in plastic or through immersion of the breast in water and identifying its volume by calculating the displaced water volume based on Archimedes' principle. Precise identification of breast volume is not easy though can be achieved using digital techniques (Veitch, Burford, Dench, Dean, & Griffin, 2012). Alonzo-Proulx et al., (2012) utilised digital mammograms to investigate some of the breast features such as the breast volume for digital mammographic images of 15,351 females. They reported that the mean breast volume for all examined cases was 687 cm^3 with small variances in several age groups. For instance, it was around 703 cm^3 for 50-55 year and 736 cm^3 for 55-65 year age groups. Diffey, (2012) found a highest mean breast volume about 820 cm^3. However, Wang et al., (2013) used ultrasound to calculate breast volume of women and they reported that the breast volume for about 57% of 306 adult women was 400-800 cm^3.

2.3 Breast Cancer

Breast cancer is an uncontrolled growth and an abnormal change of breast tissue due to abnormal cell divisions (proliferation). In a normal condition, two types of genes are responsible for controlling the division of the cell, named as a tumour suppressor and proto-oncogenes genes. These genes continuously mutate, this leads to uncontrolled cell division (Shannon & Chittenden, 2015). This cancer can metastasise or diffuse to other parts through the lymphatic system or the blood circulation (Shetty, 2015a).

Breast cancer is characterised by malignant tumours that arise from the glandular tissue within the breast. It is an insidious disease that will affect one in seven women over their lifetime (Cancer research UK, 2016). There are several types of breast cancer which can be classified by the physical characteristics of the tumour and location within the breast. One of these types is known as cancer in situ. This appears as a non-invasive disease in which the cancer cells stay inside the basement membrane and do not invade the surrounding tissues. Another type of breast carcinoma is known as an invasive breast carcinoma. This invades surrounding tissue and has the ability to metastasise, which means that the cancer transfers from one part of the body to another through the lymph system or the blood stream (Evans et al., 2002). According to Danziger and Simonsen, (2011), Invasive Ductal Carcinoma (IDC) is an example of an invasive breast cancer which involves different subtypes (Papillary Carcinoma, Medullary Carcinoma, and Tubular Carcinoma), while Ductal Carcinoma in Situ (DCIS) is an example of a non-invasive breast cancer. Other types of breast cancer (American Cancer Society, 2014) such as carcinoma, sarcoma and adenocarcinoma, originate in various lobes of the breast. Carcinomas originate in the lining layer of the breast, Sarcomas originate from connective tissues (fat, blood vessels or muscle), and Adenocarcinomas originate in the glandular tissue such as the breast lobules.

The American Cancer Society (2014) found that approximately 8 out of 10 invasive breast cancers could be categorised as IDC. The shape and margins of IDC are most commonly spiculated firm masses with ill-defined and irregular margins and it is difficult to detect. The second most common breast cancer, which starts in lobules or in the milk-producing glands, is Invasive Lobular Carcinoma (ILC). DCIS is the most common type and it originates in the milk ducts. It is also recognised that there are other types of breast cancer such as Lobular Carcinoma in Situ (LCIS) (Evans & Blanks, 2002; Winchester &Winchester, 2006).

The TDLUs are important units within the breast , as over 90 % of breast cancers originate in these units (Hogg et al., 2015). The ducts and acini consist of three layers including the epithelial lining, myoepithelial layer and the basement membrane. The epithelial layer is normally only one cell thick, but when converted to two or three cells thick it is named a hyperplasia. More proliferation is classified depending on a number of layer cells that are existent, and the appearance of the atypical cells; these situations range from atypical ductal hyperplasia to ductal carcinoma in situ. The function of the basement membrane is responsible for preventing the spread of cancer. When this membrane is breached, a carcinoma is named invasive. Male breast cancer is extremely rare compared to breast cancer in women, representing approximately less than 1% of all breast cancers (Garnett, 2015). In the UK, male breast cancer is of lower incidence than female breast cancer, with only one new case detected for every 100,000 males (around 350 to 400 cases per year). The male breast is undeveloped but is affected by testosterone and oestrogen that influences some of the breast tissue located beyond the nipple. This undeveloped tissue of breast consists of rarely ductal lobular units and mainly major sub-areolar ducts (Cancer research UK, 2016).

2.3.1 Factors Affecting Breast Cancer

An individual's likelihood of contracting breast cancer is their breast cancer risk. Many factors are responsible for breast cancer risk such as gender, age, family personal history, lifestyle factors and hormonal therapy. However, it is uncontrolled by large number of factors, and there is no full explanation about the mechanism of how these factors can stimulate the normal cells to become cancer cells (Hackney, 2015). The two essential unalterable risk factors are gender and age. In the context of gender, more than 99% of breast cancer incidences are from women (Kopans, 2007; Garnett, 2015). In women under 20 years of age, breast cancer cases are quite rare, and approximately 0.3% of the breast cancer incidences happen in women within the 20–30 age group (Finkel, 2005). However, approximately (48 %) of the breast cancer incidences occurs in females within their fifth and sixth decade (50–69 year) (Hackney, 2015). This contributed to the rationale for supporting the UK NHS breast-screening programme to invite females within the aged 50–70 year for screening mammography every three years (NHSBSP Publication No 60, 2005).

Other risk factors comprise family history, breast density and personal history. In relation to family history nearly 15% of the females with breast cancer have a family history of breast

cancer (Hackney, 2015). Breast density is a further risk factor and females that have a higher density of breast tissue have a higher incidence rate of breast cancer (Shetty, 2015a). In relation to personal history, females who have previous incidence of breast cancer are more liable to develop breast cancer by about three to five times than other females (Hackney, 2015). Additional risk factors are related to lifestyle, and they include diet, physical activity, drinking alcohol and smoking. Hormonal therapy can also cause an increase in breast cancer cases (Kopans, 2007; ACS, 2015; Hackney, 2015).

Socio-economic circumstances are also important in incidence rate with recent studies indicating that approximately 53% of breast cancer cases occur in developed nations (Hackney, 2015). There are significant differences between regions: it is at least 2-3 times less common in East Asian countries than in Western Europe and America, where the latter illustrate lesser proportions than African countries (United Nations Scientific Committee on the Effects of Atomic Radiation (UNSCEAR, 2008). Between 2002 and 2003, breast cancer studies demonstrated a significant decline of about (7%) in the United States. This decline might have come according to a decrease of using menopausal hormone therapy (ACS, 2011b). In the UK, however, obesity, hormone therapy, use of hormones as a contraceptive, and the lower proportion of pregnancies have contributed to a growing occurrence of breast cancer between 1975 and 2003 (Health Protection Agency, 2011). In 2012, a study demonstrated that the proportion of breast cancer incidences have altered to be 39%, 28%, and 15% in Asia, Europe, and the United State respectively (ACS, 2015). Breast cancer death rates have gradually reduced in developed nations. For example, in England, it decreased by 37% between 1971 and 2011 (Office for National Statistics [ONS], 2012). Likewise, a 5.2% per year decline is noticeable in North America between 1990 and 2011 (ACS, 2011b). This decline in death rate is related to earlier diagnosis of breast cancer via breast cancer screening programmes, primary prevention of breast cancer incidence reduction, and the development of better cancer treatment procedures (ACS, 2011b; Säbel & Aichinger, 1996).

2.4 Mammography

Mammography is a well-established imaging procedure which is utilised as both a screening and diagnostic mammography tool. In the United Kingdom (UK), females between 50 and 70 years of life are offered mammographic screening examinations through a screening programme to identify those with breast carcinoma, so as to offer them treatment at the earliest

possible stage. At present in the UK a randomised controlled trial is ongoing to screen women 50 years or older once every 3 years (Dewar, 2015).

Digital mammography is considered one of the greatest new technologies in screening mammography due to its superior contrast performance (Muller, 1999; Rafferty, 2007). Digital mammography has many advantages which enhance and improve sensitivity and specificity and can enhance lesion detection performance; it has also been seen to decrease diagnosis errors (Pisano and Yaffe, 2005). An observer's ability to detect cancer in its early stages is dependent on high-quality mammographic images being obtained (Kulama, 2009). Although there are several imaging modalities used for breast cancer detection, mammography is the most common, most cost effective and best screening tool for the diagnosis of breast abnormalities (Muller, 1999; Cole et al., 2003; Rafferty, 2007). There are different projections that can be taken, the most common being mediolateral oblique (MLO), and craniocaudal (CC) (Hogg et al., 2015). In screening mammography, these two projections of the breast are acquired. In situations wherein the breast lesions are not well visualised by the CC and MLO, additional mammographic projections involving the Medio-lateral (ML) and Latero-medial (LM) can be used (Lewin, D'Orsi and Hendrick, 2004; Whitman and Haygood, 2012). By utilising the different mammographic projections, the person reading / interpreting the image can study the breast anatomy and potential lesions from different perspectives in order to enhance lesion detection performance (Ortiz-Perez and Watson, 2015). **Figure 2.3** demonstrates the four mammographic projections.

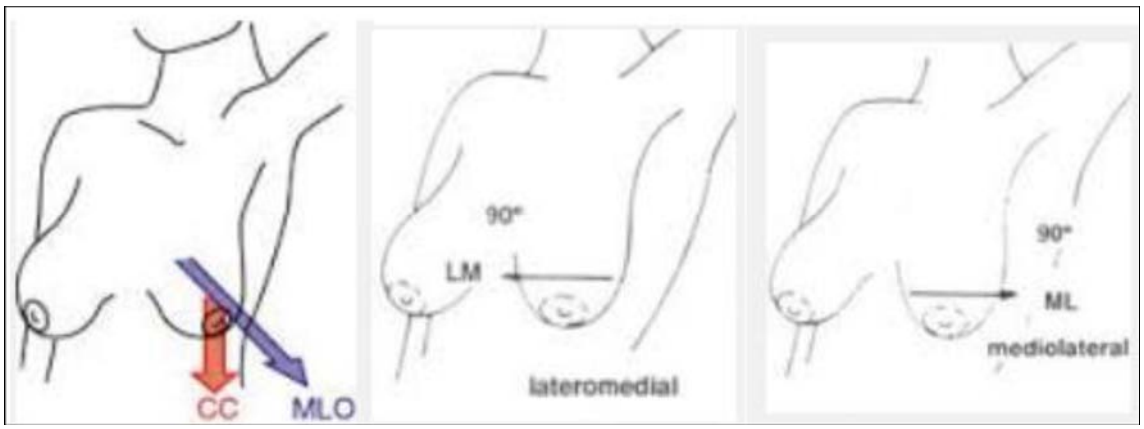

Figure 2.3 Mammographic Projections (Imaginis Corporation, 2014).

Figure 2.4 represents typical mammographic images; Cranio-Caudal Projection (A&B) and Medio-Lateral Oblique Projection (C&D) for left and right sides. The fact that there is little difference in contrast between normal breast tissue and lesions can create difficulties in lesion perception detail such as; boundaries, edges and shapes (Tabar et al., 2005; Kopans, 2006). However, other factors such individual differences in the relative proportions of high-low breast densities are found to affect accuracy in interpretation (Masotti, 2005; Al-osta, 2010). Furthermore, sub-optimal positioning is a major contributor to accurate visualisation of abnormalities on FFDM images (Debono, 2012).

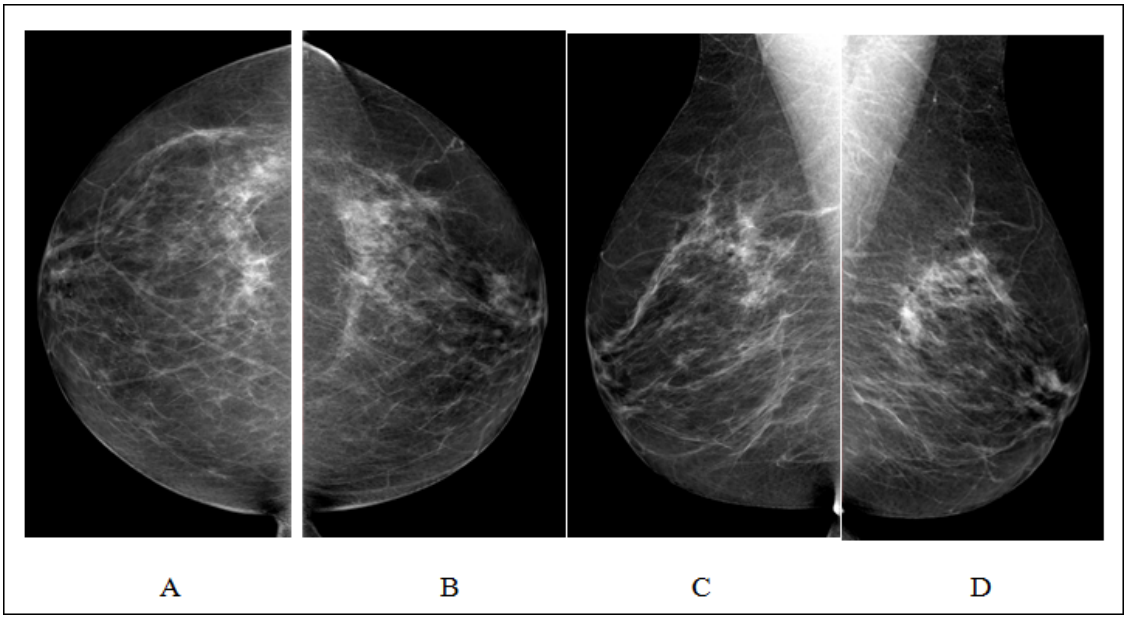

Figure 2.4 Normal mammography- Cranio-Caudal Projection (A&B) and Medio-Lateral Oblique Projection (C&D).

It is recognised that the composition of the breast varies among women and depends on the proportion of fibrous, glandular and adipose tissue. Breast composition changes with the age of women such that the quantity of adipose tissue will increase with age. The variations of breast tissue can be observed by mammography due to the attenuation of the x-ray beam that passes through different levels of tissue density. The adipose tissue is visualised as dark areas (radiolucent) in mammography while fibrous and glandular tissue appear less dark (radiopaque). Therefore, these variations of tissues are apparent in the image due to the absorption of x-ray by different densities and thicknesses of glandular and adipose tissues (Uchiyama, Nachiko & Zanchetta, 2012).

Breast tissues are highly sensitive to (x-ray) radiation and, as such, special characteristics of x-ray tube are utilised in mammography. Mammography tube characteristics are designed to achieve high image quality with low radiation dose (Uchiyama et al., 2012). Low-energy radiation is accomplished through the combination of filters and different x-ray tube targets. Mammographic x-ray tubes should have a small focal spot to achieve high resolution and sharpness (Wilson et al., 2011). The increase of x-ray energy can lead to a decrease in the contrast between different breast tissues. Therefore, low-energy radiation is used in mammography because this differentiates breast densities in order to achieve high contrast (Whitman & Haygood, 2009). It is obvious that a weakness of mammography systems is ionising radiation. However, the radiation risk regarding using x-ray within mammography is far below the risk of breast cancer (Yaffe and Mainprize, 2011). Consequently, women should continue for the procedure of screening mammography (Ali et al., 2015). Research illustrates that screening mammography reduced the mortality rate from breast cancer by approximately 1,300 per year in the UK due to the early detection of cancer (Cancer Research UK, 2014).

2.4.1 Characteristics of Malignant Microcalcifications within Mammography Images

Malignant microcalcifications have different distribution patterns; they can be clustered, diffused or punctate. Clustered microcalcifications present with a wide range of sizes compared to benign whereas malignant microcalcifications display homogeneous appearances and irregular shapes with a low-density (Kaiser, 2009; Bick, 2010) . In addition, individual malignant microcalcifications are reportedly varied in terms of their size and shape; some are linear and branching, others microscopic and fine or stellate-shaped (Schueller et al., 2008). **Figure 2.5** illustrates examples of malignant microcalcifications of several shapes, sizes and distributions patterns. Malignant microcalcifications vary in number, density, size and shape. They are often clustered within one lobe at the breast. Malignant microcalcifications are divided into two types- granular and casting, due to their physical characteristics. The granular type are very small, often ‘uncountable’, with an extended shape. The casting type contains a large number of small calcifications with different lengths and irregular contours (Shetty, 2015b). Many studies (Gathani et al., 2005; Hizukuri et al., 2013) have classified clustered microcalcifications into five different types due to histological origins: non-invasive carcinomas of the comedo type, non-invasive carcinomas of the non-comedo type, invasive carcinomas, fibroadenomas, and mastopathy. Benign microcalcifications however, are characterised by a sharp outline, a homogeneous shape and a radiolucent density (Shetty,

2015a). **Table 2.1** demonstrates the main types of benign and malignant breast microcalcifications.

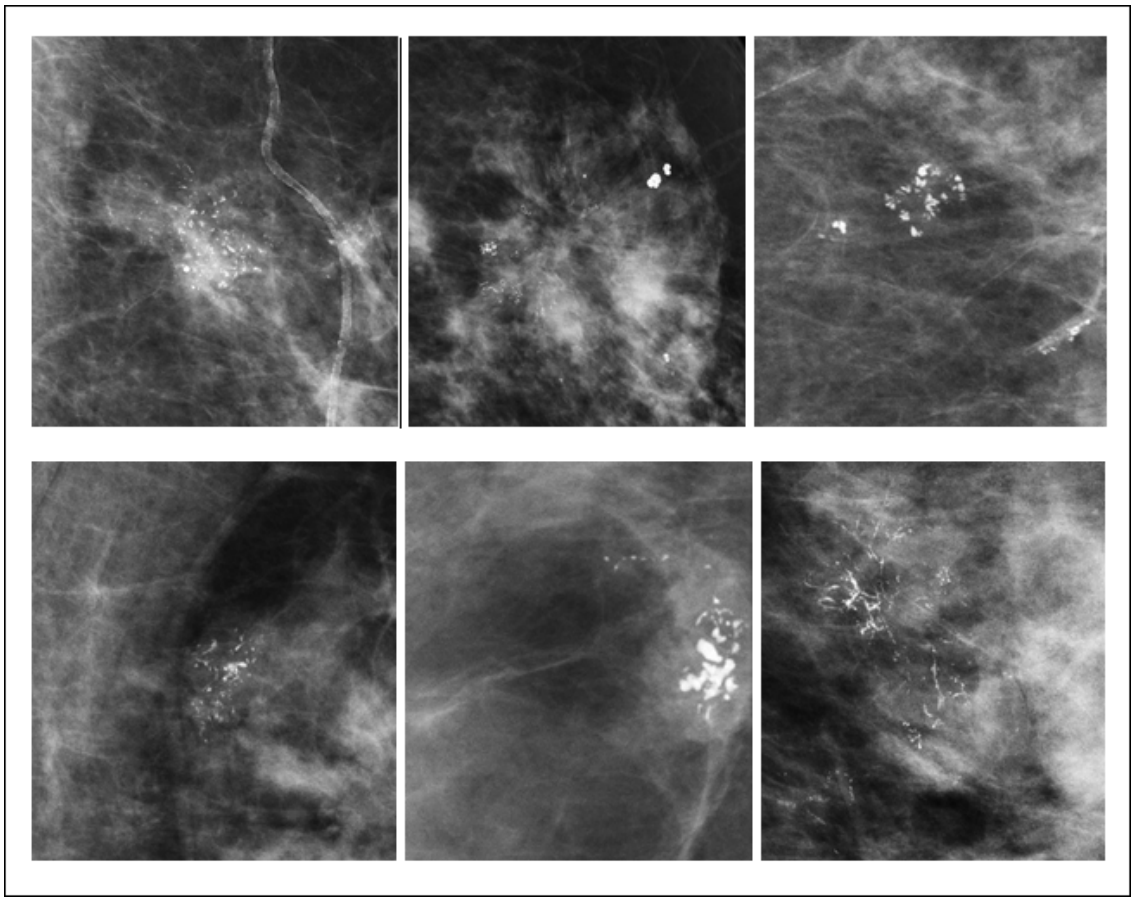

Figure 2.5 Malignant microcalcifications in different shapes, sizes and distributions pattern.

These characteristics can be difficult to interpret due to their small size and relatively little difference in contrast and this can have an impact on visual performance. The image contrast can be affected by lesion characteristics and background, according to the density of the breast. The amorphous microcalcifications presentation (**Figure 2.5**, bottom left) is considered the most difficult lesion to identify due to its poor contrast and small size.

Lesion type	Size	Shape	Density	Appearance	Distribution Pattern
Malignant microcalcification	Variation of sizes	Irregular	Low density	Inhomogeneous	Clustered innumerable
Benign microcalcification	Uniform in size	Rounder shape, coarse oval	High density	Homogeneous	Scattered or diffuse
Malignant masses	3 sizes: Large, medium, small	Circumscribed or spiculate	High density	Stellate spiculated with poorly define margins	
Benign masses		Rounded	Low density	Sharpe define margins	

Table 2.1 Main types of benign and malignant breast lesions

Contrast within FFDM images refers to the difference in luminance between a breast lesion and its background (Apelt et al., 2009). A consequence of low contrast can be that malignant microcalcifications located within a dense breast are likely to be difficult to visualise as this represents a high-density lesion within a high-density background (Sabih et al., 2011). This is also true for malignant masses with poorly defined margins. However, many benign microcalcifications are often easy to recognise by the human eye due to their high-density and homogenous appearance, which are often characterised by good contrast with its surroundings.

2.4.2 Breast Masses

The shape and margin of breast masses or lesions can indicate if the lesion is benign or malignant. The margin can be micro-lobulated, obscured, indistinct, circumscribed, or spiculated (Shetty, 2015a). The shape can be either lobulated, round, irregular, or oval. Lesions which have a round or an oval shape and involve a circumscribed margin are commonly benign while lesions with an irregular shape or lobulated are most likely to be malignant (Shetty, 2015b). **Figure (2.6)** demonstrates a set of the most common shapes and margins of breast lesions.

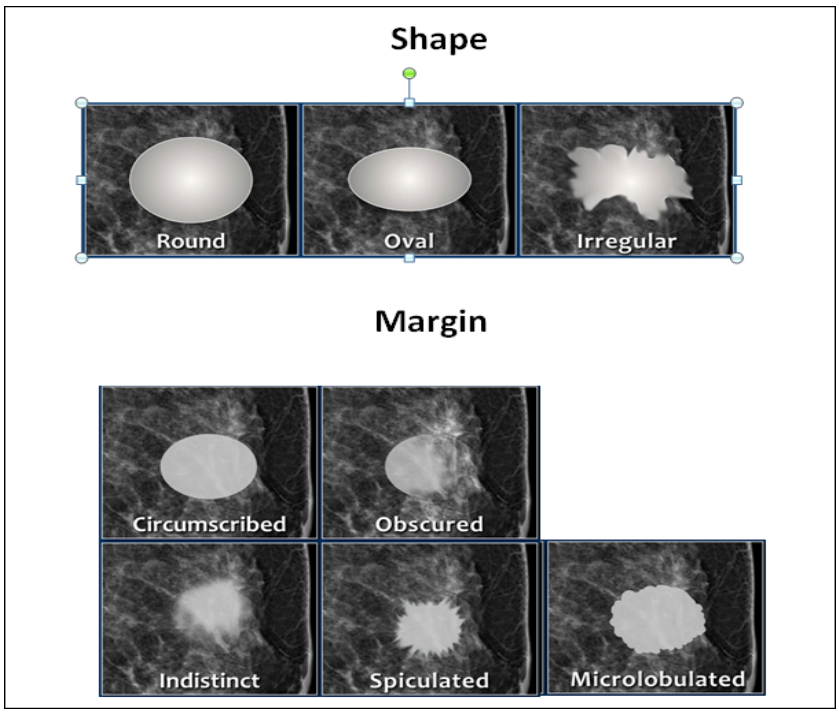

Figure 2.6 shapes and Margins of Breast Lesions (The radiology Assestant, 201

Some cases of benign circumscribed masses contain cysts and fibroadenomas. Invasive ductal carcinoma (IDC) is an example of a cancer with spiculated margins and irregular shapes, although these can also have well-defined margins (Ossati, 2015). **Figure 2.7** illustrates some malignant and benign breast masses.

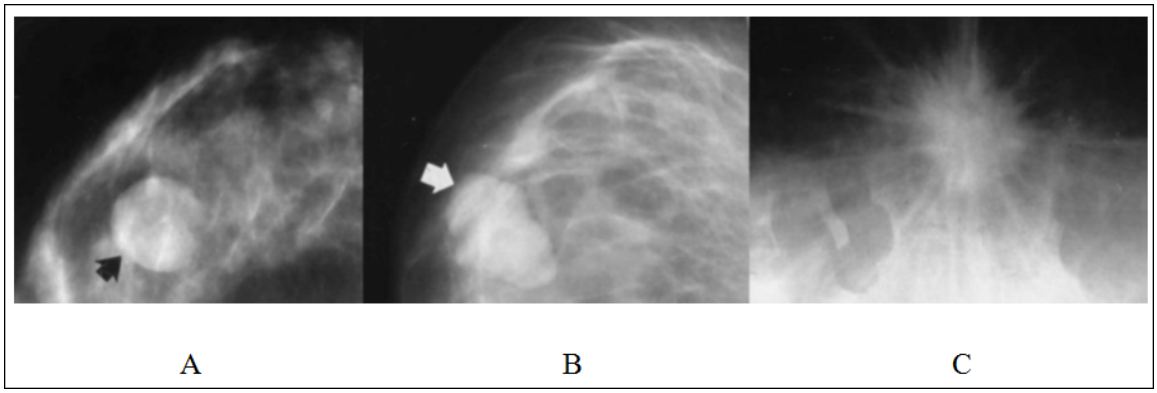

Figure 2.7 Mammographic images demonstrating benign and malignant masses
A: Cyst-round circumscribed, B: Fibroadenoma-lobular, low density and circumscribed, and, C: spiculated margins and irregular shape represents an Invasive ductal carcinoma (IDC) (Ossati, 2015). Specific lesion characteristics in mammographic images have different degrees

of detection difficulty. Some types of breast masses may be difficult to detect as the surrounding breast tissue obscures the spicules that radiate outwards (Lehman et al., 1999). In comparison, malignant microcalcifications, which are associated with a high false negative fraction (FNF), may be misdiagnosed because of the difficulty in identifying the nature of lesions of suspicious area of the image (Al Mousa et al., 2014). Architectural distortion has a subtle appearance and may appear similar to normal overlapping breast tissue; this can also result in missed lesions and lead to false negative presentation (Zwiggelaar, Schumm and Taylor, 1997).

2.5 Factors Affecting Diagnostic Efficiency

Breast cancer detection, in the early stages, can lead to the creation of more effective treatments and can result in a decrease in mortality rates. It is therefore a universal health priority when developing strategies to control breast cancer. Screening mammography represents the most efficient technique for the early detection of breast cancer; however, the sensitivity of mammography is in the 68–92% range (Beam et al., 2013). The high occurrence of breast cancer, aside from the rate of misdiagnosis, highlights the need for a better understanding of why some breast lesions go undetected.

Many studies suggest that detection performance is related to the observer in terms of experience, cognitive skills and visual performance (Nodine & Kundel 1987; Chester 1992; Reed, 2005; Manning et al., 2006; Burgess 2011; Sabih et al., 2011; Lança et al., 2015). Other studies suggest that lesion characteristics can contribute to challenges in image reading accuracy. These characteristics include the type, size, contrast, distribution and location of the lesion within the breast (**Figure 2.8**). Small lesions with indefinite borders can lead to perception difficulties (Van Overveld, 1995; Tabar et al., 2005; Kopans, 2006). In the same context, other studies suggest that factors related to the characteristics of a mammographic image (image quality, artefacts, spatial resolution, sharpness and contrast resolution) can have an influence on detection performance.

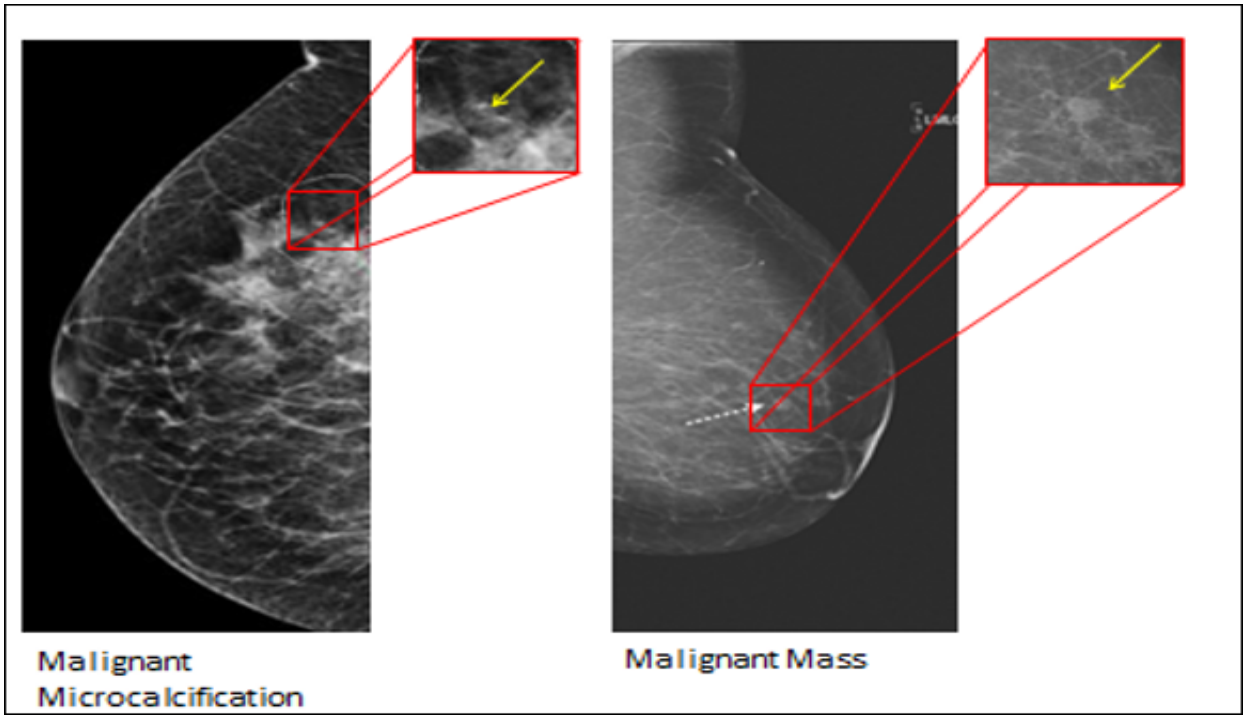

Figure 2.8 Malignant microcalcification and mass with different lesion characteristics.

Perception errors can be considered the main cause of missed cancers in mammography (Rawashdeh et al., 2014). Misdiagnosed cancers in mammography are commonly located in the retro-glandular regions (Berlin, 2001a). Whereas, Huynh et al., (1998) highlighted that the misdiagnosis of cancers were more significant within lower density breasts; they were almost visible on only one of two projections and were smaller in size. Huynh and colleagues (1998) also found that masses, rather than calcifications, are more commonly undetected (Huynh, Jarolimek and Daye, 1998). This is a concern since a large number of lesions are present as palpable, non-calcified tumours (Yankaskas et al., 2001). However, within these studies it is noted that limited data exists on the effect of other image and lesion appearances, such as texture and shape.

When interpreting a mammography image, the image can be divided into several quadrants by the image reader; this approach is known as the regions of interest (ROI) paradigm. The selections of ROIs are based on clinical considerations and the quadrants should be equal for all images. For instance, the mammographic image could be divided into four quadrants (external upper quadrant, internal upper, external lower and internal lower quadrant). The task of the observer is to rate each region for the presence of a breast lesion in that ROI (Al-osta,

2010). The rating of quadrants per image produces numeric data. It is supposed that the truth of each ROI is known, whether the lesion exists or absent in ROI and it cannot lesions that overlap ROIs.

2.5.1 Mammographic Breast Density (MBD) Assessment

There are many methods for measuring breast density. Some are quantitative whilst others are qualitative (Yaffe, 2008). Qualitative methods involve an observer scoring images using scales; examples of visual grading scales include Breast Imaging Reporting and Data System. (BI-RADS), Tabar, visual estimation and Wolfe's (Wolfe, 1976). According to Gram et al., (1997), Tabar has categorised breast density into five types:

I: A predominance of fibrous tissue with balanced proportion of all components of breast tissue (Cooper's ligaments and scalloped contours)
II: Fatty breast (predominance of fat tissue)
III: Mostly fat tissue with oval-shaped lucent areas
IV: Predominantly nodular and linear densities
V: Extremely dense (mostly fibrous tissue)

However, Wolfe's (Wolfe, 1976) grading classified breast density into four types:

(i) Fatty breasts (fibro-glandular tissues >25 % and almost all of the tissue appears to be fat
(ii) Fibro-glandular breasts (Proportion of fibro-glandular tissue 26–50 % of the breast
(iii) Heterogeneously dense breast (heterogeneously compose 51–75 % of tissues)
(iv) Extremely dense (fibrous connective tissue composes more than 75 %)

Breast Imaging Reporting and Data System (BIRADS) (American College of Radiology 2013; Carl et al., 2013; Geller, et al., 2002) is a qualitative method to assess the density of breasts which is widely utilised in mammography. **Figure 2.9** shows BIRADS for four main density classifications: (A) fatty breast; (B) fibro-glandular tissue; (C) heterogeneous dense breast; and (D) for the extremely high-dense breast. The BIRADS system categorises breast density according to a percent of its compounds, as follows: BIRADS (A) (the breasts are almost entirely fatty), BIRADS (B) (there are scattered areas of fibro-glandular density), BIRADS (C) (the breasts are heterogeneously dense, which may obscure small masses), and BIRADS (D) (the breasts are extremely dense, which lowers the sensitivity of mammography). In spite of

the BIRADS method being commonly used worldwide for reporting mammographic breast densities, the features of the mammographic image are identified subjectively (Taplin et al., 2002); this method can be susceptible to visual errors and can be influenced by the experience level of the observer.

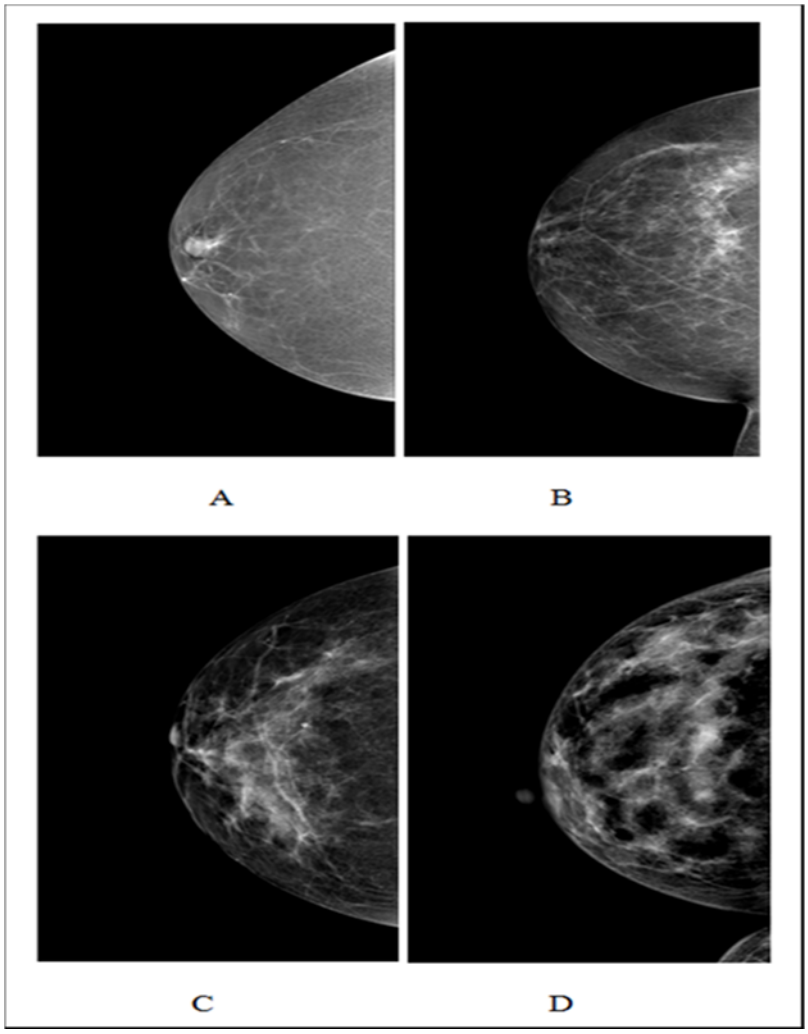

Figure 2.9 Variations in breast density according to BI-RADS classification system

2.5.2 Effect of Mammographic Breast Density on Lesion Detection Performance

A number of studies have demonstrated that the sensitivity of mammographic image-observers to detect breast cancer increases with decreasing breast density (Byng et al., 1994; Lehman et al., 1999; Kolb et al., 2002; Kriege et al., 2006; Lip et al., 2010; Chiu et al., 2010; Cook et al., 2010; Al-Mousa et al., 2014). Other studies demonstrated that lesion density contributes to challenges in screen reading accuracy (American College of Radiology, 2013; The Radiology

Assistant, 2013). It can be reasoned that small differences in contrast between lesion density and density of breast tissue (density of normal and abnormal tissue) could create difficulties in perception of important lesion details, such as margins or borders. Therefore, it is proposed that there is an inverse relationship between breast density and lesion detection performance; an increase in breast density leads to a reduction in detection performance and vice versa.

Many researchers have studied the combined influence of breast density and age on the sensitivity of mammography and have generally demonstrated lower performance in high-density mammographic images compared with the low-density breast images in both old and young age groups. For instance, Rosenberg et al., (1998) demonstrated that the sensitivity in females aged >50 was 8% higher in fatty breasts than in dense breasts and that for females aged <50 with fatty breasts, sensitivity was 19% higher than those with dense breasts. Kerlikowske et al., (1996) demonstrated that the sensitivity in females aged <50 years old was not significantly higher in low-density breast images (81.1%) compared with high density breast images (85.4%); nevertheless, the latter outcome may be accounted for by the small sample size. Just nine cases of breast cancer were included in the study. Kolb et al. (2002) demonstrated a correlation with a decrease in sensitivity of mammography and age for females with high mammographic breast density images. They concluded that sensitivity was 50% in females aged <50 years, compared to the 70.2% in females aged >50 years ($p<0.035$). Nevertheless, such age-dependency does not exist for low-dense mammographic images (Wivell et al., 2003). Chiu et al., (2010) demonstrated that less-dense breasts had a higher sensitivity than high-dense breasts (82% versus 62.8%) and this higher sensitivity was significant, regardless of age. In females within the age group >50 years, they found that sensitivity in higher-dense breasts was 55.3% and increased to 76.8% in lower-dense breasts. In the same context, a similar increment in females aged >50 years was found, with a sensitivity of 77.7% in females with dense breasts, which increased to 88.7% in females with fatty breasts (Chiu et al., 2010).

Specificity is another indicator that is utilised to determine detection performance in mammography. Studies, such as Lehman et al., 1999 and Carney et al., 2003 suggest that specificity is reduced within dense breast tissue, with magnitudes shifting from 89.6-89.9% in females with higher density to 93.5-96.5% in females with almost low-density breasts and this was the same for both older and younger females (Lehman et al., 1999; Carney et al., 2003).

Lehman et al., (1999) also conclude that females with low-density breasts have a lower probability of resulting in false-positive (FP) mammography (10.4%) than females with fatty breast tissue (6.5%). Likewise, a study by (Kriege et al., 2006) shows that false-positive (FP) value decreases from 5.9 in high-dense to 8.3 in the low-dense breast. Cook et al., (2010) demonstrated that females with highly dense breasts were more likely to be recalled for further tests. This study also shows that the measurement of the relationship between an exposure, and a consequence known as the specificity odds ratio, decreased from 0.86 in an extremely dense breast to 1.85 in almost entirely fatty breast, however, there is no change in the positive predictive value (PPV) of breast density.

2.5.2.1 Mammographic Image Assessment

In the UK, a list of criteria to ensure the quality of an image has is recommended by the National Health Service Breast Screening Programme (NHSBSP). This should be utilised during the assessment of mediolateral oblique (MLO) images (NHSBSP Publication No 63, 2006).

- The image should cover the whole breast
- Breast Nipple should in profile
- Correct annotations
- Acceptable radiation dose
- Adequate compression force
- Absence of movement
- Absence of skin folds
- Artefacts free
- Symmetrical images L (left) MLO versus R (right) MLO

Likewise, the NHSBSP advise the following image quality criteria for craniocaudal (CC) images (NHSBSP Publication No 63, 2006):

- Medial border should be imaged
- Some axillary tail should be present
- Pectoral muscle shadow may be shown
- Nipple in profile
- Correct annotations
- Appropriate exposure

2.5.3 Effect of Image Quality on Lesion Detection Performance

The ability of image observers to identify small microcalcifications is dependent upon the production of high-quality images. Artefacts can reduce image quality in mammography and can obscure abnormal structures, causing interpretation errors. The identification of artefacts can improve interpretation and minimise the description of artefacts as breast disease

(Schueller et al., 2008). Image blurring, caused by unwanted motion, is a common reason for a repeat exposure to ionising radiation in mammography. The impact of image blurring is not currently fully understood within the literature. Artefacts in digital mammography can lead to a reduction in image quality and may obscure true lesions. In addition, they can create pseudo-lesions. As such, they represent a serious concern in quality assurance, as some image observers may be unfamiliar with all possible artefacts; the understanding and knowledge of the types of artefacts in FFDM and the causes of each type is extremely important for image observers and radiographers in order to minimise them in the diagnostic process. Overall, familiarity with the various artefacts encountered can enable the image reader to provide more accurate diagnoses (Choi et al., 2014).

Chaloeykitti et al., (2006) divided the types of artefacts associated with mammography images into three causes; patient-related artefacts, software-processing artefacts and hardware-related artefacts; whilst Ayyala et al., 2008 and Schueller et al., 2008 described them as technical-related artefacts and patient-related artefacts. Some of these artefacts are similar to the artefacts in screen-film mammography, however many are unique to digital mammography. The latter include artefacts due to digital detector deficiencies and software processing errors (Chaloeykitti et al., 2006). In addition, there are digital mammographic artefacts according to the detector type (direct or indirect). Therefore, an observer is required to be able to differentiate artefacts from pathology in order to improve interpretation and prevent the identification of artefacts as breast disease (Chaloeykitti et al., 2006).

The spatial resolution of FFDM equipment means its ability to identify two neighbouring structures, or an edge (sharpness), as separate entities. Geometric blurring can cause losses of spatial resolution. Focal spot size of the x-ray tube, object image distance (OID) and subject image distance SID impact onto geometric unsharpness. Other factors might also cause loss of spatial resolution such as a detector element effective aperture and pitch, and relative motion of the X-ray source, and the breast or the image detector during image acquisition. The impacts of spatial resolution on clinical image quality can be observed when imaging fine pathological detail in the breast such as spiculations radiating from a microcalcifications or mass.

Geometric blur can by caused by the shape and design of a mammographic X-ray tube. The rotating type of the anode with slight anode angulation is used in FFDM equipment to minimise geometric blur by decreasing the size of the focal spot (Yaffe & Madiment, 2014). In a

mammographic X-ray tube, the typical size of the focal spot is 0.1 mm and 0.3 mm for small and large foci respectively. The small focus is often utilised for magnified views, while the large focus is used for conventional mammography. The geometric focal spot unsharpness can be increased due to small focal-object distance is utilised in magnification mammography. To eliminate geometric blur, the smallest focal spot is employed. However, utilisation of a small focal spot can increase the thermal load of the X-ray tube which is accounted for by utilising of the longer time of exposure. This can increase the probability of patient movement blur.

Despite the fact that image processing introduces many advantages to image quality, the user should also be aware of the potentially harmful consequences of utilising certain image processing techniques with FFDM. For instance, using some software for processing raw images or altering the display of the images can improve the sharpness of mass lesion margins; however it can make indistinct masses appear more circumscribed (Medicine, 2005; Kanal et al., 2013). Likewise, histogram-based intensity windowing can enhance the conspicuity of edges but at the cost of losing detail outside of the denser parts of the image. **Figure 2.10** demonstrates an example of using different image processing algorithms to process raw data of same breast image. The spatial resolution of image (a) is less than in image (b) for the same mammographic image.

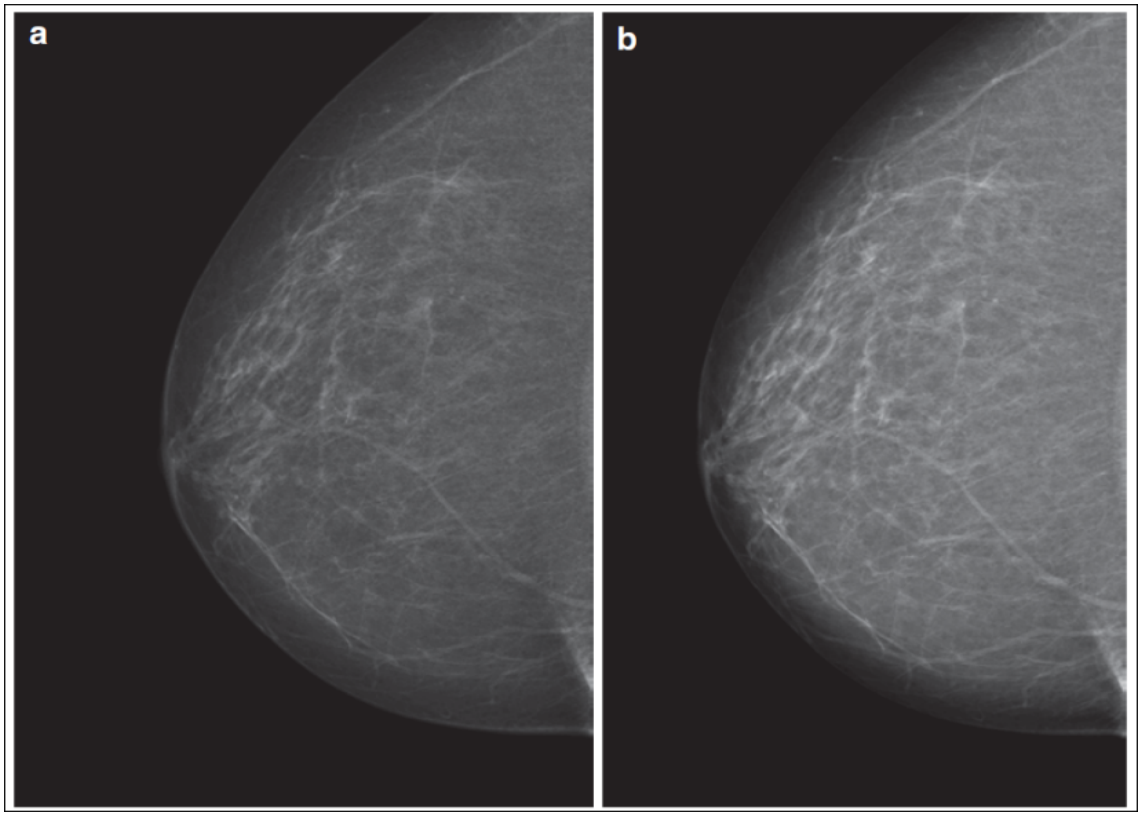

Figure 2.10 Demonstrate same breast image with different spatial and contrast resolution.
(a) Raw FFDM image reprocessed utilising image processing algorithm
(b) Raw image as in 3.10(a) but reprocessed utilising different algorithm (Zanca et al. 2009).

Contrast resolution of the image (mammographic image contrast) refers to the amount of the signal difference between the object within the region of interest and its surrounding background in the displayed image. It is affected by subject contrast and display image contrast (Woudenberg, Thijssen and Young, 2001; The American College of Radiology, 2014). Obtaining high mammographic contrast is of particular importance as it enables us to identify small differences in soft-tissue densities in normal and abnormal structures of the breast, the concurrent requirement to detect and characterise the structural characteristics of margins of masses (which is governed more by contrast resolution) and very small microcalcifications (which is governed more by spatial resolution). However, high-contrast images display two intensity levels; high and low. Therefore, the ability to identify the difference between the levels of intensity is necessary because it provides the observer with sufficient information regarding the region of interest within the mammographic images (The American College of Radiology, 2014).

According to Wilson et al., (2011) there are many specific requirements which should be taken into account to obtain acceptable mammographic image quality: fibrotic strands and small microcalcifications should be imaged sharply, with a low level of noise and high contrast resolution. Although high contrast can be achieved, the mammography image should ensure the sufficient assessment of regions with large density variations. These can be the tissue overlying the pectoralis muscle, areas of dense fibrocystic tissue in large breasts or, in small breasts, fatty areas that might be found behind the nipple or close to the skin.

Since some types of breast cancer can have a similar density to glandular breast tissue, high image contrast is necessary to distinguish normal areas from suspicious lesion appearance. There are many factors can influence the contrast between lesions and surrounding areas. These involve exposure factor optimisation, utilisation of adequate compression force and accurate breast positioning. Therefore, appropriate techniques are required to ensure sufficient lesion visibility.

2.5.4 Mammography Image Interpretation

Many studies examined the performance accuracy of radiographers to detect breast cancer and evidence has been provided which demonstrates that suitably trained and experienced radiographers have the equivalent accuracy to radiologists (Mucci et al., 1997; Debono, 2012a). Other studies have provided evidence of the capability of radiographers to participate in enhancements of the accuracy of the screening programmes. Most importantly are those that combine radiographer and radiologist in image reading to increase breast cancer detection efficiency (Wivell et al., 2003; Duijm et al., 2009; Miglioretti et al., 2011; Haneuse et al., 2012). In the UK, radiographers have been trained to be able to read and interpret the mammographic image with high accuracy. Consequently, radiographers have been employed within NHSBSP to read mammograms in the same way as radiologists (Debono, 2012; NHSSCP, 2011). Many studies have investigated the performance of radiologists and radiographers in the detection of the breast cancer. Some studies found radiographers have abilities to detect malignant breast masses in mammography (Duijm et al., 2007; Duijm et al., 2008; Duijm et al., 2009). Wivell et al., (2003) have found that radiographers are capable of detecting microcalcifications.

2.6 Full-field Digital Mammography

The U.S. Food and Drug Administration (FDA) was the first to approve FFDM systems for clinical utilisation in 2000 (Hendrick, et al., 2010). In 2006, digital radiography systems were gradually introduced in Canada. Since then, these systems have been utilised extensively in many countries (Brooks & Morley, 2013).

The principle of full field digital mammography equipment is similar to conventional film-screen mammography; however, digital detectors have replaced the film-screen system (Heddson et al., 2007; Data et al., 2009; Hambly et al., 2009; Schulz-Wendtland et al., 2009; Diekmann et al., 2011; Souza et al., 2013; Knox et al., 2015). Digital detectors were initially utilised for general radiography and after that were extended into mammography. There are many potential advantages of digital compared with film-screen mammography. These include: lower radiation dose, improved contrast resolution and the provision of a wider dynamic range (Souza et al., 2013). An easier archiving process, soft copy reviewing and patient data sharing are additional advantages of digital mammography (Taplin et al., 2002; Samei, 2003). Digital mammography machines can provide two field sizes (24×30 cm and 18×24cm) or a single field size (18×24cm) depending on the manufacturer. Magnification techniques include the electronic magnification of the image and a physical magnification platform on the FFDM machine (Whitman & Haygood, 2012).

Digital radiography (DR) systems differ due to the type of detector technology and are subdivided into indirect and direct digital radiography (Uchiyama et al., 2012). The direct digital system uses amorphous selenium photo-detectors. The detector in this type of system has a high intrinsic resolution, high X-ray absorption efficiency and low noise levels. The indirect digital system utilises Caesium iodide doped with thallium (CsI:Tl) to absorb the X-rays. These systems produce light scintillation which is detected by an array of photodiodes (Pisano & Yaffe, 2005). The early digital mammography (DR) devices used indirect conversion detectors. These detectors utilised charge couple devices (CCD) for image capturing (Aslund, 2007). The CCD technique utilises phosphor, installed with millions of optic fibres on coupling plates. The main purpose of the optic fibers is to transfer light from the phosphor to CCD. In the latter, the light is converted into an electronic signal, this is then digitised (Muller, 1999; Rafferty, 2007). The early CCD was possible for small field sizes (5cm×5cm). These detectors coincided with slit collimated X-ray beams to scan the breast in a

perpendicular direction to a patient's body producing a 22x30 cm image. Due to slit collimation of the X-ray beam, the scatter radiation is minimised, eliminating the need for a grid (Pisano and Yaffe, 2005).

Computed radiography (CR) is also known as cassette-based technology. The principle of CR devices depends on photostimulable luminescence. These devices involve photostimulable phosphor known as storage phosphor screen (SPS) which absorbs the X-ray photons, before a laser scanning mechanism is used to extract this data. Subsequently, the SPS is scanned with a red laser light in a separate device, the reader, to convert the latent image to a blue light signal, proportional to the amount of incident X-ray on the SPS. After that, a photomultiplier in the reader changes the light signal to an electronic signal which is then digitised (Rafferty, 2007). To ensure that the SPS is free from any residual charge, it is then scanned with a high-intensity white light. The main drawback of this sort of digital detector is the lack of spatial resolution due to light scattering by the detector. It is worth noting, however, that thicker phosphor layer detectors are more sensitive to radiation however greater light scattering is produced (Pisano and Yaffe, 2005; Aslund, 2007).

2.6.1 Components of FFDM Systems

The FFDM system consists of many parts; each part with a specific function in the image production process. These include a collimator, anode / focal spot, field of view, automatic exposure control (AEC), grid, compression device, collimator, and compression paddles. Technical review grade computer monitors are also components of such systems. X-ray tubes, AEC and breast compression functions are utilised to produce optimised mammographic images. The x-ray tube is an example of an electronic device known as a diode, consisting of two electrodes the negative part is known as a cathode and the positive part is known as an anode (Aslund, 2007). In most FFDM systems, the cathode consists of two tungsten-thorium filaments, one for the large focal spot and a second one for the small focal spot (Muller, 1999). The electrons that comprise the tube current within the x-ray (milliampere mA) are emitted thermionically. The current of the x-ray tube is often reduced at high or low kilovolts peak (kVp) (Pisano and Yaffe, 2005). **Figure (2.11)** demonstrates the main components of a Full-felid digital mammography unit.

Figure 2.11 Full- field digital mammography equipment (Ossati 2015; Hologic Inc., 2014).

Breast compression is a significant factor in mammographic practice to ensure optimal diagnostic performance and can be described as the compression of the breast describes that between the compression paddle and the support table. Compression of the breast is applied to increase image quality by reducing the amount of scattered radiation, while also reducing the mean glandular radiation dose. In addition, it spreads apart overlapping tissues, and in this way can allow for a reduction of false negative and false positive findings (Kallenberg & Karssemeijer, 2012). Decreased breast thickness can also result in several benefits, such as shorter exposure time. Compression also aids in immobilisation of the breast, which can reduce movement unsharpness (blur).

High image quality is required and is essential for the early detection of breast cancer. However, certain image quality measures are subjective. Image quality can be assessed in terms of exposure, positioning, the sufficiency of compression force utilisation, noise, sharpness and contrast (Kallenberg and Karssemeijer, 2012; Murphy et al., 2014). Sharpness is linked with several factors, including an absence of client/equipment motion, positioning and the sufficiency of compression force and application exposure. Appropriate exposure is essential to achieve adequate image contrast, also to produce an appropriately noise-limited image (Haimo Liu, 2012).

2.6.2 Automatic Exposure Control (AEC)

Automatic exposure control (AEC) as a key component in mammography has a vital function in FFDM. It offers appropriate optimal image exposure despite variances in the skill level of the radiographers, breast density and breast size (Bick & Diekmann, 2010). It is used to determine the intensity of the X-ray does not increase up to the limit of the digitizer or detector (Yaffe, 2010). Though the importance of AEC is essential to determine the exposure level to the breast and detector, the main function of AEC is to achieve appropriate exposure rather than identifying the brightness or contrast of the image and to help perform the signal to noise ratio (SNR) (Yaffe, 2010).

2.6.3 Paddles

The paddle is a plastic 'plate' in a mammography system that is used for compressing and fixing the breast during image acquisition. The compression process is performed between the support table and the compression paddle. The shape and size are different according to the purpose of mammography test. Choosing the suitable size of the paddle has an impact on image quality. Using a large paddle for small breast may prevent access to the breast. Likewise, the using a small paddle on a large breast might lead to inadequate compression and can cause inadequate compression of some border areas (Defreitas, Pellegrino, Farbizio, Janer, & Hitzke, 2008). Several sorts of paddles can be utilised for diagnostic and screening purposes depending mammography procedure. In spot compression, the concentration of compression is on a specific region of the breast; consequently, a small paddle is utilised to acquire the mammographic image. Spot compression can also be utilised to detect microcalcifications (Canadian Cancer Society, 2014). Biopsy, magnification and male breast paddles are additional forms of paddles used for different mammographic purposes (AR Custom Medical Products, 2007). Usually, in breast screening mammography two sizes of the paddle (24x30 cm and 18x24 cm) are used. These parallel and flat paddles equivalent the detector size. Flat rigid paddles can be replaced by flexible paddles during the obtaining mammograms. The tilting mechanism of these spring-loaded paddles gives more uniform compression from the chest wall to the nipple (Bushberg, Seibert, Leidholdt, & Boone, 2012). Although manufacturers of mammographic systems have recommendations for using the

flexible paddles to minimize discomfort and the pain for females, there is no robust study regarding the correlation between the pain experience and these two kinds of paddles. However, the rigid paddle has been recommended for use in CC and MLO Projections because it promotes better contrast (Broeders et al., 2015). Ma et al., (2016) suggested one solution to reduce the probability of motion blur is to utilise the fixed paddle with caution, as their results demonstrate that there is a significant difference in motion for flexible and fixed paddles. Ma et al., (2014) demonstrated that flexible paddles have approximately less motion in the compressed state than fixed paddles. Therefore, the radiographer should take extra caution with fixed paddles when positioning clients.

2.7 Motion Blur in Mammography Images

Motion blur occurs due to the motion of the patient or imaging system, distorting the image in one or more directions (Cao, Zhao and Ni, 2010). In mammography, motion blur results when the breast structures or the paddle are relaxing and are moved during time; this motion can produce blur or motion unsharpness (Massanes and Brankov, 2011; Choi et al., 2014). The movement of patient or body organs, such as respiratory system and chest wall, is also a source of motion blur in FFDM images. It appears as un-sharpness in the detail of mammographic images, especially with low contrast edges of breast tissues. However, this type of artefact can be reduced by minimising exposure time to reduce the movement of the patient during image acquisition (Lu et al., 2005).

Image blurring in FFDM images has the potential to obscure breast lesions and lesions which have low contrast to background ratios; as a result, clinically significant abnormalities could go undetected which may impact negatively on diagnosis. The source of motion in FFDM can be related to the patient or equipment (Chaloeykitti, Muttarak and Ng, 2006). The movement of the patient is one of the problems during the exposure time (Allec et al., 2012). It can be acknowledged that FFDM images are more vulnerable to image blurring with the increase in image resolution. Image blurring was no doubt apparent within conventional film mammography yet probably more difficult to detect due to variation in image resolution (Allec et al., 2012; Choi et al., 2014; Geiser et al., 2011).

Although there are anecdotes within the UK National Health Breast Screening Programme (NHSBSP) in the UK about image blurring and the requirement to repeat the images because of blurring, this technical problem continues to be under-reported and there is a scarcity of literature about it. According to the NHSBSP, (2005) the repeat and technical recall images for screening have a duty to be under 3% with a target of 2% within the (Public Health England and NHS Screening Programme, (2017). Some studies (Berry-Smith & Lonsdale, 2000; Wilson et al., 2011; Bisset, 2014; Rourke et al., 2016) have calculated the repeat and technical recall with direct reference to image blurring. A study by Rourke et al., (2016) found, within one screening service, that 86% of females were recalled due to image blurring, forming approximately one third (29%) of the 3% maximum admissible rate for repeated images (Rourke et al., 2016). Another study by Seddon et al., (2000) found that more than 90% of their total technical recalls were due to image blurring. Other studies have shown that image blurring is one of the highest reasons behind repeat mammographic images (Kelly at al., 2012; Ma et al., 2014). However, more research studies are required to determine the causes and effects of this blurring phenomenon in FFDM. The need to repeat mammography images due to blurring has a direct effect on the female in question; this includes an increase in radiation dose, if a repeated image is required, coupled with an increase in patient anxiety. Repeated images will also increase the work load on the mammographic units, which requires effort and is time consuming.

Ma et al., (2016a) proposed that some of the blurred images can be only detected if they are displayed on 5MP monitors during reporting of mammograms. In many cases, motion blur goes undetected during the assessment of images for technical accuracy in mammography imaging rooms as these use lower grade monitors (less than 5MP). Ma et al., (2017) suggested that this lack of detection of blurring could be related to the low quality of the non-diagnostic monitors utilised in clinical rooms coupled with variable and generally brighter ambient lighting compared to reporting rooms. However, surprisingly, little research has been conducted into the technical review monitors specifically for the technical review purposes utilised within imaging rooms (Ma et al., 2017).

In breast cancer screening mammography, the first study by Kinnear and Mercer, (2016) aimed to compare different types of monitors used in breast screening. They reported the capability of observers to detect simulated image blur visually in FFDM images on 1MP and 5MP

monitors. They found that higher resolution monitors resulted in a higher visual detection rate for blurred images. Following this Ma et al., (2017) utilised a more robust method to compare different monitors in the detection of motion blur visually. Compared with Kinnear's work, Ma's was superior in quality, and they increased the number of observers allowing inter-observer variances to be considered (28 observers evaluated 120 images for motion blur). Second, simulated motion blur was utilised in Ma's study in which the magnitude of motion blur was known exactly, so this allowed for better control of the experimental conditions.

2.7.1 Causes and Effects of Image Blurring

There are several publications that have studied the causes and effects of blurring on image quality (Van Overveld 1995; Badano, 2003). However, there is no precise description about the magnitude of image blurring which can influence the appearance of anatomical structures within the image and how image blurring can affect the visualisation and sharpness of abnormalities within general radiographic images. To better understand image blurring, researchers have added simulated blurring to images using algorithms that apply a Gaussian mask. This was carried out to determine the effect of blurring on edges and to establish how the impact of image blurring could be minimised using de-blurring (Elder & Zucker, 1998; Yap et al., 2003; Wee et al., 2007; Wallis & Georgeson, 2009).

Consideration of image blurring has increased in recent times because FFDM images are more vulnerable to blur with the improvement of contrast resolution. Several studies have investigated methods to reduce the impact of image blurring with image processing software (Badano, 2003; Young et al., 2008; Cao et al., 2010). These studies are encouraging, however there is a noticeable absence of accurate identification of the amount of image blur which can cause obscured or unperceived breast lesions. Therefore, there is a requirement for an index to demonstrate how much image blurring can obscure the breast lesion within FFDM images. Also there is a paucity of information about repeated mammographic images relating to the amount of motion blur within FFDM images. Saunders et al., (2007) demonstrate that the existence of blurring and noise within the image can significantly decrease the accuracy of lesion detection. They examined the influences of various noise levels and resolution on task performance in digital mammography. The noise influences were most common for the detection of microcalcifications and the discrimination performance of breast mass. They reported that the changes of noise from full clinical dose to quarter clinical dose could lead to

a decrease in the detection performance of microcalcifications from 89% to 67%. Likewise, this change can lead to a reduction in the discrimination of breast mass from 93% to 79%, whereas malignant mass detection performance stayed comparatively constant with values of 88% and 84%, respectively.

2.7.2 Paddle Movement Effects

(Hauge et al., 2011) were the first researchers to report that compression paddles move slightly after compression force had ceased. Subsequently, research by Kelly et al., (2012) hypothesised that paddle motion may cause image blur. Ma et al., (2014) assessed 'Paddle Motion' and they utilised a breast phantom to assess six FFDM paddles to determine whether paddle movement occurred. The breast phantom was mounted in a semi-mobile fashion to a rigid backboard. Calibrated linear potentiometers were used to document paddle motion at 0.5-second intervals for 90 seconds. The paddle motion for all acquisition conditions was an average of 1.8 mm and a range of=0.44–7.46 mm. This research gave the first insight into paddle movement during exposure times in FFDM. However, the limitation of this study is that the breast phantom they used cannot completely represent the compression characteristics of the female breast. The silicone within breast phantom demonstrates a purely elastic compression characteristic, while the woman's breast demonstrates a visco-elastic compression characteristic (Geerligs, Peters, Ackermans & Oomens, 2010).

Another study by Ma et al., (2014a) introduced a new method to assess image blurring, by considering compression paddle motion in FFDM machines. Image blurring was determined by measuring the distortion of the ball-bearing diameter using a computer software. It showed that ball-bearing diameters were increased, indicating the impact of compression paddle motion on the images. The largest alteration in ball-bearing diameter affected the nipple area. They concluded that the increase in ball-bearing diameter means that image blurring caused by paddle movement could be utilised as an indicator of movement severity (Ma et al., 2014a). The advantages of this study were introduced a novel method to measure paddle movement leading to important initial results. However, some limitations in this study were related to the limited number of points in time during which exposures that could be made after compression force ceased. Previous studies into paddle movement demonstrate that about 60% of motion happens within the first 20 seconds of paddle compression (Kelly et al., 2012). Whereas, the

mammography system used in Ma's (2014a) study only allowed for repeat imaging after an average time of 29.5 seconds (Ma et al., 2014). Therefore, many exposures per unit time would be better, from the point after compression forces ceases to be applied.

A more recent study by Ma et al., (2014b) suggested that patient movement occurring during the exposure time represents a source of image blurring. In his work two calibrated linear potentiometers were used to measure the movement at the paddle. A hypothesis was proposed between the amount of movement and the amount of blurring that could lead to a lesion being obscured due to movement-related unsharpness in the image. It was suggested that the quantity of extra patient movement during FFDM imaging could be assessed utilising a linear relationship between paddle movement and the change in compression force (Ma et al., 2014b). There are some limitations to this study related to the materials and the method. Firstly, the FFDM system was only one type; so, the results are likely to be restricted to that system - Hologic Selenia Dimensions machines. Secondly, only one type of breast phantom was used to simulate real breasts. Female breasts differ in size, composition and shape, therefore, the phantom used by Ma et al., (2014b) did not simulate the potential range of women's breasts.

Recent research by (Ma et al., 2016) identified paddle motion being present in a number FFDM machines during in the clamping phase, with estimates of motion being as high as 1.7 mm. Compression paddle motion has been reported to occur during the 'clamping' phase and it has been hypothesised that this may cause image blur (Ma et al., 2016). They utilised a deformable breast phantom to simulate a woman breast. Vertical motion at the paddle was calculated utilising two calibrated linear potentiometers. The motion in millimetres was calculated every 0.5s for 40s for each paddle, whereas the compression force of 80N. They concluded that most motion occurred within the first 10s of clamping, and after 4s, paddle motion will probably be clinically insignificant. However, the limitation of this work related to the phantom utilised by Ma et al., (2016) cannot fully represent the compression features of the woman breast.
Other research by Ma et al., (2015) identified the amount of simulated image blurring that can be detected visually. The findings of this study have determined that the amount of simulated motion blur for a hard edge software/mathematical simulation mask is 0.8mm and soft edge software/mathematical simulation mask is 0.7mm, while Gaussian blur software/mathematical simulation mask is 0.4mm. Whilst the sample size in this study was small (25 cases, 2 observers) and did not provide adequate statistical power, the results are however of interest.

Another study by W. K. Ma et al. (2016) assessed the visual detection of motion blur on a 2.3MP monitor and a 5 MP monitor of report grade; also they suggested an observer standard for the detection blurring visually on a 5 MP monitor. The findings of this study demonstrated that the technical recall rate for 2.3 MP monitor is 20.3 % while for 5 MP monitors it is 9.1%. The minimum magnitude of motion blur which can be detected visually is 0.4 mm of motion blur on 5-MP monitors. For a small amount of motion blur (0.2 mm), the visual detection difference was not statistically significant between the 5 and 2.3 MP monitors. This study has some limitations for instance the viewing environment may not fully represent the normal screening scenario. For instance, practitioners in clinical imaging rooms predominately do not work in dim light levels consistent with standard conditions of reporting and the volunteers in Ma's study possibly had different amounts of time compared to image observers and practitioners to interrogate the image to determine whether blurring is present.

2.7.3 Thixotropic Behavior and Breast Tissue Characteristics

Thixotropic behaviour, the proportion of adipose tissue within the breast, mechanical properties of breast tissues, patient movement, paddle movement, and the amount of breast compression during the mammographic image acquisition are all factors that can cause motion blur in FFDM images. Geerligs et al., (2010) suggested that thixotropic behaviour of the breast tissue may be one of the main causes of movement at the paddle. Thixotropic behaviour of the breast tissue is related to the structural changes in the adipose tissue caused by mechanical loading during paddle compression. Geerligs et al., (2008) examined the long-term behaviour of adipose tissue under slight pressure and its response to several large compression magnitudes. The outcomes demonstrate that the shear modulus increases dramatically when increase loading period, but returns to its initial value within three hours of recovery from loading. They concluded that adipose tissue probably behaves as an (anti-) thixotropic material.

Mechanical load transfer from a superficial contact region on skin to deeper tissues has an impact on various tissue layers. A previous study by Geerligs et al., (2008) on the linear behaviour of adipose tissue demonstrated that the linear strain is valid only for low strains (Geerligs et al., 2008). In most fields, however, much higher deformations happen in the adipose tissue for a longer period of time and with higher pressure. In uniaxial tension experiments, adipose tissue shows a non-linear stress against strain response; at small strain levels, the response is linear while at high strain levels, the tissue 'lock-up' and the stress level

rises promptly. Adipose tissue is capable of changing its microstructure such that at high strains or long periods of harmonic excitation the material behaviour changes dramatically. This structural change is reversible after long periods of rest.

A study by (Peters, 2010) reviewed many published studies to provide data on the behaviour of adipose tissue, most of these are inadequate, and either only concentrate on some sides of the substance, such as relaxation or creep behaviour (Linder-Ganz et al., 2007) , only compare the characteristics of tissues (Patel, Smith and Patrick, 2005) or are highly concentrated on one sort of tissue. However, neither of these studies is comprehensive enough to establish a specific description about the importance of adipose tissue and breast compression. On the other hand, some researchers (Samani, Zubovits and Plewes, 2007) used the mechanical properties of breast tissue to increase the detection performance of breast cancer. Several studies suggested imaging the stiffness distribution in breast tissue to improve detection of breast lesions (Wellman et al., 1999). They proposed that cancers are much stiffer than the surrounding tissue. A study by (Wellman et al., 1999) proposed that there is a relationship between elastic modulus in compression and histological diagnosis. They also hypothesised that cancer exhibits non-linearity and its change in modulus with pressure is larger normal breast tissue. The study results reported that there is a significant difference in the stiffness and the rate of increase in stiffness with compression between benign and malignant breast tissues.

2.8 Physics of Mammography System

2.8.1 X-ray Spectrum

A mammography system is provided with distinctive anode/filter configurations in order to work in the suitable range of kilo-voltage (kVp). The typical kVp range differs depending on several studies. For instance, the International Atomic Energy Agency (IAEA) proposed the typical range of kilo-voltage as (24-32 kVp), whereas Zhang and Liua, (2012) suggested the typical range is (18-42 kVp) for conventional mammography (Zhang & Liua, 2012). Likewise, Ranger et al. (2010) considered the kVp settings ranged between 23–35 kVp (Ranger, & Samei, 2010). These differences in settings of kilo-voltage among several studies may be due to utilising different models and makes of mammography machines from various manufacturers. In conventional mammography equipment, the anode/filter combinations are commonly molybdenum/rhodium (Mo/Rh) or molybdenum/molybdenum (Mo/Mo). Some mammography systems are provided with a dual-track anode which gives more flexibility to the radiographer

for choosing either rhodium or molybdenum (Sprawls, 1995). Moreover, due to developments in modern digital detector devices, additional anode/filter combinations such as tungsten/rhodium (W/Rh) and rhodium/rhodium (Rh/Rh) can be used in the mammography equipment (Chevalier et al., 2012). Mo/Mo or Mo/Rh are typically utilised in mammography units (e.g. Hologic Selenia). A study by (Baldelli, Phelan and Egan, 2010) demonstrates that the W/Rh target/filter is the better choice regarding image quality with the optimal dose of radiation. This target/filter combination is able to work as the best selection for all breast structures and thicknesses for diagnosis abnormalities (Baldelli, Phelan, & Egan, 2010). The energy spectrum of molybdenum comprises of a Bremsstrahlung and characteristic energies (see **Figure 2.12**). The molybdenum anode produces two types of characteristic X-ray energies (19.5 keV and 17.9 keV). These provide high contrast mammographic images for breasts with average thickness. The X-ray beam that has energies higher than (20 keV), are removed by a molybdenum filter and the mammographic image results from the low-energy spectrum. Most Bremsstrahlung energies above the binding energy of the K-shell electrons are attenuated when using a molybdenum filter (**Figure 2.12**). The removal of high energies X-ray spectrum above 20 keV enhances the subject contrast (Huda & Slone, 2007; Sprawls, 1995).

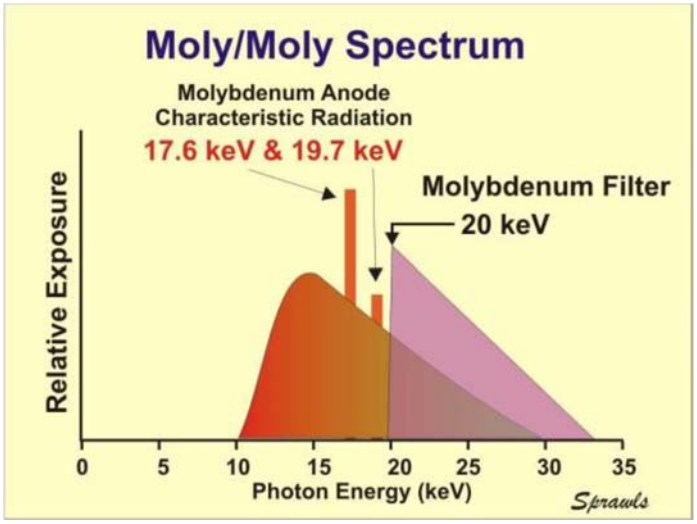

Figure 2.12 Molybdenum / Molybdenum spectrum (Sprawls, 1995)

A rhodium filter which is either chosen by the radiographer or the mammography system utilising AEC is an alternative filter. This is commonly contained within mammographic systems with double filters. The k-edge boundary is shifted to a higher energy (23.22 keV)

compared to a molybdenum filter (20 keV) (**Figure 2.13**). Moving to a higher energy means that the Bremsstrahlung radiation between (20 and 23.22 keV) is included in the beam of the X-ray. This extra radiation has a higher penetration and can be utilised for thicker or denser breasts (Sprawls, 1995). For most clients, the Mo/Mo filter is used. However, for denser/thicker breasts, a Mo/Rh setting with a higher kVp is automatically designated (Yaffe, 2010).

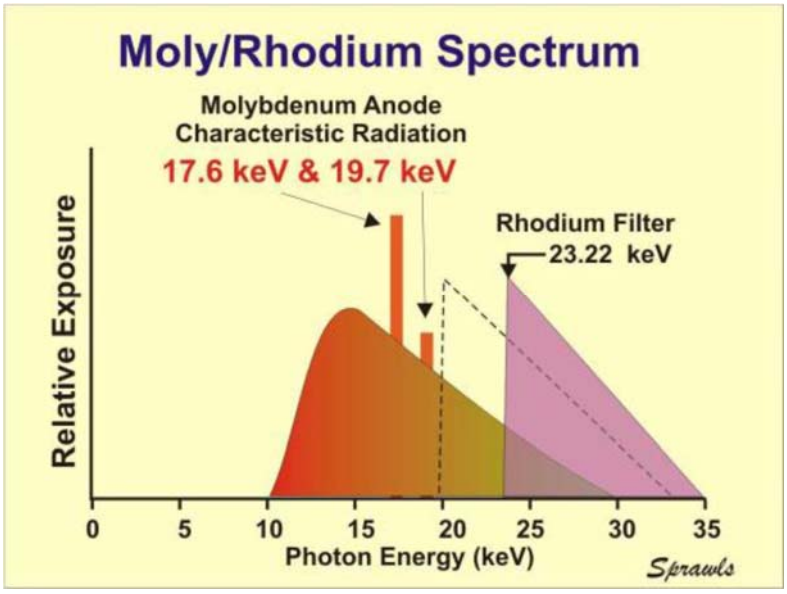

Figure 2.13 Molybdenum / Rhodium spectrum (Sprawls, 1995).

The interaction of X-ray is often among different types of detectors. Three essential atomic interaction forms happen between the photons of X-ray and the detectors of mammography system. These interactions involve the photoelectric effect, Compton (inelastic) scattering, and elastic scattering (Yaffe, 2010). In elastic scattering, the emitted photon from the matter has the same energy as the incoming photon. This means the energy of the scattered emitted photon does not disperse when interacting with the material. In Compton scattering (**Figure 2.14**), some of the photon energy is absorbed when the photons liberate a recoil electron which is a low binding electron. The rest of the energy stays in the scattered photon (Yaffe, 2010). Consequently, elastic scattering leads to contrast reduction, increased noise and loss of spatial resolution (Toennies, 2012). The Compton scattering amount increases with the increase of photon energy. The scattered photon can be dissipated in any orientation and also can be dangerous for the operator of X-ray system (Zhang, Li and Liu, 2012).

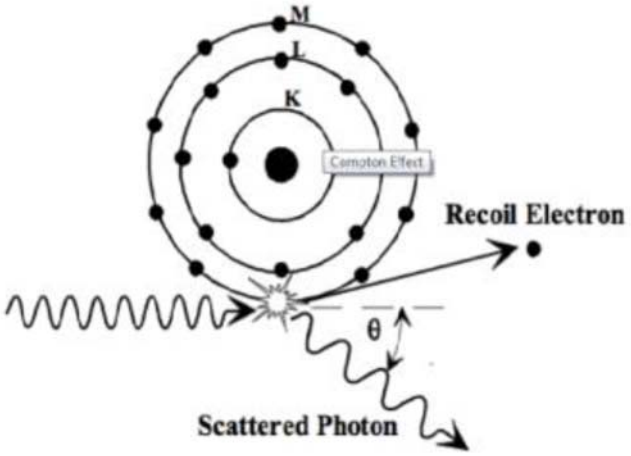

Figure 2.14 The interaction of X-ray through Compton scatter (Haidekker, 2013).

The probability of photoelectric absorption per unit mass is related to the following equation.

$$\frac{Z^3}{E^3} \quad \ldots\ldots\ldots\ldots (2.1)$$

Where: Z is the atomic number of object and E is the energy of the X-ray (Bushberg, Seibert, Leidholdt, & Boone, 2012). This equation demonstrates the opposite relationship between the increment of energy and the photoelectric interaction. At low kVp levels the photoelectric interaction dominates over Compton scattering, while at high kVp levels, Compton interaction happens more often. Therefore, since a low energy is required in mammography, the photoelectric effect represents the essential interaction of X-ray in the detectors (Saha, 2013). The types of material utilised as detectors have an important impact on the increase of the photoelectric effect. The high atomic number materials are appropriate materials for making detectors such as selenium and iodine. At 20 keV, 96% of the interactions of X-ray will occur via photoelectric interaction for selenium and 94% for iodine (Yaffe, 2010). As photoelectric absorption needs low photons energies and low photons energies are required in mammography to obtain images with better visibility, these types of materials are appropriate for mammography detectors.

2.8.2 X-rays Incident on the Detector

As **Figure 2.12** and **Figure 2.13** illustrate, mammographic machines operate using on low-energy photons. In order to clarify the cause of utilisation low-energy photons to output mammographic images, the relationship between the thickness of the region of interest in the breast, the attenuation coefficient of the breast abnormality and the mammography detector are discussed. Since the photon of an X-ray transmits through tissues of the breast, different reactions occur between X-ray and difference densities of the breast tissues (Yaffe, 2010). **Figure 2.15** illustrates two samples of paths that an incident X-ray transfer through the breast, A and B. In path A, the photon moves through the normal tissue, in path B there is a breast abnormality with the thickness 'a'.

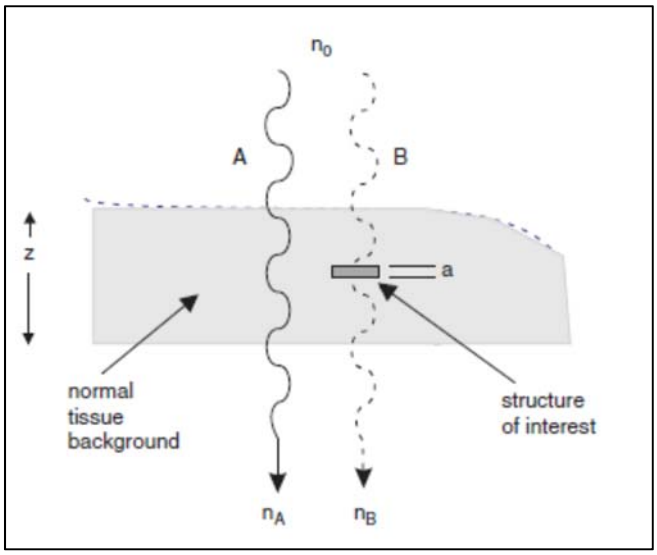

Figure 2.15 The pathways of transmitted X-ray A: through normal tissue of breast B: during interest structure (Yaffe, 2010).

2.8.3 Digitization

In digital mammography, the process of converting the analogue data to a digital signal is named digitisation. This process includes two stages: sampling and quantization. The analogue data is produced by a detector initially, and then the detector converts it to digital data using special electronic circuit named analogue-to-digital convertors (ADCs). The digital signal transfers to a computer in order to digitize and store it digitally. In digital mammography, the last step in the process of image formation is the image processing application. Image processing is utilised to improve the diagnostic information within the image. This can be achieved by improving the contrast and edge definition or through decreasing image noise

(Warren et al., 2014). Every manufacturer utilises their own image processing algorithms, and the appearances of the image after this processing can vary between manufacturers. Many studies have investigated the impact of these variations in image appearance (Pisano et al., 2000; Sivaramakrishna et al., 2000) and objective studies (Chen et al., 2010; Goldstraw et al., 2010; Kamitani et al., 2010; Warren et al., 2012). Some studies concluded that the difference between several image-processing algorithms was significant (Goldstraw et al., 2010; Visser et al., 2012), and others found that the difference was not significant (Kamitani et al., 2010; Cole et al., 2003; Warren et al., 2014). In digital images many reviewed studies have attempted to detect and estimate motion blur in digital images. A study by (Ramakrishnan, 2010) investigated some algorithms which used to detect blurred images. However, no robust empirical study has been published to detect image blurring in FFDM images mathematically. Accurate identification of motion blur visually in digital images is not easy and can be carried out using mathematical methods.

2.8.4 Pixel Size in Mammography

Pixel size and spacing affects the spatial resolution of a digital mammogram. However, more pixels do not always offer a higher spatial resolution due to the fact that image blurring can produce scattering of X-ray, scattering of light, and scattering of both in the detector (Chotas, Dobbins & Ravin, 1999). For instance, the pixel size of direct selenium (about 70 μm) has higher spatial resolution than a scintillator based system which has larger pixel size of about (100 μm) per pixel. Commonly, the pixel size on current detectors of mammography systems is between the range 50 -100 μm per pixel **(**Freitas, Kemp, Louveira, Fujiwara, & Campos, 2006).

Chapter Three: Medical Images Assessment Methods

3.1 Chapter Overview

Image quality assessment (IQA) is increasingly important to medical image enhancement applications. These applications use several technologies to improve the visual appearance of the medical images. Conventional IQA indices, such as signal-to-noise ratio (SNR) and mean squared error (MSE), are used extensively but they do not take into account the human visual system (HVS) (Krupinski, 2011). Medical images require human interpretation, and despite software approaches like computer-aided detection, image analysis ultimately requires visual and cognitive skills. A number of the IQA metrics based on HVS are used to assess perceptual image quality. The assessment of medical imaging procedures or systems should involve the observer since the observer's opinion is considered an integral part of the medical diagnostic procedure. The measurement of physical parameters is not sufficient to assess the success of the process. Receiver operating characteristics (ROC) methods are considered a robust approach involving performance of observer and imaging techniques (Thompson, Manning & Hogg, 2013). **Figure 3.1** demonstrates the relationship between visual performance, image interpretation and image quality assessment methods.

This chapter is organized into six main themes. The first theme will focus on the relationship between visual performance and medical image interpretation (section 3.2). The second theme will focus on the human visual function (section 3.3); the third theme will focus on the receiver operating characteristics (ROC) methods (section 3.4). The fourth theme will focus on a location sensitive method of observation study, the free-response receiver operating characteristics (FROC) method (section 3.5), which will be used for data collection. The fifth theme will focus on perceptual measures (section 3.6), and finally the sixth theme will focus on the physical measures of mammographic images and the factors which affect the conspicuity of the breast lesions (section 3.7).

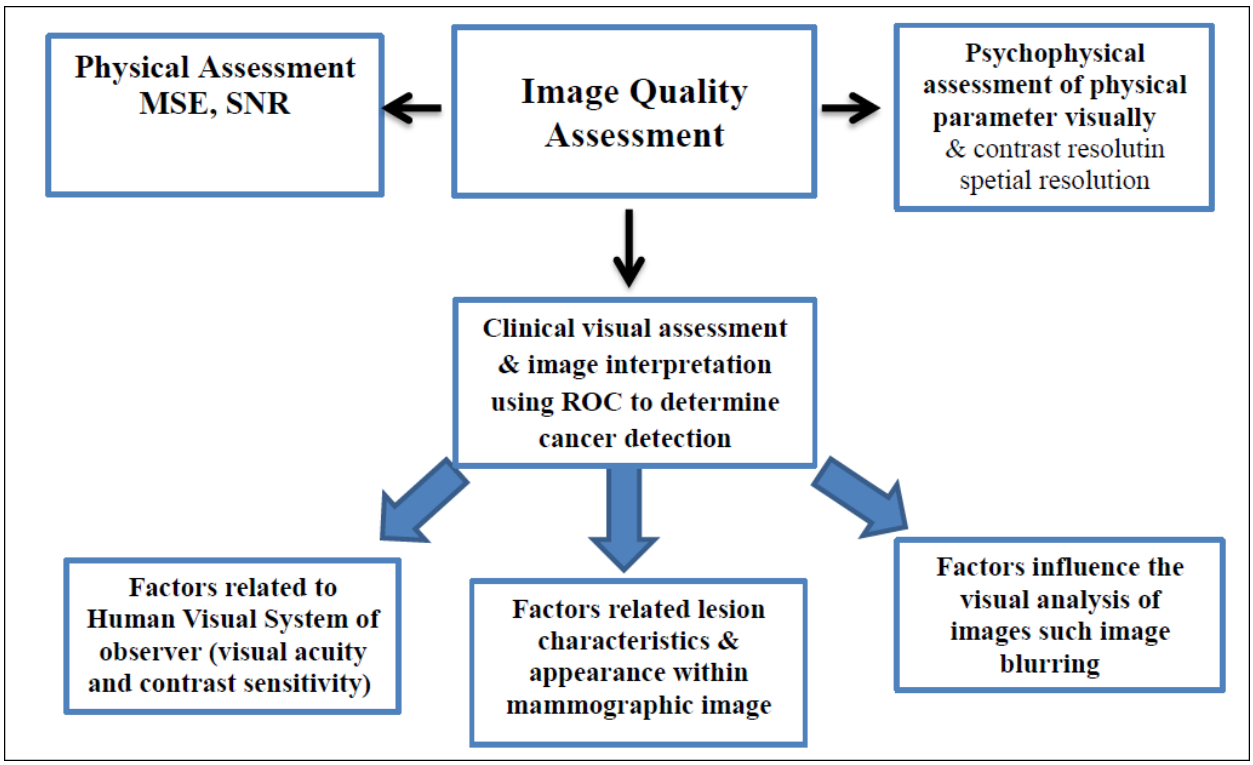

Figure 3.1 Relationship between visual performance, image interpretation and image quality assessment methods.

3.2 The Relationship between Visual Performance and Medical Image Interpretation

Visual perception represents the ability to interpret the surrounding environment by processing information that is contained in visible light. Research in neuroscience, cognitive science and psychology, collectively referred to as vision science, concerns certain physiological components which make up the visual system (Watson & Null, 1997; Manning, 1998). Medical image interpretation is based on visual performance of an observer and visual appearance of image. A psychophysical study by Apelt et al., (2009) has illustrated that human detection performance does not predict pattern recognition performance, which has contributed to the creation of a visual processing hierarchy. The process evolves as follows: detection→ discrimination→ identification→ recognition. However, it is often impossible to predict the results at a given hierarchy level based on the results obtained at a different level (Apelt et al., 2009). Factors affecting error in mammographic image reading are complex and difficult to isolate. One prospective source of error could be related to reduced visual performance, which

in turn decreases an observer's ability to correctly identify tiny breast lesions (Reed, 2005). Errors related to visual perception can be classified into two categories: cognitive or visual errors. Cognitive errors represent approximately 45% of all errors and this concerns the observer who makes the incorrect decision (Samei & Krupinski, 2010). Visual errors represent approximately 55% of all errors and relate to an incomplete search of the image. Manning et al., (2004) concluded that most errors in image perception were failures of decision-making instead of detection (Manning, Ethell and Donovan, 2004b). Visual errors may occur due to not seeing the abnormal area or not focusing on lesion location for enough time (Samei, 2003).

Interpretation of mammographic images can be a tedious task, given its repetitive nature of this task; but the unique nature of each mammogram means there is a unique map for every individual. Furthermore, the mammogram of a woman changes through time, related to the age, menopausal status, and hormonal changes (Zuley, 2010). Since breast cancer is a commonly diagnosed cancer in females, it is important to understand visual perception in mammography (Zuley, 2010). According to Zuley (2010), the mistakes in perceiving mammographic images can be categorised into three types: search errors, recognition errors and decision-making errors. If a lesion is not identified by the observer this is considered a search error. However, if the lesion 'catches the observer's eye' but is then quickly dismissed it is considered a recognition error. This will lead to the lesion going unnoticed. Other errors such as decision-making errors can happen when the lesion is present, however the assessment of its nature is made incorrectly. This can result in a lesion being falsely identified as malignancy; a false-positive (FP), or dismissed as benign when it is actually malignant, a false-negative (FN). Anatomical noise or normal tissue structure in mammography can mask the abnormal tissue. Decision-making errors can lead to either FP or FN decisions whereas search and recognition errors can lead to only FN (Zuley, 2010). **Figure 3.2** demonstrates the three categories of perceptual mistakes in observing mammograms. Therefore, there is a well-known search type called 'satisfaction of search' to demonstrate why the lesions stay undetected after finding the initial lesions (Mello-Thoms, Trieu, & Brennan, 2014). Satisfaction of search can play an essential role in missing pathologies within an image. In this condition, an expert image reader may be ignoring other possible lesions after locating the first one.

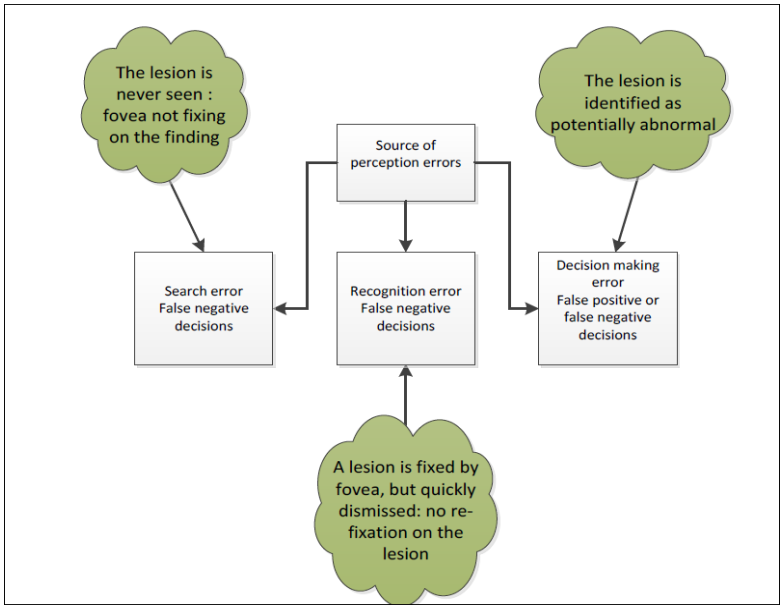

Figure 3.2 Three categories of perceptual mistakes in observing mammograms (Zuley, 2010; Ossati, 2015).

3.3 Human Visual Function

Vision is the eye's ability to detect an electromagnetic spectrum of light; the brain then interprets this information. The main function of the eye is to convert light into electrical signals which are then transferred to the brain by the optic nerve (Gao et al., 2010). This process includes several stages, starting with the light of an object passing through the lens to a reversed visible image on the retina (Chester, 1992). There are several main concepts related to human visual function; these can be evaluated with visual tests such as visual acuity, contrast sensitivity and stereopsis. These visual parameters are recommended to evaluate and decide if an observer has adequate eye function to participate in medical imaging observer studies (Lanca et al., 2014). The expression *visual acuity* is used to designate the capacity of the eye to resolve the size of an object. *Contrast sensitivity* makes the discrimination of low and high contrast frequency information possible. This can be linked to the perception of complex patterns in FFDM images (Apelt et al., 2009). *Stereopsis* can describe depth perception of objects in the central visual area, enhancing vision quality through binocular summation. Perceived visual errors are computed based on the visual error sensitivities to various factors of HVS, such as brightness, contrast sensitivity and visual attention (Gao et al., 2010).

The main functions of the human eye are to distinguish colours and shapes and to reveal light in the darkness. This process usually happens when light passes through the lens to a reversed visible image on the retina (Osberger, 1999; Nadenau et al., 2000). **Figure 3.3** illustrates the anatomical structure of the human eye. The light passes through the cornea and is focused by the lens to form an image on the retina. *The retina* is located at the back of the eye. It contains two types of photoreceptors: the first, known as cones, are responsible for colour and high-acuity (photopic) vision; the second, known as rods, are responsible for low light level (scotopic) vision. At light levels between the photopic and scotopic range, i.e., the mesopic region, both cones and rods provide vision (Gao et al., 2010). Rod cells are extremely sensitive to small levels of luminance, however, they are capable only of low resolution and are therefore of little relevance to medical imaging (Kundel, 1995). The pupil works as a diaphragm to control the amount of light entering the eye. The lens elastically focuses at different distances; a process referred to as *accommodation.* The diameter of the eye's pupil at relaxation is approximately 1.5 mm (Chester, 1992).

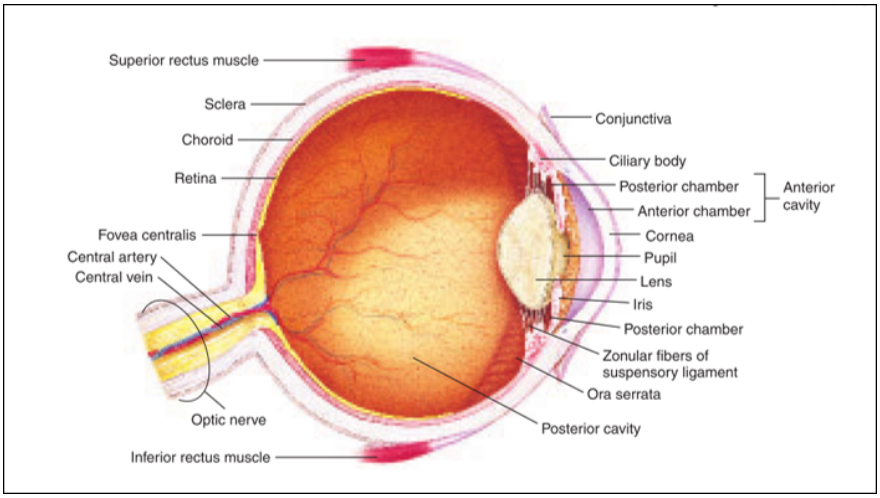

Figure 3.3 Anatomical structures of the human eye (Van De Graaff, 2001)

The construction of an image can be put through many processes at several steps in the *visual pathway* from the retina to the cortex area. The retina consists of bipolar and ganglion cells, which are responsible for transmitting electrical impulses to the brain. Cells such as horizontal and amacrine work on lateral connections between ganglion and bipolar cells. The transmission of electrical signals from cones to bipolar cells is responded to with a chain of electrical

impulses. The strength of response is coded at all the nervous systems, according to the frequency of the electrical signal (Osberger, 1999). *The visual cortex* contains cells which are responsible for image analysis and is located at the back of the brain. It can be categorised into simple, complex, hyper-complex and higher-order hypercomplex cells. The primary visual cortex contains simple cells which have Receptive Fields (RFs) and are characterised by extremely structured and restricted regions of space. In spite of the fact that a limited quantity of image processing may occur in the retina and lateral geniculate bodies, the visual cortex is considered the essential part of image analysis (Chester, 1992).

3.3.1 Visual Acuity

Visual acuity is a measure of the eye's ability to distinguish detail. The ability of the eye to detect small detail is a significant factor in the diagnosis of medical images. The processing of visual information by the HVS is connected to the ability of an observer to interpret the medical image (Safdar et al., 2009). Visual acuity is the most commonly measured aspect of visual function (Colenbrander, 2001; Kaiser, 2009). This function could determine an observer's ability to determine small objects correctly, such as solitary pulmonary nodules (Bass & Chiles, 1990; Thompson et al., 2017). Several factors influence visual acuity, including illumination, contrast, refractive error and the site of the retina being stimulated (Holladay, 2004). The impact of the tested object features on visual acuity is related to different factors, such as contrast of the test object, luminance distribution in the field of view, colour, movement of test object and criterion for detection of detail (Kaiser, 2009). However, visual acuity is a complex task. The lowest separation concerns the decision of the site of a visual target, commonly related to another part of the same target (Holladay, 2004).

3.3.2 Contrast Sensitivity

Two concepts must be considered and differentiated in the discussion of contrast sensitivity such as objective and subjective contrast. Objective contrast (photometric) concerns the variation in luminance of objects or adjacent grounds. Subjective contrast (physiologic) concerns subjective phenomena, such as the modification in the ostensible brightness of objects of a given luminance, which is related to the luminance of the background. Overall, visual acuity reduces with a decline in photometric contrast; this becomes clearer with small test objects (Watson & Null, 1997). The influence of physiologic contrast is important. The borderline between a dark and luminous surface causes a blurred, unfocused retinal image to

be produced by the veiling effect of stray light and the optical aberrations of the eye. These impacts are off-set by physiologic contrast. The image on a white background appears whiter, the image on a black background appears darker and the border becomes sharp when the two edges meet each other (Apelt et al., 2009). With low contrast levels, visual acuity changes significantly; but at high degrees of contrast, comparatively great variations in objective contrasts have minimal impact on visual acuity (Jackson, 1996).

3.3.3 Visual Function Assessment

There are different techniques that can be used to measure and specify visual acuity and in its measurement, it is essential to use eye-validated charts. Typically, these contain capital letters organised in rows with the largest letters at the upper part of the chart decreasing gradually to the smaller letters at the bottom of the chart. There are several charts which can be used for visual acuity measurements, examples include senllen and ETDRS (Kaiser, 2009). The ETDRS chart is considered to be the gold standard for vision measurement in clinical trials (Kaiser, 2009). Visual acuity measures are used to describe the capacity of the eye to resolve the size of an object. It is the sharpness or clearness of vision and this is defined based on the clarity of focus in the retina of the eye. However, the processing of visual information by the human visual system describes the ability of the observer to interpret and understand the (medical) images. The reduced visual acuity might significantly raise the contrast threshold required to identify high-frequency information. Visual acuity hinges on the site of the retinal stimulus and reduces sharply with a rise in the distance of the image of an object from the centre of the fovea. The complex patterns of mammography perception are related to the contrast sensitivity of the visual system (Apelt et al., 2010). Pattern-detection ability is provided by eye contrast sensitivity for stimuli of various sizes and if abnormal contrast sensitivity is present, low-contrast targets are difficult to appreciate and can be missed. The limitation of visual acuity is caused by aberrations, diffraction and photoreceptor density in the eye (Holladay, 2004). In comparison, contrast sensitivity measurement is known as the ratio of the average background intensity to the peak amplitude of the spatial sinusoid at the threshold that is used as the test stimulus.

There is an additional factor which affects visual performance measurements known as *contrast sensitivity function (CSF)*. Grading the contrast sensitivity function is a valuable measure of visual function. It quantifies the capability of an observer to perceive small changes

in luminance between areas which are not isolated by definite borders (Arden, 1978; Apelt and Peitgen, 2008). Higher contrast sensitivity includes the identification of sinusoidal gratings, which are a model of black parallel bars and parallel light that measure the sensitivity of the eye through bar widths or a range of spatial frequencies (Drum, Calogero and Rorer, 2007). Visual Attention is the process of concentration in the sense of excitation, whether this excitation is sensory or mental. Perceptual quality measures are based on models of human visual perception. Several perceptual image quality metrics are proposed as alternatives to objective metrics, such as methods incorporating models of luminance adaptation and Contrast Sensitivity Function (CSF)(Gao et al., 2010). An early study by Riggs (1965) described the relationship between luminance intensity and visual acuity; it has been utilised within test objects within a white background. Riggs (1965) illustrated that visual acuity is low at dark levels where peripheral rod receptors or parafoveal dominate. As the light intensity level rises, the cone receptor thresholds increase and acuity rises sharply. As the intensity increases once more, a level of maximum acuity is reached and this can be maintained across further increases in intensity. The influence of luminance on visual acuity includes *the pupil size*. The ideal visual acuity is related to the pupil size of approximately 2 mm. However, the optimal size changes with levels of luminance, the size of the test object and other characteristics. A large pupil means more light will pass through the eye but this can also lead to visual aberrations. Luminance of the ambient lighting in a radiology reporting room typically should be below 10 lux. These aberrations are reduced with a smaller pupil size, but a very small pupil size can lead to decreased visual acuity because the impact of light diffraction, through decreasing retinal luminance, is raised. Luminance of the ambient lighting can significantly affect the detection of microcalcifications in high density breasts (Thompson et al., 2017).

3.4 Receiver Operating Characteristics (ROC) Methods

The receiver operating characteristic (ROC) method is considered a valuable tool to evaluate the combined performance of the imaging system and observer in radiology. The historical background of ROC was established upon the fundamental principles of signal detection theory (SDT) (Li et al., 2010). This paradigm originated in the 1950s when it was used to establish a radar's ability to detect approaching aircrafts. In 1960, a number of studies and books were published by Dr Lusted that encouraged the utilisation of ROC analysis in diagnostic radiology (Metz, 2008). However, this recommendation was not implemented until the 1970s, when

many laboratory studies were conducted by some researchers at The University of Chicago that led ultimately to the adoption of ROC analysis in medical imaging, and this lead to the development of new analytic techniques (Metz, 2008).

There are many applications for ROC methods; they can be utilised in several modalities for different purposes. The ROC modalities can be used to compare old imaging techniques with a modern alternative. For instance, the ROC method can be used to make a comparison of the diagnostic performance between different models and it is a common choice of model (Bator and Chmielewski, 2008). Also, the ROC method can be used to compare between two new technologies in mammography such as digital mammography versus digital breast tomosynthesis (Gennaro et al., 2010). In digital mammographic image screening trials, both film screening (SF) and full field digital mammography FFDM can be obtained in each patient and the diagnostic performance of the observers for the two mammograms can be compared. The ROC paradigm can be generally described as a graphical curve that shows the performance of a binary classifier process, which consists of the true positive fraction known as sensitivity (equation 1) plotted against the false positive fraction known as 1-specificity (equation 2) (Metz, 2008).

$$Sensitivity = \frac{number\ of\ true\ positive\ cases}{true\ positive\ cases + false\ negative\ cases} \quad \text{..... (3.1)}$$

$$Specificity = \frac{true\ negative\ cases}{true\ negative\ casese + false\ positive\ cases} \quad \text{..... (3.2)}$$

The performance of any screening programme can be evaluated by three relevant parameters: sensitivity, specificity and positive predictive value. The expression of sensitivity and specificity is a measure of the observer performance of a binary decision; yes or no. This is a limitation in that it is difficult to help the observer estimate the probability of lesions in individual cases (Akobeng, 2007). A true positive (TP) decision occurs when the disease is present and identified by the observer while a false negative (FN) decision occurs when the disease is present and either overlooked or misinterpreted by the observer (Equation 2). The remaining possibilities are true negative (TN) decisions, wherein the disease is absent and the observer agrees, and false positive (FP) decisions, wherein the disease is absent and the observer disagrees (Obuchowski, 2005).

Positive predictive value and negative predictive value can be affected by disease prevalence. Negative predictive value is the probability that the lesion is not present when the result of the test is negative while positive predictive value means the ratio of the actual number of cancer cases to the number of abnormal cases detected by the programme (Equation 3). The same test can produce different results in two populations (Chakraborty, 2011).

$$Positive\ Prdective\ value = \frac{\boldsymbol{true\ positive\ cases}}{\boldsymbol{true\ positive\ cases + false\ positive\ cases}} \quad \ldots\ldots\ldots\ldots\ldots\ldots (3.3)$$

The operating characteristics can be expressed in several forms projected by the search method from which they have been extracted. Table 3.1 outlines concisely several ROC methods.

Table 3.1 Summary of development and comparison between ROC methods.

Full name	Abbreviation	Description	Description of plot	Properties & comparison between each method
Receiver Operator Characteristic	**ROC**	Differentiates between normal and abnormal images	TPF versus FPF	Does not consider the location of the lesions. Low statistical power
Localisation ROC	**LROC**	Identifies localisation of one abnormality in the images. This can be used as it is still a single rating per case/image	TPF versus FPF	Incorrect location of lesion considered as false positive
Free-response ROC	**FROC**	Identifies and localises several abnormalities within the images Discriminates between malignant and benign	LLF versus NLF	localised several abnormalities Mark-rating according to BI-RADS Confidence level Multi-reader multi-cases
Jackknife alternative FROC Analysis	**JAFROC**	A re-sampling method that does not assume independence of responses within the same study applied to FROC	AFFROC curve is a plot of LLF versus FPF	A high statistical power method required multiple observers and multi-cases
The ROC curve is the graphical scheme of true positive fraction (TPF) versus false positive fraction (FPF) while the FROC curve is the graphical scheme of lesion localisation fraction (LLF) versus non lesion localisation fraction (NLF) and the AFROC curve is the scheme of LLF versus FPF				

The ROC modalities have several measures which can be used, according to the design or the purpose of each study. According to Metz (2008), the ROC study can be divided into two types

of designs: clinical and laboratory studies. This refers to where the image-reading data is collected, either in clinical or laboratory based research, and it is important to understand the pros and cons of each approach. In laboratory studies, data collection can be most closely controlled so that statistical variation is decreased with increased statistical power, and the situations that led to the study's conclusion are better understood (Gur, 2007; Metz, 2008). However, in the routine clinical practice, the data collection better represents the 'real world' with regard to a condition which we would like to draw conclusions about (Metz, 2008).

ROC analysis considers the ability of human observers to distinguish between patients that are actually negative and positive for disease, which has been previously confirmed by a suitable arbiter (Metz, 2008). Since the performance in ROC methods depends on the human observer, there is a reasonable probability that the performance may be affected by the individuality of the observer; for instance the expertise of the image reader, fatigue, display environment and other conditions (Chakraborty and Yoon, 2008). Rating scales utilised in ROC analysis allow an observer to provide a numeric rating to an image, based on the perceived probability that disease is present (Chakraborty, 2002). This rating is used to assess the disease existence or absence. The low confidence level means that the observer believes that the image is more likely to be negative for disease (normal). In contrast, the higher confidence ratings reserved for cases that the observer believes are positive for disease (abnormal) (Chakraborty, 2011). The decision threshold is a scalar quantity; not a random variable, used in an observer performance study. It is different from the confidence level; a random variable.

The capabilities of the classic ROC analysis can be limited in some applications. For instance, the location of the lesion is ignored and the task of the observer is just to decide if a case is normal or abnormal (Chakraborty and Yoon, 2008). The true positive (TP) is insufficient if the lesion location is obscure or incorrectly localised (Chakraborty and Berbaum, 2004). In addition, the classical method may not take into consideration if there is more than one lesion present in the same image. This can lead to clinical consequences resulting from missing lesions and can have an effect on the truth of image quality description (Svahn and Tingberg, 2005). The ROC method is extensively described (Park et al., 2004; Chester, 1992; Metz, 2008) and has been the method predominantly chosen to assess the detection performance of a single pathology for many years. However, there are some limitations associated with the classic method. For example, not all of the information available within an image is taken into account

and the system has trouble coping with multiple pathologies. Although ROC methods are considered the typical process to evaluate performance and ROC is very useful for evaluating diffuse disease such as chest infection or pneumonia, the limitations discussed above are considerable and have led to the development of more advanced methods such as FROC and AFROC.

3.5 Free-Response Receiver Operating Characteristics (FROC) Method

The free-response ROC (FROC) method takes into account the precise location of disease, where it can accurately measure cancer detection performance in FFDM images (Ruschin, Timberg and Båth, 2007a). In a FROC study, theoretically unlimited numbers of abnormalities can be localised in a single image by observers, with each localisation requiring an individual rating to describe the observer's certainty that the abnormality (suspected lesion) is malignant. The FROC method allows observers to localise multiple lesions in each case (Chakraborty and Berbaum, 2004). The main aspect of the FROC method is the ability to penalise incorrect localisations and to reward correct localisations, this means making the use of location information efficient. It should be acknowledged that the FROC method has more clinical relevance than the ROC for masses and lesions; however, it is a demanding perceptual task for the observer. In the FROC method, the observer does not know the number of lesions that might exist in an image. Thereby, the observer's task is to search the image for disease and mark all areas which raise suspicion of an abnormality; for each of these marks they must also provide a rating from a confidence scale; this process is known as creating a series of mark-rating pairs, which is considered the basic unit of data.

The fundamental variations between ROC and the Free-response ROC methods are in the figure of merit (FOM) quantifying observer performance and in the data collection step (Chakraborty and Yoon, 2008). In the ROC paradigm, lesion localisation is not required and a single rating is collected for each image, while in the free-response ROC paradigm, the data involves mark-rating pairs. These are classified into lesion-localisation (LL) and non-lesion localisation (NL) by a proximity criterion (Chakraborty, 2002). Secondly, in a ROC study, the FOM refers to the areas under the ROC curve. In contrast, computation of the FROC FOM includes creating two lists: an abnormal-list and a normal list. The abnormal-list is a record of the ratings for each lesion. The normal list is a record of the higher mark-rating (essentially a non-lesion) for each normal image (Chakraborty, 2010a). The number of normal images

represents the number of entries in the normal list. The total number of lesions is the corresponding number for the abnormal-list. The calculation of FOM includes making all probable comparisons between the quantities in the two lists (Chakraborty and Berbaum, 2004). The FOM is considered as the possibility that a lesion rating skips all non-lesion localisation ratings on normal images (Ruschin, Timberg and Båth, 2007a).

3.5.1 Constructing Curves from FROC Data

In FROC, the observer's task is to search the image and mark areas, which are expected to have lesions. The ROC curve can be computed in a similar process to those for the FROC curve. Nevertheless, they are normalised to a different denominator. The LLF is normalised to the number of lesions whereas the NLF stays normalised to the number of cases. The significant variation between accounts of the operating points for the FROC curve is that it covers all of the ratings that are made for each image within its calculations, whereas the ROC curve only considers the highest ratings.

The overriding value of observer performance studies is the calculation of a figure of merit (FOM) to summarise the performance of the imaging system and observer, which rewards correct decisions and penalises wrong decisions. It provides a single value summarising performance which can be compared statistically. For instance, to compare two types of imaging systems, one calculates a FOM for each method and a statistical test is performed to identify the difference between two FOMs and whether the difference is considered large enough to be different in consideration of the pre-test value of alpha (Chakraborty, 2011). The value of probability is quantified by the p-value (Chakraborty, 2011) When the p-value is smaller than 0.05, one deduces that there is a significant statistical performance variation between two modalities - a difference greater than would be expected by chance alone. The calculation of the overall regions of interests (ROIs) produces the nonparametric area under the curve (AUC) of a receiver operating characteristic curve known as a figure of merit (FOM) (Chakraborty et al. 2011).

The AFROC curve is represented as the plot of LLF versus FPF. It can be noted that the difference between the ROC curve and AFROC curve is just in the descriptions of the y-axes, which means TPF versus LLF. Lesion localisation can be distinguished in good assessments by using the FOM or the area under the AFROC curve while non-lesion localisations on the normal image can be penalised to different marks. For instance, an upper rated FP is penalised

more than a lesser rated FP. **Figure 3.4** demonstrates use of the FROC method to localise breast lesions. In the FROC method, two different types of the curve can be generated: the FROC curve and the alternative FROC (AFROC) curve. On the FROC curve the y-axis is normalised to the number of lesions (LLF) rather than the number of abnormal cases, as in ROC analysis. Thus, ROC is a case based analysis and the observers make case based decisions, whereas FROC is lesion based analysis.

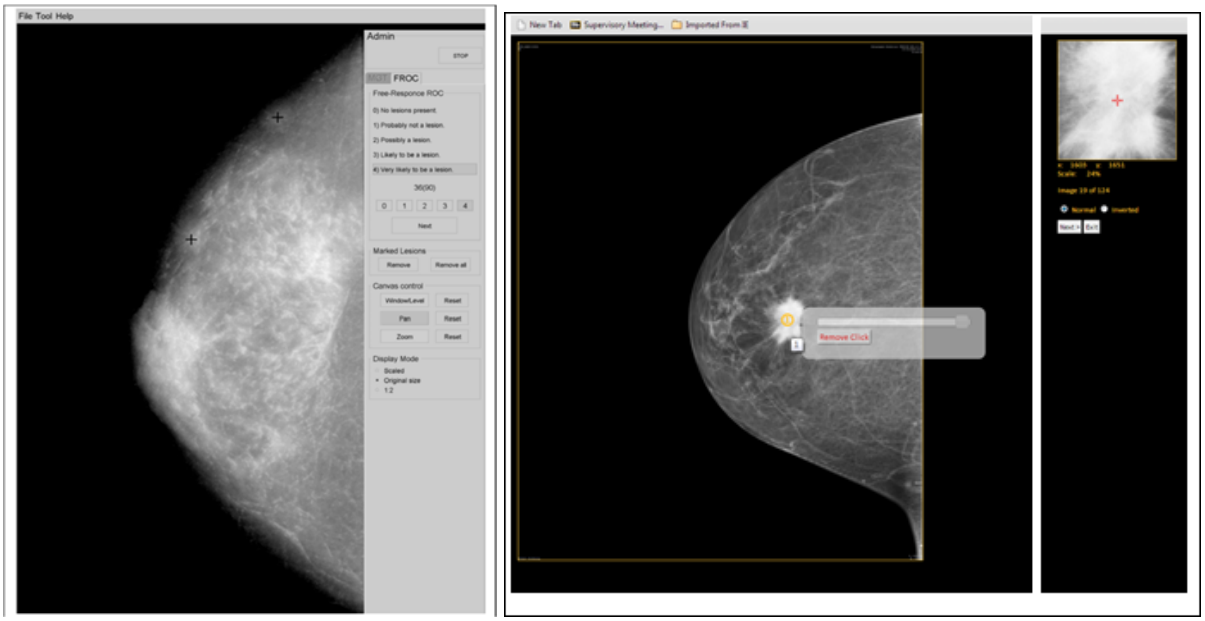

3.4(A) 3.4 (B)

Figure 3.4 The use of FROC methods to localise breast lesions
(A) 5 confidence levels and other available functions (Chakraborty, 2002).
(B) ROCView tools utilised within in this study

3.5.2 FROC Data Analysis

An increase in the number of observers that read or assess the same image set, leads to an increase in the statistical power of the study. This procedure is known as the *multi-reader multi cases* (MRMC) method. Furthermore, an increase in the number of cases in the study leads to an increase in the statistical efficiency. JAFROC analysis successfully overcomes obstacles such as the limitations in the classical ROC method, through the use of the multi-reader multi cases method (Federica Zanca *et al.*, 2012). The JAFROC figure of merit refers to the probability that lesions ratings (LL marks) are rated higher than all noise sites (NL marks) on

normal images (Chakraborty & Berbaum, 2004). There are two approaches for MRMC analysis, (i) the Obuchowski-Rockette (OR) method and (ii) the Dorfman-Berbaum-Metz (DBM) method. The OR and DBM methods are equivalent and are precisely equal when the jackknife method is utilised (Hillis, Berbaum, & Metz, 2008). The DBM-MRMC process is a widely utilised method in ROC analysis, whereas the AUC (Area under the curve) is utilised as the FOM and data are analysed utilising analysis of variance (ANOVA) (Obuchowski *et al.*, 2004; Buissink et al., 2014). The DBM method distinguishes between the variables of case difference and the variance within and among observers to evaluate whether the observed difference is caused by the observers or by the cases of the study. This is known as the jackknife method, where pseudovalues are computed by systematically excluding one case at a time and then searching the variance in accuracy assessments between the evaluation of all data and with that case excluded (Chakraborty, 2010a).

3.5.3 Jackknife Analysis of FROC Data (JAFROC)

The JAFROC method is the equivalent method for analysing free-response rating data and the JAFROC figure of merit refers to the probability that lesions ratings (LL marks) are rated higher than all noise sites (NL marks) on normal images. The JAFROC figure of merit is the trapezoidal under the AFROC curve, θ. The JAFROC figure of merit can be described by equation 4:

$$\theta = \frac{1}{N_N \; N_L} \; \sum_{i=1}^{N_N} \sum_{j=1}^{N_L} \psi(X_i \, , Y_j \,) \ldots\ldots\ldots\ldots\ldots\ldots \; (3.4)$$

Where Xi is the maximum noise rating (mark on a normal case) for a case i, Y_j is the rating for the jth lesion, NN is the number of normal cases, and NL is the number of lesions. The psi (ψ) function is the comparison of the highest rated noise rating and the lesion rating (Chakraborty, 2010c). For the ψ function, if Xi (abnormal) is greater than Y_j (normal) then ψ=1; if Xi is less than Y_j, then ψ=0; if they are equal ψ=0.5 (Chakraborty, 2010b).

Chakraborty et al., (2006) illustrated that the statistical power of JAFROC is greater than the statistical ability of the previous ROC methods (Chakraborty and Berbaum, 2004). JAFROC was developed as a multi-reader, multi-cases process in order to be able to deal with the limitations in the classic ROC method. The statistical power of diagnostic performance of JAFROC analysis is increased according to the sample size, in comparison with ROC.

The similarities are recognised by the pseudovalue denotation in JAFROC analysis (Equation 5):

$$PV_{ijk} = N_T\theta ij - (N_T - 1)\theta_{ij(k)} \quad \ldots\ldots\ldots\ldots\ldots (3.5)$$

Where the pseudovalue for each modality i, observer j and case k is defined by PV_{ijk}, N_T is the total number of cases, θ_{ij} is the figure of merit for modality i and observer j for all data, and $\theta_{ij(k)}$ is the figure of merit with case k removed – identifying the dependence of each case (Chakraborty and Berbaum, 2004).

3.6 Perceptual Measures

When comparing methods of image quality assessment, perceptual and physical methods, perception methods are considered more helpful to determine diagnostic abilities than objective methods (Goossens et al., 2013). However, some human observer studies, such as two alternate forced choice (2AFC), may be time consuming, and therefore expensive, so supplementary objective measures are helpful to support human observer studies (E. Burgess, 1994; Richard and Siewerdsen, 2008). The 2AFC method can be utilised to compare the subtle variances between the performances of different imaging modalities (Burgess, 2011). Revesz et al., (1974) calculated the conspicuity of lung nodules. Image observers were requested to find the existence of a lesion and localise it. They concluded that the computed conspicuity correlated with the possibility to detect an abnormality within a limited range of conspicuity values. Samei et al., (2003) calculated the contrast-diameter product, according to local anatomical noise, and concluded a correlation between the ability to detect lesions and this measure. However, attempting to find a correlation between human observer studies and objective measures has not proved successful (Samei et al., 2003). Manning et al., (2002) demonstrated a poor relationship between the measure of conspicuity index and undetected lesions in chest radiography and pointed out that decision errors were more common detection errors**.** However, it must be noted that the study size was small, and only four regions around the lesion (four profiles) were used which means that the computing of conspicuity had some limitations. The study also included other categories of observer error as initially mentioned by Kundel et al., (1974) (Manning and Ethell, 2002). Mello-Thoms et al. (2005) demonstrated, through an eye tracking study, that undetected lesions predominantly received sufficient visual attention. Other eye tracking studies such as (Chesters, 1992; Manning, Ethell and Donovan, 2004a;

Mello-Thoms, 2006) demonstrated that lesion conspicuity, or the period of time it is viewed, is not the only reason they go undetected. Mello-Thoms et al., (2005) assessed the effects of breast masses' conspicuity on the decision outcome of the observers. They suggested that breast mass conspicuity has an impact on the visual search in a mammography reading. They compared the visual search strategy utilised by an expert in mammography and concluded that most undetected malignant masses did attract a certain amount of visual attention; nevertheless, it was in the processing of the produced information in the lesion location that most errors happened. In summary, errors in Radiology are unlimited to observers missing lesions because they are poorly clarified; it is valuable to inform efforts to enhance the radiological task with calculated image quality that utilise functional data on visual performance (Mello-Thoms et al., 2005).

3.7 The Physical Measures of Mammographic Images

The image quality of mammographic images can be assessed in several methods. Medical imaging devices are quality controlled utilising structured phantoms; measures such as spatial resolution, in terms of modulation transfer function (MTF), signal to noise ratio (SNR) and contrast to noise ratio (CNR) are utilised to assess if the equipment is working within acceptable performance standards (Samei, 2003; NHSBSP Equipment Report, 2007). However, these physical parameters are not exemplifications of a diagnostic image and their output measure is not related to any particular radiological task (Samei, 2003). Therefore, there is a requirement that these measures (SNR and CNR), and other parameters, are utilised to determine the effect of image quality on detection performance and to provide support investigations about the influence of physical measures on visual appearance of lesion futures within the images (Desai, Singh & Valentino, 2010). Other parameters such as the conspicuity of lesions, the size and contrast of lesions is helpful to characterise lesion features (Manning et al., 2004a).

3.7.1 Measuring Conspicuity Index

Initially, conspicuity was introduced as a concept to quantify errors made by observers in radiology. The conspicuity of a lesion represents a ratio between the contrast of a lesion and its surrounding complexity. A study by Kundel et al., (1976), introduced a new method to describe and determine the conspicuity of the lesion. They utilised a measurement of lesion conspicuity

to describe the probability of detection of a lung nodule in the chest X-ray. The lesion contrast is represented by the density alteration around the lesion edge, while the surrounding complexity is the rate of change of the density around the lesion border. This produces a description of anatomical, or structural, noise which puts into consideration the surrounding structures and artefacts. However, Szczepura & Manning, (2016) identified that this equation does not take into account other characteristics that can affect lesion conspicuity such as noise, contrast and lesion size.

In observer studies, Likert scales are commonly utilised in attempts to measure conspicuity, whilst drawing comparisons between different acquisition parameters or utilising varying contrast agents (Van Ravesteijn et al., 2013; Marin et al., 2013). The Likert scales within these studies were quite different in terms of the number of points included on the scale and terms set for each point. This means that the scale is entirely task dependant. However, Likert scales are open to bias as both cognitive and perceptual errors may become involved within the task, as such the use of Likert scales is not an ideal measure of conspicuity (Weiner, 2010).

Conspicuity can be measured utilising just noticeable difference techniques, such as two 2AFC methods, which the task of the observer is to select between two images. The first image is known as a static reference image and the other differs based on the research question being asked. According to the design technique of the studies, this method is more likely to be un-bias than Likert scales and has a low variability (Szczepura & Manning, 2016). The 2AFC method requires a considerable group of images and is time consuming, according to the number of observers that are required; this leads to raise the cost of the study. Furthermore, the observer can be asked a number of questions via 2AFC, not only about conspicuity, which can lead to the obtainment of a more complex depth of data (Burgess, 2011). In 2AFC, the order of data should be taken into account. This means a creation of ordinal data, where the images are arranged in order, and the variance between the ranks are presumed to be equal. Thus, the outcomes are in accordance to the dataset utilised within the study. Brook et al., (2013) and Chang et al., (2013) utilised region of interest data to evaluate conspicuity with a comparison made between the lesion and its surrounding background. In spite of being an objective method to quantify lesion conspicuity, it does consider other factors such as sharpness and lesion size, which affect the conspicuity of a lesion.

3.7.2 Factors Affecting Conspicuity

Szczepura & Manning, (2016) summarised the factors affecting lesion conspicuity; these factors are the; sharpness of the edges, lesion size, structural noise (within and surrounding a lesion) and contrast. Following is a review each of these factors individually:

3.7.2.1 Sharpness

Sharpness means the capability of the system to demonstrate distinctive anatomical structures within the object being imaged (Samei, 2003). For example, the sharpness of the edge of a lesion is important because it affects its visibility. There are mathematical methods to quantify the sharpness of system. Point and line spread functions and their Fourier transform, the MTF, all measure the resolving ability (Samei, 2003) or spatial resolution of a system. They take a number of things into consideration that can lead to blurring of borders, such as: the poly energetic beam, focal spot size and any magnification. Blurring can also occur because of movement of the imaging system or patient. Blurring is the reason behind reduction of visibility of fine details, decreased spatial resolution and minimal sharpness of image.

3.7.2.2 Lesion Size

The size of a focal lesion is a significant factor used to determine the conspicuity of a lesion. A study by Plöckinger (2012) demonstrated that small lesions, of less than 1cm, can be undetected when imaged by 2-dimensional images (Plöckinger, 2012). According to Delrue et al., (2011) 3mm is considered the threshold size limit for perceiving a lesion. If the edges of the tested object are parallel to the X-ray beam, or when the borders are bevelled (either caused by blur, or anatomical reasons) then this affects the visible threshold size (Delrue, Gosselin & Ilsen, 2011). Birdwell et al., (2001) demonstrated that in mammography about 81% of undetected lesions in their study were less than 20mm. In addition, a study by Michealson et al., (2008) demonstrated that the median size of detected lesions by screening mammography was 7mm, with 40% of lesions measuring 5mm (Michealson et al., 2008). Anatomical structure superimposition: during the measurement of contrast to noise ratio or signal to noise, the noise is commonly calculated from a background that does not involve complex surrounding structures; thereby these complexities that affect the lesion detection can be unrecognised with these standard measures (Eckstein and Whiting, 1995).

3.7.2.3 Noise

Noise refers to undesirable changes within an image that do not exist within the imaged subject. (Samei, 2003), when considering lesion conspicuity, said there are two types of noise that should be taken into account, radiographic noise and structural noise. Radiographic noise can be calculated utilising SNR, and offers information about the capability of the system, nevertheless it does not give the full information about the noise within a clinical image. It is stochastic in nature and due to several factors, such as the detector capability and the exposure factors utilised (Samei, 2003). Radiographic noise, however, is not dependent on the subject being imaged (Szczepura & Manning, 2016). During the explanation of radiographic noise, two terms should be clarified: absolute noise and relative noise. The term noise is commonly utilised to describe both quantities, (relative and absolute). Relative noise represents the amount of image changes relevant to the signal existing in the image; for instance, it is equal pixel standard deviation divided by mean signal. Relative noise represents the relevant factor in the detection of lesions. When unqualified, the term noise is predominantly referring to relative noise whilst absolute noise is referring to the absolute amount of changes within the image, which equals pixel standard deviation (Samei, 2003).

3.7.2.4 Contrast

Contrast is an important measurement of the diagnostic ability of a device. SNR and CNR are standard measurements used to characterise this within the clinical evaluation of images and in quality control. They refer to the variance in signal amplitude between the lesion and the background (Michaelson et al., 2003). Both SNR and CNR are utilised as an objective measure of the image quality. Calculations are made based on the signal of the abnormality and the signal of the surrounding regions; this data is then utilised to measure either the SNR or the CNR.

Chapter Four: Methodology

4.1 Chapter Overview

This chapter gives an overview of methods used in the thesis. The chapter commences by outlining the design of the free-response study and how simulated motion blur was applied to the FFDM images. The study comprised of 8 logical steps, using five different software applications; each having a specific function in the study.

Step 1: Image selection- In the first step it was necessary to identify a selection of suitable FFDM mammography images with half of them containing disease (malignant mass or microcalcification) and the remaining half being disease free. The cases were selected via a retrospective review of 420 cases from a single UK Hospital Trust.

Step 2: Image assessment- The selected images were assessed by an experienced reporting consultant radiographer with two purposes in mind (i) to ensure that the images were free from motion blur, and (ii) to confirm the precise anatomical location of all malignant lesions.

Step 3: Applying and validating simulated motion blur- Novel mathematical simulation software was used to mimic the effect of blurring produced by breast movement during image acquisition. Different magnitudes of simulated blurring were applied to the images. A face validity check was performed with 8 mammography practitioners. This was done to establish whether a difference in appearance could be detected between simulated blur and real blur.

Step 4: Observer performance study- The design of the free-response study gave due consideration to sample size, in order to produce a statistically powerful outcome. Other aspects to consider included data collection, monitor specification, ambient lighting, fatigue, case memory, training, the truth status (location of disease) of the images, and the acceptable level of error for localisation.

Step 5: Statistical analysis- Data analysis of free-response data was performed using Rjafroc (Chakraborty and Zhai, 2015); where I also used alternative FOMs to provide values of sensitivity (FOM = HrSe) and specificity (FOM = HrSp). A method is also described for combining data to represent the dual reporting that occurs in clinical practice in the UK.

Step 6: Lesion conspicuity (Masses) - Conspicuity software was used examine the physical parameters of malignant lesions; this included the conspicuity index, edge angle, contrast, and

SNR. The objective is to identify a relationship between physical parameters, lesion detectability, and the impact of different magnitudes of simulated blurring.

Step 7: Dispersion Index (Microcalcifications)- It is not possible to evaluate conspicuity for very small objects. A Dispersion Index (DI) is proposed to evaluate the detectability of microcalcifications: this accounts for the spread of microcalcifications (units of distance), contrast, and SNR.

Step 8: Missed lesion analysis- This was completed in an attempt to establish a reason why observers failed to detect lesions, and where the changes in detection occurred because of image blurring. The following question was posed: What affects the ability of the observer to differentiate/characterise lesions into benign and malignant categories? The method for this thesis is summarised into the following steps (**Figure 4.1**).

Figure 4.1 Key Steps within thesis methodology

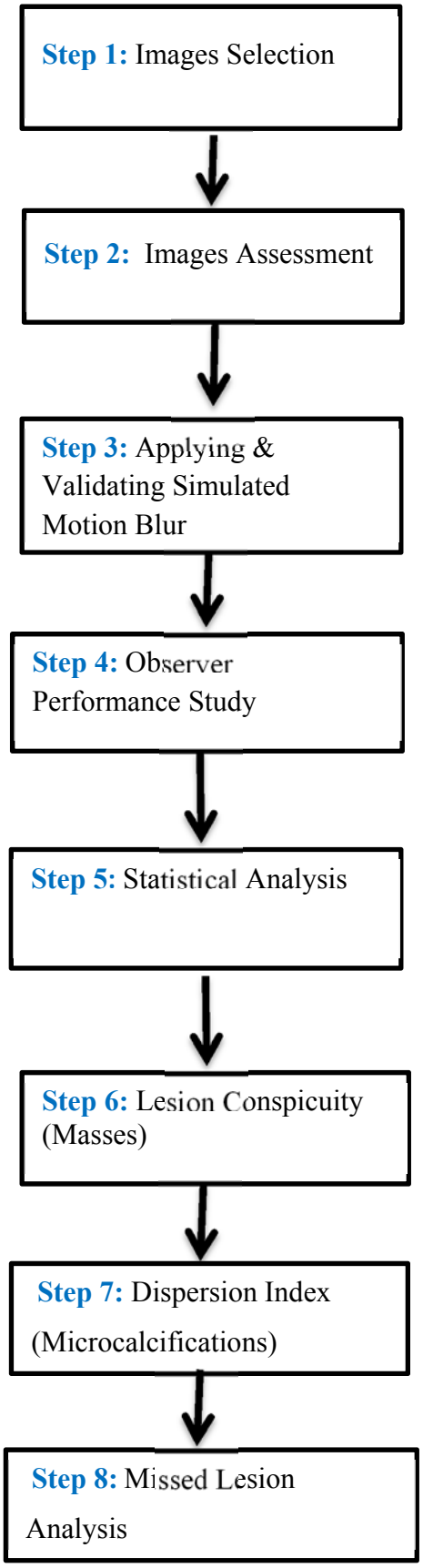

4.2 Step 1: Image Selection

In total, 420 retrospective cases were provided by *the Predicting of Cancer at Screening (PROCAS)* data set under the supervision of a Hospital Trust; ethical approval was granted via organisational management consent (Appendices A, B & C). Each case included four images (Right and Left CC and MLO), 150 of these cases were classified as normal and 270 cases were reported as abnormal and contained biopsy proven cancers. The abnormal cases were further classified into microcalcifications (120 cases) and masses (150 cases). All abnormal cases were evaluated by a reporting consultant radiographer with 17 years reporting experience to confirm the presence and precise location and disease and to determine (i) the distribution of different types of breast cancer (according to shape, size, and distribution) and (ii) breast density within this sample. The Breast Imaging-Reporting and Data System (BI-RADS) was used to categorise cancers by shape, distribution, and size of lesion. This reporting consultant radiographer also assessed the images to ensure that they were free from motion blur. Tables of the Collected Data (see section 4.12) demonstrate the features mammographic images (view of image, breast density, and number of lesion per image). The characteristics of malignant breast masses with different shapes of margins, lesions' BI-RADS and sizes of lesions are presented in (**Appendix G**).

The GE Seno Essential FFDM system was used to acquire images for all the cases in the PROCAS dataset. This FFDM unit has a 23x19.2 cm^2 field of view, alpha-Si flat panel coupled with a CsI (Tl) scintillator image receptor with 100-micron pixel size and spatial resolution of 7.1 lp/mm; this conforms to the standards of the UK Breast Screening Programme. This system was operating within the NHSBSP quality assurance guidelines for mammography quality control in the UK (NHSBSP Publication No 60, 2005; NHSBSP Publication No 63, 2006; NHSBSP Publication No 59, 2011). The working principle of the FFDM machine has been discussed in Chapter 2.

4.3 Step 2: Image Assessment

The normal images were previously formally reviewed and identified as normal through the standard NHS Breast Screening Programme double reading process by two breast imaging professionals. In addition, two different breast imaging professionals verified the images were correctly classified as normal. The verification task was conducted with ambient lighting levels set to less than 10 lux, being similar to hospital reporting rooms.

Artefact-free mammographic images were selected from a set of FFDM images. The images were assessed visually to ensure that all anatomical structures had distinct /sharp edges. Two clinicians classified the images and then subdivided according to the following criteria:

a) Type of lesion (malignant microcalcification and malignant masses)
b) Lesion localisation (determining the location of the lesion within the breast and marking the lesion)
c) Denoting whether the image is sharp/unsharp (free of motion blur or not)
d) Identifying lesion size (measurement the size and create the acceptance radius).
e) Determining the lesion BI-RADS according to suspicion suspicious of malignancy of breast lesion.
f) The breast density: the images were subdivided into four groups according to BI-RADS.

When denoting whether the image was sharp or unsharp the two clinicians took the following into consideration (Taplin et al. 2002; European Commission 1996):

a) Visualisation of pectoral muscle margin fibrous strands and all vessels should be sharp (absence of movement)
b) Visually sharp medial breast tissue and lateral glandular tissue.
c) Visualisation of skin structure along the pectoral muscles should be sharp.
d) Visualisation of the retroglandular fat tissue and skin outline should be sharp.

4.4 Step 3: Applying & Validating Simulated Motion Blur

A mathematical model was used to simulate motion in the FFDM images (Ma et al., 2015). Simulated motion blur was applied using a convolution mask that provided a 3 standard deviation (3SD) distribution of blur over the desired blur radius. The 3SD range is consistent with the application of a Gaussian blur mask, typically used to generate generic blur effects (equivalent to a semi-transparent film being placed over an image). However, the Gaussian distribution profile did not match the characteristics of a typical blur effect. To determine an appropriate blur distribution function a simulation of image pixel motion, under elastic restitution, was made. This allowed an individual pixel to be displaced by a random vector (within the range of the blur effect) and the pixel contribution to the overall image sampled by sub-steps, as the pixel returned to the central position. Sampling of the motion pixel was enacted as a pixel sized Gaussian distribution within a super-sampled image frame to allow for

fractional motion within each sub-step. Repeated iterations of this process enabled a representative distribution profile to be generated that showed a sharper central peak, more rapid initial distribution decay, and longer continuation, than with a traditional Gaussian function. Multiple applications of the simulation were made to define an average distribution function. To ensure that the intensity window of the pixel values remained the same after blurring, the pre-blurring minimum and maximum pixel intensities were corrected post-blurring through intensity scale and shift.

Ma et al. (2014) suggested that paddle motion could be one source of motion blur. They concluded that the extent of paddle motion, through acquisition of mammographic images, could be as much as 1.5 mm in the vertical plane. Ma et al. (2015) illustrated that simulated motion blur at 0.7 mm is the minimum amount of simulated breast movement required for visual detection of blurring. Therefore, the minimum and maximum visual levels for blurring were selected as 0.7mm and 1.5mm respectively. **Figure 4.2** shows an example of FFDM images, with and without simulated blur imposed.

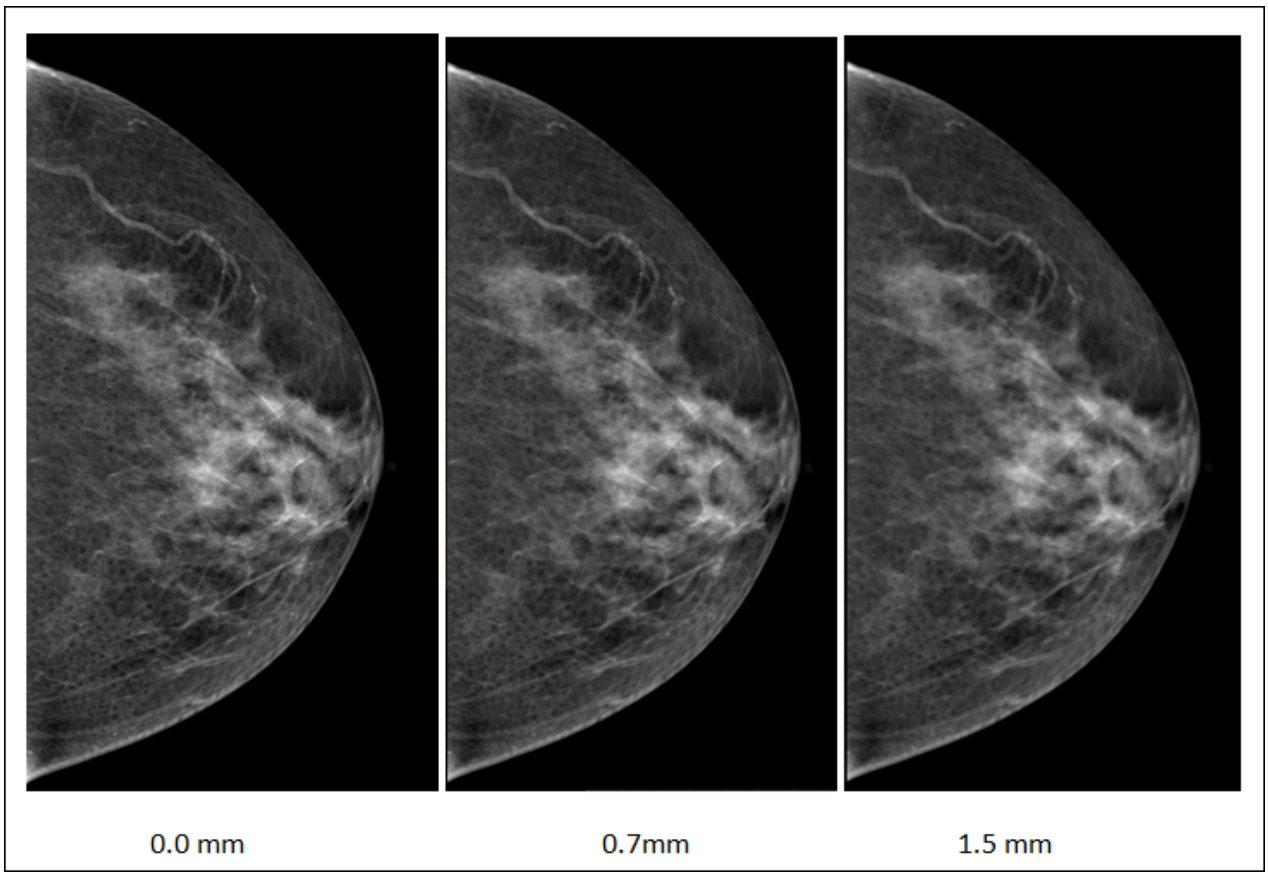

Figure 4.2 Example of FFDM images with two levels of simulated blur and without simulated blur

4.4.1 The Convolution-based Operations and Blurring masks

The fundamental process in image processing is a digital convolution in the spatial domain and is utilised to either sharpen or smooth an image. It includes a "shift" and a "sum-of-products" operation. The main concept is that a kernel or *mask*, principally a matrix of k × k elements, is rotated by 180° and animated in a bitmap model across an input image of M×M pixels; k is normally an odd integer, considerably lesser than the linear size of the image. Every pixel of the output image is the weighted sum of the input pixels within an area known via the mask, with the elements of the mask which set the weights (Tobergte & Curtis, 2013).

When the input image is F (of size M×M), and the convolution mask is H (size k × k), the output image G is given by:

$$G = F * H \quad \ldots\ldots\ldots\ldots \quad (4.1)$$

The above mathematical process is demonstrated in **Figure 4.3**. The mask is rotated by 180° and is placed on top of the input image beginning at the upper left position. The mask components are doubled by the corresponding pixel value in the image beneath and the outputs are summed and normalised to create a measured restraint, which is the value of the product pixel at the placement congruous to the middle of the mask. Nearly all the mask ***k*** is selected to be odd so that the middle of the mask is readily visible. After that, the mask is moved one place to the right, the total of products re-studied and normalised to show the following pixel amount in the production image. This operation is reduplicated as the mask is passed towards the inserted image in a raster scan (Tobergte & Curtis, 2013).

Predominantly, the "sum-of-products" formulation can result in pixel overflow. Normalisation, by dividing the total of the mask components, produces a weighted response that stays within the initial range of pixel values in the input image. The product of output image pixels predominantly have non-integral values. Therefore, working with floating-point numbers is important to avoid "round-off" errors (Young et al., 2008).

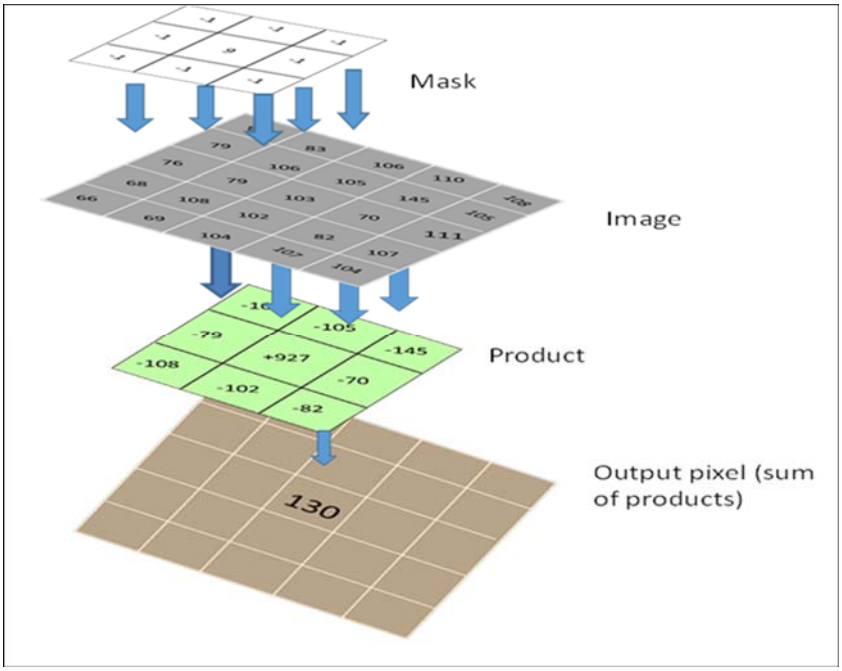

Figure 4.3 Digital convolution: the mask is put on the original image, mask components are multiplied pixel values, and the outcomes added to form an output pixel (Tobergte & Curtis 2013).

The primary rotation of the mask through 180° is not obvious when the mask is circularly symmetric, as it is for several common masks utilised in sharpening and smoothing. However, this is not usually the case for the masks utilised in locating vertical and horizontal edges in an image. This initial rotation is what distinguishes correlation from convolution. The cross-correlation includes two images that are approximately similar sizes, while the sum of product, scanning and replacement processes happens without the initial 180° rotation. The outcomes of the cross-correlation function are utilised predominantly for locating the characteristics of one image that appears in another and can be utilised for registering or aligning images.

Gedraite & Hadad, (2011) and Fallis, (2013) demonstrated that the pixels surrounding the boundaries of the input image have deficiency a full series of neighbours. For convolution with a 3 × 3 mask this includes pixels in a boundary one pixel wide surrounding the input image, while for convolution with a 5 × 5 mask, the boundaries are two pixels wide, and so on. It is not an important problem if k is much smaller than M. It can be alleviated through extending image (A) using different techniques such as repeating its boundary pixels, or stuffing it out with zeroes or considering that the input image wraps surround the vertical and horizontal trends (cyclic convolution). The complexity calculation for the convolution of an image of M×M pixels with a mask of size k × k is the organisation of k 2 per pixel, according to the

number of multiply and-adds (MADDs). This can lead to problems for big masks, like this alternative process to convolution utilising calculations within the spatial frequency field. Gaussian blurring is commonly utilised in graphics software to change image quality and to reduce fine detail and image noise. However, the simulated motion blur in this thesis is based on a real motion of the subject through the capture time of the pixel. Therefore, it is not appropriate to replicate the features of blur viewed in this type of image (Ma et al., 2015).
Despite the convolution mask utilised in the Gaussian blurring method, the same magnitude of simulated motion blur is used as with the soft edge method, it is creates a larger distribution of the pixel intensity through a more gradual spread of the function within the specific motion. The simulation technique, which has been implemented by replicating the motion of the subject as a stochastic sampling procedure, illustrates that the profile of distribution within a motion-based blur is described by a function in which the intensity drop-off is much more rapid (Ma et al., 2015). This shows that the same level of simulated motion applied by a Gaussian-based function produces a larger level of visual blur than the estimated mask used in this thesis proposes. This explains the reason why the human visual system is more sensitive to the Gaussian blurring method at smaller magnitudes.

The visual impact of the smooth blur of the Gaussian technique is similar to displaying the image using a translucent screen (Yap et al., 2003). On the other hand, computer vision algorithms use Gaussian smoothing as a pre-processing stage to enhance image constructs at different scales (Yap et al., 2003). Applying the Gaussian blur to an image mathematically is similar to convolving the image with a Gaussian function. **Figure 4.4** shows a wireframe image of two-dimensional Gaussian function (Ma et al., 2015). It has the impact of decreasing the high-frequency of image structures; therefore, a Gaussian blur acts as a low pass filter (Waltz & Miller, 1998).

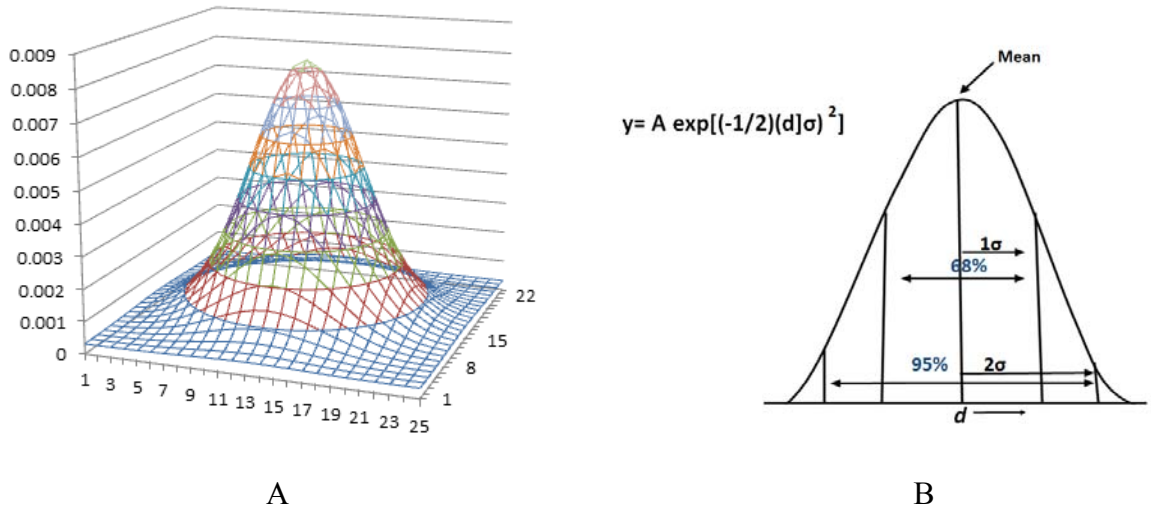

A B

Figure 4.4 (A) Demonstrates wireframe image of two-dimensional Gaussian (Ma et al., 2015) (B) Demonstrates Gaussian profile (one-dimensional) (Tobergte & Curtis, 2013)

A simple example of the smoothing process is that of neighbourhood averaging; this means that every pixel in the output image is created from the average of the pixel values in a region around the pixel in the input image at that location. The mask that implements this is a k × k mask, with all coefficients equal to unity (**Figure 4.5** (i) and (ii)) acting as constant pre-multiplier of $1/k_2$; it is known as an averaging or box mask. The averaging procedure decreases the abrupt differences in local pixel values, smoothing the input image by decreasing its noise. A reduced smoothing effect can be obtained by utilising a weighted-average mask (**Figure 4.5**(iii)).

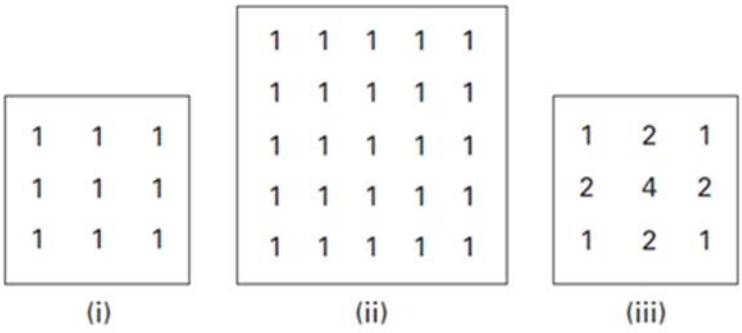

Figure 4.5 Shows different convolution masks; (i) averaging mask (3x3); (ii) averaging mask (5x5); (iii) weighted-average mask (3x3) (Tobergte & Curtis, 2013).

According to Fallis (2013), the fact that the averaging mask blurs the edges in an image is a significant drawback. However, smoothing an image can minimise the signal-to-noise ratio and shift the grey-level histogram of the images. Therefore, there are many advantages of this

operation. One function of smoothing is to blur out features smaller than the mask. In addition, smoothing can be helpful as a precursor to segmentation of an image into a region of interest. Furthermore, it can be utilised as a mask to smooth out the false contours that can happen in images obtained with an inadequate number of grey levels. In practice, the size of the mask, k, must be larger than or equal to 2w + 1 when characteristics of diameter (w) are to be blurred out; k must be lesser or equal to 2w − 1 when characteristics like these are to be retained while decreasing the overall noise.

The novel motion simulation software used in this thesis can be applied with 15 magnitudes, from 0.0 to 1.5 mm stepping through 0.1 mm increments. This produces a total of 15 images with different magnitudes of blur from each original image (no blur). Simulated motion blur was achieved mathematically via the accumulated pixel points moving randomly. The simulated motion blur software can add blurring equivalents to the actual motion to the mammographic images. This blurring has been created using image processing techniques to produce soft edge mask estimation (Dougherty, 2009).

4.4.2 Validation Method for Simulated Motion Blur Software

Simulated blur has been used as it is extremely difficult to control and/or measure sub-millimetre movement of the breast during mammography in a physical study. Attempting to replicate motion in patients at the point of imaging would result in an unwanted and unethical increase in radiation dose. Since simulation was being performed, it was important to ensure that simulated motion blur gave the same appearance as real blur. A validation check was performed with 8 mammography practitioners who had been trained to recognise the appearance of real blur. The practitioners comprised mammography qualified radiographers, ranging from basic grade through advanced practitioner to consultant level. A forced choice study was prepared to evaluate the performance of practitioners in recognising simulated blur, and thus indicating the overall success of the procedure to simulate motion blur. The practitioners were informed that all images contained blur; either real or simulated and that they must decide which was present.

Twenty images containing real blur and 20 images containing simulated blur were shown to the 8 practitioners in a different randomised order. The twenty images containing real blur had been selected by an expert in mammography reporting. These images contained a range of magnitudes of real blur, affecting different image features, including breasts of different shapes

and density. The twenty images containing simulated blur had two magnitudes of simulated blurring (10 at 0.7mm and 10 at 1.5mm). For images containing simulated blurring the average incorrect rate was 34% (SD=13.8); for real blur, the average incorrect rate was 34% (SD=20). The incorrect rate refers to the proportion of images incorrectly identified as either real blur or simulated blur. On this basis, it can be proposed that the visual appearance of simulated blur to be comparable to that of a real blur.

4.5 Step 4: Observer Performance Study

The free-response receiver operating characteristic (FROC) method has been determined to be the appropriate method as it accounts for the precise localisation of lesions and can deal with multiple decisions (localisations) per case. This is an advantage over traditional ROC methods that only permit a single rating to be applied to each case and do not distinguish between correct and incorrect identifications of pathology on abnormal cases. Several previous studies have applied FROC methods in detection studies in mammography (Obuchowski et al., 2000; Chakraborty & Berbaum, 2004; Bator & Chmielewski, 2008; Chakraborty, 2011; Biltawi, Al-Najdawi & Tedmori, 2012; Zanca et al., 2012). In an FROC study the observer is instructed to localise all suspicious areas of the image, as defined by the task. In this thesis the observers are instructed to localise all lesions (masses or microcalcifications) that they believe may be malignant. For each localisation, the observers are required to provide a confidence rating. The higher the level of suspicion of malignancy, the higher the rating. The lower end of the rating scale can be used for lesions where the observer is unsure if the lesion is benign or malignant.

One of the most important aspects of an observer study is to ensure that there is sufficient statistical power to ensure that the results of the study are meaningful. This requires a statistical power calculation based on several different criteria relating to the design of the study. Fortunately, this process has been made relatively straightforward with sample size estimation tables provided by Obuchowski (Obuchowski, 2000).The sample size calculation in this thesis was based on recruiting a minimum of 6 observers. All observers participate in the NHSBSP approved biannual external audit which evaluates their performance for difficult cases specifically selected by expert radiologists (Wivell et al., 2003; Van den Biggelaar et al., 2008). Local Directors of screenings would be notified of any outliers regarding poor performance. One of the difficulties in an observer study is getting the balance between a sufficient number

of abnormal cases to test the intervention proposed (in this case simulated motion blur) against the prevalence of disease in a clinical situation. It is nearly impossible to accurately represent the reality of a screening population, where the prevalence of disease is extremely low. The burden on the group of observers would be too high when trying to get a meaningful evaluation of detection performance in the presence of simulated blur. The primary outcome of the study is not to evaluate the performance of individual practitioners, but to test the impact of simulated blurring. This is a key concept to remember.

It was decided that a 50:50 ratio of normal-to-abnormal images would be selected. This would ensure adequate variation in the type of lesion and the density of the breast. In total, 124 cases (62 normal, 62 abnormal) were selected for the evaluation of masses and the same number for microcalcifications. These would be displayed to each observer in the following three conditions (i) no simulated blur (0 mm) and two magnitudes of simulated blurring, (ii) 0.7 mm and, (iii) 1.5 mm. Overall, this would require three image evaluations, assessing 248 images on each occasion. These were reviewed visually to identify a range of BIRADS density grades and to ensure that the cases did not contain blurring. Cases were chosen from a bank of 300 to ensure a representative distribution of breast density (A=10%, B=40%, C=40%, D=10%) while also excluding cases where the pathology was too obvious to control difficulty and also excluding cases that contained artefacts other than blurring. **Table (4.1)** shows the number of cases used, with the normal distribution of population breast density.

Table 4.1 Demonstrates the sample size of the images and the number of the observers with the normal distribution of the population of breast density for this study.

Number of observers	Number of images	NO. OF Images	Total sample size	Breast density	
7	62 normal	62 breast masses	124	A	12
				B	50
				C	50
				D	12
7	62 normal	62 single calcification	124	A	12
				B	50
				C	50
				D	12

It would have been acceptable to have one single set of normal images which could have been used in both FROC studies. However, a decision was taken to use two separate sets of normal images. This increased case variation which made for a study which more closely simulated clinical routine in breast screening. Microcalcifications and masses could have been included as one large dataset and then that dataset could have been split into two sub-sets for the observer study. This approach would have achieved the same outcome as the use of one dataset for micro calcifications and one for masses, however it was hypothesised that simulated image blurring may have a different impact on micocalcification and masses. Therefore, a decision was taken to separate the images into masses and microcalficiations dataset. Furthermore, the use of separate masses and microcalcifications datasets allowed for easier display and analysis. Importantly, observers were blinded to what the case mix was, in terms of microcalcifications and masses, and they did not know whether they were looking for microcalcifications or masses.

The following factors were taken into account during the design of the protocol in order to reduce error and minimise unwanted variation. To minimise the influence of inter-observer variation, seven observers (advanced and consultant radiography mammography practitioners) with approximately similar years of experience (average 10 years' experience reporting mammograms) participated in the study. The purpose of performing a multi-reader multi-case (MRMC) study is to decrease the effect of observer experience and variance in the difficulty of the interpreted images such that any observed variance between the compared modalities (magnitudes of simulated blurring) is not masked (Chakraborty, 2011b). The environment where image viewing occurs makes a contribution to the overall accuracy of the procedure (Gur et al., 2003). Viewing conditions were therefore carefully controlled, with ambient lighting set to be lower than 10 lux for all image evaluations. A 5-megapixel grey-scale reporting grade monitor (2560x2048, 21.3"EIZO RadiForce GS521-CL-LCD, 12-bit) was used to view the mammographic images for all aspects of the work (case selection, validation of simulated blurring, observer study). The monitor was calibrated prior to each image evaluation to the digital imaging and communications in medicine (DICOM) greyscale standard display function (GSDF) standard (Wilson et al., 2011). The images were presented in a random order to observers for both microcalcification and masses datasets. Observers were also blinded to the proportion / number of confirmed cancer cases within each dataset, whether blurring was

present or whether they were looking for microcalcifications or masses. ROCView (Thompson et al., 2012) was used for image display and recording of free-response data.

For the observer study, it is necessary to mark the true location of lesions (masses and microcalcifications) in each abnormal case. This was done using the data provided by the experienced image reader, as described in Step 1. This localisation data is saved in a database in ROCView and all subsequent localisations made by the observers are compared to these marks. The marks made by the observers are classified as true (lesion localisation, LL) or false (non-lesion localisation, NL) by a proximity criterion, which in this case is an acceptance radius. The size of the acceptance radius has been determined by the size of the masses or the spread of the cluster of microcalcifications. The acceptance radius, was based on the largest lesion size (Chakraborty, 2011; Haygood et al., 2012) emanate from the centre of the lesion. The acceptance radius was set at 42 pixels (11 mm) for masses and 50 pixels (13 mm) for microcalcifications. This was based on measurements made in ImageJ (Schindelin et al., 2012).

If the localisation made by the observer is within the acceptance radius emanating from the centre of the true lesion, then the localisation will be considered as LL; otherwise it will be considered NL. All LL marks are stored in a database that indicates the observer number, modality (magnitude of simulated blurring), case number, lesion number, and the rating (confidence). All NL marks are stored in a separate database that indicates the observer number, modality, case number, and rating. Notice that there is no lesion number for the NL database as these all represent incorrect localisations, where no real lesion is present.

The aims and objectives of the study were explained to all observers (Appendix H); those who agreed to take part were trained to use the software and how to using the rating scale to assign a confidence rating to localisation. Prior to their first evaluation, a 5-minute presentation was given to explain the difference between a mammographic report and the FROC study, and what was required from the observer. The observers were then able to familiarise themselves with the software and task with a training dataset of 15 cases, that were not used in the main study. The cases included different lesion types and different magnitudes of simulated blurring.

Each abnormal image contained 1 or more lesions. The observers were asked to localise any areas of the image that they thought were suspicious of malignancy and then rate their suspicion of malignancy using a confidence scale. **Figure 4.6** (A&B) demonstrates a mammographic image containing a malignant mass and demonstrates a scoring with a high level of confidence.

(A)The main image (scaled) demonstrates a mark that prompted the confidence scale to appear. (B) The image in the top right hand corner of the screen shows the main image at 100% size, without observer marks for a re-evaluation of uncertain areas.

Figure 4.6 Screenshot of ROCView

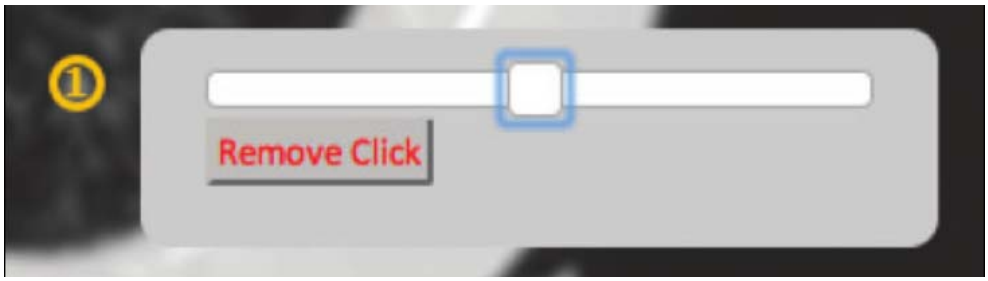

Figure 4. 6 (C) Confidence scale variant.

Figure 4.6 (C) demonstrates the confidence scale variant. The observer clicks the mouse and the slider bar appears; the observer then rates their confidence from relatively low (left side of the bar) to high (right side of the bar) and can leave the cursor at any point in between these two points. A minimum period of 2-weeks was imposed between image evaluations to reduce the influence of case memory. Each observer completed the evaluations (0 mm, 0.7 mm, and 1.5 mm) in a different order to reduce the dependence of evaluation order on the overall figure of merit (FOM). Observers interpreting the images then marked the suspicious locations in the image (**Figure 4.7**); the marked locations were checked against the true locations using the acceptance radius within ROCView. The raw data was then automatically collected into a log

file and exported to MS Excel, where it was transformed and saved as a text file to be analysed by the JAFROC software. In this way, the data was analysed very shortly after its production.

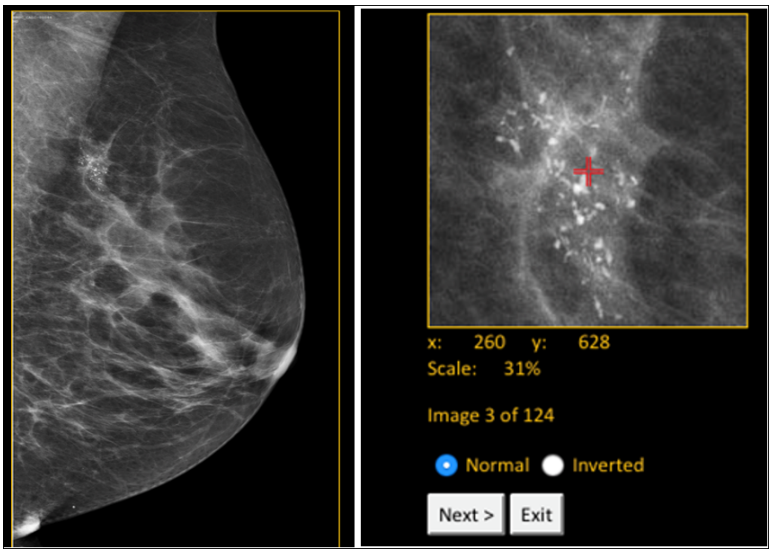

Figure 4.7 A mammographic image containing malignant clustered microcalcification and the mark placed in the centre of the clusters using ROCView software.

4.6 Step 5: Statistical Analysis

The equally weighted jackknife alternative free-response receiver operating characteristic (wJAFROC) figure of merit (FOM) defines the empirical weighted probability that a lesion rating (LL) is rated higher than a non-lesion rating (NL) on a normal case (Chakraborty & Berbaum, 2004). The wJAFROC FOM is the equivalent to the trapezoidal area under the wAFROC curve. Chakraborty et al., (2006) demonstrated that the statistical power of JAFROC is greater than the statistical ability of the previous ROC methods. JAFROC has been developed as a solution to the analysis of MRMC data when it is desirable to account for the precise localisation of pathology. The statistical power of the JAFROC analysis method can be measured by d-parameter. A low d-value means that it is comparatively difficult to identify a difference between two technique conditions while a high d-value is considered relatively easy to detect a contrast between each status (Chakraborty & Yoon, 2008). The statistical power of diagnostic performance of JAFROC analysis is increased according to the sample size, and this is something that does not happen with ROC. The JAFROC method requires an accurate response from the observer, which includes *mark-rating* of confidence information and lesion localisation for each suspicious lesion in the image (Zanca et al., 2012). The wAFROC curve

is determined as the plot of lesion localisation fraction (LLF) vs false positive fraction (FPF) plus a straight-line segment linking the uppermost operating point to (1, 1).

4.6.1 Data Analysis for Single Observer Free-response Method

Data analysis was performed using Rjafroc (Chakraborty & Zhai, 2015) where alternative FOMs were used to provide values of sensitivity (FOM = HrSe) and specificity (FOM = HrSp). Test alpha was set at 0.05 to control the probability of Type I error. The calculation of wJAFROC FOM is performed to reward true lesion localisations and penalise incorrect lesion localisations. It provides a single value summarising performance of single observer which can be compared statistically. For example, comparing two magnitudes of simulated blurring one calculates a FOM for each method and a statistical test is performed to identify the difference between the two FOMs. When the difference is large enough to be different in consideration of the pre-test value of alpha (0.05), then there is a statistical difference, if the result of the overall F-test is also significant (Chakraborty, 2011). The result of the overall F-test and the 95% confidence interval (CI) of each pair of modalities must not include zero for a difference in detection performance to be considered significant. The F-statistics, the denominator degree of freedom (the numerator degree of freedom was always one) and the p-values. The observer averaged FOM and 95% CI will be reported for all magnitudes of simulated blurring.

4.6.2 Data Analysis for Combined Observer Data Method

The double reporting method in screening mammography involves two observers interpreting the same case independently (Taplin et al., 2000). The aim of the double method is to analyse the combined two observers' reports in the same process in clinical practice (Tanaka et al., 2015). Consequently, additional analysis method was conducted utilising the same data from FROC study obtained (248 cases) to determine the benefit of double reporting on lesion detection performance in sharp and blurred FFDM images. In this analysis method, the simulated double reporting evaluations were conducted by performing a comparison between free-response data from one observer, with combined free-response data from two observers. This is a secondary analysis of data from a first free response study which evaluates the impact of simulated motion blur on observer performance. The single observer analysis demonstrated a detrimental effect of simulated motion blur on the detection of masses and microcalcifications for the sample of seven observers. Secondary analysis of data was deemed important partly 'mimic' this combined data result.

The observer study was split into two components: the evaluation of (i) microcalcifications and (ii) masses. Seven observers (15±5 years' clinical reporting experience in mammography) have previously evaluated images with no simulated blurring (0 mm), and with 0.7 and 1.5 mm of simulate blurring. These have acted as the distinct modalities (1st, 2nd, and 3rd) that were compared statistically. In this secondary analysis of data, these three modalities have been combined. The 1st modality in the current work comprises of all observer data created for images of 0.0 mm, 0.7 mm, and 1.5 mm of simulated motion blur for six single observers. The 2nd modality in the current study comprises of the combined observer data for the six single observers with each combined with an additional (seventh) observer. It has used the following rules to combine the data from the free-response study. For lesion localisations (LL) the highest rating for the two observers was adopted, regardless of whether one or both of the observers had successfully localised the lesion. For non-lesion localisations (NL) all unique data was maintained. This follows a similar method to the work of (Tanaka et al., 2015). The overall F-test, p-values for FOM pairs (pairs of motion blur levels), and the observer averaged FOM and 95% confidence interval (CI) of double reporting for each magnitude of simulated motion blur are reported. The F-statistics, the denominator degree of freedom (the numerator degree of freedom was always one) and the p-values are also reported. The rating score in combined two observers' data congruent cases was automatically assigned the highest rating provided by one of the two observers see (**Table 4.2**).

Table 4.2 Shows the single and combined two observers' data assessments and the rating score for each case

	Single observer 1	Single observer 2	Double observer	Rating score
Situation 1	True	True	True	Higher rating adopted
Situation 2	True	False	True	Rating of true observer
Situation 3	False	True	True	Rating of true observer
Situation 4	False	False	Rejected	Rejected

4.7 Step 6: Lesion Conspicuity (Masses)

Measuring the conspicuity of lesions attempts to characterise the visibility of a lesion in terms of the imaging systems diagnostic capabilities, and the lesion structure within the tissue surrounding it (Kundel et al., 1976). The purpose of this method is to identify physical parameters, such as lesion conspicuity, SNR, and lesion edge angle and the relationship they have with detection in the presence of different magnitudes of simulated motion blur. In addition, the behaviour of image blurring software has been evaluated. A new conspicuity software programme and associated Excel spread sheet has been used to perform objective measures of the expected visual detectability of focal breast lesions (masses) (Szczepura & Manning 2016). However, the conspicuity index using this software could not be applied to microcalcifications due to their individual size and their wide distribution pattern.

Manning and Ethell, (2002) initially suggested a procedure to evaluate lesion conspicuity; this method combines the factors that define conspicuity into a single equation (Manning et al., 2002). The conspicuity equation, which takes into consideration all factors that influence conspicuity of a lesion, depends on the appearance of the image characteristic to the visual system. Line profiles were built around a lesion, covering the immediate surrounding background and the equation for conspicuity measure was developed, and can be given by:

$$\chi = \frac{d\tan[\theta-1]\Delta GL}{\sqrt{\sigma_s^2+\sigma_n^2}} \quad \ldots\ldots\ldots\ldots\ldots\ldots (4.2)$$

Where:

χ = conspicuity index

d = maximum lesion dimension

θ = is the maximum slope angle to the edge of the lesion profile in degrees

SNR for the nodule $= \Delta GL/\sqrt{\sigma_s^2 + \sigma_n^2}$

σ_s = mean noise within the lesion

σ_n= mean background noise

A study by Manning et al., (2004) used the physical characteristic measurements of the lesions to determine the conspicuity (x) of the nodules and to investigate possible causes of false

detection. The term conspicuity helped to understand why some lesions are missed by the observers (Manning, Ethell & Donovan, 2004a).

This part of the thesis is focused on the physical measures of mammographic images. It utilises a new software implementation by Szczepura and Manning, (2016) for measuring the conspicuity of lesions and other physical parameters, such as edge angles of lesions, contrast and SNR. The method is as follows:

1. A JAVA based programme allows the operator to draw a region of interest (ROI) around a lesion (**Figure 4.8**)
2. Line profiles are then drawn 180° surrounding the area of interest and are extended by one lesion dimension outside the drawn lesion (**Figure 4.8**)
3. A fit is applied for every line profile (**Figure 4.8 and Figure 4.9**) wherein:
    a. The edges of the region of interest drawn by the operator are denoted by green lines
    b. The line profile is denoted by a blue line
    c. The plotted fit is denoted by a red line
4. The regions of interest data sets are stored as TSV files in the same directory as the analysed images
5. The image file name is labelled first, the region of interest second (starting at 0).
6. The data is transferred from the TSV file into the Raw Data worksheet in the Excel spreadsheet.
7. Conspicuity is automatically calculated in the conspicuity index worksheet (**Table 4.3**)

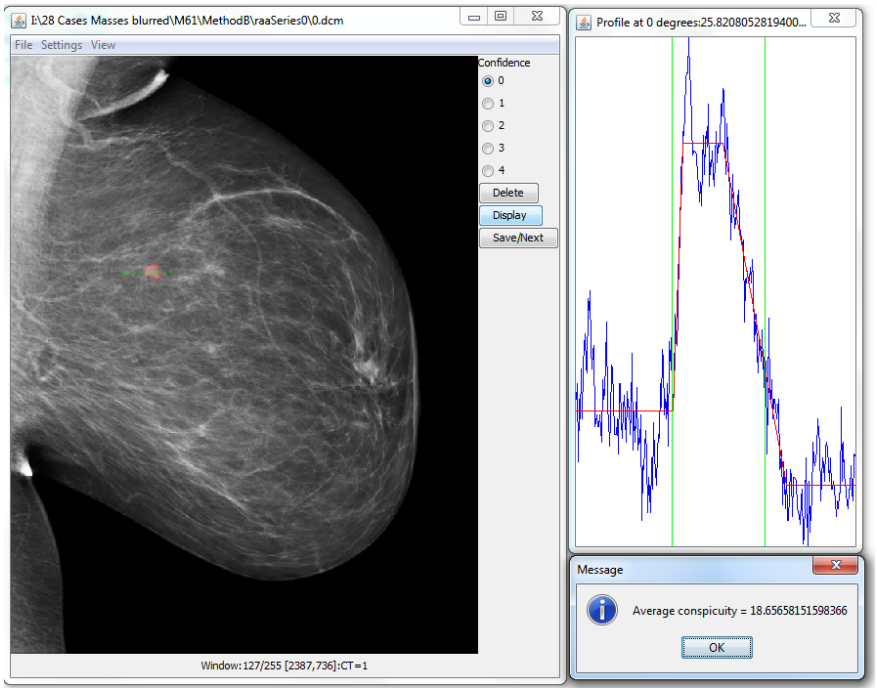

A B

Figure 4.8 The conspicuity software demonstrates the measurement of a breast mass. (A) Demonstrates the first stage through selecting the region of interest while (B) shows the second stage, where line profiles are drawn 180° surrounding the region of interest and are extended one lesion dimension outside the drawn lesion. Only DICOM images can be utilised with this software.

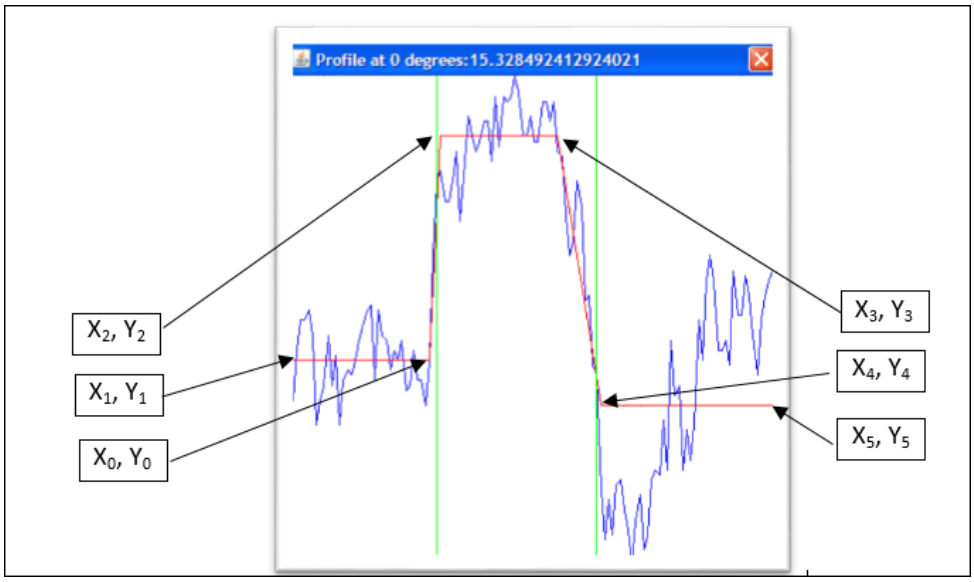

Figure 4.9 Line profiles are drawn 180° surrounding the region of interest.

The X and Y are co-ordinates of each of the plotted fit edges (X_0, Y_0; X_1, Y_1; etc), the standard deviation of the Y values between X_2 & X_3 (SD_{Top}) are utilised to represent the lesion noise

and the standard deviations of the Y values between X_0 & X_1 (SD_1) and X_4 & X_5 (SD_2) are utilised to represent the noise of background.

Table 4.3 Illustrates the physical measures of breast lesion with three levels of simulated motion blur using conspicuity software

Blur Level mm	Conspicuity Index	d (max lesion diameter)	θ (degrees)	ΔGL	σ Lesion	σ Background	μ Lesion	μ Background
	Cases 1							
0.0	51.631	24.450	63.765	88.903	42.734	69.744	192.939	104.036
0.7	66.389	18.589	61.030	93.344	21.061	40.134	194.894	101.550
1.5	74.993	17.133	59.797	93.600	16.109	31.417	194.417	100.817
	Cases 2							
0.0	71.577	42.183	69.151	69.483	60.864	82.009	178.011	108.528
0.7	101.672	39.644	67.259	70.189	34.217	51.973	178.272	108.083
1.5	110.622	38.578	66.415	69.886	27.714	45.491	178.044	108.158

4.8 Step 7: Dispersion Index

The second part of the physical measures analysis in this thesis is focused on the physical features of microcalcifications. ImageJ software was utilised for measuring a new metric, which has been called the Dispersion Index (D.I). Dispersion index of microcalcifications repsesents the number of calcifications within a specified area divided by the area (equation 4.2). DI was measured because the conspicuity index could not be applied to microcalcifications due to their individual size and their wide distribution pattern. This takes into account the contrast of lesions, SNR and D.I. x contrast. The purpose of this method is to demonstrate the relationship between dispersion index, contrast, SNR and lesion detection. The aim was to assess the impact of simulated motion blur on the detection of microcalcifications. The method is as follows:

1. A JAVA based programme (ImageJ) allows the operator to draw a region of interest (ROI) around a cluster of microcalcifications for three levels of simulated motion blur (**Figure 4.10**).

2. The area of a cluster of microcalcifications will be measured using analysis tool manager of imageJ software (**Figure 4.11 A**).

3. The ROI data sets are stored as TSV files in the same directory as the analysed images (**Figure 4.11 B**). After that, the data is transferred from the TSV file into the Raw Data worksheet in the Excel spreadsheet to calculate the dispertion of microcalcifications.

4. The number of microcalcifications per cluster are calculated manually by the operator for each image of with for three conditions: no motion blur (0 mm) and two magnitudes of simulated motion blur 0.7 mm and 1.5 mm (**Figure 4.12**). A quality control test was performed to minimise error on this, two observers have counted them individually and were blinded to each other's answers.

5. Dispersion index, lesion contrast and SNR are automatically calculated in the Excel worksheet (**Table 4.4**).

The equation for the dispersion index measure was used and can be given by:

$$D.I = C/A \quad \text{(4.3)}$$

Where:

D.I = Dispersion Index

C = the number of single calcifications per clustered

A = Area of selected region of interest

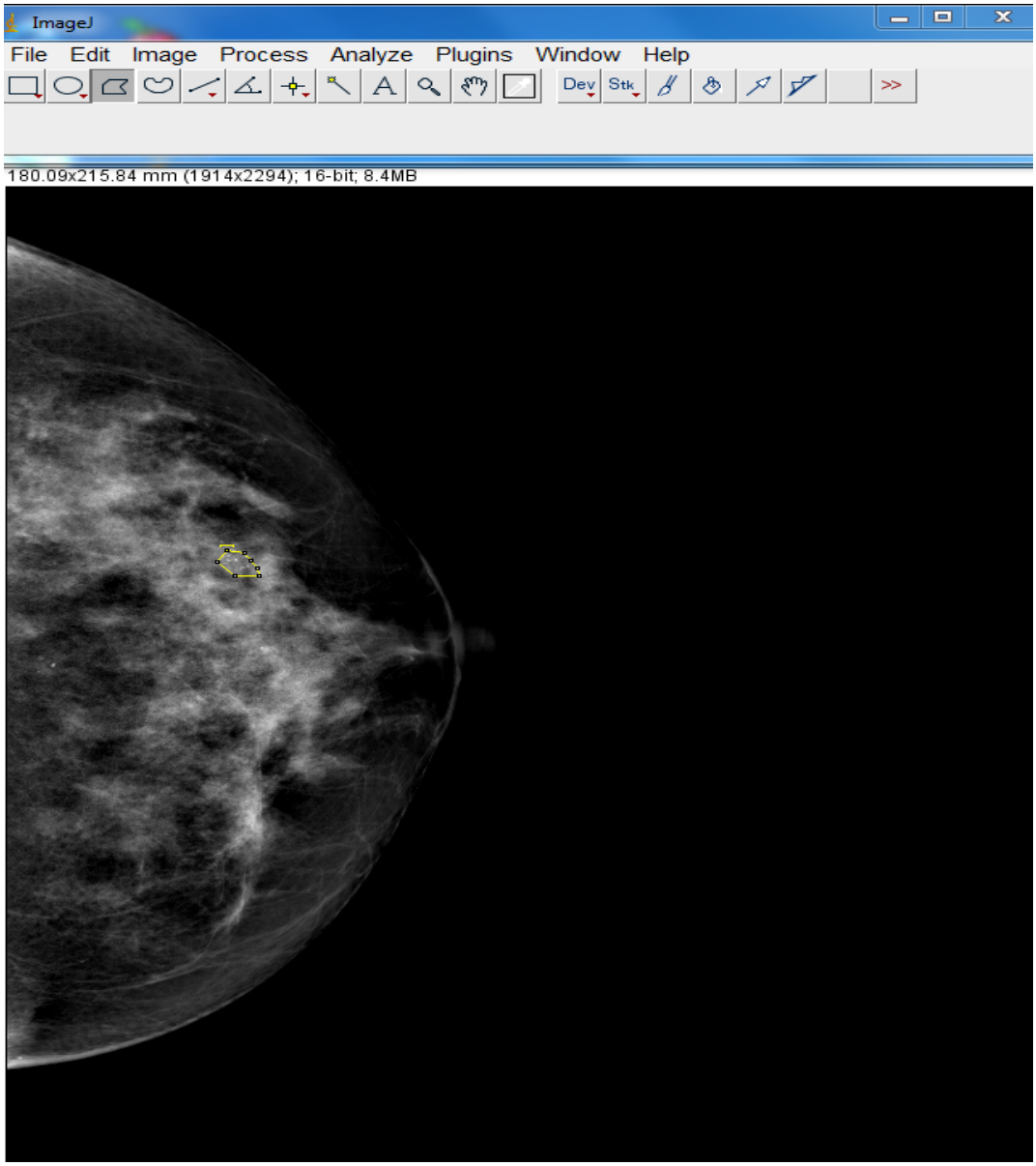

Figure 4.10 The Imagej software demonstrates the measurement of breast microcalcification. Shows the first stage for selecting the region of interest

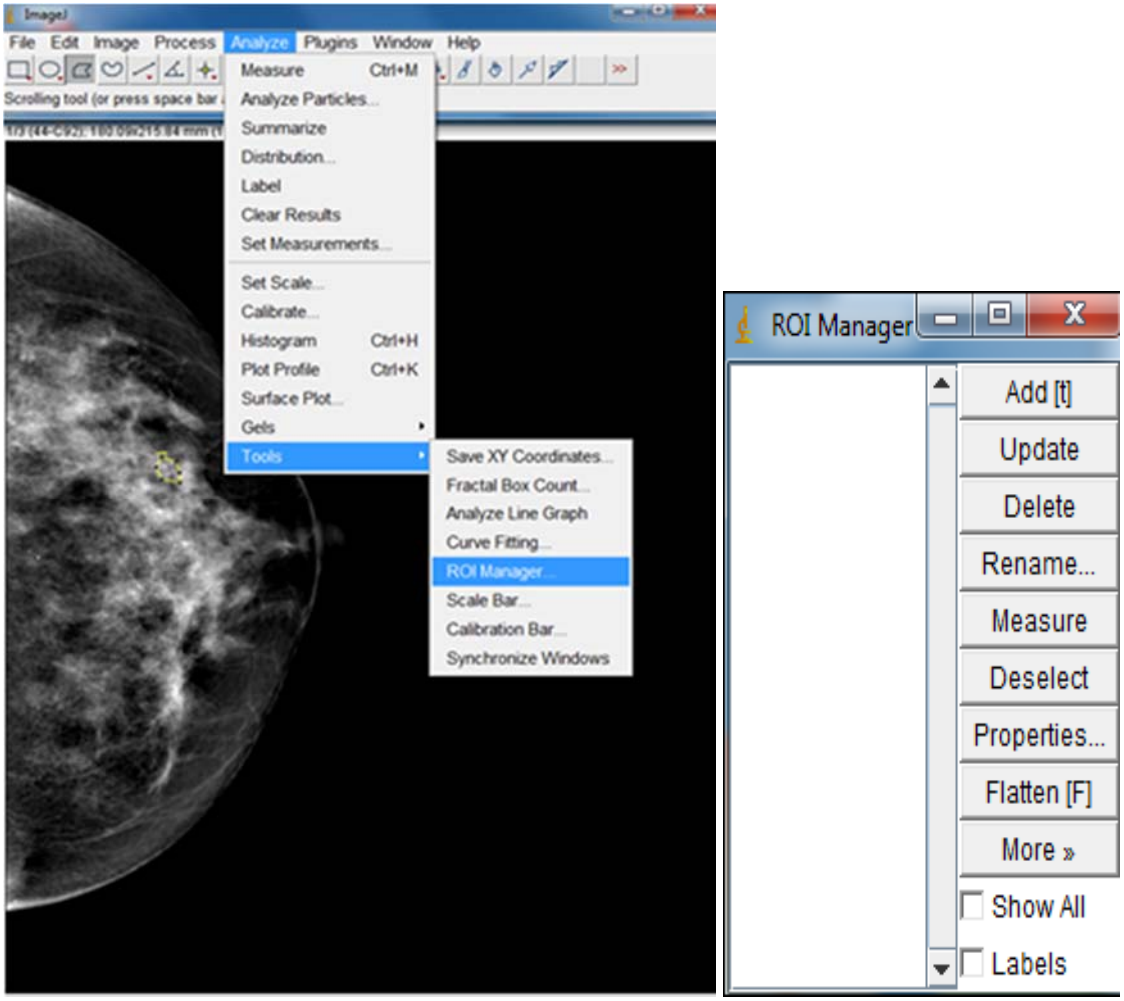

A

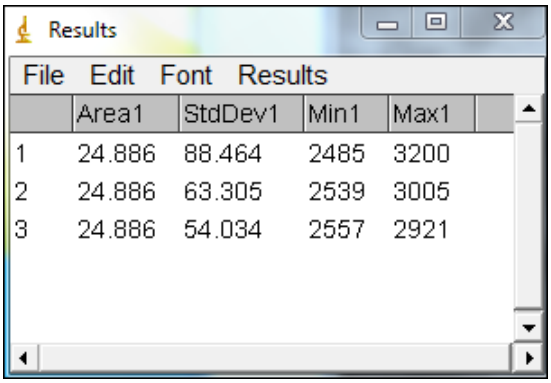

B

Figure 4.11 (A) Demonstrates the step 2 of measurement of breast microcalcification using Imagej software. (B) demonstrates the regions of interest data sets are stored as TSV files in the same directory as the analysed images for three levels of simulated motion blur.

0.0 mm 0.7mm 1.5mm

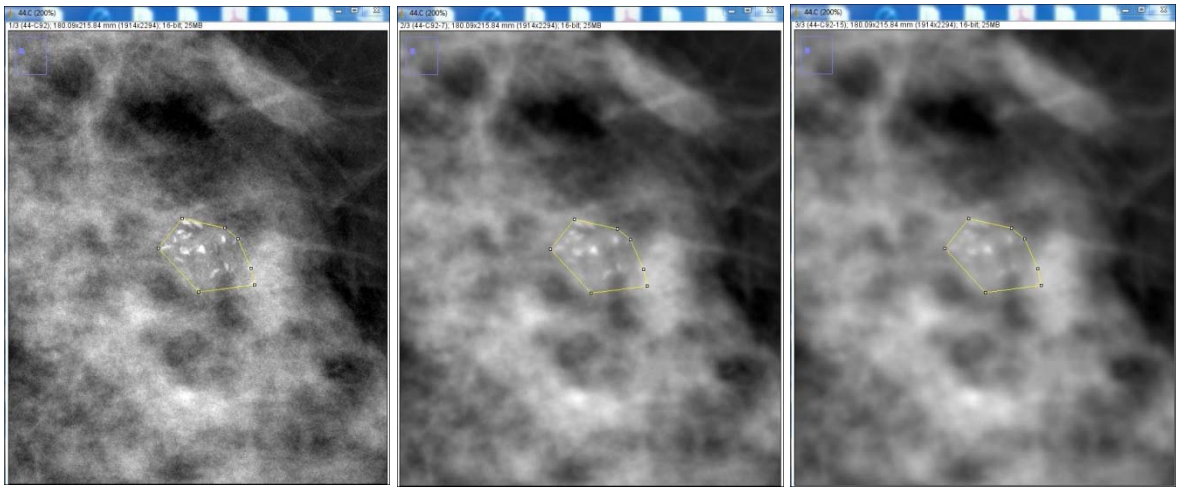

Figure 4.12 Demonstrates the same region of interest for clustered microcalcification for the three levels of simulated motion blur.

Table 4.4 Demonstrates the physical measures of breast lesion with three levels of simulated motion blur using ImageJ software

	Area1	Mean1	StdDev1	Min1	Max1	Calc. NO.	DI	Contrast	DI x Con	SNR	Detect ability
Case 1											
0.0 mm	13.731	2609.767	62.231	2457	2933	11	0.801	0.890	0.220	41.937	1.00
0.7 mm	13.731	2607.006	39.558	2544	2774	11	0.801	0.940	0.753	65.903	1.00
1.5 mm	13.731	2604.941	32.185	2555	2718	11	0.801	0.958	0.768	80.936	0.85
Case 2											
0.0 mm	23.549	2967.666	89.657	2702	3361	25	1.062	0.883	0.937	33.100	1.00
0.7 mm	23.549	2966.361	73.434	2766	3191	25	1.062	0.930	0.987	40.395	1.00
1.5 mm	23.549	2965.665	69.593	2776	3137	25	1.062	0.945	1.004	42.614	0.85

4.9 Step 8: Missed Lesion Calculation Method

The calculation of missed lesions was used to identify the detectability of each lesion by each observer. A comprehensive table has been created to present a full detailed explanation to the seven observers on three levels of simulated motion blur. This table shows the sensitivity of each lesion for all images related to the each level of simulated motion blur (**Table 4.11**). The detectability of each lesion represents the number of observers detect the lesion divided on the total number of observers. For instance, when all the observers detected the lesions (7/7), this means that the percentage detecting the abnormality is 100% in 0.0 mm of motion blur. Whereas, if only six observers detected the lesion from seven (6/7) the detectability will be reduced to 85.8 % for 0.7 mm of simulated motion blur , and to 57.2% (4/7) for 1.5 mm of simulated motion blur (see case 3 and case 5 **Table 4.5**).

Table 4.5 demonstrates the missed lesion calculation method

	Observer 1			Observer 2			Observer 4			Observer 5			Observer 6			Observer 7			Observer 9			Detectability of each lesion by the observers		
	0.0	0.7	1.5	0.0	0.7	1.5	0.0	0.7	1.5	0.0	0.7	1.5	0.0	0.7	1.5	0.0	0.7	1.5	0.0	0.7	1.5	0.0	0.7	1.5
1	✓	✓	X	✓	✓	X	✓	✓	X	✓	✓	✓	✓	✓	✓	✓	✓	✓	✓	✓	✓	1.00	1.00	0.572
2	✓	✓	X	✓	✓	✓	✓	✓	✓	✓	✓	✓	✓	✓	✓	✓	✓	✓	✓	✓	✓	1.00	1.00	0.850
3	✓	✓	X	✓	X	X	✓	✓	✓	✓	✓	X	✓	✓	✓	✓	✓	✓	✓	✓	✓	1.00	0.858	0.572
4	X	X	X	✓	✓	X	✓	X	X	✓	X	X	X	✓	X	✓	✓	X	X	X	X	0.572	0.429	0.00
5	✓	✓	X	✓	X	X	✓	X	X	✓	✓	X	✓	X	X	X	✓	✓	✓	X	X	0.858	0.429	0.143
6	✓	✓	✓	✓	✓	✓	✓	✓	✓	✓	✓	✓	✓	✓	✓	✓	✓	✓	✓	✓	✓	1.00	1.00	1.00
7	✓	✓	✓	✓	✓	✓	✓	✓	✓	✓	✓	✓	✓	✓	✓	✓	✓	✓	✓	✓	✓	1.00	1.00	1.00
8	✓	✓	X	✓	✓	✓	✓	✓	X	✓	✓	✓	X	✓	X	✓	✓	✓	✓	X	X	1.00	0.858	0.429
9	✓	✓	X	✓	✓	X	✓	X	✓	✓	✓	✓	✓	✓	✓	✓	✓	X	✓	✓	X	1.00	0.858	0.429
10	✓	✓	X	✓	X	✓	X	✓	X	✓	✓	✓	✓	✓	✓	✓	✓	X	✓	X	X	1.00	0.715	0.429

The mark (✓) represents the detected lesion while mark (X) represents the missed lesion.

4.10 Ethical Issues

As this study involved human participation, special care must be paid to the rights of the participants (Polit and Beck, 2003). Ethical approval for this study was granted by the University of Salford (HSCR15-107) (Appendix A and B) and with consent from The University Hospital of North Manchester, Nightingale Centre (Appendix C). This was a retrospective study of breast screening images. Ethical approval has been provided by the University of Salford (UOS). Most of the observation sessions took place at the University of Salford medical imaging facility; the sessions included the explanation of the study using an information sheet (Appendix D) and an explanatory PowerPoint presentation (Appendix H). The observers were invited to participate in the study through several ways, such as Participant Invitation Letter (Appendix E) and Poster (Appendix F).

All participants in this study signed a consent form before conducting the tasks. Participants were informed that the results of the study would be included in a research thesis, would be discussed at research conferences and published in peer-reviewed research journals. Data was anonymised and stored on a password protected computer. No financial reward or otherwise was offered. Participants were advised that their involvement may help to improve quality and raise awareness of the impact of motion blur on cancer detection performance. All the observers have received feedback on the outcomes of this study. They have received e-mail told them there was a statistically significant impact of motion blur on the detection performance of malignant masses and microcalcifications.

The Data Protection Act (DPA) 1998 (Legislation.gov.uk, 1998) can be applied to all observer studies. Participants should be provided with adequate information about the study to enable them to make a decision to participate in a study. All participants must inform and know the target of the data collection, the period of the data can be kept and what will be achieved with the data when it has been completed.

4.10.1 Ethical Approval in Observers' Studies

In general, ethical issues aim to ensure the integrity and interests of persons and adherence to standards. In the observer study implemented for this Ph.D. thesis, it was necessary to conserve the privacy of all the observers and to make sure that any collected data was not definable to them. Duquenoy et al., (2008) suggested that the ethical standards for electronic collection data

should be established in the code of ethics to ensure security, material quality, integrity, accessibility, and usability. Therefore, this thesis reviewed by the University of Salford Research and Ethics Committee, to protect the participants' safety, rights, wellbeing, and dignity. This Committee is run by the University of Salford, but its members are not connected to the research they examine.

The Declaration of Helsinki (World Medical Association, 2013) summed up the role of individuals participant in medical researches. The integrity and interests of the participants should be the primary concern through the study, and while this declaration mentions to participants as patients, the same standards must be utilised to those who participate as observers. According to (Duquenoy et al., 2008), the medical informatics require that the regulations in place ought to support the study, prevent the participants from experiencing danger and keep information confidential. This is applicable to the existing work.

4.11 Chapter Summary

In summary, a novel mathematical simulation method has been designed to determine whether simulated motion blur has an influence on lesion detection performance using observer performance study. The stages of this observation method can be summarised into several phases. First, suitable FFDM images were selected. Next, simulated motion was applied through a novel mathematical technique within computer software. Then, the mammographic images have been evaluated using an FROC method. Finally, JAFROC was used to analyse the data for assessing the impact of simulated motion blur on lesion detection performance.

In this thesis, several additional methods have been used to manipulate the data. To start with, two methods were used to analyse the FROC data combined two observers' data and single observer data (see the results chapter 5). After that, two physical methods have been applied to investigate the impact of simulated motion blur on the physical parameters of the breast masses using conspicuity software. ImageJ software was used to investigate the impact of motion blur on microcalcifications. Finally, the missed lesion calculated method has been utilised to determine the detectability for each lesion by each observer.

Chapter Five: Results

5.1 Chapter Overview

This chapter presents the results of the free response study. The presentation of results is organised into three main sections. The first section shows the results of seven observers (single reporting) of the free response study to determine the impact of simulated motion blur on the detection of malignant masses and malignant microcalcifications. The results demonstrate that there is a statistically significant influence of simulated motion blur on lesion detection performance between images without motion blur (0.0 mm) and images with two levels of motion blur (0.7 and 1.5 mm) for masses and microcalcification.

Section two presents the results of second analysis method; this is where two observers' data have been combined in an attempt to mimic the double reporting method in screening mammography. The results of combining two observers' data demonstrate that there is a reduction in the impact of motion blur on detection performance compared to single observer. However, there is still a statistically significant impact of simulated motion blur on lesion detection performance between three levels of simulated motion blur for masses and microcalcification.

Section three involves a comparison between the detection performance of single observer and the detection performance of combining two observers' data. The result of the third section demonstrates that there is a significant difference between single and combined two observers analysis of microcalcification lesions, whereas there no statistically significant difference for detection performance of masses. This means that the impact of simulated motion blur remains significant even when double reporting implemented.

5.2 Section One: Results of the Free-response Study

5.2.1 Overview of wJAFROC Analysis

An equally weighted jackknife alternative free-response receiver operating characteristic (wJAFROC) analysis was performed to analyse the detection of: (i) microcalcifications, and (ii) masses, for three conditions (0.0 mm (no motion blur), 0.7 mm simulated motion blur, and 1.5 mm simulated motion blur). Random observer random case analysis was reported for both analyses.

For these analyses the following data has been reported:

- F-statistic and p-value
- Observer averaged wJAFROC figure-of-merit (FOM) for all conditions and 95% confidence intervals (CI)
- Observer averaged sensitivity and specificity derived from the highest ratings
- FOM difference and 95% CI for all treatments pairs of simulated motion blur
- wAFROC curves for all magnitudes of simulated motion blur

In this analysis, the free-response data for seven observers is reported. For a difference in detection performance to be declared statistically significant, the result of the overall F-test must be significant and the 95% confidence interval of the treatments pair must not include zero.

5.2.2 Microcalcifications

For microcalcifications, the observer averaged wJAFROC FOM and 95% confidence intervals (CIs) are displayed in **Table (5.1)**. Differences between FOM treatment pairs are displayed in **Figure 5.1,** with the p-values to indicate significance. For a difference in FOMs to be declared significant, the 95% CI of the FOM treatment pairs must not include zero, in addition to the result of the overall F-test being significant. The observer averaged wAFROC curves for microcalcifications are displayed in **Figure 5.2**.

When sensitivity (HrSe) was used as the FOM, a significant difference was found between all treatment pairs of magnitudes of simulated motion blur ($F(2,18) = 10.48$, $p=0.0010$). This implies that the false negative rate was increasing significantly as the magnitude of simulated motion blur was increased. When specificity (HrSp) was used as the FOM, there was no

significant difference between magnitudes of simulated motion blur ($F(2,13) = 0.21$, $p=0.8110$). This reveals that the false positive rate did not increase significantly with image blurring (**Table 5.3**).

Average number of non-lesion localisation marks per observer on non-diseased cases	0.094
Average number of non-lesion localisation marks per observer on diseased cases	0.393
Average number of lesion localisation marks per observer	0.888

Table 5.1 Demonstrates a summary of the wJAFROC FOM with confidence interval (95% CI), sensitivity and specificity analysis for microcalcifications case.

Higher sensitivity (HrSe) corresponds to higher negative predictive value and higher specificity (HrSp) corresponds to higher positive predictive value is the ideal property of a test.

Magnitude of Simulated Motion blur (mm)	wJAFROC FOM (95% CI)	Sensitivity % (HrSe)	Specificity % (HrSp)
0 mm	0.899 (0.859,0.939)	97.9	84.8
0.7 mm	0.813 (0.757,0.870)	86.4	84.3
1.5 mm	0.746 (0.679,0.812)	76.5	86.6

Table 5.2 Demonstrates the wJAFROC FOM with confidence interval (95% CI), sensitivity and specificity analysis for each observer for the image with no motion blur and two levels of simulated motion blur of microcalcifications.

	wJAFROC FOM			Sensitivity % (HrSe)			Specificity % (HrSp)		
Observer	0mm	0.7mm	1.5mm	0.0mm	0.7mm	1.5mm	0.0mm	0.7mm	1.5mm
1	0.896	0.728	0.690	98.4	72.6	53.2	85.5	90.3	98.4
2	0.937	0.818	0.813	100	96.8	90.3	93.5	83.9	91.9
3	0.902	0.822	0.781	95.2	82.3	74.1	96.8	96.8	98.4
4	0.885	0.799	0.715	100	79.0	59.7	91.3	87.1	87.1
5	0.913	0.859	0.776	96.8	82.3	80.6	98.4	100	88.7
6	0.902	0.874	0.782	95.2	93.5	83.9	96.8	88.6	87.1
7	0.858	0.794	0.662	100	98.4	93.5	30.6	43.5	54.8
Average	**0.899**	**0.813**	**0.746**	**97.7**	**86.4**	**76.5**	**84.8**	**84.3**	**86.6**

Table 5.3 Shows a comparison of the p-values difference between treatment pairs of average wJAFROC FOMs (95%) of single observer for microcalcification images.

Magnitude of Simulated Motion blur (mm)	The p-value difference between two pairs of average wJAFROC FOM (95% CI)
0.0 – 0.7 mm	0.0016
0.0 – 1.5 mm	0.0000
0.7 - 1.5 mm	0.0043
Overall F-test & average wJAFROC FOM (95% CI)	F (2, 12) = 18.13, p = 0.000)

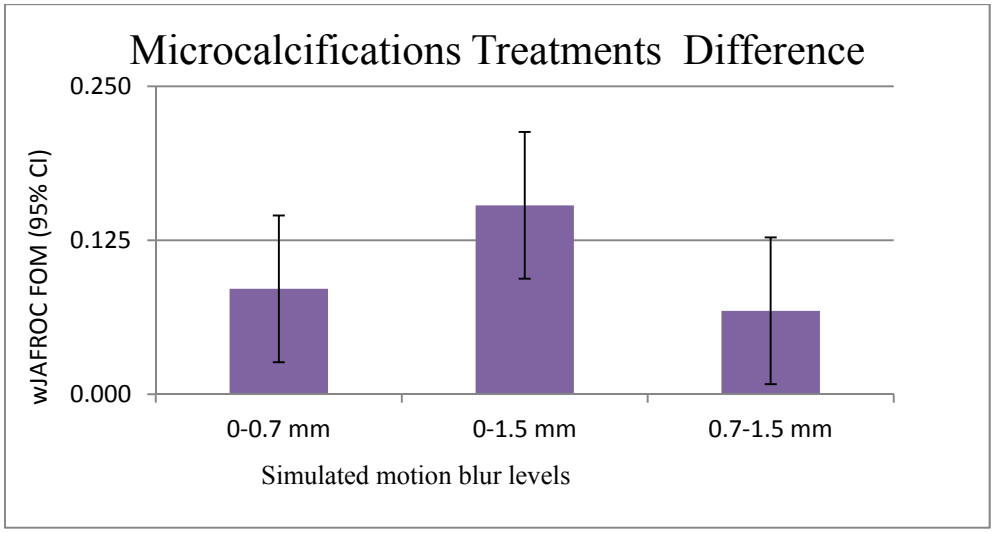

Figure 5.1 Demonstrates the distribution of FOM difference and 95% CIs for all FOM treatment pairs in the analysis of microcalcifications (this is the same data as indicated in **Table 5.3**).

This displays the inter-levels differences for the three treatment pairs (0.0 mm v 0.7 mm; 0.0 mm v 1.5 mm; 0.7 mm v 1.5 mm) for the analysis of microcalcifications. For a difference to be declared statistically significant the 95% confidence interval of the treatment pair must not include zero and the overall F-test must be significant.

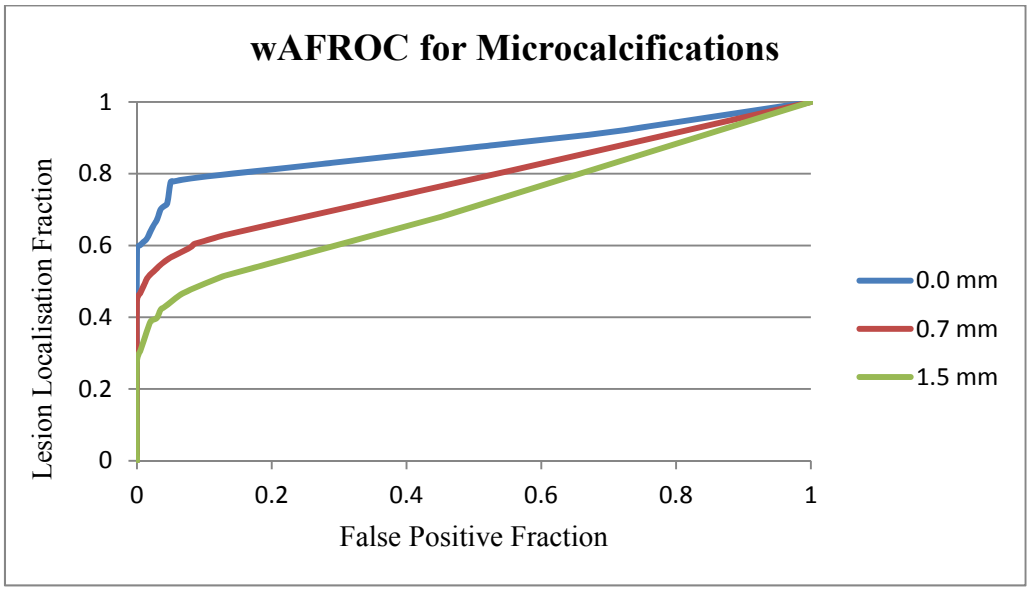

Figure 5.2 Demonstrates the wAFROC curve of microcalcification cases with three levels of motion blur. The highest performance is represented in level 0.0 mm (blue line) and the performance decreased with increase motion blur 0.7 mm (red line). The lowest performance is represented in level 1.5 mm of motion blur (green line).

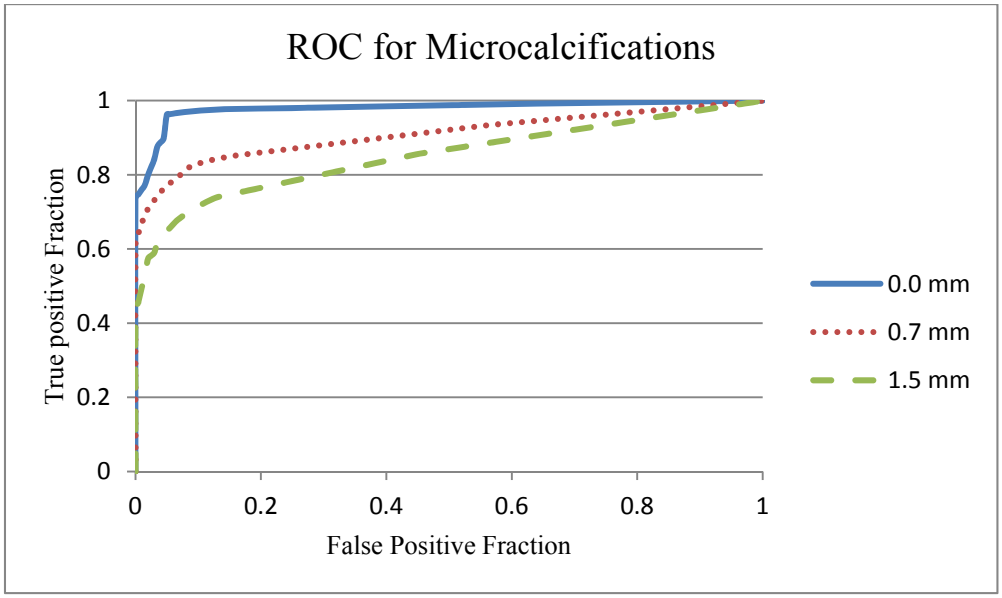

Figure 5.3 demonstrates the highest-rating inferred ROC curve of microcalcification for the image with no motion blur and two levels of simulated motion blur.

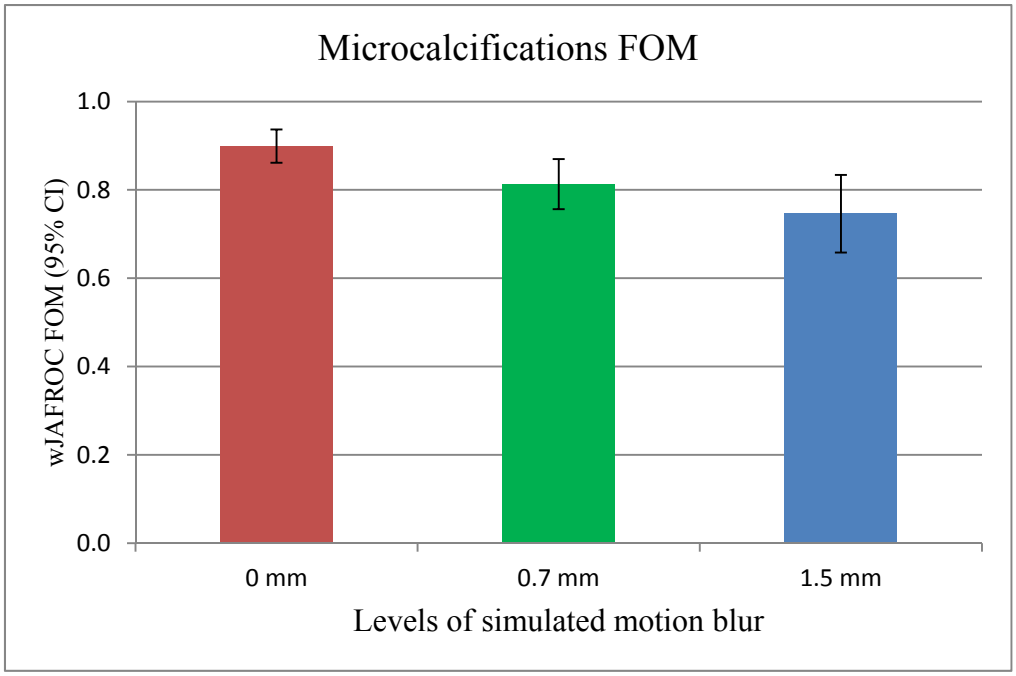

Figure 5.4 The observers averaged FOM of microcalcifications for the image without motion blur and two levels of simulated motion blur.

5.2.3 Masses

For masses, the observer averaged wJAFROC FOM and 95% confidence intervals (CIs) are displayed in **Table 5.4**. Differences between FOM treatment pairs (magnitudes of simulated motion blur) are displayed in (Table 5.5) with the p-values to indicate significance. The observer averaged wAFROC curves for masses are displayed in **Figure 5.5**.

When sensitivity (HrSe) was used as the FOM, there was no significant difference between magnitudes of simulated motion blur ($F(2, 16) = 0.43$, $p=0.6575$). This implies that the false negative rate was not changing significantly as a result of simulated motion blur. When specificity (HrSp) was used as the FOM, again there was no significant difference between magnitudes of simulated motion blur ($F(2, 12) = 1.31$, $p=0.3043$) (see **Table 5.5**).

Average number of non-lesion localisation marks per observer on non-diseased cases	0.217
Average number of non-lesion localisation marks per observer on diseased cases	0.211
Average number of lesion localisation marks per observer	0.885

Table 5.4 A summary of the wJAFROC analysis for masses. Shows the observer averaged wJAFROC FOM and 95% confidence intervals (CIs), Sensitivity % (HrSe) and Specificity % (HrSp).
Higher sensitivity (HrSe) corresponds to higher negative predictive value and higher specificity (HrSp) corresponds to higher positive predictive value is the ideal property of a test.

Magnitude of Simulated Motion blur (mm)	wJAFROC FOM (95% CI)	Sensitivity % (HrSe)	Specificity % (HrSp)
0	0.905 (0.859,0.952)	92.3	82.7
0.7	0.869 (0.814,0.924)	91.19	73.3
1.5	0.862 (0.810,0.915)	90.5	77.6

Table 5.5 Demonstrates a comparison of the p-value difference between two treatment pairs of average wJAFROC FOMs (95%) and the p-value difference between two sensitivity and specificity for single observer of masses cases.

Magnitude of Simulated Motion blur (mm)	The p-value difference between two levels of average wJAFROC
0.0 – 0.7 mm	0.0122
0.0 – 1.5mm	0.0041
0.7 - 1.5 mm	0.6408
Overall F-test & average wJAFROC FOM (95% CI)	F(2,21.53) = 6.01, p= 0.0084

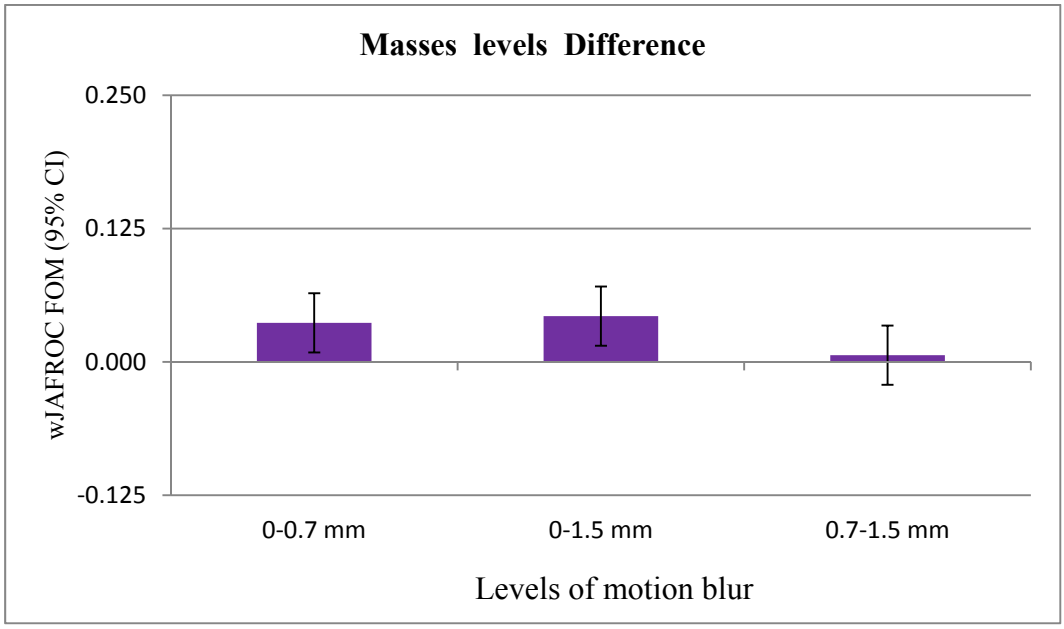

Figure 5.5 Demonstrates the distribution of FOM difference and 95% CIs for all FOM treatment pairs in the analysis of masses (this is the same data as indicated in Table 5.5).

This displays the inter- levels differences for the three level pairs (0.0 mm v 0.7 mm; 0 mm v 1.5 mm; 0.7 mm v 1.5 mm) for the analysis of masses. For a difference to be declared statistically significant the 95% confidence interval of the levels pair must not include zero and the overall F-test must be significant. Therefore, in this case, the level pairs 0.0 mm v 0.7 mm, and 0.0 mm v 1.5 mm are significantly different, while 0.7 mm v 1.5 mm, which does include zero is not significantly different despite the overall F-test does reach significant levels. The treatment differences were all a lot smaller for masses than microcalcifications (see **Figure**

5.8). This means that the malignant masses is less affected by motion blur than microcalcifications.

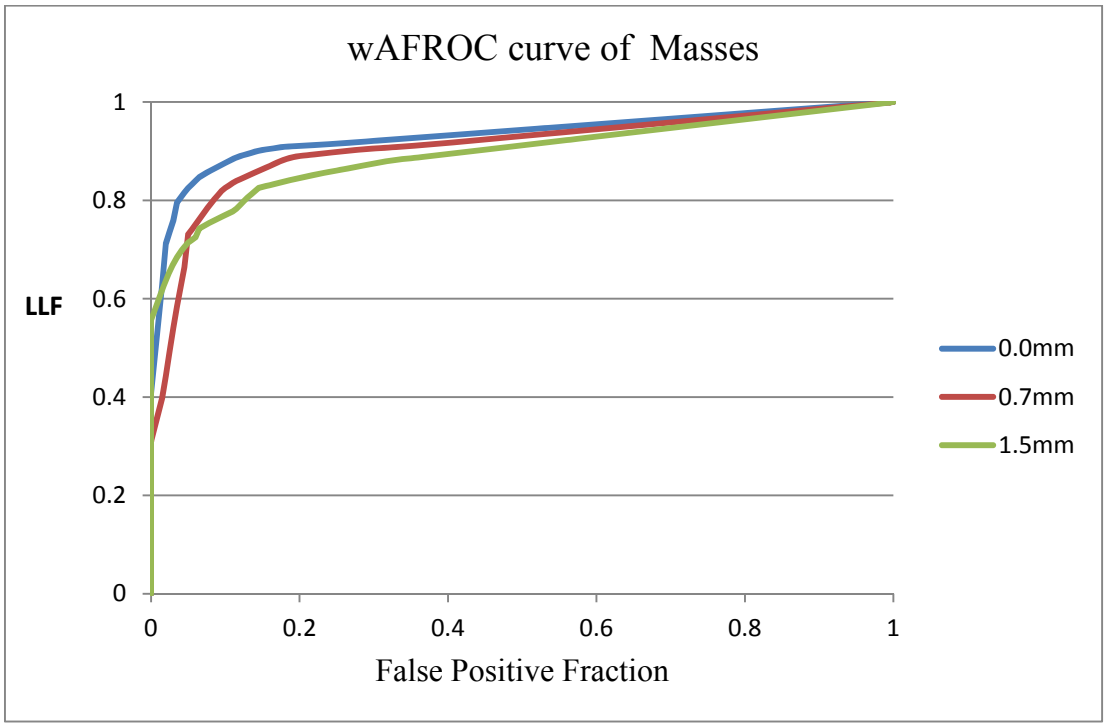

Figure 5.6 Demonstrates the wAFROC curve of masses in image with no blur (0.0 mm) and two levels of simulated motion blur (0.7 & 1.5 mm).

The highest performance is represented in images with no simulated motion blur 0.0 mm (blue line) and the performance decreased with increase motion blur 0.7 mm (red line). The lowest performance is represented in level 1.5 mm of motion blur (green line).

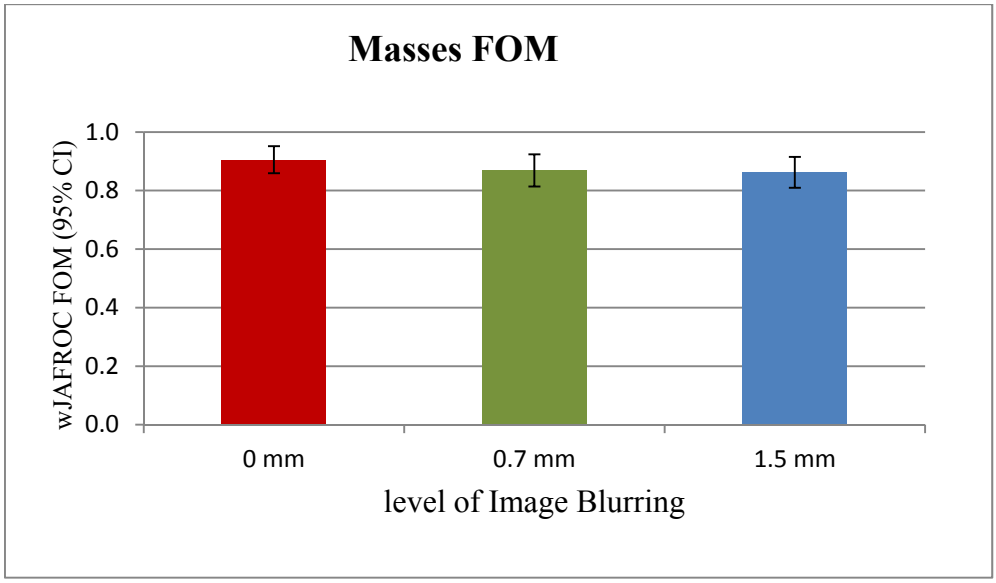

Figure 5.7 Demonstrates the observers averaged FOM of masses at 0.0 mm, 0.7 mm, and 1.5 mm of simulated motion blur.

Table 5.6 The wJAFROC FOM with confidence interval (95% CI), sensitivity and specificity analysis for each observer at 0 mm, 0.7 mm, and 1.5 mm of simulated motion blur for masses.

Masses cases	**wJAFROC FOM (95% CI)**			**Sensitivity % (HrSe)**			**Specificity % (HrSp)**		
Observer	0.0 mm	0.7 mm	1.5 mm	0.0mm	0.7mm	1.5mm	0.0mm	0.7mm	1.5mm
1	0.898	0.833	0.802	85.5	82.3	79.0	96.8	91.9	85.5
2	0.943	0.879	0.876	96.8	96.8	87.0	85.5	62.9	85.5
3	0.836	0.816	0.843	90.3	87.0	88.7	69.4	80.6	83.9
4	0.936	0.895	0.907	96.8	87.1	92.0	75.8	88.7	87.1
5	0.925	0.922	0.900	93.5	98.4	98.4	88.7	80.6	66.1
6	0.920	0.930	0.894	93.5	98.4	96.8	90.3	72.6	79.0
7	0.879	0.808	0.816	90.3	93.5	91.9	72.6	35.5	56.5
Average	**0.905**	**0.869**	**0.862**	**92.3**	**91.9**	**90.5**	**82.7**	**73.3**	**77.6**

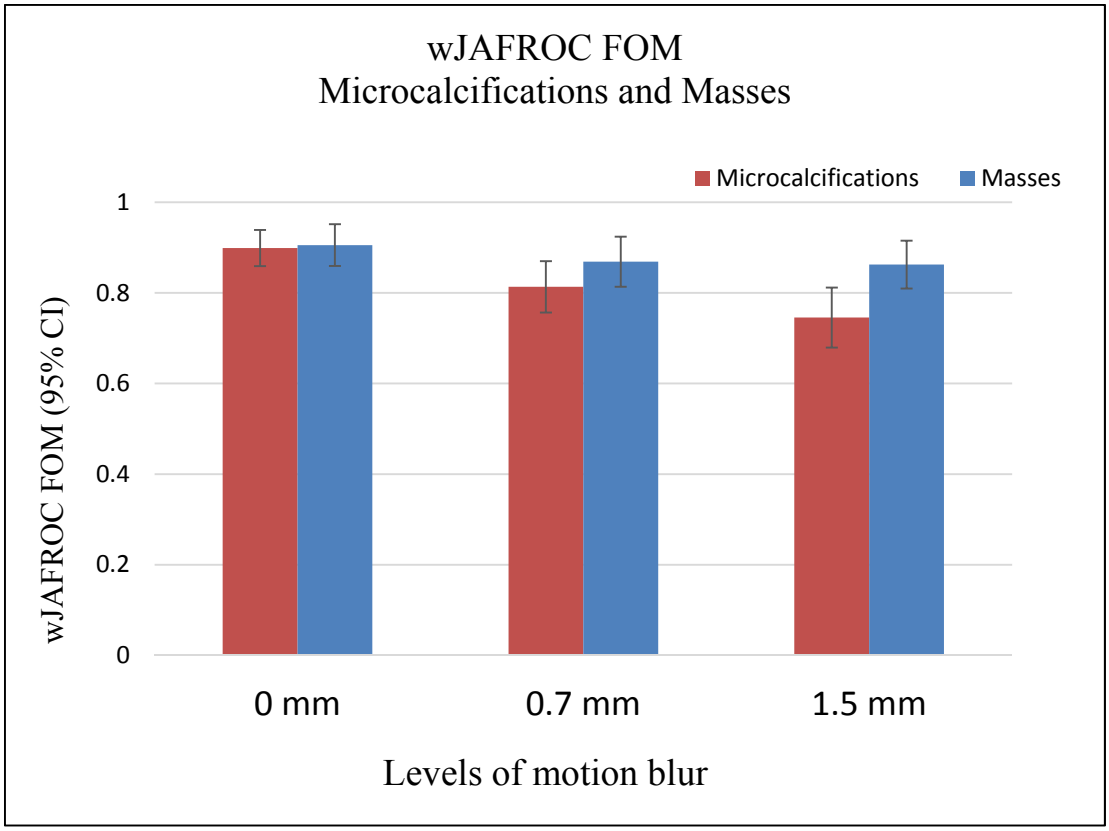

Figure 5.8 The wJAFROC FOM and 95% confidence intervals for microcalcifications and masses at 0.0 mm, 0.7 mm, and 1.5 mm of simulated motion blur.

5.3 Section Two: Results of the Combining Two Observers' Data

As it is recognised that double reporting is an essential element of NHSBSP standards, secondary analysis of the data was deemed essential to partly 'mimic' this combined data result. In this analysis 'a single result for each observer' is compared to 'the combined result of this observer and a second observer; the latter being referred to as a 'combined result'. The outcome of the combined result is classified as follows: a positive outcome is assigned if one of the two observers suspects a lesion; the negative outcome is assigned if both observers indicate no lesion present. Seven observers completed the study and their data was analysed collectively to establish the impact of simulated motion blur on detection of breast lesions. This means that observer ratings have been combined. For the TP worksheet, the highest rating of the two observers was adopted as the rating for each lesion. For the FP worksheet, all unique ratings were kept (see Appendix I and Appendix J).

Since the results of combining two observers' data process have used the same data of the free-response study, the data for observers' pairs from combining two observers' data is implemented and the following data analysis will be reported:

- F-statistic and p-value
- Observer averaged wJAFROC figure-of-merit (FOM) for all conditions and 95% confidence intervals (CI)
- Observer averaged sensitivity derived from the highest ratings
- FOM difference and 95% CI for all treatment pairs of simulated motion blur
- wAFROC curves for all magnitudes of simulated motion blur

For a difference in detection performance to be declared statistically significant, the result of the overall F-test must be significant and the 95% confidence interval of the treatment pairs must not include zero.

Two observers' data were combined for the detection of malignant microcalcifications and masses for three conditions; (i) no simulated motion blur (0 mm), and for two magnitudes of simulated motion blur (ii) 0.7 mm, and (iii) 1.5 mm. A statistically significant difference was found for the detection of masses ($F(2, 48) = 5.64$, $p < 0.0038$) and for the detection of microcalcifications ($F(2, 12) = 18.13$, $p < 0.0000$). For both analyses, a significant difference was observed between 0.0 mm and 0.7 mm, and between 0.0 mm and 1.5 mm of simulated motion blur, and also between 0.7 mm and 1.5 mm for microcalcifications. No significant

difference was detected between 0.7 mm and 1.5 mm for masses. Rjafroc was also used to calculate observer averaged sensitivity (FOM = HrSe) and specificity (FOM = HrSp) as the FOM for all conditions for microcalcifications and masses, (**Table 5.7 & Table 5.9**).

5.3.1 The Combining Two Observers' Data of Microcalcifications

A statistically significant difference for the detection performance of microcalcifications was demonstrated ($F(2, 11) = 13.68$, $p = 0.000$) between all three levels pairs 0.0 mm V 0.7 mm ($p < 0.01$). All FOM pairs (0 mm V 1.5 mm, and 0.7 mm V 1.5 mm) were significantly different (Figure 5.11). The observer averaged wJAFROC FOMs and 95% CIs are presented in (**Table 5.7**).

Average number of non-lesion localisation marks per observer on non-diseased cases	0.459
Average number of non-lesion localisation marks per observer on diseased cases	0.126
Average number of lesion localisation marks per observer	0.943

Table 5.7 A summary of the wJAFROC analysis of microcalcification. Shows the observer averaged wJAFROC FOM and 95% confidence intervals (CIs), Sensitivity % (HrSe) and Specificity % (HrSp) of combining two observers' data.

These results demonstrate there is a reduction in the impact of motion blur on detection performance compared to single observer.

Magnitude of Simulated Motion blur (mm)	wJAFROC FOM (95% CI)	Sensitivity % (HrSe)	Specificity % (HrSe)
0	0. 923 (0.883,0.964)	99.7	72.0
0.7	0.876 (0.831,0.921)	96.0	70.9
1.5	0.826 (0.771,0.880)	89.6	75.3

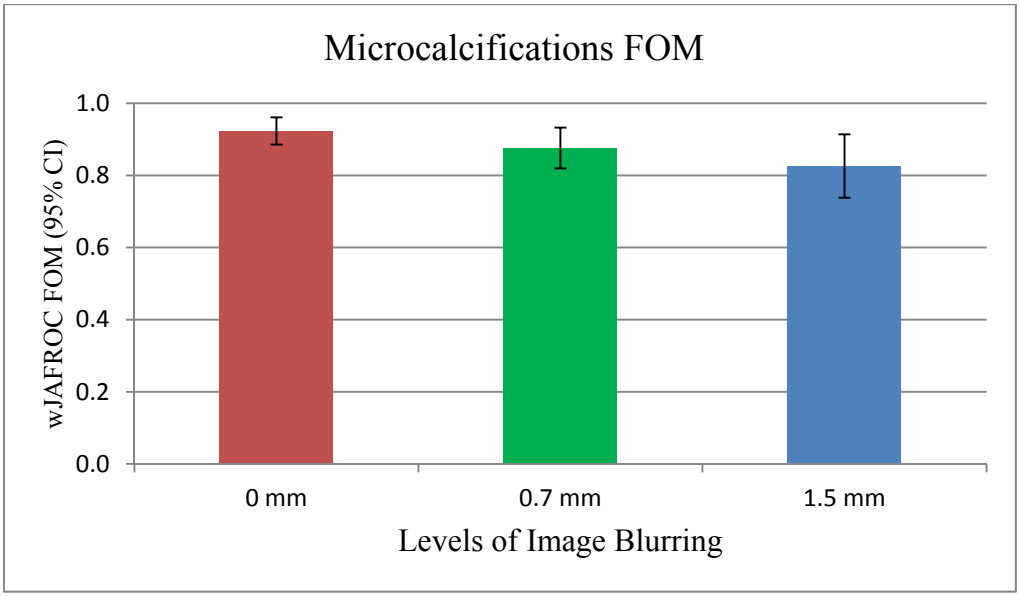

Figure 5.9 Demonstrates averaged FOM of the combining two observers' data of microcalcifications at 0 mm, 0.7 mm, and 1.5 mm of simulated motion blur.

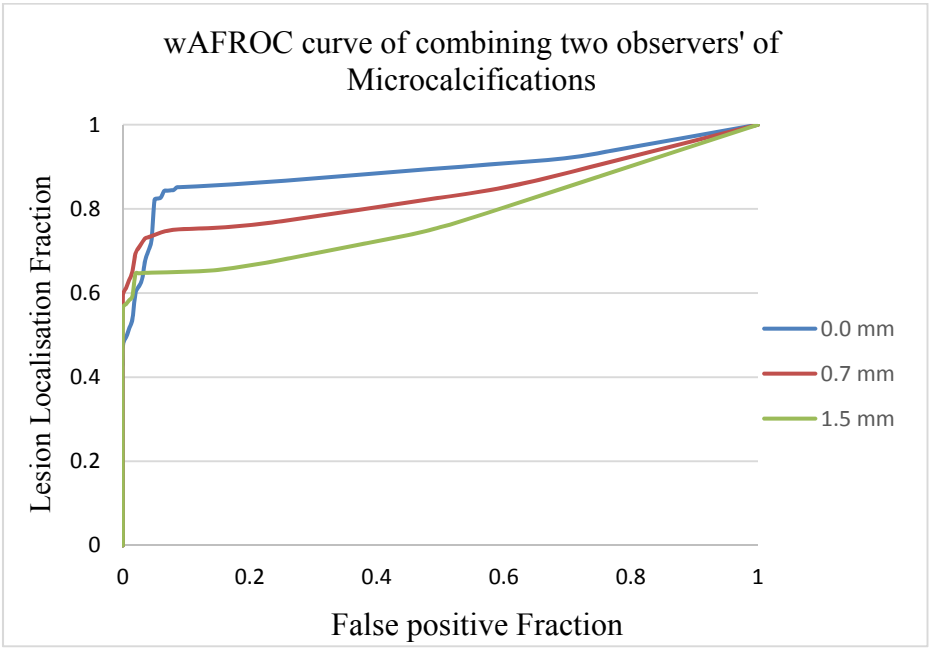

Figure 5.10 Demonstrates wAFROC curve of combined two observers' data of microcalcifications cases at 0.0 mm, 0.7 mm, and 1.5 mm of simulated motion blur.

The highest performance is represented in level 0.0 mm (blue line) and the performance decreased with increase motion blur 0.7 mm (red line). The lowest performance is represented in level 1.5 mm of motion blur (green line).

5.3.2 Combining Two Observers' Data of Masses

A statistically significant difference for the detection performance of masses was demonstrated (F (2,484) = 5.64, p = 0.0038). The observer averaged wJAFROC FOMs and 95% CIs are presented in (**Table 5.11**). A statistically significant difference was detected between all motion blur levels pairs except between 0.7 and 1.5 mm for masses (**Table 5.13**)

Average number of non-lesion localisation marks per observer on non-diseased cases	0.369
Average number of non-lesion localisation marks per observer on diseased cases	0.392
Average number of lesion localisation marks per observer	0.873

Table 5.8 A summary of the wJAFROC analysis of masses. Shows the observer averaged wJAFROC FOM and 95% confidence intervals (CIs), Sensitivity % (HrSe) and Specificity % (HrSp) of combined two observers' data.

These results demonstrate that there is a reduction in the impact of motion blur on detection performance.

Magnitude of Simulated Motion blur (mm)	wJAFROC FOM (95% CI)	Sensitivity % (HrSe)	Specificity % (HrSe)
0	0. 948 (0.915, 0.982)	98.2	70.5
0.7	0.915 (0.873,0.954)	97.9	55.1
1.5	0.913 (0.874,0.956)	97.5	62.7

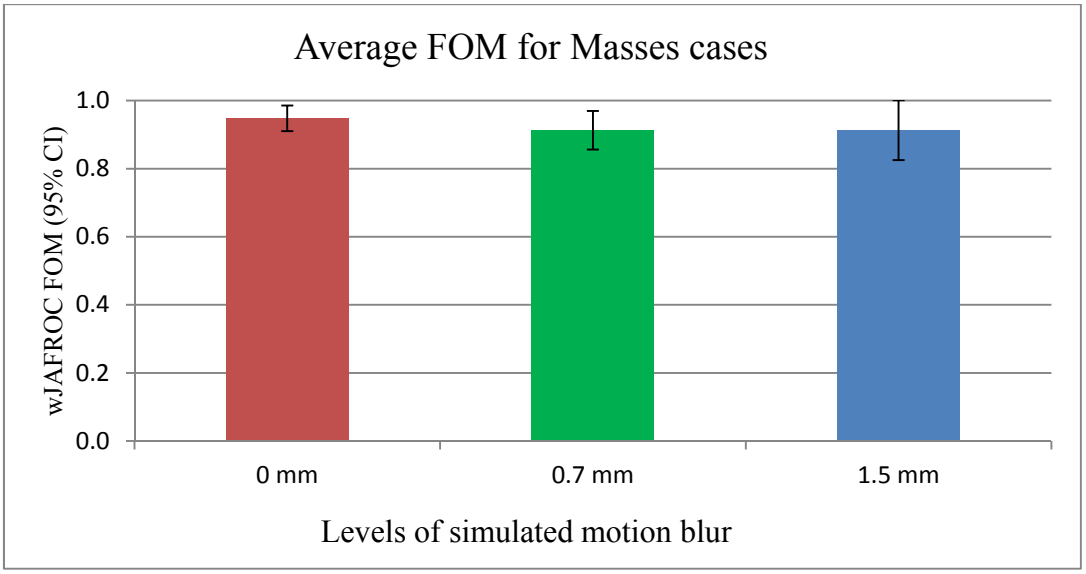

Figure 5.11 Demonstrates averaged FOM of the combining two observers' data in images with no motion blur and two levels of simulated motion blur of masses

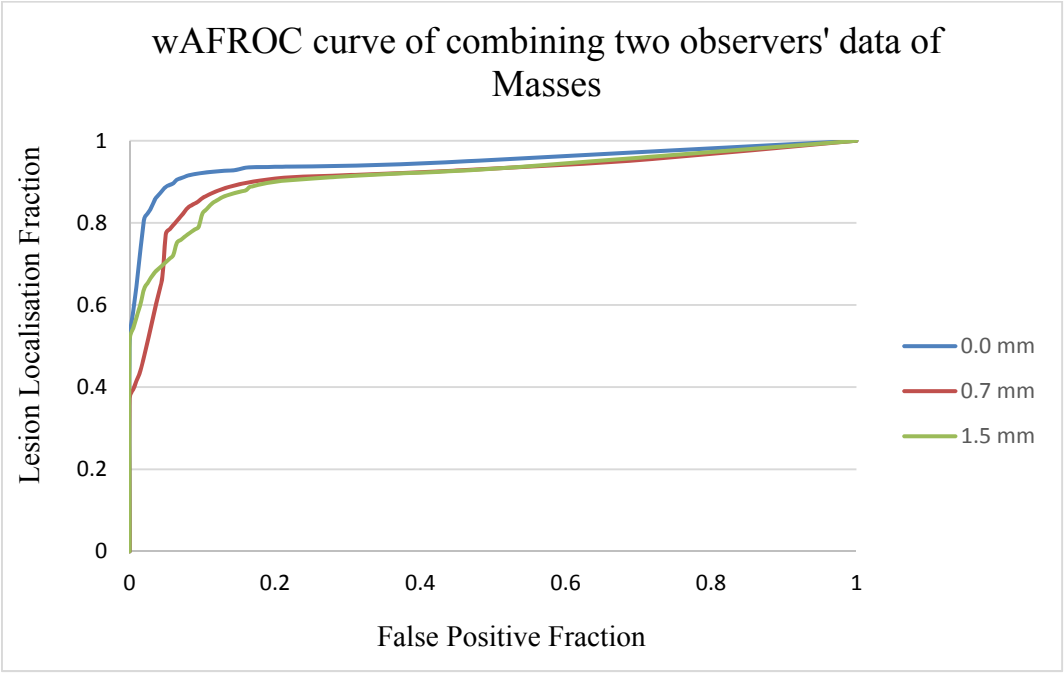

Figure 5.12 Demonstrates wAFROC curve of combined two observers' data of masses with three levels 0.0 mm, 0.7 and 1.5 mm.

The highest performance is represented in level 0.0 mm (blue line) and the performance decreased with increase motion blur 0.7 mm (red line). The lowest performance is represented in level 1.5 mm of motion blur (green line).

5.4 Section Three: A Comparison between the Results of Single Observer and the Combining Two Observers' Data

5.4.1 Microcalcification

A statistically significant difference for the detection performance of microcalcifications was demonstrated ($F(2, 11) = 13.68$, $p = 0.000$) between single observer and combined two observers' data (see **Figure 5.13**); **Figure 5.13** demonstrates the difference between wAFROC curve of single observer and combined two observers' data of microcalcifications cases.

Table 5.9 Demonstrates the comparison between wJAFROC FOMs, sensitivity and specificity of single and combined two observers' data with three levels of simulated blur.

Simulated Motion blur	wJAFROC FOM (95% CI)		Sensitivity % (HrSe)		Specificity % (HrSe)	
	Combined two observers' data	Single Observer	Combined two observers' data	Single Observer	Combined two observers' data	Single Observer
0 mm	0. 923 (0.883,0.964)	0.899 (0.859, 0.939)	99.7	97.9	72.0	84.8
0.7 mm	0.876 (0.831,0.921)	0.813 (0.757,0.870)	96.0	86.4	70.9	84.3
1.5 mm	0.826 (0.771,0.880)	0.746 (0.679,0.812)	89.6	76.5	75.3	86.6

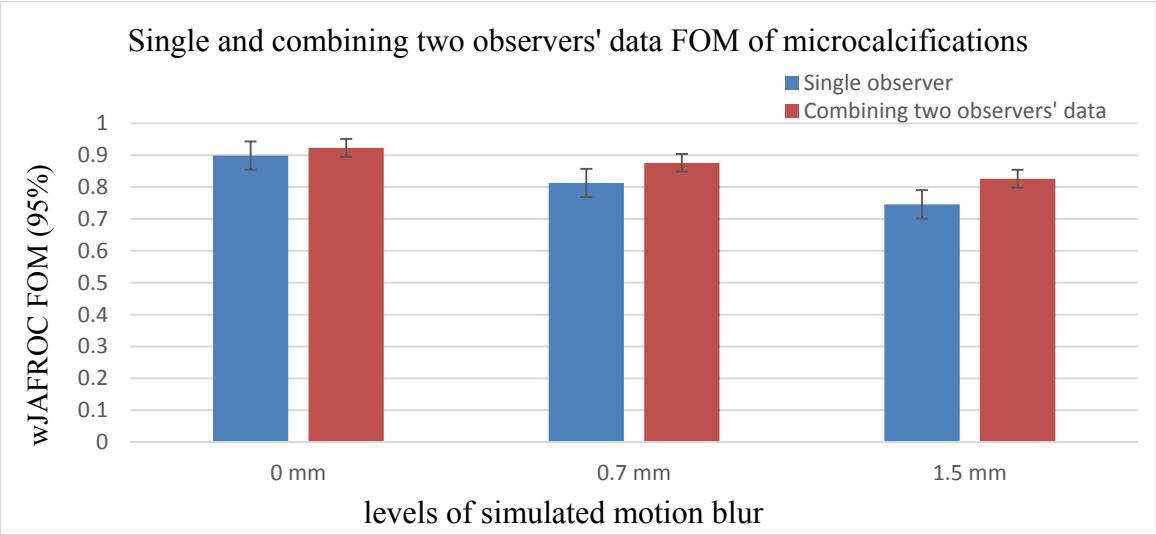

Figure 5.13 The comparison between wJAFROC FOMs for single observer and combined two observers' data in microcalcification.

Table 5.10 Demonstrates a comparison of the p-value difference between treatment pairs of average wJAFROC FOMs (95%) and the p-value difference between two sensitivity and specificity for single observer and combined two observers' data of microcalcifications.

Magnitude of Simulated Motion blur (mm)	The p-value difference between two pairs of average wJAFROC FOM (95% CI)	
	Combined two observers' data	Single Observer
0.0 – 0.7 mm	0.0000	0.0016
0.0 – 1.5 mm	0.0000	0.0000
0.7 - 1.5 mm	0.0000	0.0043
Overall F-test & average wJAFROC FOM (95% CI)	F (2, 12) = 18.13, p = 0.0000. significant	F (2, 12) = 18.13, p = 0.000. significant

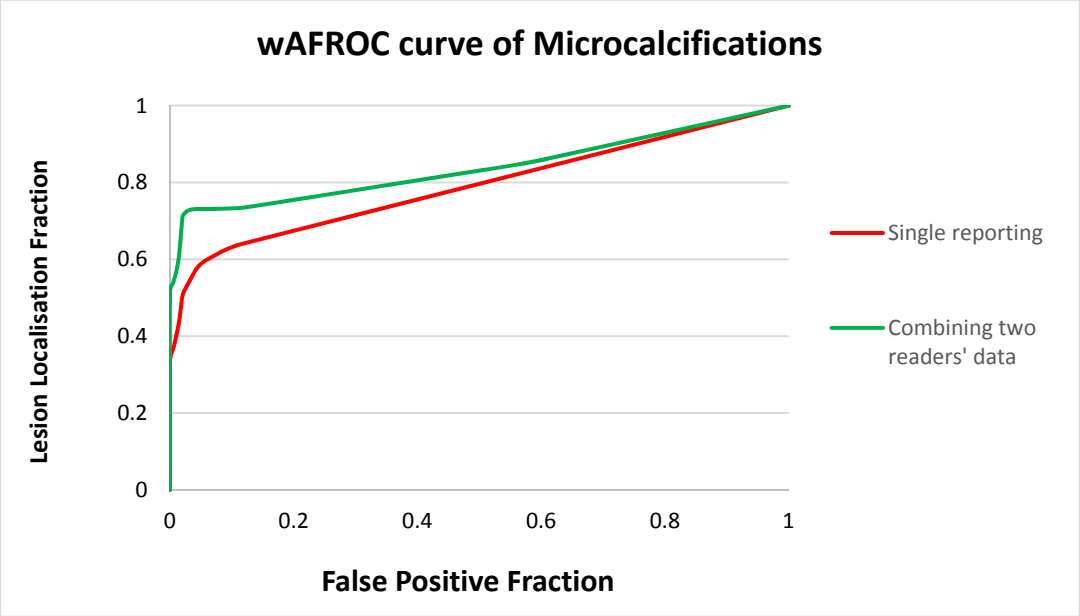

Figure 5.14 The difference between the wAFROC curve of single observer and combined two observers' data of microcalcifications.

There is a reduction in the impact of motion blur when using the combined two readers' data (green line), the results demonstrate there is a statistically significant difference for detection performance of microcalcification.

5.4.2 Masses

For masses, no significant difference for the detection performance was demonstrated (F (1,5) = 4.04, p = 0.1001) between single observer and combined two observers' data (see **Figure 5.16**); **Figure 5.16** demonstrates the difference between wAFROC curve of single observer and combined two observers' data of masses cases.

Table 5.11 Demonstrates a comparison between wJAFROC FOMs and sensitivity and specificity for single observer and combined two observers' data of masses.

Magnitude of Simulated Motion blur (mm)	wJAFROC FOM (95% CI)		Sensitivity % (HrSe)		Specificity % (HrSe)	
	Combined two observers' data FOMs	Single Observer FOMs	Combined two observers' data	Single Observer	Combined two observers' data	Single Observer
0	0. 948 (0.915,0.982)	0.905 (0.859,0.952)	98.2	92.3	70.5	82.7
0.7	0.913 (0.873,0.954)	0.869 (0.814,0.924)	97.9	91.19	55.1	73.3
1.5	0.915 (0.874,0.956)	0.862 (0.810,0.915)	97.5	90.5	62.7	77.6

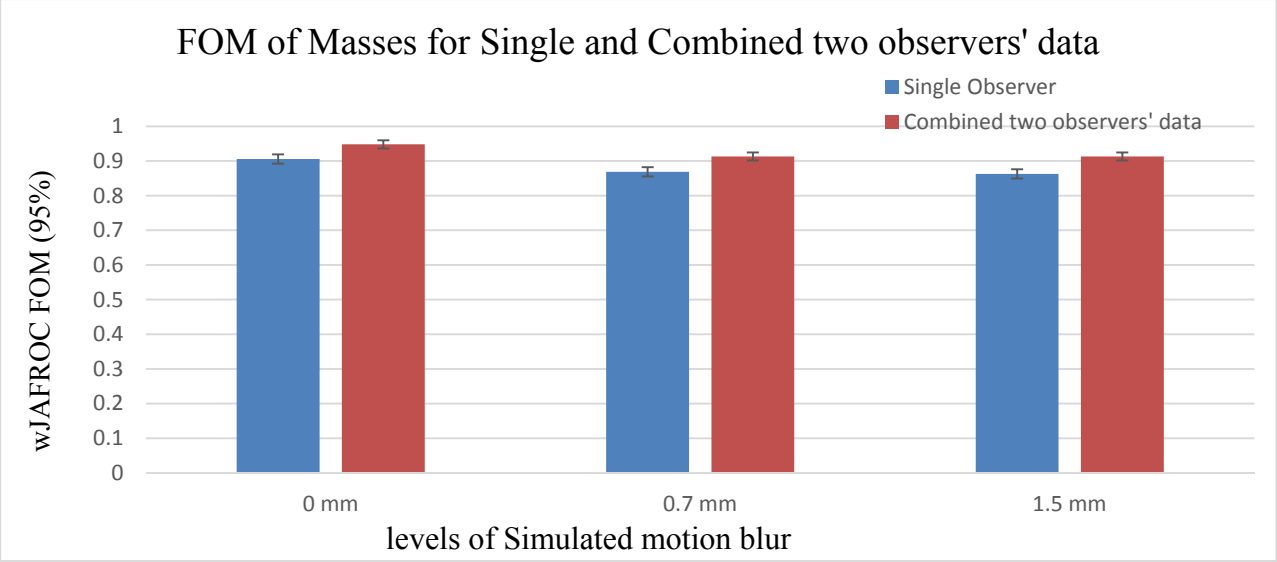

Figure 5.15 The comparison between wJAFROC FOMs for single observer and combined two observers' data of masses.

Table 5.12 Demonstrates a comparison of the p-value difference between two treatment pairs of average wJAFROC FOMs (95%) of masses.

Magnitude of Simulated Motion blur (mm)	The p-value difference between two levels pairs average wJAFROC	
	Combined two observers' data	Single Observer
0.0 – 0.7 mm	0.0031	0.0122
0.0 – 1.5 mm	0.0047	0.0041
0.7 - 1.5 mm	0.8952	0.6408
Overall F-test & average wJAFROC FOM (95% CI)	F(2,484.78) = 5.64, p = 0.0038 significant	F(2,21.53) = 6.01, p= 0.0084. significant

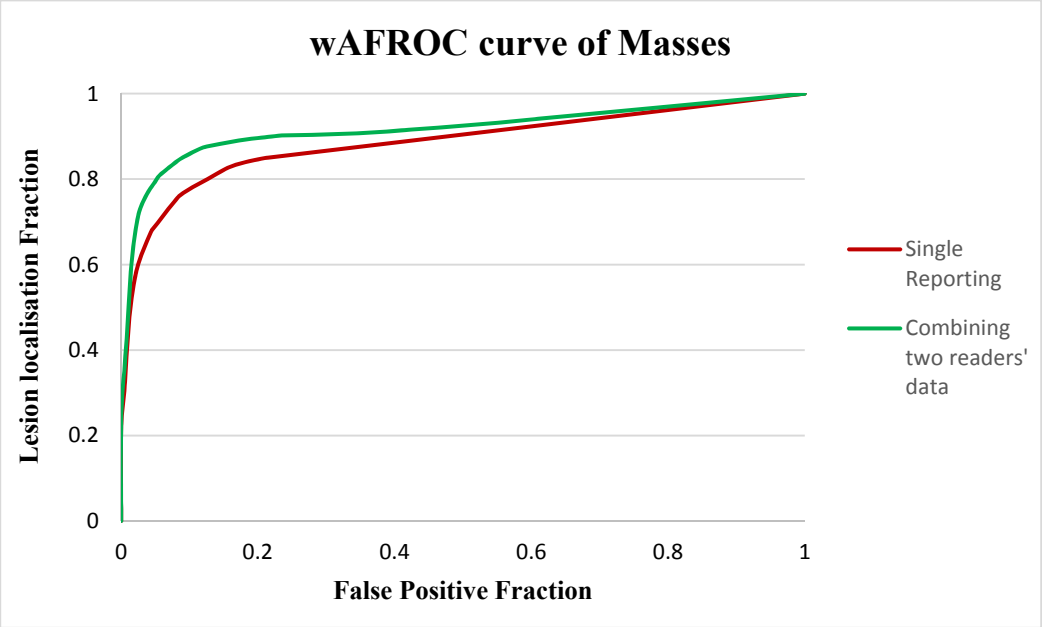

Figure 5.16 The difference between wAFROC curve of single and combined two observers' data of masses.

Despite the slight reduction in the impact of motion blur when using combined two observers' data method and increase the detection performance (green line), the results demonstrate there no statistically significant difference for detection performance of masses between two methods. This means that the impact of motion blur remains even when two observers' data have been combined.

Table 5.13 The wJAFROC FOM and 95% confidence intervals (CI) for single and combined observers for masses and microcalcifications.

Analysis	Modality	wJAFROC FOM (95% CI)	Difference (95% CI)	Sensitivity HrSe (%)	Specificity HrSp (%)
Masses	1st (single)	0.885 (0.844,0.927)	-0.03 (-0.07,0.01)	92	82
	2nd (combined)	0.916 (0.885,0.947)		97	63
Micro-calcifications	1st (single)	0.820 (0.780,0.860)	-0.06 (-0.10,-0.17)	85	92
	2nd (combined)	0.876 (0.842,0.909)		93	82

The inter-modality difference and confidence intervals are also presented for the analysis of masses and microcalcifications. For a difference to be declared statistically significant, the result of the overall F-test must be significant and the 95% CI of the modality difference must not include zero. The sensitivity and specificity were calculated in Rjafroc using the HrSe and HrSp FOMs.

Chapter Six: Results of Physical Measures

6.1 Chapter Overview

This chapter presents physical measures taken from the cases containing lesions. The results are organised into three main themes:

The first theme focuses on calculating the impact of motion blur on focal lesions (masses). This is primarily done using conspicuity index software (Szczepura & Manning, 2016). The conspicuity of a lesion represents a ratio between the contrast of a lesion and its surrounding complexity. Conspicuity index help to explain the function of the blurring software (e.g. how the edge angle degreases with increasing blur simulation) and how it impacts on the visual characteristics of the masses' images.

The second theme focuses on the impact of simulated motion blur on microcalcifications. This includes a novel metric, that has been named the 'dispersion index' (DI), lesion contrast, and dispersion index X contrast (DI x contrast). A relationship between lesion detectability and these physical measures has been investigated.

The third theme focuses on an analysis of missed lesions. This aspect focusses purely on detection, ignoring the confidence rating assigned for the free-response study. In this case, detectability is defined as the number of successful detections (for all observers) over the total number of opportunities to detect the lesion.

6.2 Part I: Physical Measures of Breast Masses

Several parameters, such as conspicuity index (χ), maximum lesion diameter (d), edge angle of the lesion (θ), mean noise within the lesion (σ_s), and mean background noise (σ_n) were recorded for all breast masses using conspicuity index software. This was not possible for microcalcifications due to their size and distribution patterns; this represents a limitation of the conspicuity software. This prompted the development of the Dispersion Index; see section 6.3.1). Overall, simulated motion blur has a significant impact on the edge angle of the lesion. In addition, these results illustrate the relationship between simulated motion blur and a change in grey level (ΔGL) of the image. Where ΔGL represents the difference between contrast of the lesion (μ_L) and background (μ_b). **Table 6.1** displays the results of the conspicuity data of breast masses with different levels of motion blur. This resulted in the conspicuity index for 23 cases out of 62 cases being measured because of limitations in the conspicuity software. Only masses which have clear edges can be measured by conspicuity software. The SNR for images is also presented to illustrate the impact of simulation motion blur on the image noise. When the magnitude of simulated motion blur increases, there is a reduction in the image noise as consequence of a smoothing effect incurred by blurring. A full range of physical measures acquired data for masses for image without simulated motion blur (0.0 mm), and images with simulated motion blur (0.7 & 1.5 mm) is presented in (**Appendix K**).

Table 6.1 Physical measurements of breast masses within mammographic images using conspicuity software.

The physical measurements include the conspicuity index (χ), the θ represents the maximum slope angle to the edge of the lesion profile in degrees, the change of grey level (ΔGL) and SNR.

	Magnitude of Simulated Motion Blur (mm)											
	0.0				0.7				1.5			
Case No.	χ	Edge angle (θ)	ΔGL	SNR	χ	Edge angle (θ)	ΔGL	SNR	χ	Edge angle (θ)	ΔGL	SNR
1	51.63	63.77	63.77	2.77	66.39	61.52	93.34	4.86	74.99	59.80	93.60	6.19
2	71.58	69.15	69.48	2.93	101.67	67.26	70.19	5.21	110.62	66.42	69.89	6.42
3	45.00	66.95	76.64	3.60	55.62	72.36	84.80	3.74	58.38	62.93	79.35	12.15
4	108.88	73.24	84.33	2.38	153.36	67.95	67.71	2.49	169.43	71.57	84.60	4.54
5	66.27	70.83	66.46	1.73	78.11	67.95	67.71	2.49	81.13	66.38	68.27	2.87
6	40.11	65.04	59.04	2.15	43.76	58.81	63.08	4.00	47.46	57.77	63.04	4.69
7	170.73	70.65	133.19	2.99	252.59	70.53	133.54	4.12	272.50	70.26	133.61	4.54
8	140.63	72.61	96.36	2.98	222.31	71.96	96.80	5.74	238.35	71.29	96.84	6.83
9	113.44	72.97	99.35	2.96	150.18	71.94	99.56	4.48	162.84	71.20	98.87	5.44
10	124.98	71.21	108.73	2.23	169.81	70.48	109.86	4.38	181.56	70.15	109.91	5.21
11	116.22	73.52	115.36	2.72	155.95	72.93	114.86	4.01	168.74	72.24	114.26	4.83
12	82.89	69.51	107.98	2.71	117.32	68.93	108.10	5.22	127.94	68.53	107.41	6.21
13	123.43	71.09	86.52	2.76	179.01	69.64	87.26	4.52	192.82	68.76	87.49	5.15
14	127.07	69.54	127.66	3.47	166.60	69.14	128.66	5.89	178.28	68.76	128.76	7.39
15	57.37	62.53	60.31	1.92	81.94	58.64	61.53	3.87	85.67	57.08	61.61	4.66
16	79.12	67.11	106.27	3.30	91.03	65.51	107.71	6.28	94.90	64.99	107.72	7.71
17	80.79	71.39	70.40	2.98	111.91	69.11	71.13	5.49	116.82	67.75	71.31	7.19
18	85.85	71.76	106.42	3.66	100.98	70.68	107.37	5.73	102.30	70.07	107.34	6.52
19	53.48	66.07	114.96	2.85	55.35	64.89	115.66	4.62	56.32	64.52	115.58	5.24
20	76.51	72.45	92.41	3.05	92.79	71.38	93.15	4.15	99.26	70.82	92.85	4.60
21	53.21	62.49	101.20	1.58	53.40	60.80	102.91	2.19	51.83	59.82	103.81	2.57
22	56.28	71.26	57.73	3.27	63.86	68.75	58.54	5.37	62.09	67.09	58.04	6.64
23	82.01	64.38	121.77	2.08	111.60	64.82	126.05	2.23	119.60	64.76	127.35	2.43
Max	170.73	73.52	133.19	3.662	252.59	72.929	133.54	6.279	272.5	72.239	133.61	12.148
Min	40.113	62.49	57.73	1.575	43.759	58.64	58.54	2.194	47.462	57.08	58.04	2.429
Ave.	87.282	69.109	92.450	2.741	116.328	67.63	94.326	4.394	124.080	66.649	94.848	5.653

6.2.1 Normality Test of Masses Data

Normality test of the data of the physical measures is required to check the suitability of the overall data for further analysis (Field et al., 2013). For this data, the Kolmogorov-Smirnov test and Shapiro-Wilk test showed that the physical parameters data such as the conspicuity index, the change in grey level and SNR were normally distributed with $P \geq 0.05$, and the edge angle data was not normally distributed with $P \leq 0.05$ as illustrated in (**Table 6.2**).

Table 6.2 Values of Kolmogorov-Smirnov test and Shapiro-Wilk normality test for the physical measures data of breast masses

	Kolmogorov-Smirnov[a]			Shapiro-Wilk		
	Statistic	df	Sig.	Statistic	df	Sig.
Conspicuity Index 0.0 m	0.169	23	0.089	0.934	23	0.133
Edge Angle 0.0 mm	0.190	23	0.031	0.899	23	0.024
GL 0.0 mm	0.131	23	0.200*	0.945	23	0.227
SNR 0.0 mm	0.171	23	0.080	0.955	23	0.376
Conspicuity Index 0.7 mm	0.145	23	0.200*	0.928	23	0.099
Edge Angle 0.7 mm	0.182	23	0.047	0.888	23	0.014
GL 0.7 mm	0.149	23	0.200*	0.946	23	0.245
SNR 0.7mm	0.119	23	0.200*	0.936	23	0.150
Conspicuity Index 1.5 mm	0.138	23	0.200*	0.927	23	0.092
Edge Angle 1.5 mm	0.138	23	0.200*	0.904	23	0.030
GL 1.5 mm	0.114	23	0.200*	0.959	23	0.451
SNR 1.5 mm	0.162	23	0.123	0.892	23	0.180

*. This is a lower bound of the true significance

a. Lilliefors Significance Correction

6.2.2 Conspicuity Index (χ)

The conspicuity of a mass represents a ratio between the contrast of a mass and its surrounding complexity. A paired sample t-test (2-way) was performed to test the hypothesis that the conspicuity index of masses was equal on images with no motion blur (0.0 mm) (M= 87.282, SD= 34.715) and images with 0.7 mm motion blur (M= 116.33, SD=56.169), 1.5 mm motion blur (M= 124.08, SD= 61.566). Prior to conducting the analysis, the assumption of normally distributed difference scores was examined, and the data was normally distributed see (**Table 6.2**). The Conspicuity Index difference between the two magnitudes of simulated motion blur and no motion blur were statistically significant for all comparisons (See **Table 6.3**). This could influence on lesion characteristics and the changes in the features of breast masses could have negatively influence the differential diagnosis between malignant and benign masses. **Figure 6.1** graphical represents the means and confidence interval 95% of the two magnitudes of simulated motion blur and no motion blur. As can be seen, the conspicuity index increases significantly when simulated motion blur increases from 0mm to 0.7 mm and then to 1.5mm. The diagram illustrates a variety of different box plot positions and shapes. The box plot of conspicuity index in images without motion blur (0.0 mm) is comparatively short. This suggests that the distribution of overall data is convergent. The median is about (80.790, 101.672, and 110.622) for images without blur 0.0mm, images with blur 0.7 mm and 1.5mm respectively.

Table 6.3 The results of conspicuity index of 23 masses cases for images with no motion blur and two levels of simulated motion blur.

Conspicuity Index of 23 masses		**0.0 mm**	**0.7 mm**	**1.5 mm**
Mean		87.282	116.33	124.08
95% Confidence Interval for Mean	Lower Bound	72.270	92.038	97.4570
	Upper Bound	102.294	140.617	150.703
5% Trimmed Mean		85.449	112.939	120.307
Median		80.790	101.672	110.622
Std. Deviation		34.715	56.169	61.566
Minimum		40.11	43.76	47.46
Maximum		170.73	252.59	272.50
Range		130.62	208.83	225.04
Interquartile Range		59.94	89.56	94.44

T-test Pairs	**Result of T-test / Difference (95% CI)**
0.0 mm – 0.7 mm	$t(22) = -6.158$, $p<0.000$ / -29.046 (-38.827,-19.264)
0.0 mm – 1.5 mm	$t(22) = -6.273$, $p<0.000$ / -36.798 (-48.964, -24.633)
0.7 mm – 1.5 mm	$t(22) = -6.231$, $p<0.000$ / -7.752 (-10.333, -5.172)

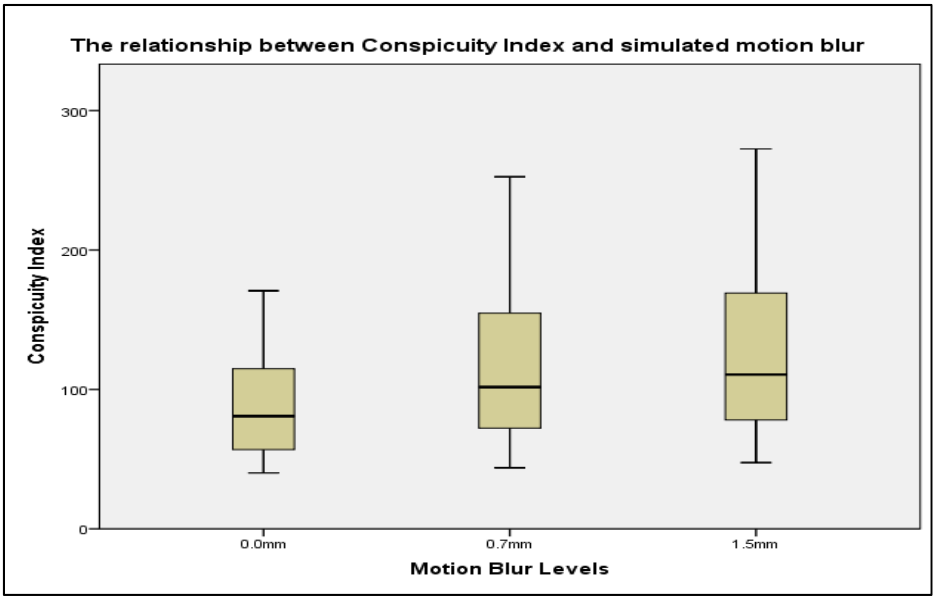

Figure 6.1 Demonstrates the relationship between the magnitudes of simulated motion blur and conspicuity index of breast masses.

As can be seen, the conspicuity index increases significantly when simulated motion blur increases from 0mm to 0.7mm and then to 1.5mm.

6.2.3 Edge Angle

The edge angle of a mass represents the maximum slope angle across the edge of a lesion profile in degrees. A non-parametric test was performed to test the hypothesis that edge angle of masses in images with 0.7mm simulated blur (M= 67.63, SD=4.308), 1.5 mm simulated motion blur (M= 66.650, SD= 4.546) and edge angle of masses in images with no motion blur (0.0mm) (M= 69.110, SD= 3.556) are equal. Prior to conducting the analysis, the assumption of normally distributed difference scores was examined and the data was non-normally distributed (See **Table 6.2**). The edge angle difference between the two magnitudes of simulated motion blur and no motion blur were statistically significant for all comparisons (see **Table 6.4**). The edge angle decreased along with the increasing level of simulated motion blur. Simulated motion blur has an impact on the edge angle of breast masses and this could influence on image of the lesion characteristics. This means that any changes in the image characteristics of breast masses could negatively affect the identification of malignant masses. **Figure 6.2** demonstrates the mean of both edge angle and confidence interval 95% of the two magnitudes of simulated motion blur and no motion blur. Each of the box plots in (**Figure 6.2**) shows a different skewness pattern. The distribution of the 0.0mm box plots is skewed up whilst the distribution of box plots 0.7mm and 1.5mm are skewed down. The median was pointed by the horizontal line that runs up the centre of the boxes. The median was (67.750) for images with no motion blur and the median for blurred images 0.7mm, 1.5 mm were 68.925, 70.653, respectively.

Table 6.4 Demonstrates the results of edge angle measures for 23 masses cases of images with no motion blur and two levels of simulated motion blur.

Edge Angle		**0.0 mm**	**0.7 mm**	**1.5 mm**
Mean		69.110	67.63	66.650
95% Confidence Interval for Mean	Lower Bound	67.571	65.770	64.683
	Upper Bound	70.647	69.492	68.615
5% Trimmed Mean		69.233	67.838	66.870
Median		70.653	68.925	67.750
Variance		12.648	18.555	20.667
Std. Deviation		3.556	4.308	4.546
Minimum		62.490	58.64	57.080
Maximum		73.520	72.930	72.240
Range		11.030	14.290	15.160
Interquartile Range		5.690	5.790	5.740

T-test Pairs	Result of T-test / Difference (95% CI)
0.0 mm – 0.7 mm	$t(22) = 3.232$, $p<0.004$/ 1.4794 (0.530, 2.429)
0.0 mm – 1.5 mm	$t(22) = 6.592$, $p<0.000$ / 1.4794 (1.686, 3.234)
0.7 mm – 1.5 mm	$t(22) = 2.234$, $p<0.036$/ 0.980 (0.070, 1.891)

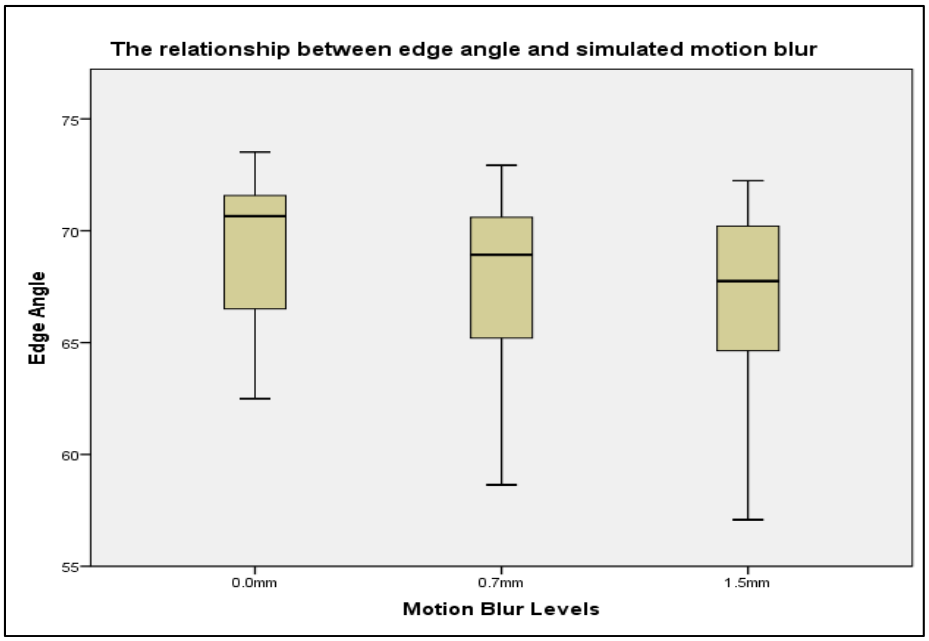

Figure 6.2 Demonstrates the relationship between the magnitudes of simulated motion blur and edge angle of masses.

6.2.4 The Grey Level Change (ΔGL):

The grey level change (ΔGL) represents the difference between the contrast of the lesion (μ_L) and the background (μ_b). The same analysis process used for conspicuity index has been used to analyse the grey level change data. A paired sample t-test was performed to test the hypothesis that the grey level of masses in images with 0.7 mm simulated blur (M= 94.326, SD=22.864), 1.5 mm level (M= 94.848, SD= 22.444) and the grey level of masses in images with no motion blur (0.0mm) (M= 92.450, SD= 23.394) are equal. The assumption of normally distributed difference scores was examined, and the data was normally distributed (see **Table 6.2**). The grey level difference between the two magnitudes of simulated motion blur and no motion blur were no statistically significant for all comparisons of motion blur levels (see **Table 6.5**). **Figure 6.3** shows the means of ΔGL and confidence interval 95% of the two magnitudes of simulated motion blur and no motion blur. The boxes of the ΔGL in (**Figure 6.3**) have approximately the same distribution (similar position and shape).

Table 6.5 Demonstrates the grey level measures of 23 masses cases for images with no blur and two levels of simulated motion blur.

Grey Level change		0.0mm	0.7 mm	1.5 mm
Mean		92.450	94.326	94.848
95% Confidence Interval for Mean	Lower Bound	82.333	84.439	85.143
	Upper Bound	102.566	104.213	104.554
5% Trimmed Mean		92.146	94.150	94.749
Median		96.358	96.797	96.836
Variance		547.282	522.755	503.724
Std. Deviation		23.394	22.864	22.444
Minimum		57.73	58.54	58.04
Maximum		133.19	133.54	133.61
Range		75.46	75.00	75.57
Interquartile Range		39.25	39.67	38.60

T-test Pairs	**Result of T-test / Difference (95% CI)**
0.0 mm – 0.7 mm	$t(22) = -1.226$, $p>0.233$/ -1.877 (-5.053, 1.299)
0.0 mm – 1.5 mm	$t(22) = -1.868$, $p> 0.075$/ -2.399 (-5.062, 0.264)
0.7 mm – 1.5 mm	$t(22) = -0.663$, $p>0.514$ / -0.522 (-2.154, 1.111)

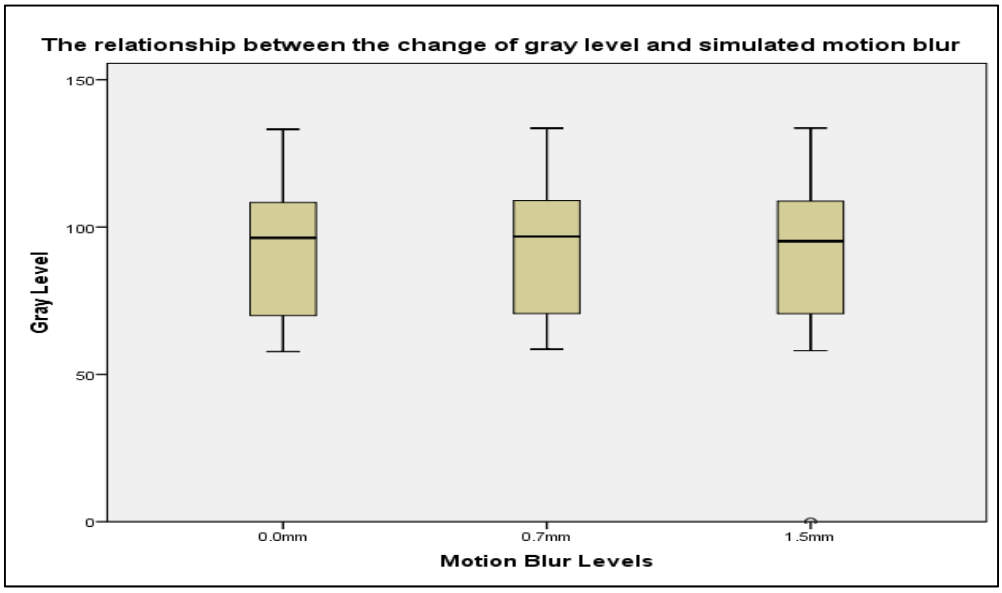

Figure 6.3 The relationship between the magnitude of simulated motion blur and the grey level of breast masses.

6.2.5 Signal to Noise Ratio (SNR):

A paired sample t-test was performed to test the hypothesis that SNR in images with simulated blur (0.7 mm) level (M= 4.394, SD=1.188), 1.5 mm simulated motion blur (M= 5.653, SD= 2.029) and SNR of images without motion blur (0.0mm) (M= 2.741, SD= 0.576) are equal. The assumption of normally distributed difference scores was examined, and the data was normally distributed (see **Table 6.2**). The SNR difference between the two magnitudes of simulated motion blur and no motion blur were statistically significant for all comparisons (See **Table 6.8**). **Figure 6.4** illustrates relationship between the magnitude of simulated motion blur and SNR of breast masses. It can be noted that SNR increases significantly with increase the level of simulated motion blur as consequence of the smoothing process. Each of the box plots in (**Figure 6.4**) is different in size and positions. The distribution of (0.0mm) box plots is lower than of box plots (0.7 & 1.5 mm). The median of SNR was pointed by the horizontal line, which runs up the centre of the boxes. The medians of SNR were 2.848 for images without blur 0.0mm, and (4.479, 5.653) for images with simulated motion blur 0.7mm and 1.5 mm respectively.

Table 6.6 Demonstrates SNR measures of 23 masses cases for images with no motion blur and two levels of simulated motion blur.

SNR		0.0 mm	0.7 mm	1.5 mm
Mean		2.741	4.394	5.653
95% Confidence Interval for Mean	Lower Bound	2.492	3.880	4.776
	Upper Bound	2.990	4.908	6.531
5% Trimmed Mean		2.754	4.414	5.503
Median		2.848	4.479	5.238
Variance		0.332	1.413	4.116
Std. Deviation		0.576	1.188	2.029
Minimum		1.581	2.191	2.430
Maximum		3.660	6.280	12.151
Range		2.091	4.090	9.720
Interquartile Range		0.820	1.501	2.040

T-test Pairs	**Result of T-test / Difference (95% CI)**
0.0 mm – 0.7 mm	$t(22) = -9.307$, $p<0.000$ / -1.653 (-2.021, -1.285)
0.0 mm – 1.5 mm	$t(22) = -8.608$, $p<0.000$ / -2.913 (-3.614, -2.211)
0.7 mm – 1.5 mm	$t(22) = -3.714$, $p<0.01$ /-1.260 (-1.963, -0.556)

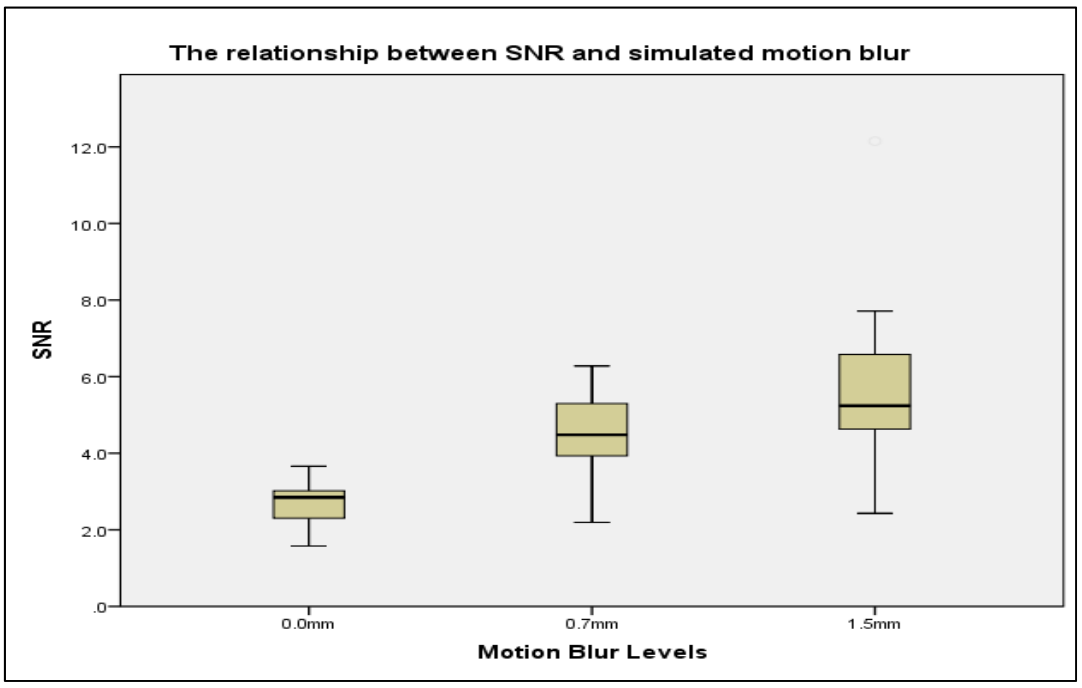

Figure 6.4 The relationship between the magnitude of simulated motion blur and the signal to noise ratio (SNR) of breast masses.

6.3 Part II: Physical Measures of Microcalcifications

Disperion Index (DI) has been developed for this thesis to test the dispersion index of microcacifications and also to investigate the relationship between physical measures of microcalcifications and their detectability. Dispersion index of microcalcifications repsesents the number of calcifications within a specified area divided by the area. DI was measured within Imagej software (Schindelin et al., 2012) because the conspicuity index could not be applied to microcalcifications due to their individual size and their wide distribution pattern. This represents a limitation of the CI software. No validation has been conducted on DI, but this could be a focus for post doctoral work. However, during conducting this thesis no alternative technique existed (aside to DI) to gain a meaningful physical measure in relation to microcalcifications.

6.3.1 Normality Tests of Microcalcifications Data

For this data, the Kolmogorov-Smirnov test and Shapiro-Wilk test showed that the physical parameters data such as dispersion index, the contrast and DI x Contrast were not normally distributed with $P \leq 0.05$, and that the SNR data was normally distributed with $P \geq 0.05$ as illustrated in (**Table 6.7**). A normality test of the data of the physical measures of microcalcifications is required to check the suitability of the overall data for further analysis (Field et al., 2013).

Table 6.7 Values of Kolmogorov-Smirnov test and Shapiro-Wilk normality test for the physical measures data of breast masses

	Kolmogorov-Smirnov[a]			Shapiro-Wilk		
	Statistic	df	Sig.	Statistic	df	Sig.
Dispersion Index 0.0 mm	0.166	62	0.000	0.854	62	0.000
Contrast 0.0 mm	0.148	62	0.002	0.913	62	0.000
DI x Contrast 0.0 mm	0.166	62	0.000	0.849	62	0.000
SNR 0.0 mm	0.076	62	0.200*	0.984	62	0.611
Dispersion Index 0.7 mm	0.168	62	0.000	0.854	62	0.000
Contrast 0.7 mm	0.188	62	0.000	0.867	62	0.000
DI x Contrast 0.7 mm	0.159	62	0.000	0.846	62	0.000
SNR 0.7 mm	0.065	62	0.200*	0.983	62	0.535
Dispersion Index 1.5 mm	0.168	62	0.000	0.854	62	0.000
Contrast 1.5 mm	0.200	62	0.000	0.841	62	0.000
DI x Contrast 1.5 mm	0.163	62	0.000	0.846	62	0.000
SNR 1.5 mm	0.077	62	0.200*	0.976	62	0.257

*. This is a lower bound of the true significance.

a. Lilliefors Significance Correction

6.3.2 Dispersion Index (DI) of Microcalcifications

The results demonstrate that the dispersion index of clustered microcalcifications decreases with an increase in the level of simulated motion blur (**Table 6.8**). Simulated motion blur has a statistically significant and negative impact on DI of microcalcifications (**Table 6.9**). This means that the changes in the image characteristics of microcalcifications as motion blur increases from no motion blur could negatively influence the differential features of malignant microcalcifications. **Figure 6.5** graphically illustrates of the mean and confidence interval 95% of the two magnitudes of simulated motion blur and no motion blur with DI. Each of the box plots in (**Figure 6.5**) demonstrates a different skewness pattern. The distribution of (0.0 mm) box plots is skewed up while the distribution of box plots 0.7 mm and 1.5 mm are skewed down. The median is (0.687, 0.541 and 0.416) for images without blur 0.0 mm and for images with simulated motion blur 0.7 mm and 1.5 mm respectively.

Table 6.8 Demonstrates dispersion index of microcalcifications between images without motion blur (0.0 mm), and images with simulated motion blur (0.7 mm & 1.5 mm).

Dispersion Index		0.0 mm	0.7 mm	1.5 mm
Mean		0.963	0.743	0.594
95% Confidence Interval for Mean	Lower Bound	0.765	0.592	0.468
	Upper Bound	1.161	0.894	0.7197
5% Trimmed Mean		0.876	0.688	0.545
Median		0.687	0.541	0.416
Variance		0.628	0.364	0.253
Std. Deviation		0.792	0.604	0.503
Minimum		0.110	0.051	0.021
Maximum		4.131	3.001	2.631
Range		4.020	2.95	2.600
Interquartile Range		0.801	0.610	0.470

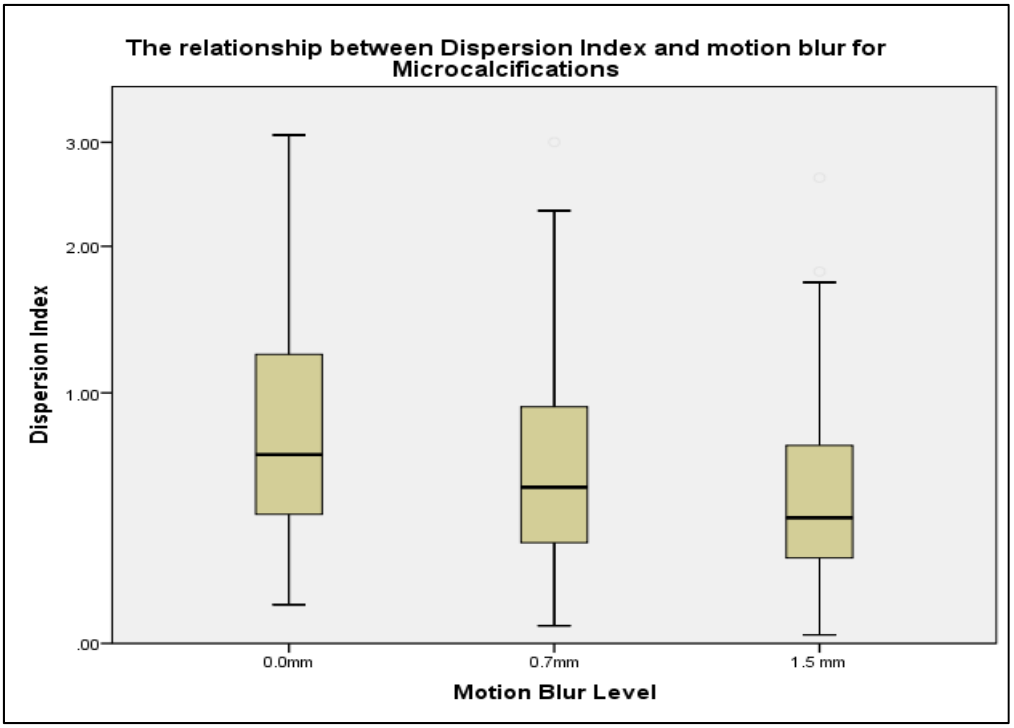

Figure 6.5 The relationship between the magnitude of simulated motion blur and dispersion index.

Table 6.9 Demonstrates the P-values of Wilcoxon Signed Ranks Test of physical measures of microcalcifications between images with no motion blur (0.0 mm), and images with simulated motion blur (0.7 mm & 1.5 mm).			
Simulated motion blur level	Dispersion Index	Contrast	DI x Contrast
0.0 mm - 0.7 mm	0.000	0.000	0.253
0.0 mm- 1.5 mm	0.000	0.000	0.000
0.7 mm- 1.5 mm	0.000	0.000	0.000

6.3.3 Contrast of Microcalcifications

The results demonstrate that the contrast of clustered microcalcifications increases with an increase in the level of simulated motion blur (**Table 6.10**). A non-parametric test (Wilcoxon Signed Ranks Test) was performed to investigate the hypothesis that contrast in images with simulated blur at 0.7 mm, 1.5 mm and contrast in images with no motion blur (0.0mm) are equal. Prior to conducting the analysis, the assumption of normally distributed difference scores was examined and the data was non-normally distributed (**Table 6.8**). **Figure 6.6** shows the means of contrast and confidence interval 95% of the two magnitudes of simulated motion blur and no motion blur. The contrast of microcalcifications increases with increase the level of simulated motion blur. The diagram illustrates a variety of different box plot that positions and shapes. The distribution of (0.0 mm) box plots is skewed down while the distribution of box plot (0.7 mm) is skewed up and box plot of 1.5 mm is much higher. The three sections of the box plot are different in size and position.

Table 6.10 Demonstrates contrast of microcalcifications for images without motion blur (0.0 mm), and images with simulated motion blur (0.7 & 1.5 mm).

Contrast of Microcalcifications		**0.0 mm**	**0.7 mm**	**1.5 mm**
Mean		0.839	0.897	0.916
95% Confidence Interval for Mean	Lower Bound	0.825	0.884	0.904
	Upper Bound	0.852	0.910	0.927
5% Trimmed Mean		0.842	0.901	0.920
Median		0.848	0.910	0.930
Variance		0.003	0.003	0.002
Std. Deviation		0.053	0.051	0.047
Minimum		0.680	0.730	0.750
Maximum		0.930	0.970	0.980
Range		0.260	0.240	0.230
Interquartile Range		0.060	0.050	0.040

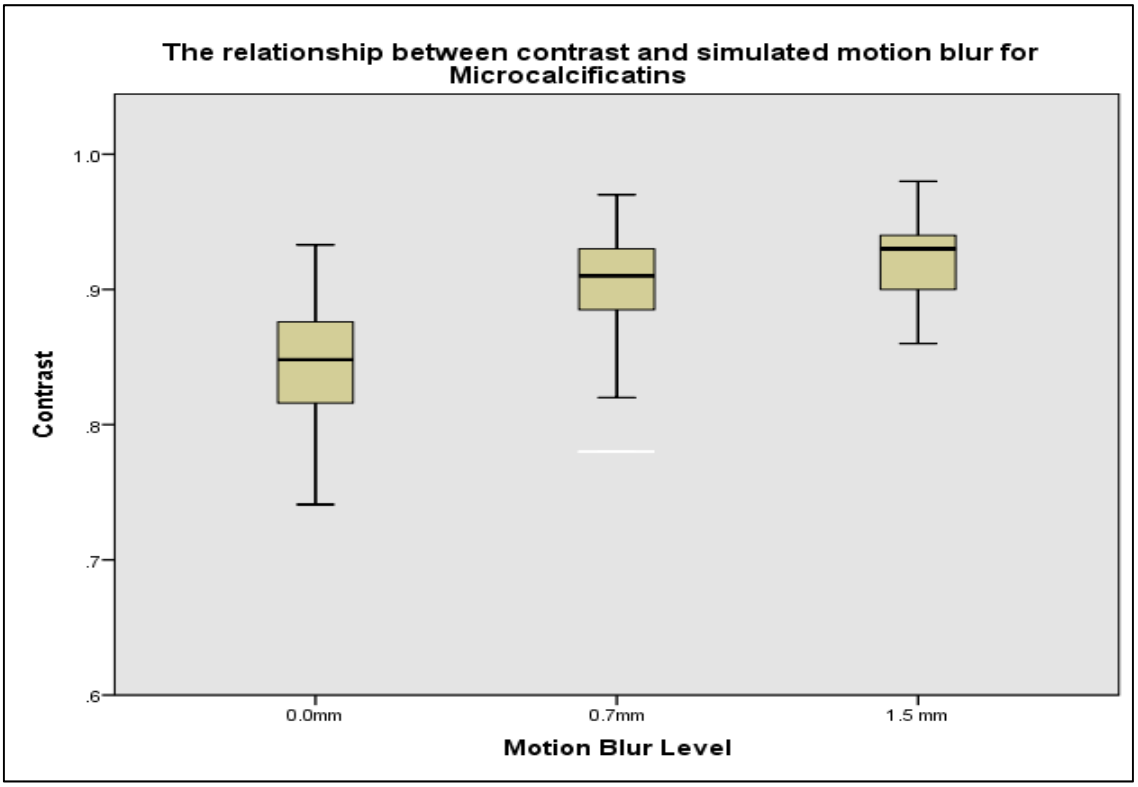

Figure 6.6 The relationship between the magnitudes of simulated motion blur and contrast of malignant microcalcifications.

6.3.4 Dispersion Index and Contrast of Microcalcifications

The results demonstrate that DI x contrast of clustered microcalcifications decreases with an increase in the level of simulated motion blur (**Table 6.11**). A non-parametric test (Wilcoxon Signed Ranks Test) was performed to test the hypothesis that DI x contrast in images with simulated blur 0.7 mm, 1.5 mm and DI x contrast in images without motion blur (0.0mm) are equal. Prior to conducting the analysis, the assumption of normally distributed difference scores was examined and the results were non-normally distributed. Simulated motion blur has a statistically significant negative impact on DI x contrast of microcalcifications (Table 6.8). A graphical representation of the means and adjusted 95% confidence interval is displayed in (**Figure 6.7**).

Table 6.11 Demonstrates measures DI x contrast of microcalcifications for images without motion blur (0.0 mm), and images with simulated motion blur (0.7 & 1.5 mm).

DI x Contrast of Microcalcifications		**0.0 mm**	**0.7 mm**	**1.5 mm**
Mean		0.824	0.815	0.640
95% Confidence Interval for Mean	Lower Bound	0.646	0.655	0.508
	Upper Bound	1.002	0.975	0.771
5% Trimmed Mean		0.742	0.761	0.592
Median		0.587	0.596	0.466
Variance		0.506	0.410	0.276
Std. Deviation		0.711	0.640	0.525
Minimum		0.080	0.060	0.030
Maximum		3.850	3.100	2.690
Range		3.770	3.040	2.660
Interquartile Range		0.700	0.650	0.520
Skewness		2.007	1.463	1.654
Kurtosis		5.011	1.896	2.942

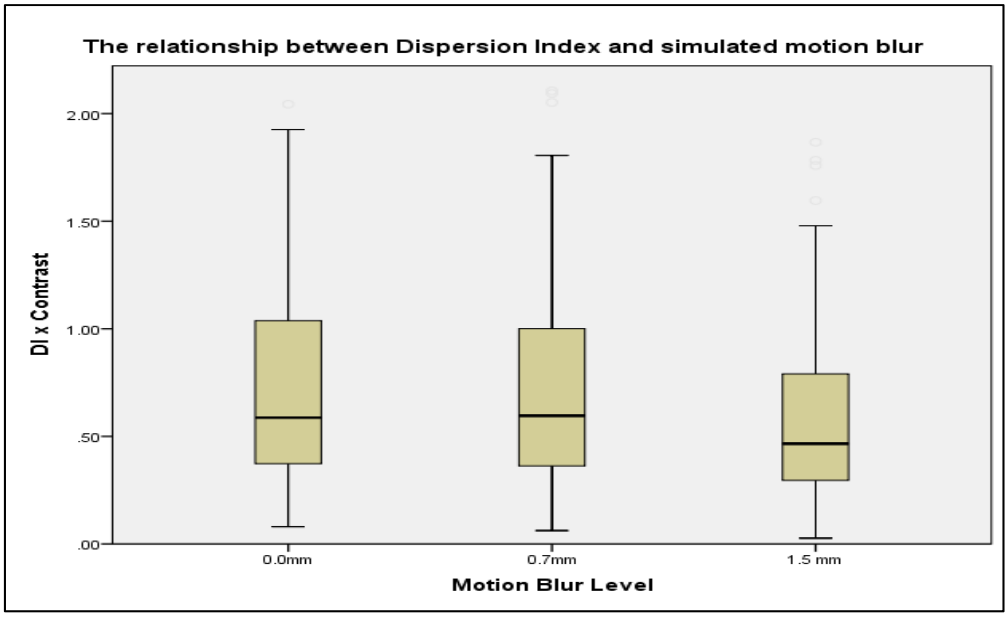

Figure 6.7 The relationship between the magnitude of simulated motion blur and DI x contrast of microcalcifications.

6.3.5 Signal to Noise Ratio (SNR) of Microcalcifications Images:

A paired sample t-test was performed to test the hypothesis that SNR in images with simulated blur (0.7 mm) (M= 34.413, SD=13.958), 1.5 mm simulated motion blur (M= 38.035, SD= 17.361) and SNR in images without motion blur (0.0mm) (M=26.97, SD= 7.859) are equal. Prior to conducting the analysis, the assumption of normally distributed difference scores was examined and, the data was normally distributed. The SNR difference between the two magnitudes of simulated motion blur and no motion blur were statistically significant for all comparisons (See **Table 6.12**).

A graphical representation of the means and adjusted 95% confidence interval is displayed in (**Figure 6.8**). Each of the box plots in (**Figure 6.8**) shows a different skewness pattern. The distribution of (0.0mm) box plots is skewed down while the distribution of box plots (0.7 & 1.5mm) are skewed up. The box plot in 0.0mm is much lower than the box plots in 0.7mm and 1.5mm respectively. The three sections of the box plot are different in size. The box plot in 0.0mm level is comparatively short. The medians of SNR are generally close to the average, which are approximately (26.725, 33.065, and 37.075) for images without blur 0.0mm and for images with motion blur 0.7mm and 1.5 mm respectively.

Table 6.12 demonstrates SNR of microcalcification for images with no blur and two levels of simulated motion blur.

SNR of Microcalcifications		**0.0 mm**	**0.7 mm**	**1.5 mm**
Mean		26.97	34.413	38.035
95% Confidence Interval for Mean	Lower Bound	25.011	30.926	33.702
	Upper Bound	28.938	37.899	42.375
5% Trimmed Mean		26.963	34.132	37.427
Median		26.725	33.065	37.075
Variance		61.779	194.849	301.424
Std. Deviation		7.859	13.958	17.361
Minimum		7.740	6.480	3.850
Maximum		43.320	66.740	82.380
Range		35.580	60.260	78.530
Interquartile Range		10.430	20.200	25.250

T-test Pairs	**Result of T-test / Difference (95% CI)**
0.0 mm – 0.7 mm	$t(61) = -7.598$, $p<0.000$ / -7.438 (-9.394, -5.482)
0.0 mm – 1.5 mm	$t(61) = -7.705$, $p<0.000$ / -11.064 (-13.934, -8.195)
0.7 mm – 1.5 mm	$t(61) = -6.246$, $p<0.000$ / -3.626 (-4.786, -2.466)

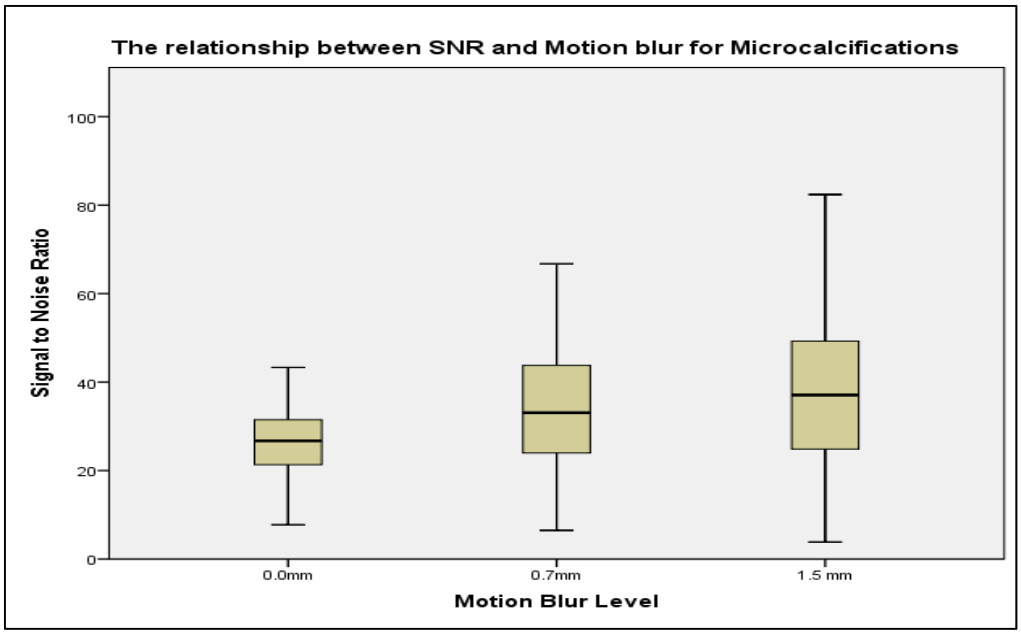

Figure 6.8 The relationship between the magnitude of simulated motion blur and SNR of microcalcifications.

6.4 The Relationship between Physical Measures and Detectability of Microcalcifications

The results of this focuses on the physical parameters of breast microcalcifications such as D.I, contrast, DI x contrast, signal to noise ratio (SNR) and detectability of lesions with different levels of motion blur (**Table 6.13**). A full range of physical measures acquired data for microcalcifications for image without simulated motion blur (0.0 mm), and images with simulated motion blur (0.7 & 1.5 mm) is presented in (**Appendix M**).

Some microcalcifications cases are highly affected by motion blur when the number calcifications is higher than 10 per cluster; where cluster refers to a collection of microcalcifications within a specified area. Some studies (Farshid et al., 2011) & Shao et al. (2011) suggested the probability of malignancy increases with the extent of the lesions on mammograms. Therefore, a DI metric has been performed to investigate the relationship between the physical measures of microcalcifications and their detectability with three levels of motion blur. From **Figure 6.9 to Figure 6.17** show there is no relationship between simulated motion blur and physical measures (D.I, contrast, DI x contrast, and SNR).

Table 6.13 The physical measures of microcalcifications in image with no simulated motion blur (0.0 mm), and images with simulated motion blur (0.7 & 1.5 mm).

	Motion blur levels														
	0.0 mm					0.7 mm					1.5 mm				
Lesion No.	**DI**	**Cont.**	**DI x Con**	**SNR**	**Detect ability**	**DI**	**Cont.**	**DI x Con**	**SNR**	**Detect ability**	**DI**	**Cont.**	**DI x Con**	**SNR**	**Detect ability**
1	1.384	0.890	1.231	41.937	1.00	1.092	1.064	1.162	65.903	1.00	0.801	1.043	0.836	80.936	0.57
2	1.231	0.883	1.087	33.100	1.00	0.934	1.076	1.005	40.395	1.00	1.189	1.058	1.258	42.614	0.85
3	0.918	0.882	0.810	31.978	1.00	0.660	1.077	0.711	38.439	0.86	0.488	1.059	0.516	40.489	0.57
4	0.371	0.850	0.316	25.417	0.57	0.272	1.074	0.292	28.612	0.43	0.198	1.062	0.210	30.236	0.00
5	0.343	0.705	0.242	16.994	1.00	0.225	1.360	0.306	18.511	1.00	0.216	1.296	0.279	19.178	1.00
6	0.426	0.818	0.348	17.616	0.57	0.290	1.154	0.334	18.885	0.43	0.256	1.126	0.288	19.511	0.14
7	0.834	0.820	0.684	26.729	1.00	0.660	1.109	0.732	36.783	1.00	0.487	1.073	0.522	42.352	1.00
8	1.079	0.874	0.943	30.416	1.00	0.863	1.064	0.919	35.927	1.00	0.648	1.050	0.680	37.319	1.00
9	0.292	0.835	0.244	22.641	0.86	0.243	1.146	0.279	24.575	0.57	0.178	1.129	0.202	25.472	0.14
10	0.316	0.829	0.262	24.361	1.00	0.278	1.091	0.303	26.537	0.86	0.215	1.068	0.229	27.239	0.43
11	0.863	0.874	0.754	30.416	1.00	0.648	1.064	0.689	35.927	0.85	0.504	1.050	0.529	37.319	0.43
12	0.524	0.868	0.455	32.058	0.85	0.434	1.089	0.473	38.371	0.72	0.315	1.067	0.336	40.661	0.43
13	1.091	0.861	0.940	25.826	1.00	0.755	1.078	0.814	35.850	0.57	0.587	1.059	0.622	42.052	0.86
14	1.644	0.836	1.375	30.497	1.00	1.644	1.098	1.806	45.660	1.00	1.644	1.070	1.759	52.843	1.00
15	1.039	0.817	0.849	19.745	1.00	0.873	1.142	0.997	26.128	0.57	0.748	1.111	0.831	29.915	0.72
16	3.081	0.902	2.779	36.045	1.00	2.311	1.050	2.427	62.583	0.43	1.797	1.039	1.867	76.603	0.29
17	0.135	0.755	0.102	17.475	0.57	0.072	1.177	0.084	18.153	0.14	0.024	1.151	0.027	18.432	0.29
18	0.138	0.770	0.106	17.204	0.43	0.050	1.236	0.062	17.686	0.29	0.044	1.200	0.053	17.860	0.00
19	0.324	0.814	0.264	19.087	1.00	0.281	1.132	0.318	20.348	0.43	0.195	1.102	0.215	20.891	0.29

20	0.519	0.837	0.434	26.142	1.00	0.424	1.106	0.469	29.235	0.43	0.377	1.085	0.409	29.860	0.57
21	1.123	0.847	0.951	26.718	0.72	0.898	1.085	0.974	43.555	0.43	0.786	1.060	0.833	55.100	0.86
22	0.527	0.816	0.430	23.446	1.00	0.461	1.121	0.517	33.045	1.00	0.395	1.089	0.430	40.379	1.00
23	0.610	0.741	0.452	19.164	1.00	0.529	1.217	0.643	21.824	1.00	0.437	1.163	0.508	22.927	1.00
24	0.593	0.816	0.484	23.446	1.00	0.527	1.121	0.591	33.045	0.72	0.461	1.089	0.502	40.379	0.29
25	1.798	0.851	1.529	30.094	1.00	1.498	1.075	1.611	43.183	1.00	1.199	1.053	1.262	51.730	0.72
26	0.400	0.818	0.328	24.267	1.00	0.308	1.120	0.345	27.066	0.14	0.246	1.100	0.271	28.234	0.43
27	0.504	0.873	0.441	29.445	1.00	1.979	1.058	2.094	52.393	1.00	1.715	1.039	1.783	65.020	1.00
28	3.035	0.878	2.666	30.421	1.00	0.395	1.079	0.426	32.785	0.29	0.307	1.068	0.328	34.208	0.00
29	0.355	0.879	0.312	29.415	1.00	0.210	1.084	0.228	33.079	0.86	0.178	1.076	0.191	34.510	0.00
30	1.807	0.813	1.469	22.563	1.00	1.536	1.113	1.709	30.590	1.00	1.084	1.073	1.164	34.509	0.72
31	0.407	0.885	0.360	42.163	1.00	0.356	1.084	0.386	58.661	0.72	0.305	1.063	0.324	68.306	0.72
32	0.344	0.845	0.291	30.250	0.72	0.325	1.054	0.343	50.527	0.43	0.344	1.072	0.369	36.830	0.29
33	1.154	0.857	0.989	23.797	1.00	0.938	1.096	1.027	33.335	1.00	0.649	1.063	0.690	40.408	1.00
34	0.708	0.918	0.650	43.316	1.00	0.472	1.043	0.492	59.089	1.00	0.393	1.035	0.407	62.587	0.72
35	0.797	0.903	0.720	39.172	1.00	0.545	1.058	0.577	50.048	0.43	0.336	1.043	0.350	55.125	0.14
36	1.219	0.896	1.092	37.352	0.72	0.914	1.051	0.961	50.704	0.14	0.711	1.042	0.741	58.915	0.00
37	0.808	0.856	0.692	24.545	0.86	0.539	1.115	0.601	27.471	1.00	0.350	1.098	0.384	28.689	0.72
38	2.195	0.877	1.926	28.573	1.00	1.596	1.072	1.711	41.712	1.00	1.397	1.055	1.474	47.745	1.00
39	0.992	0.875	0.868	33.865	1.00	0.850	1.084	0.922	44.094	1.00	0.709	1.058	0.750	48.152	0.86
40	0.227	0.790	0.179	15.869	0.86	0.212	1.189	0.253	16.741	0.86	0.191	1.169	0.223	17.229	0.72
41	0.949	0.877	0.833	33.421	0.00	0.576	1.086	0.626	45.533	0.00	0.509	1.063	0.541	53.154	0.00
42	0.577	0.778	0.449	21.297	1.00	0.577	1.185	0.684	26.301	1.00	0.577	1.148	0.663	28.756	1.00
43	2.336	0.875	2.044	30.619	1.00	1.934	1.061	2.052	49.347	1.00	1.531	1.042	1.596	58.999	1.00
44	0.800	0.850	0.680	30.134	1.00	0.695	1.106	0.769	40.874	1.00	0.556	1.075	0.598	46.925	0.72
45	0.677	0.863	0.584	28.022	0.86	0.542	1.081	0.586	33.045	0.57	0.316	1.068	0.338	34.799	0.14
46	0.476	0.883	0.421	37.722	0.72	0.278	1.065	0.296	47.684	0.29	0.238	1.046	0.249	51.536	0.00
47	0.521	0.853	0.445	24.452	0.86	0.521	1.118	0.583	27.135	0.72	0.521	1.103	0.575	28.191	0.72
48	0.503	0.820	0.412	21.925	0.72	0.258	1.165	0.300	23.383	0.29	0.225	1.146	0.258	24.122	0.29
49	0.179	0.779	0.139	17.682	0.86	0.124	1.201	0.149	18.750	1.00	0.080	1.168	0.093	19.202	0.86
50	1.605	0.847	1.359	32.138	1.00	0.843	1.088	0.917	40.854	1.00	0.522	1.063	0.554	43.838	0.57
51	2.076	0.845	1.753	30.503	1.00	1.639	1.090	1.787	43.539	0.86	1.202	1.066	1.281	50.335	0.29
52	4.128	0.933	3.852	42.565	1.00	3.002	1.033	3.101	66.743	0.43	2.627	1.023	2.687	82.383	0.29
53	1.304	0.880	1.148	30.465	1.00	1.043	1.082	1.129	36.054	0.86	0.626	1.066	0.667	37.848	0.59
54	2.207	0.812	1.792	18.588	1.00	1.891	1.113	2.106	27.941	0.86	1.366	1.082	1.479	34.383	1.00
55	0.696	0.848	0.590	20.017	0.86	0.544	1.122	0.611	21.552	1.00	0.302	1.108	0.335	21.844	0.57
56	2.064	0.874	1.805	31.030	1.00	1.622	1.103	1.789	6.748	0.86	1.032	1.107	1.142	4.760	0.43
57	0.457	0.848	0.388	38.224	1.00	0.373	1.112	0.414	51.145	1.00	0.288	1.081	0.311	58.309	1.00
58	0.608	0.847	0.515	22.595	1.00	0.405	1.110	0.450	25.336	1.00	0.262	1.097	0.288	26.495	0.86
59	0.399	0.715	0.286	12.505	0.00	0.318	1.288	0.410	13.200	0.00	0.288	1.244	0.359	13.464	0.00
60	0.490	0.802	0.393	19.823	1.00	0.327	1.211	0.396	21.454	1.00	0.272	1.191	0.324	22.394	0.72
61	0.113	0.709	0.080	13.458	0.72	0.083	1.260	0.105	14.581	0.29	0.053	1.192	0.063	14.990	0.29
62	1.266	0.675	0.854	7.745	0.86	1.022	1.363	1.393	6.480	0.72	0.876	1.336	1.171	3.848	0.43
Min.	0.113	0.675	0.080	7.745	0.000	0.050	1.033	0.062	6.480	0.000	0.024	1.023	0.027	3.848	0.000
Max.	4.128	0.933	3.852	43.316	1.000	3.002	1.363	3.101	66.743	1.000	2.627	1.336	2.687	82.383	1.000
Ave.	0.977	0.838	0.837	26.911	0.890	0.754	1.119	0.827	34.438	0.715	0.603	1.096	0.649	38.118	0.556

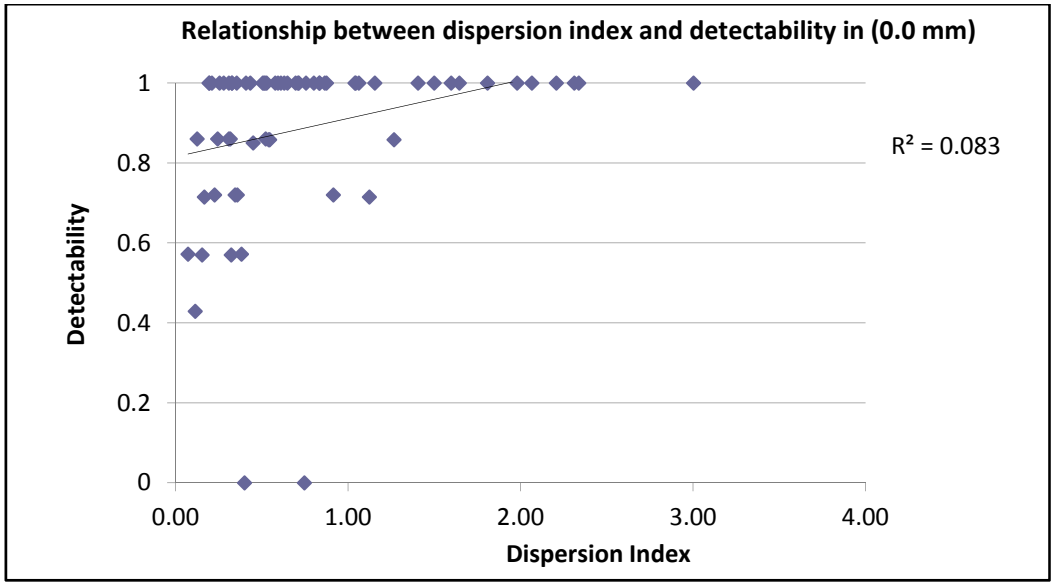

Figure 6.9 Shows the relationship between dispersion index of microcalcifications and their detectability in images without motion blur. This figure demonstrates there is no relationship (R2= 0.083) between the detectability and dispersion index of microcalcifications.

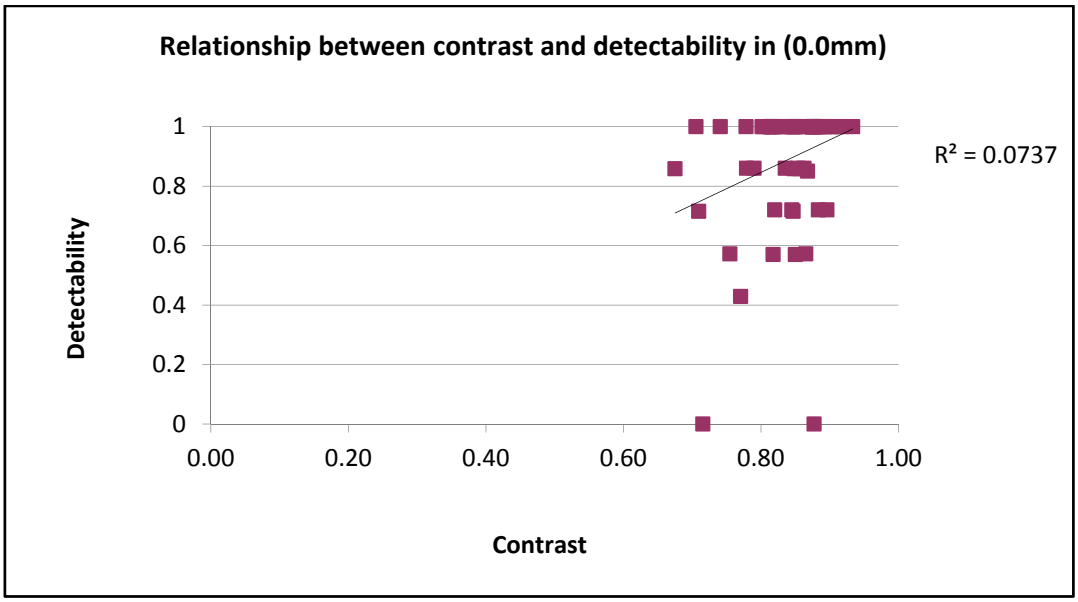

Figure 6.10 Demonstrates the relationship between the contrast of microcalcifications and their detectability in images without simulated motion blur. There is no relationship (R2= 0.0737) between contrast and detectability of microcalcifications.

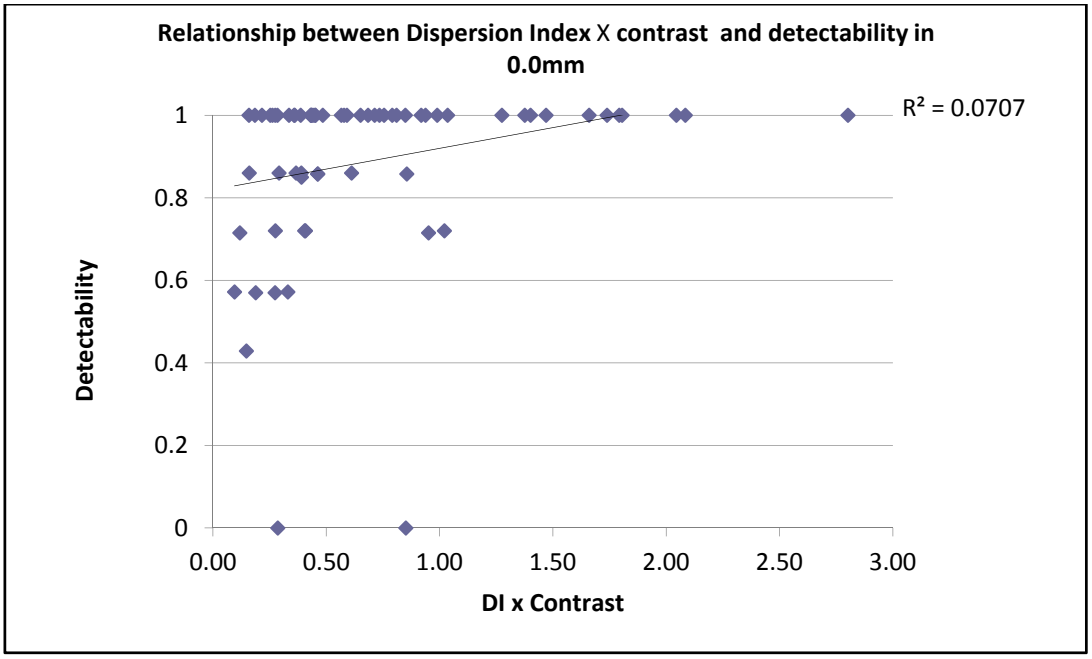

Figure 6.11 Demonstrates the relationship between the DI x contrast of microcalcifications and their detectability in images without simulated motion blur. There is no relationship (R2=0.070) between the DI x contrasts of microcalcification and the detectability of the lesion.

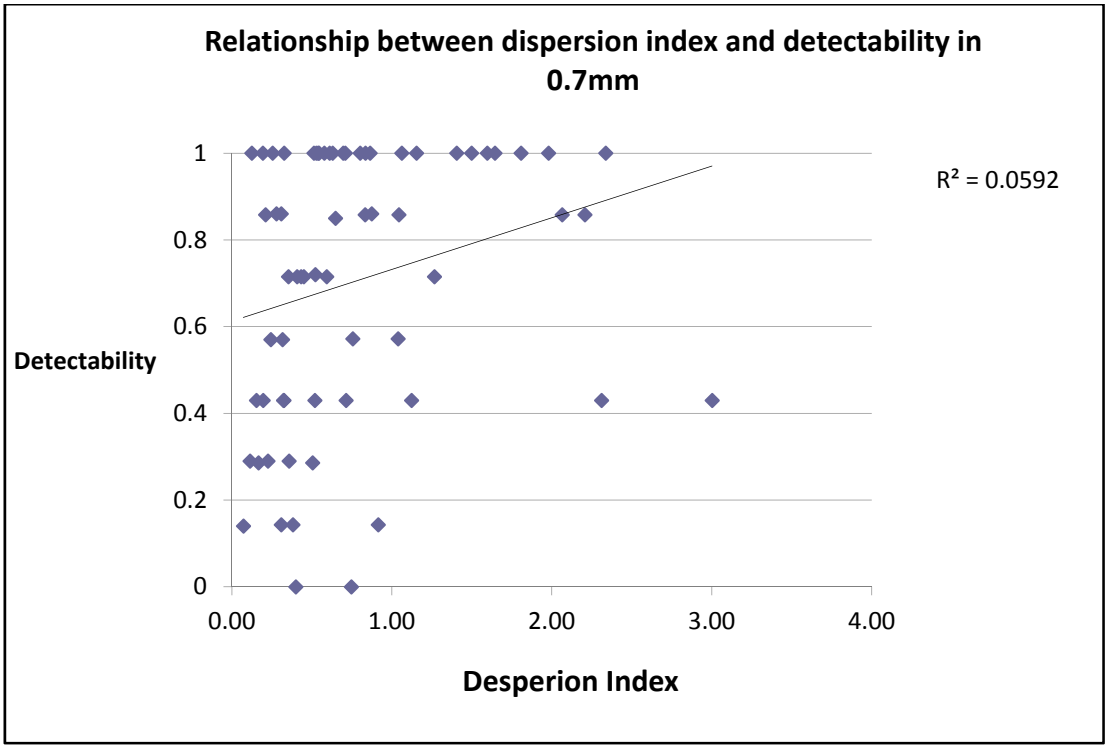

Figure 6.12 Demonstrates there is no relationship between dispersion index of microcalcifications and the detectability of the lesion in images with simulated motion blur (0.7mm).

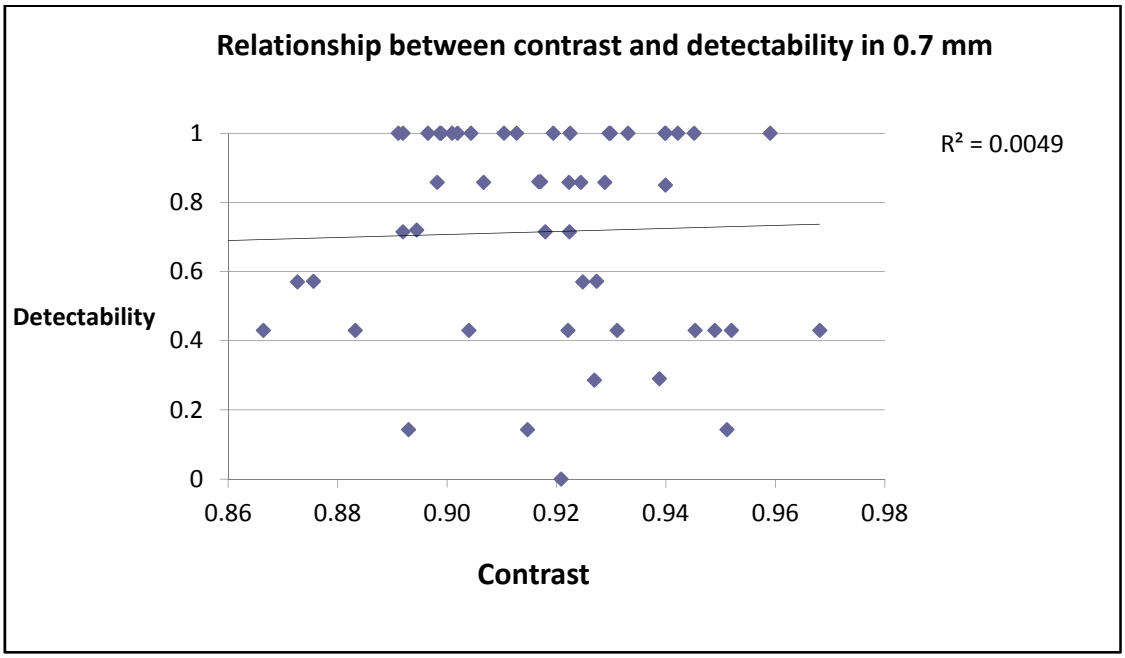

Figure 6.13 Demonstrates there is no relationship between the contrast of microcalcifications and the detectability of the lesion in images with simulated motion blur (0.7mm).

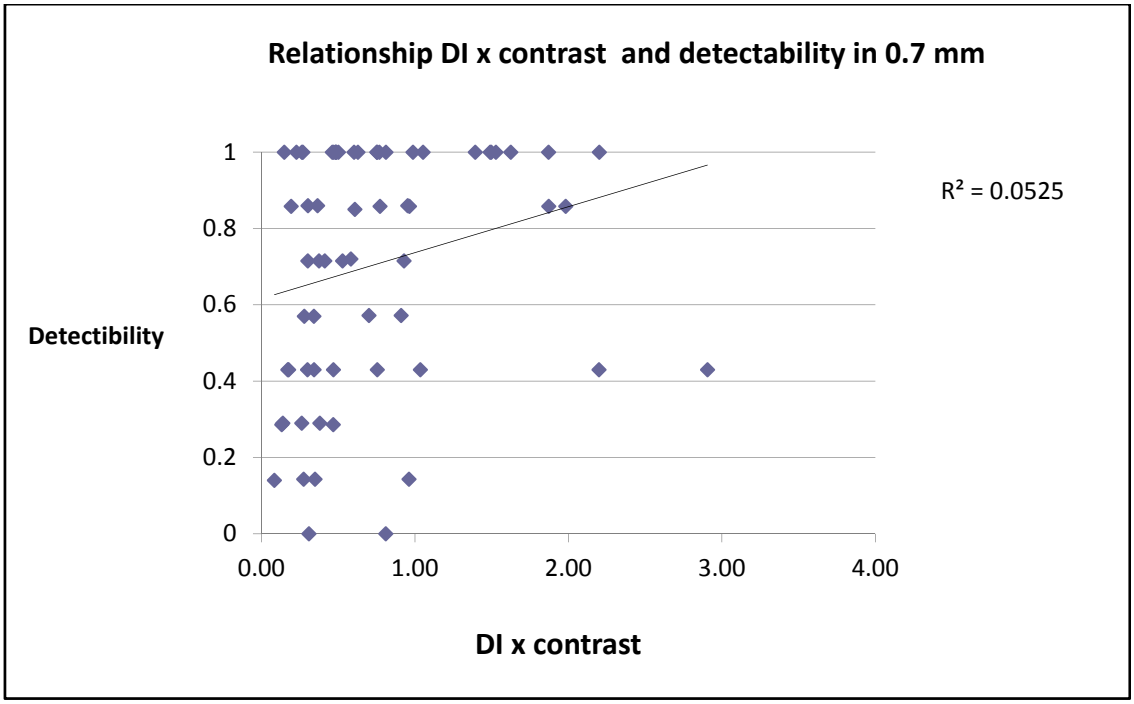

Figure 6.14 Demonstrates there is no relationship between DI x contrast of microcalcifications and the detectability of the lesion in images with simulated motion blur (0.7mm).

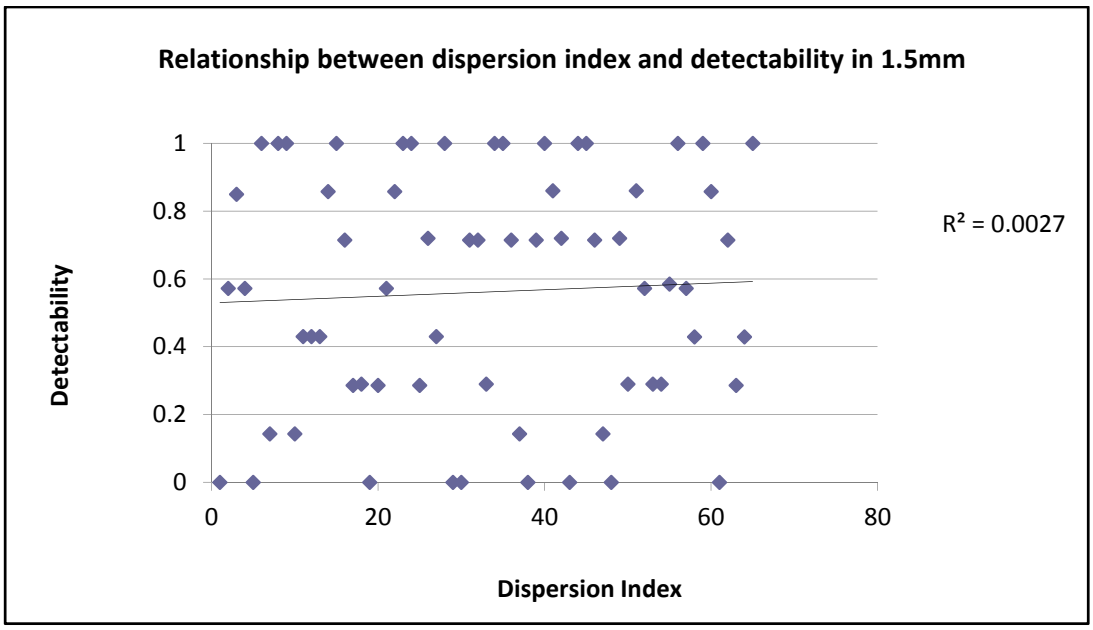

Figure 6.15 Shows the relationship between dispersion index of microcalcifications and their detectability in images with (1.5 mm) motion blur. This figure demonstrates there is no relationship (R2 = 0.0027) between the detectability and dispersion index of microcalcifications.

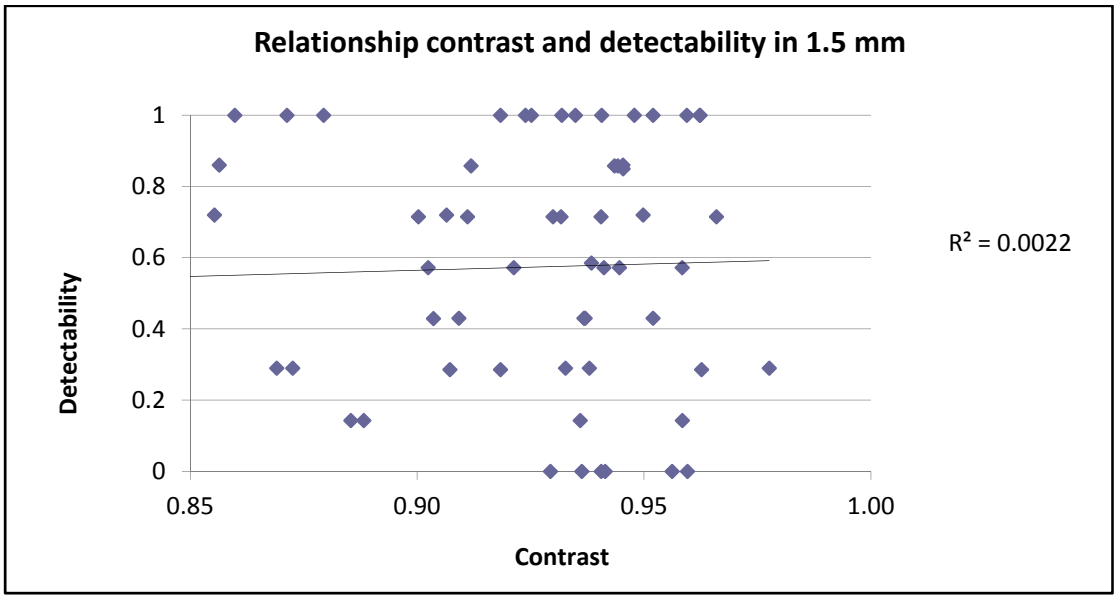

Figure 6.16 Demonstrates that there is no relationship between dispersion index of microcalcifications and the detectability of the lesion in images with motion blur (1.5 mm).

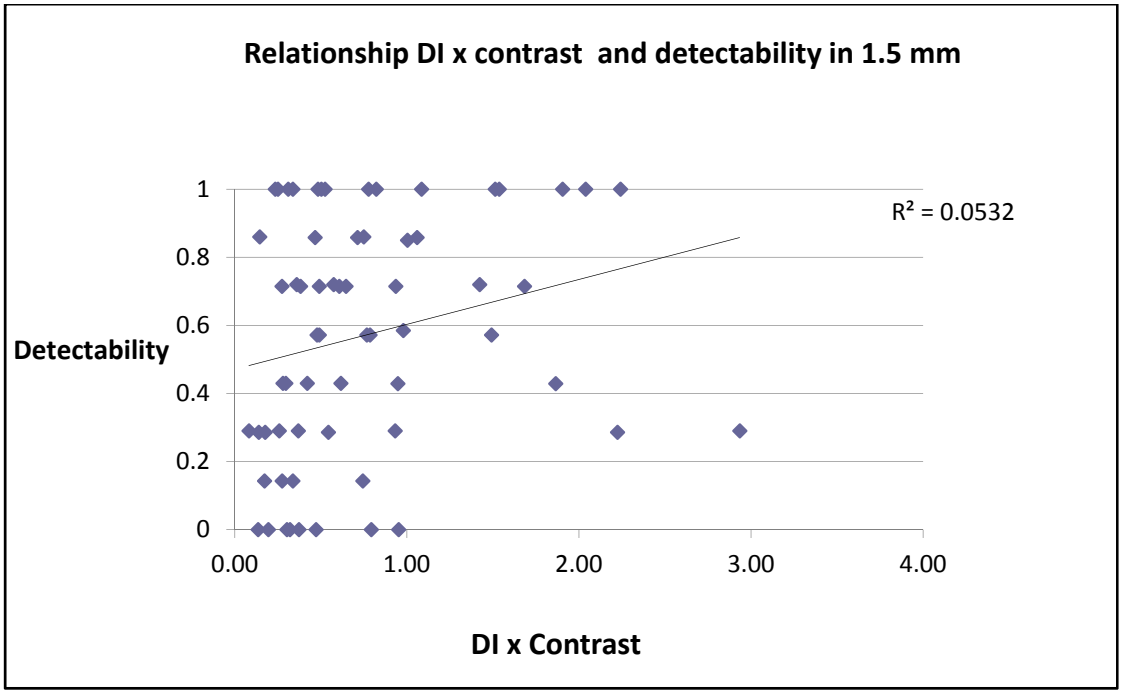

Figure 6.17 Demonstrates there is no relationship between DI x contrast of microcalcifications and the detectability of the lesion in images with simulated motion blur (1.5 mm).

6.5 Missed Lesion Analysis

Missed lesion analysis (i.e. no detection in the free-response study) has been used to evaluate trends and to identify particular lesion types that have been overlooked frequently. This analysis has been done for all magnitudes of simulated motion blur such that the impact of simulated motion blur can be assessed for different lesion types. Comprehensive tables presented in (**Table 6.14 & Table 6.15**) to exhibit a list of all lesions missed and detected, describing detectability as the primary outcome. The detectability for each lesion is represented by the number of observers who successfully detected the lesion divided by the total number of opportunities for detection. For instance, when the all observers detected the lesions (7/7), this means that the detectability is 100%.

Table 6.14 The detectability of malignant masses by the observers in images without motion blur (0.0 mm), and images with simulated motion blur (0.7mm & 1.5 mm).

No.	Observer 1			Observer 2			Observer 4			Observer 5			Observer 6			Observer 7			Observer 9			Detect ability %	Detect ability %	Detect ability %
	0.0	0.7	1.5	0.0	0.7	1.5	0.0	0.7	1.5	0.0	0.7	1.5	0.0	0.7	1.5	0.0	0.7	1.5	0.0	0.7	1.5	0.0 mm	0.7 mm	1.5 mm
1	✓	✓	✓	✓	✓	✓	✓	✓	✓	✓	✓	✓	✓	✓	✓	✓	✓	✓	✓	✓	✓	100%	100%	100%
2	✓	✓	✓	✓	✓	✓	✓	✓	✓	✓	✓	✓	✓	✓	✓	✓	✓	✓	✓	✓	✓	100%	100%	100%
3	X	X	X	x	X	X	X	X	X	X	X	X	X	x	X	X	X	X	X	X	X	0%	0%	0%
4	✓	✓	✓	✓	✓	✓	✓	✓	✓	✓	✓	✓	✓	✓	✓	✓	✓	✓	✓	✓	✓	100%	100%	100%
5	✓	✓	✓	✓	✓	✓	✓	✓	✓	✓	✓	✓	✓	✓	✓	✓	✓	✓	✓	✓	✓	100%	100%	100%
6	✓	✓	✓	✓	✓	✓	✓	✓	✓	✓	✓	✓	✓	✓	✓	✓	✓	✓	✓	✓	✓	100%	100%	100%
7	✓	✓	✓	✓	✓	✓	✓	✓	✓	✓	✓	✓	✓	✓	✓	✓	✓	✓	✓	X	✓	100%	86%	100%
8	✓	✓	✓	✓	✓	✓	✓	✓	✓	✓	✓	✓	✓	✓	✓	✓	✓	✓	✓	✓	✓	100%	100%	100%
9	X	X	X	✓	✓	X	✓	X	X	✓	✓	X	✓	✓	✓	X	X	X	✓	X	✓	71%	43%	29%
10	✓	X	X	✓	X	✓	✓	✓	✓	✓	✓	✓	✓	✓	✓	✓	X	✓	X	✓	✓	86%	57%	86%
11	X	✓	✓	✓	X	✓	✓	X	✓	✓	✓	✓	✓	✓	✓	✓	✓	✓	X	X	✓	71%	57%	100%
12	✓	✓	✓	✓	✓	✓	✓	X	✓	✓	✓	✓	✓	✓	✓	✓	✓	✓	✓	✓	✓	100%	86%	100%
13	X	✓	✓	✓	✓	✓	✓	✓	✓	✓	✓	✓	✓	✓	✓	✓	✓	✓	✓	✓	✓	86%	100%	100%
14	✓	✓	✓	✓	✓	✓	✓	✓	✓	✓	✓	✓	✓	✓	✓	✓	✓	✓	X	✓	✓	86%	100%	100%
15	✓	✓	✓	✓	✓	✓	✓	✓	✓	✓	✓	✓	✓	✓	✓	✓	✓	✓	✓	✓	✓	100%	100%	100%
16	✓	✓	✓	✓	✓	✓	✓	✓	✓	✓	✓	✓	✓	✓	✓	✓	✓	✓	✓	✓	✓	100%	100%	100%
17	✓	X	✓	✓	✓	✓	✓	✓	✓	✓	✓	✓	✓	✓	✓	✓	✓	✓	✓	✓	✓	100%	86%	100%
18	✓	✓	X	✓	✓	✓	✓	✓	✓	✓	✓	✓	✓	✓	✓	✓	✓	✓	✓	✓	✓	100%	100%	86%
19	✓	✓	✓	✓	✓	✓	✓	✓	✓	✓	✓	✓	✓	✓	✓	✓	✓	✓	✓	✓	✓	100%	100%	100%
20	✓	✓	✓	✓	✓	✓	✓	✓	✓	✓	✓	✓	✓	✓	✓	✓	✓	✓	✓	✓	✓	100%	100%	100%
21	✓	X	✓	✓	✓	✓	✓	X	✓	✓	✓	✓	✓	✓	✓	✓	X	✓	✓	X	✓	100%	43%	100%
22	✓	✓	✓	✓	✓	✓	✓	✓	✓	✓	✓	✓	✓	✓	✓	✓	✓	✓	✓	✓	✓	100%	100%	100%
23	✓	✓	✓	✓	✓	✓	✓	✓	✓	✓	✓	✓	✓	✓	✓	✓	✓	✓	✓	✓	✓	100%	100%	100%
24	✓	✓	✓	✓	✓	✓	✓	✓	✓	✓	✓	✓	✓	✓	✓	✓	✓	✓	✓	✓	✓	100%	100%	100%
25	✓	✓	✓	✓	✓	✓	✓	✓	✓	✓	✓	✓	✓	✓	✓	✓	✓	✓	✓	✓	✓	100%	100%	100%
26	✓	✓	✓	✓	✓	✓	✓	✓	✓	✓	✓	✓	✓	✓	✓	✓	✓	✓	✓	✓	✓	100%	100%	100%
27	X	X	X	✓	✓	✓	✓	X	✓	✓	✓	✓	✓	✓	✓	✓	✓	X	X	X	X	71%	57%	57%
28	✓	✓	X	✓	X	✓	✓	✓	✓	✓	X	✓	✓	✓	✓	✓	✓	✓	X	✓	X	86%	71%	71%
29	X	X	X	X	X	X	X	X	X	✓	X	X	X	✓	X	X	X	X	X	X	X	14%	14%	0%
30	✓	X	✓	✓	✓	✓	✓	✓	✓	✓	✓	✓	✓	✓	✓	✓	✓	✓	✓	X	✓	100%	71%	100%

31	✓	✓	✓	✓	✓	✓	✓	✓	✓	✓	✓	✓	✓	✓	✓	✓	✓	✓	✓	✓	✓	100%	100%	100%
32	✓	✓	✓	✓	✓	✓	✓	✓	✓	✓	✓	✓	✓	✓	✓	✓	✓	✓	✓	✓	✓	100%	100%	100%
33	✓	✓	✓	✓	✓	✓	✓	✓	✓	✓	✓	✓	✓	✓	✓	✓	✓	✓	✓	✓	✓	100%	100%	100%
34	✓	X	X	✓	X	X	✓	✓	✓	✓	✓	✓	✓	✓	✓	✓	✓	✓	X	✓	X	86%	71%	57%
35	✓	✓	✓	✓	✓	✓	✓	✓	✓	✓	✓	✓	✓	✓	✓	✓	✓	✓	✓	✓	✓	100%	100%	100%
36	✓	✓	✓	✓	✓	✓	✓	X	✓	✓	✓	✓	✓	✓	✓	✓	✓	✓	✓	✓	✓	100%	86%	100%
37	✓	✓	✓	✓	✓	✓	✓	✓	✓	✓	✓	✓	✓	✓	✓	✓	✓	X	✓	✓	✓	100%	100%	86%
38	✓	✓	✓	✓	✓	✓	✓	✓	✓	✓	✓	✓	✓	✓	✓	✓	✓	✓	✓	✓	✓	100%	100%	100%
39	✓	✓	✓	✓	✓	✓	✓	✓	✓	✓	✓	✓	✓	✓	✓	X	✓	✓	✓	✓	✓	86%	100%	100%
40	X	X	X	X	X	X	X	X	X	X	X	X	X	X	✓	X	X	X	X	X	X	0%	0%	14%
41	✓	X	X	✓	✓	✓	✓	✓	✓	X	✓	✓	X	✓	✓	X	✓	X	X	✓	X	43%	86%	57%
42	✓	✓	✓	✓	✓	✓	✓	✓	✓	✓	✓	✓	✓	✓	✓	✓	✓	X	✓	X		86%	100%	86%
43	✓	✓	✓	✓	✓	✓	✓	✓	✓	✓	✓	✓	✓	✓	✓	✓	✓	✓	✓	✓		86%	100%	100%
44	✓	X	X	✓	X	✓	✓	X	X	✓	✓	✓	✓	✓	X	✓	✓	X	✓	✓	X	100%	57%	29%
45	✓	✓	✓	✓	✓	✓	✓	✓	✓	✓	✓	✓	✓	✓	✓	✓	✓	✓	✓	X	X	100%	86%	86%
46	X	✓	X	✓	✓	✓	X	X	X	✓	✓	X	✓	✓	✓	X	X	X	✓	X	✓	71%	57%	43%
47	✓	✓	✓	✓	✓	✓	✓	✓	✓	✓	✓	✓	✓	✓	✓	✓	✓	✓	✓	✓	✓	100%	100%	100%
48	X	X	✓	✓	✓	X	✓	✓	✓	✓	X	✓	✓	X	✓	X	X	X	✓	✓	✓	71%	43%	71%
49	✓	✓	✓	✓	✓	✓	✓	✓	X	✓	✓	✓	✓	✓	✓	✓	✓	✓	✓	✓	✓	100%	100%	86%
50	X	✓	X	X	✓	✓	✓	X	✓	✓	✓	✓	X	✓	X	X	✓	X	X	✓	X	29%	86%	43%
51	✓	X	X	✓	✓	✓	✓	✓	✓	✓	X	✓	X	✓	X	X	X	✓	✓	X	X	71%	43%	57%
52	✓	✓	✓	✓	✓	✓	✓	✓	✓	✓	✓	✓	✓	✓	✓	✓	✓	✓	✓	✓	✓	100%	100%	100%
53	✓	✓	✓	✓	✓	✓	✓	✓	✓	✓	✓	✓	✓	✓	✓	✓	✓	✓	✓	✓	✓	100%	100%	100%
54	X	X	✓	✓	✓	✓	✓	✓	✓	✓	✓	✓	✓	✓	✓	✓	✓	✓	✓	✓	✓	86%	86%	100%
55	✓	X	X	✓	✓	X	✓	✓	✓	✓	✓	✓	✓	✓	✓	X	✓	✓	✓	✓	✓	86%	86%	71%
56	X	X	X	✓	✓	✓	X	✓	X	✓	✓	✓	✓	✓	✓	✓	✓	✓	✓	X	X	57%	71%	57%
57	✓	✓	✓	✓	✓	✓	✓	✓	X	✓	✓	✓	✓	✓	✓	✓	✓	✓	✓	X	✓	100%	86%	86%
58	✓	✓	✓	✓	✓	✓	✓	✓	✓	✓	✓	✓	✓	✓	✓	✓	✓	✓	✓	✓	X	100%	100%	86%
59	✓	✓	✓	✓	✓	X	✓	✓	X	✓	✓	✓	✓	✓	X	✓	✓	✓	✓	✓	✓	100%	100%	57%
60	✓	✓	X	✓	✓	✓	✓	✓	✓	✓	✓	✓	✓	✓	✓	✓	✓	✓	✓	X	✓	100%	86%	86%
61	✓	✓	✓	✓	✓	✓	✓	✓	✓	✓	✓	✓	✓	✓	✓	✓	✓	✓	✓	✓	✓	100%	100%	100%
62	✓	X	X	✓	✓	✓	✓	✓	✓	✓	✓	✓	X	✓	X	✓	✓	✓	✓	X	X	86%	71%	57%

The mark (✓) represents the detected lesion while mark (X) represents the missed lesion. The highlighted results in three columns on the right side represents the average performance of the observers for lesion which is highly affected by motion blur. The detectability of each lesion represents the number of observers who detected the lesion divided by the total number of observers. For instance, when all the observers detected the lesions (7/7), this means that the percentage detecting the abnormality is 100%. While if only four observers detected the lesion from seven (4/7) the detectability will be 57.1 %. The highlighted cases represent the affected cases due to reduce in the detectability of the seven observers as the level of motion blur increases. The non-highlighted cases represent the non-affected cases due to the detectability of the observers remaining the same as increase the level of motion blur increases. This means that some lesion types are not affected by simulated motion blur at all. This table is complimented by an explanation in the discussion (Chapter Seven) as to why one type is not affected and why another is affected by simulated motion blur according to lesion features and breast characteristics.

Table 6.15 The detectability of malignant microcalcifications by the observers in images without motion blur (0.0 mm), and images with simulated motion blur (0.7mm & 1.5 mm).

No.	Observer 1			Observer 2			Observer 4			Observer 5			Observer 6			Observer 7			Observer 9			Detectability of each lesion by each observer		
	0.0	0.7	1.5	0.0	0.7	1.5	0.0	0.7	1.5	0.0	0.7	1.5	0.0	0.7	1.5	0.0	0.7	1.5	0.0	0.7	1.5	0.0 mm	0.7 mm	1.5 mm
1	✓	✓	X	✓	✓	X	✓	✓	X	✓	✓	✓	✓	✓	✓	✓	✓	✓	✓	✓	✓	1.00	1.00	0.572
2	✓	✓	X	✓	✓	✓	✓	✓	✓	✓	✓	✓	✓	✓	✓	✓	✓	✓	✓	✓	✓	1.00	1.00	0.85
3	✓	✓	X	✓	X	X	✓	✓	✓	✓	✓	X	✓	✓	✓	✓	✓	✓	✓	✓	✓	1.00	0.858	0.572
4	X	X	X	✓	✓	X	✓	X	X	✓	X	X	X	✓	X	✓	✓	X	X	X	X	0.572	0.429	0.00
5-1	✓	✓	✓	✓	✓	✓	✓	✓	✓	✓	✓	✓	✓	✓	✓	✓	✓	✓	✓	✓	✓	1.00	1.00	1.00
5-2	✓	✓	X	✓	X	X	✓	X	X	✓	✓	X	✓	X	X	X	✓	✓	✓	X	X	0.858	0.429	0.143
6	✓	✓	✓	✓	✓	✓	✓	✓	✓	✓	✓	✓	✓	✓	✓	✓	✓	✓	✓	✓	✓	1.00	1.00	1.00
7	✓	✓	✓	✓	✓	✓	✓	✓	✓	✓	✓	✓	✓	✓	✓	✓	✓	✓	✓	✓	✓	1.00	1.00	1.00
8	✓	X	X	X	X	X	✓	✓	X	✓	✓	X	✓	✓	✓	✓	✓	X	✓	X	X	0.858	0.572	0.143
8	✓	✓	X	✓	✓	✓	✓	✓	✓	✓	✓	✓	X	✓	X	✓	✓	✓	✓	X	X	1.00	0.858	0.429
9	✓	✓	X	✓	✓	✓	✓	X	✓	✓	✓	✓	✓	✓	✓	✓	✓	X	✓	✓	✓	1.00	0.858	0.429
10	✓	✓	X	✓	X	✓	X	✓	X	✓	✓	✓	✓	✓	✓	✓	✓	X	✓	X	X	1.00	0.715	0.429
11	✓	✓	✓	✓	✓	✓	✓	X	X	✓	X	✓	✓	✓	✓	✓	✓	✓	✓	X	✓	1.00	0.572	0.858
12	✓	✓	✓	✓	✓	✓	✓	✓	✓	✓	✓	✓	✓	✓	✓	✓	✓	✓	✓	✓	✓	1.00	1.00	1.00
13	✓	X	✓	✓	✓	✓	✓	X	X	✓	✓	✓	✓	X	X	✓	✓	✓	✓	✓	✓	1.00	0.572	0.715
14	✓	X	X	✓	X	X	✓	✓	X	✓	X	X	✓	✓	✓	✓	✓	X	✓	X	✓	1.00	0.429	0.286
15	X	X	X	✓	X	X	✓	X	X	✓	X	✓	X	✓	✓	X	X	X	✓	X	X	0.572	0.143	0.285
15	X	X	X	✓	X	X	✓	X	X	✓	X	X	X	X	X	X	X	X	X	✓	X	0.429	0.285	0.00
16	✓	X	X	X	X	X	✓	X	X	X	X	✓	✓	✓	X	X	X	X	X	X	X	0.429	0.143	0.143
16-2	✓	X	X	✓	✓	✓	✓	✓	X	✓	X	✓	✓	✓	✓	✓	✓	✓	X	✓	X	0.858	0.715	0.572
17	✓	✓	X	✓	✓	✓	✓	X	X	✓	X	✓	✓	X	X	✓	✓	X	✓	X	X	1.00	0.428	0.285
18	✓	X	X	✓	✓	✓	✓	X	X	✓	✓	✓	✓	X	✓	✓	✓	✓	✓	X	X	1.00	0.428	0.572
19	X	✓	✓	✓	X	✓	✓	X	✓	X	X	X	✓	X	X	✓	✓	✓	✓	✓	✓	0.715	0.428	0.858
20	✓	✓	✓	✓	✓	✓	✓	✓	✓	✓	✓	✓	✓	✓	✓	✓	✓	✓	✓	✓	✓	1.00	1.00	1.00
21	✓	✓	✓	✓	✓	✓	✓	✓	✓	✓	✓	✓	✓	✓	✓	✓	✓	✓	✓	✓	✓	1.00	1.00	1.00
22	✓	X	X	✓	✓	✓	✓	✓	X	✓	X	X	✓	✓	✓	✓	✓	X	✓	✓	X	1.00	0.715	0.286
23	✓	✓	✓	✓	✓	✓	✓	✓	X	✓	✓	✓	✓	✓	✓	✓	✓	X	✓	✓	✓	1.00	1.00	0.715
24	✓	✓	✓	✓	✓	✓	✓	✓	✓	✓	✓	✓	✓	✓	✓	✓	✓	✓	✓	✓	X	1.00	1.00	0.858
25	✓	X	X	✓	X	✓	✓	X	X	✓	X	✓	✓	X	X	✓	✓	X	✓	X	X	1.00	0.143	0.286
26	✓	✓	X	X	✓	✓	✓	✓	X	✓	✓	✓	✓	✓	✓	✓	✓	X	✓	✓	X	1.00	1.00	0.43
27	✓	✓	✓	✓	✓	✓	✓	✓	✓	✓	✓	✓	✓	✓	✓	✓	✓	✓	✓	✓	✓	1.00	1.00	1.00
28	✓	X	X	✓	X	X	✓	✓	X	✓	X	X	✓	✓	X	✓	X	X	✓	X	X	1.00	0.286	0.00
29	✓	X	X	✓	✓	X	✓	✓	X	✓	✓	X	✓	✓	X	✓	✓	X	✓	✓	X	1.00	0.858	0.00
30	✓	✓	✓	✓	✓	X	✓	✓	✓	✓	✓	✓	✓	✓	✓	✓	✓	X	✓	✓	✓	1.00	1.00	0.715
31	✓	X	X	✓	✓	✓	✓	X	✓	✓	✓	X	✓	✓	✓	✓	✓	✓	✓	✓	✓	1.00	0.858	0.715
32-1	X	✓	X	X	✓	X	✓	X	X	✓	X	X	✓	✓	X	✓	X	X	✓	X	X	0.858	0.429	0.285
32-2	✓	✓	✓	✓	✓	✓	✓	✓	✓	✓	X	✓	✓	✓	✓	✓	✓	✓	✓	✓	✓	1.00	0.858	1.00
33	✓	✓	✓	✓	✓	✓	✓	✓	✓	✓	✓	✓	✓	✓	✓	✓	✓	✓	✓	✓	✓	1.00	1.00	1.00
34	✓	✓	X	✓	✓	X	✓	✓	✓	✓	✓	✓	✓	✓	✓	✓	✓	✓	✓	✓	✓	1.00	1.00	0.715
35-1	✓	X	X	✓	X	✓	✓	✓	X	✓	X	X	✓	X	X	✓	✓	X	✓	X	X	1.00	0.429	0.143
35-2	✓	X	X	✓	X	X	✓	X	X	✓	X	X	✓	✓	X	X	X	X	✓	X	X	0.715	0.143	0.00
36	✓	✓	X	✓	✓	✓	✓	✓	X	✓	✓	✓	✓	✓	✓	X	✓	✓	✓	✓	✓	0.858	0.858	0.715
37	✓	✓	✓	✓	✓	✓	✓	✓	✓	✓	✓	✓	✓	✓	✓	✓	✓	✓	✓	✓	✓	1.00	1.00	1.00
38	✓	✓	✓	✓	✓	✓	✓	X	✓	✓	✓	✓	✓	✓	✓	✓	✓	✓	✓	✓	✓	1.00	1.00	0.858
39	✓	X	X	✓	✓	✓	✓	✓	✓	X	✓	X	✓	✓	✓	✓	✓	✓	✓	✓	✓	0.858	0.858	0.715
40	X	X	X	X	X	X	X	X	X	X	X	X	X	X	X	X	✓	X	X	X	X	0.00	0.00	0.00
41	✓	✓	✓	✓	✓	✓	✓	✓	✓	✓	✓	✓	✓	✓	✓	✓	✓	✓	✓	✓	✓	1.00	1.00	1.00
42	✓	✓	✓	✓	✓	✓	✓	✓	✓	✓	✓	✓	✓	✓	✓	✓	✓	✓	✓	✓	✓	1.00	1.00	1.00
43	X	✓	✓	✓	✓	✓	✓	✓	✓	✓	✓	✓	✓	✓	✓	✓	✓	✓	✓	✓	✓	0.858	1.00	1.00
44	✓	✓	✓	✓	✓	✓	✓	✓	✓	✓	✓	✓	✓	✓	X	✓	✓	✓	✓	✓	✓	1.00	1.00	0.715

45-1	✓	X	X	✓	✓	X	✓	X	X	✓	✓	X	✓	✓	✓	X	✓	X	✓	X	X	0.858	0.572	0.143
45-2	✓	X	X	X	X	X	✓	X	X	✓	X	X	✓	✓	X	X	✓	X	✓	X	X	0.715	0.286	0.00
46-1	✓	X	X	✓	✓	✓	✓	✓	✓	✓	✓	X	✓	✓	✓	✓	X	✓	✓	✓	✓	0.858	0.715	0.715
46-2	✓	✓	✓	X	X	X	X	X	X	X	X	X	X	X	X	✓	✓	✓	X	X	X	0.715	0.285	0.285
47	✓	✓	✓	✓	✓	✓	✓	✓	✓	✓	✓	✓	✓	✓	✓	✓	✓	✓	X	✓	X	0.858	1.00	0.858
48-1	✓	✓	X	✓	✓	X	✓	✓	✓	✓	✓	✓	✓	✓	✓	✓	✓	X	✓	✓	✓	1.00	1.00	0.572
48-2	✓	X	X	✓	✓	X	✓	✓	✓	✓	✓	✓	✓	✓	X	✓	✓	X	✓	✓	✓	1.00	0.858	0.286
49	✓	X	X	✓	✓	✓	✓	X	✓	✓	✓	X	✓	✓	X	✓	X	X	✓	X	X	1.00	0.429	0.286
50	✓	X	X	✓	✓	✓	✓	✓	✓	✓	✓	X	✓	✓	X	✓	✓	✓	✓	✓	✓	1.00	0.858	0.585
51	X	X	X	✓	X	✓	✓	✓	X	✓	X	✓	✓	X	✓	✓	X	X	X	X	X	0.715	0.143	0.572
52	✓	X	✓	✓	✓	✓	✓	✓	✓	✓	✓	✓	✓	✓	✓	✓	✓	✓	✓	✓	✓	1.00	0.858	1.00
53	✓	✓	X	X	✓	✓	✓	✓	✓	✓	✓	✓	✓	✓	X	✓	✓	X	✓	✓	✓	1.00	1.00	0.572
54	✓	✓	✓	✓	✓	✓	✓	X	X	✓	✓	✓	✓	✓	X	✓	✓	X	✓	✓	X	1.00	0.858	0.429
55	✓	✓	✓	✓	✓	✓	✓	✓	✓	✓	✓	✓	✓	✓	✓	✓	✓	✓	✓	✓	✓	1.00	1.00	1.00
56	✓	✓	✓	✓	✓	✓	✓	✓	✓	✓	✓	✓	✓	✓	✓	✓	✓	✓	✓	✓	✓	1.00	1.00	0.858
57	X	X	X	X	X	X	X	X	X	X	X	X	X	X	X	X	X	X	X	X	X	0.00	0.00	0.00
58	✓	✓	X	✓	✓	✓	✓	✓	X	✓	✓	✓	✓	✓	✓	✓	✓	✓	✓	✓	X	1.00	1.00	0.715
59	✓	X	X	✓	X	X	X	X	X	✓	✓	✓	X	X	X	✓	✓	X	✓	X	X	0.715	0.286	0.286
60	✓	X	X	✓	✓	✓	X	✓	X	✓	✓	✓	X	✓	✓	✓	✓	✓	X	X	X	0.858	0.715	0.429
61	✓	✓	✓	✓	✓	✓	✓	✓	✓	✓	✓	✓	✓	✓	✓	✓	✓	✓	✓	✓	✓	1.00	1.00	1.00
62	✓	✓	X	✓	X	✓	✓	✓	X	✓	✓	✓	✓	✓	✓	✓	X	X	✓	✓	X	1.00	0.715	0.429

The mark (✓) represents the detected lesion while mark (X) represents the missed lesion. The highlighted results in three columns on the right side represents the average performance of the observers for lesion which is highly affected by motion blur. The highlighted cases were selected according to the decrease of the detectability when increases simulated motion blur. The detectability of each lesion represents the number of observers who detected the lesion divided by the total number of observers. For instance, when all the observers detected the lesions (7/7), this means that the percentage detecting the abnormality is 100%. While if only four observers detected the lesion from seven (4/7) the detectability will be 57.1 %. The highlighted cases represent the affected cases due to reduce in the detectability of the seven observers as the level of motion blur increases. The non-highlighted cases represent the non-affected cases due to the detectability of the observers remaining the same as increase the level of motion blur increases. This means that some lesion types are not affected by simulated motion blur at all.

Chapter Seven: Discussion

7.1. Overview

This chapter evaluates the results of the free-response study and the physical measures performed on the lesions under different magnitudes of simulated blur. The discussion is organised into five main themes. The first theme will discuss the impact of motion blur on the detection performance of breast masses and microcalcifications for single observer data. The second theme will focus on the result of simulating a dual read versus a single read via the combination of observer data. The third theme will focus on the impact of simulated motion blur on the physical characteristics of breast masses and microcalcifications. The fourth theme will focus on the commonly missed lesions in this study and the impact of motion blur on lesion characteristics. The physical measures of malignant masses include the conspicuity index, edge angle, grey level change, image noise and SNR. The physical measures of malignant microcalcifications include a new novel metric known as the 'dispersion index', contrast, image noise and SNR with the impact of motion blur. The fifth theme will focus on the impact of motion blur on the image characteristics of malignant masses; discussing the cases where observer performance was affected by simulated motion blur and those that were not. Finally, the limitations of the work will be discussed.

7.2 Free-response Performance Study (single observer)

This thesis has investigated the impact of computer simulated motion by means of shifting accumulated pixel points to blur the resultant image. The results of the single observer free-response study demonstrate that simulated motion blur had a significant effect on observer performance, with performance becoming statistically worse for the detection of microcalcifications as motion blur increased from 0 mm to 0.7 mm, and then on to 1.5 mm. A similar trend was observed for masses, with the only difference being that there was no statistically significant difference in lesion detection performance as the magnitude of simulated motion blur was increased from 0.7 mm to 1.5 mm. For both broad categories of lesions, it should be noted that motion blur in the magnitude of 0.7 mm and above will have an adverse impact on lesion detection performance.

Previous work by Ma et al., (2015) suggested that motion blur could be visible at 0.7 mm for 'soft-edged' motion blur using software simulation, and the findings of my PhD thesis appear

to confirm that a similar effect was observed with a computer simulation motion blur on clinical mammographic images. This observation may have implications for practice. It suggests that if motion blur is identified in an image, repeat imaging should be considered as in clinical work one would simply not know how much motion blur is present or what impact it is having in terms of masking lesions or potentially changing the appearance of lesions. If image motion blur has this type of impact it could lead to an incorrect classification of disease status. In order to explain the significance of motion blur, several scenarios are presented:

Scenario 1– repeated case

Motion blur is detected at the time of image acquisition and a decision is made to repeat the image while the client is still within the mammography department. The image is repeated directly after image acquisition and the client is still in the mammography department. This occurs when the radiographer detects blur during the quality assessment of the image whilst still in the mammography imaging room. This process will lead to increased cost and radiation dose, lost time and effort. From the clients perspective, repeating the image at the time of attendance is better than a recall (i.e. reduced anxiety). However, the image blurring could go undetected in imaging rooms if low resolution monitors are used (Ma et al., 2016).

Scenario 2– recall case

If motion blur is not identified at the time of acquisition, and is only picked up during the review of images (on a higher specification of monitor display) then the client may be recalled for further imaging. This scenario can lead to an increase in client and family anxiety because they might suspect that an abnormality has been detected. In addition, the decision to recall a client means a new appointment must be scheduled, which can ultimately lead to delays in the detection and treatment of breast cancer.

Scenario 3– missed lesion

If motion blur is not detected at any point during the diagnostic decision making stage and a lesion is 'missed', there is a chance that this lesion could later present at follow-up imaging or as an interval cancer. An interval cancer represents a breast cancer which is detected in the interval between scheduled screening sessions (Hofvind & de Wolf, 2015).

In the performance study, there were several categories of lesion. First, lesions that are detected by all observers when motion blur is absent and then missed by the observers in images containing simulated motion blur (0.7 mm and 1.5 mm), providing a clear indication about the impact of motion blur on detection performance. Second, some lesions were not affected by

the magnitudes of simulated motion blur used in this study. Third, lesions that are either difficult to detect or decide if they are malignant, when lesions are missed by all observers in images without blur and in images with motion blur (0.7 mm & 1.5 mm); this means that in some difficult cases, lesions were missed anyway and blurring had no impact on their detection performance. In this study, we do not know if it is due to decision or detection error; further work with eye-tracking may help to answer this.

The impact of motion blur on lesion detection performance could vary with lesion characteristics. Each lesion within the mammography image has a range of characteristics along with a range of background features in which the lesion sits. Some of the lesion types, such as spiculated or indistinct masses, could be affected by motion blur due to the impact of simulated blur on the edge between the lesion and background tissues; while others, such as well circumscribed oval or round masses, might be affected or not affected at all. A lesion-by-lesion analysis of detection performance revealed that larger malignant masses were not affected by simulated motion blur. In addition, breast masses that have high lesion-to-background contrast did not demonstrate a detection deficit in the observer study. However, some smaller, low-contrast breast masses were associated with poorer detection performance. For example, some small breast masses were detected in images without motion blur by all observers and missed when simulated motion blur was applied (at 0.7mm and 1.5mm simulated motion blur) (See **Table 6.15** on page 155).

In the observer study, a high FOM and sensitivity were achieved for images without motion blur for microcalcifications and masses. For microcalcifications, the observer averaged wJAFROC FOM was 0.899 (0.757,0.870) in images without motion blur, whereas this decreased to 0.813 (0.757,0.870) in 0.7mm and 0.746 (0.679,0.812) in 1.5mm levels of simulated motion blur . For masses, the FOMs in images without motion blur was 0.905 (0.859,0.952) compared with blurred images 0.7mm 0.869 (0.814,0.924) and 0.862 (0.810,0.915) in1.5mm . However, it should be noted that there is no statistically significant difference between 0.7mm and 1.5mm levels of simulated motion blur for the latter; this gives an indication that the levels between 0.7 and 1.5 have the same impact on lesion detection performance.

There are many factors that affect lesion detection performance and these should be taken into account in both the empirical work presented here and in clinical practice. Many studies suggest that detection performance is related to the observer in terms of experience, cognitive skills and

visual performance (Reed, 2005; Manning et al., 2006; Sabih et al., 2011; Burgess, 2011; Lança et al., 2015). Other studies suggest that lesion characteristics could contribute to the challenges of interpreting an image accurately. Lesion characteristics are particularly important in breast disease. Malignant breast lesions with indefinite edges for normal and pathological tissue can lead to difficulties in perception (Van Overveld, 1995; Tabar et al., 2005; Kopans, 2006). Other studies suggest that factors related to the characteristics of mammographic images (e.g. image quality, artefacts, spatial resolution, sharpness and contrast resolution) can also influence detection performance (Li et al., 2010; Spuur et al., 2011; Zanca et al., 2012).

7.2.1 Microcalcifications

Free-response data were analysed for the detection of malignant microcalcifications for three conditions; (i) no simulated motion blur (0.0 mm), and for two magnitudes of simulated motion blur (0.7 and 1.5 mm). A significant difference was observed between 0 mm and 0.7 mm, and between 0 mm and 1.5 mm of simulated motion blur, and also between 0.7 mm and 1.5 mm. This means all levels equal to and above 0.7mm have the potential to obscure lesions or cause interpretation error. In addition, an even higher significant difference was detected between (0.0 mm V 1.5 mm, p= 0.004) compared with 0.0mm and 0.7mm (p= 0.0016). This suggests that the negative impact of simulated motion blur on detection performance increases as the level of simulated motion blur increases. It should be noted that no study was found in the literature to compare the results of the impact of motion blur on lesion detection performance in FFDM, so comparisons to what is already known cannot be done.

Lesions which contain less than 10 calcifications in a cluster and are classified as punctate or granular types of microcalcifications illustrating irregularity in density, variety, size, or shape were affected by simulated motion blur and tended to be associated with poorer detection rates. **Figure 7.1** provides an illustration of this, where the calcifications are indicated by red arrows. The microcalcifications appear as non-focal clusters with irregular outlines. In contrast, the results demonstrated that the microcalcifications which have definite edges (similar shape, density and size of individual microcalcifications) with focal clustering were not affected by motion blur. Overall, detection performance decreased as simulated motion blur increased. In the case described in **Figure 7.1**, 100% (7/7) of the observers detected microcalcifications with no blur (0.0mm), this decreased to 14.3% (1/7) at 0.7mm and 29% (2/7) at 1.5mm of simulated motion blur.

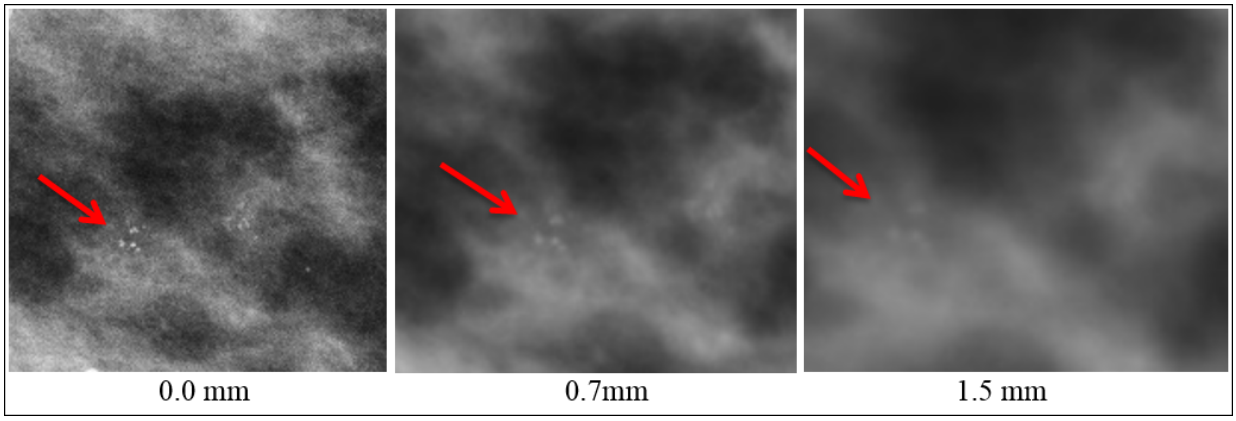

Figure 7.1 Magnified area of right cranio-caudal projection. Demonstrates a cluster of microcalcifications have irregular shapes.

The cases used in this observer study have been classified into two types according to the influence of motion blur on detection performance; affected and not affected. The detection performance of some image characteristics of malignant calcifications are affected by motion blur more than others. **Figure 7.2** describes an example that contains several different shapes of calcification, such as pleomorphic, diffuse and punctate. These have all been detected by the observer in images without motion blur (0.0mm). The same microcalcifications have been missed by the observers when simulated motion blur had been applied in the magnitude of 0.7mm and 1.5mm levels of simulated motion blur. This suggests that motion blur could obscure certain types of small calcifications. In general, sensitivity represents a measure of accuracy determined by the true positive rate which is the ability of the observer to accurately identify cases of disease while specificity represents a measure of the true negative rate or the ability of the observer to accurately identify cases without lesion. Since the FOM decreased as simulated motion blur increased, this implies that the false negative rate also increased. This relationship, between the FOM and motion blur, was significant ($F(2,18) = 10.48$, $p=0.0010$). The results demonstrate that the sensitivity of images without simulated motion blur (0.0mm) was 97.9, and the sensitivities for blurred images (0.7mm and 1.5mm) were 86.4 and 76.5 %, respectively. When specificity (HrSp) is used as the FOM, there was no significant difference between magnitudes of simulated motion blur ($F(2,13) = 0.21$, $p=0.8110$). This suggests that the false positive rate did not increase significantly with increasing motion blur. Although the false positive (FP) rate at the 1.5mm level was more than 0.0mm level, a low confidence level

was provided by the observers (1.5 mm) and the free-response study is designed to not penalise errors if the observers gives low confidence level.

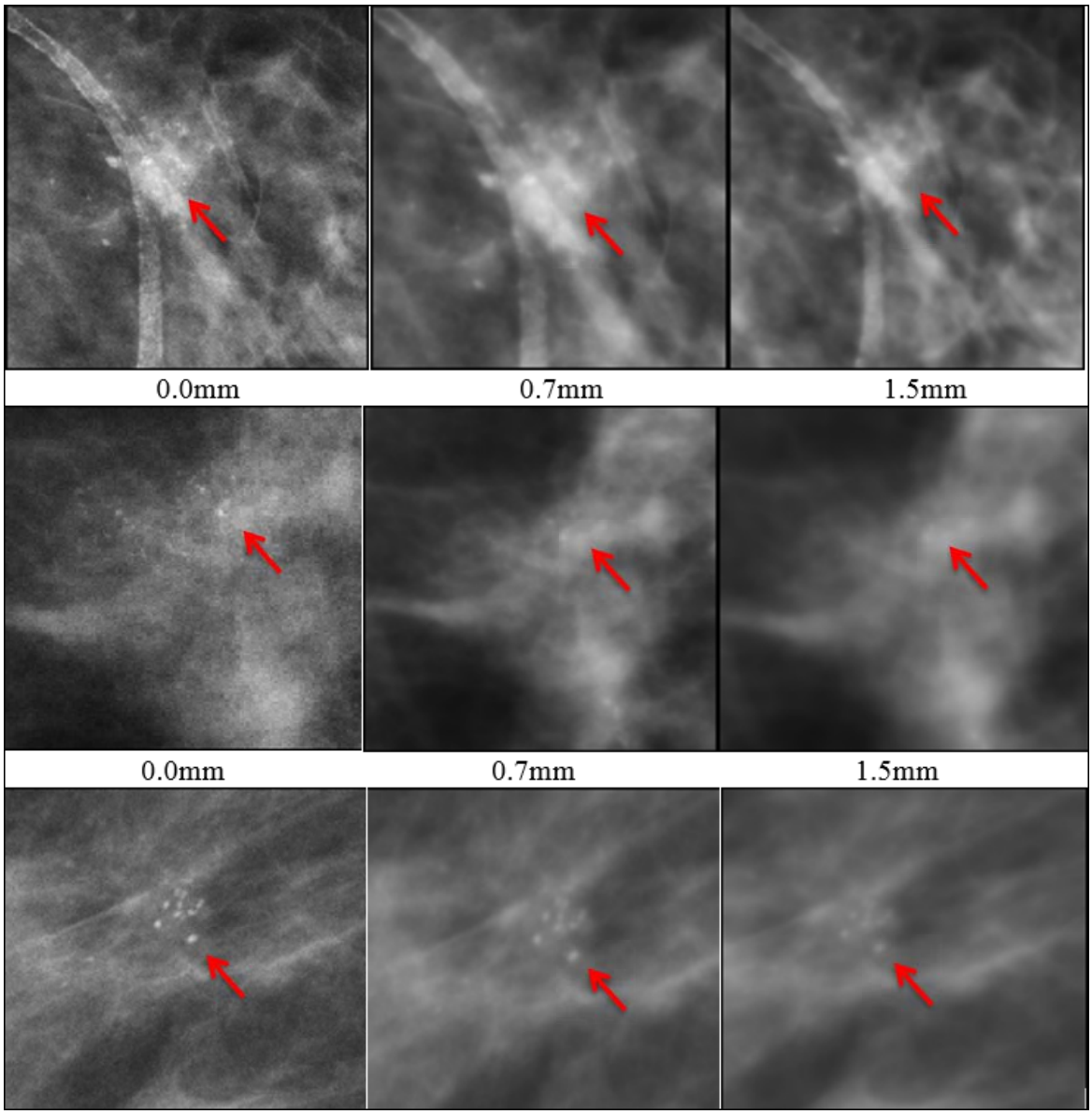

Figure 7.2 Magnified views of images without simulated motion blur (0.0mm) and blurred mammography images (0.7mm & 1.5mm). The images illustrate a cluster of malignant microcalcifications, which were affected by simulated motion blur.

7.2.2 Masses Cases

For masses, a statistically significant difference was detected between two levels (0 mm V 1.5 mm, p=0.0041), this means that detection performance was reduced between images containing no blur and those containing 1.5mm of simulated motion blur. The result also showed that there

was no significant difference between the two magnitudes of simulated motion blur (0.7 mm and 1.5 mm; p=0.640). This means that all magnitudes of motion blur above 0.7 have a similar negative impact on mass detection. When sensitivity (HrSe) was used as the FOM, there was no significant difference between different magnitudes of simulated motion blur (F (2, 16) = 0.43, p=0.6575). This implies that the false negative rate did not change significantly as a result of simulated motion blur. The sensitivity of images without motion blur (0.0 mm) was 92.3% and the sensitivity for blurred images were 91.9% and 90.5% for levels 0.7mm and 1.5mm, respectively. The sensitivity of lesion detection decreases with increasing levels of motion blur, but not to a significant level. When specificity (HrSp) was used as the FOM, again there was no significant difference between magnitudes of simulated motion blur (F (2,12) = 1.31, p=0.3043). Specificity reduces with an increase in the level of simulated motion blur especially in cases of breast masses, with magnitudes shifting from 82.7% for images without motion blur (0.0 mm) to 73.3% in blurred images (0.7 mm).

In summary, for both microcalcifications and masses, there was a reduction in sensitivity as the magnitude of simulated motion blur increased. For masses, this was not statistically significant and the values in (**Table 5.5** on page111) demonstrate that the false negative rate did not change that much as motion blur increased. For microcalcifications, this was not the case and there was a statistically significant reduction in sensitivity, (**Table 5.3** on page 107) suggests that an increase in motion blur caused the smaller lesions to become visually imperceptible. The change in specificity was not significantly different for masses or microcalcifications.

The literature is relatively sparse on studies that have looked at the impact of motion blur artefacts, however there are some isolated cases from other image modalities that have assess the impact of motion blur. Let us now compare the mass results in this thesis with other studies. Donnelly and Thompson, (2017) assessed the impact of simulating respiratory motion on the detection of lung nodules in CT. Low-dose images were generated with the intention with the primary application of CT attenuation correction (CTAC) of nuclear medicine SPECT image data. They used an anthropomorphic chest phantom and a variety of simulated spherical lung nodules of different size and density. Physical motion blur was introduced through use of a mechanical device used to simulate the rate and amplitude of respiratory motion. Five observers assessed the images with and without simulated motion using a free-response study

to determine the detection performance of the nodules. Data were analysed using the wJAFROC FOM. It was concluded that simulated respiratory motion has a significant negative impact on nodule detection performance ($F(1,4.00) = 10.88$, $p=0.0300$).

In comparison to other previous observer studies, the FOM achieved in images containing no simulated motion blur were associated with generally better performance. This must be considered in some caution due to differences in study design, purpose of the research, and the population of client images, and the experience of the observers. For instance, a study by (Debono, 2012a) evaluated the diagnostic accuracy of reporting radiographers in screening mammography according to types of breast lesions. Debono used ROC method to assess the accuracy of 10 radiographers through measuring the area under the curve (AUC). Debono found that individual sensitivity levels ranged between 76.0% and 92.0%, and individual specificity levels ranged between 74.8% and 96.2%. Debono (2012a) also summarised previous studies and found that radiographer sensitivity levels varied between 61.0% and 91.42%, and specificity levels varied between 45.0% and 99.1%. Debono's study found radiologist sensitivity levels were between 63.9% and 100%, and specificity levels between 81.0% and 99.2% (Debono, 2012a). In my thesis, the FROC method was used to determine the detection performance; this is more advanced method than ROC, since ROC ignores location information. Typically, it is expected that an inflated FOM is generated if location information is ignored. However, this general level of agreement in performance is encouraging.

7.2.3 Reflection – comparison of laboratory and clinical studies

A laboratory study, as conducted in this thesis, is very different to the clinical reality of reviewing mammographic images. In a laboratory study there is a heightened expectation of disease since there is an enriched dataset and the observers know they are probably looking for a higher proportion of lesions. The consequence of this is that observers are more likely to indicate the presence of a lesion. This can lead to changed behaviour and in this situation the likelihood of making more localisation, leading to increased true and false decisions, has little consequence other than an increase in sensitivity or a reduction in specificity (**Table 5.2** on page 101 **and Table 5.6** on page 107**)**. When compared to the clinical scenario, the image reader also has to consider their recall rate and the risk of over-investigation. It is difficult to predict how image readers will behave during a laboratory study and consequently this can lead

to differences in sensitivity and specificity. This is why laboratory studies are conducted using multiple readers and cases.

7.3 The Combined two Observers' Data

Double reading is a routine procedure to interpret mammographic images in breast cancer screening programmes. In the UK NHSBSP, double reading is ideally conducted blinded for all cases (Wilson et al., 2011). Discordant cases are arbitrated under locally agreed protocols. In the case of a suspicious area being noted, a decision is then made to either recall the client for further assessment or allow them to carry on as normal in routine triennial screening. Double reading is standard and recommended in many breast screening programmes (e.g. European and Australia breast cancer screening programmes) due to the advantages of increased accuracy and sensitivity through decreasing the chance of undetected lesions (Perry et al., 2008; Debono et al., 2015). With the above in mind, there was an opportunity to combine the data from individual observers to simulate the outcome of a double reading. The purpose of combined two observers' data was to assess the impact of combined observer free-response data on lesion detection performance in blurred images. Since this was a retrospective analysis of the data acquired by individual observers, the method to achieve this in my thesis cannot be generalised to NHSBSP practice as no consensus meeting or arbitration process took place for discordant cases. However, it is reasonable to assume that the combined read used in this thesis will give a higher positive outcome rate because in the clinical setting within NHSBSP the double reading consensus meeting will result in some cases being 'downgraded' from positive to negative.

Different combinations of two observers' data was likely to enhance the detection performance of the observers. For random reader random case analysis of breast masses, there was no statistically significant difference in lesion detection performance between single and combined free-response data ($F(1,6)=4.04$, $p=0.1001$). For the analysis of microcalcifications, a statistically significant difference in lesion detection performance was demonstrated between single and combined free-response data ($F(1,6)=12.28$, $p=0.0122$). For both masses and microcalcifications, there was an increase in sensitivity (HrSe) when using two observers in combination rather than one observer in isolation. This is due to the method used to combine the data, where the highest rating was taken as the single rating. This means that if one of the

two observers correctly localised the lesion it would be classed as true positive. Conversely, the simulation of a double reading also increased the number of false positive localisations thus reducing the specificity, as shown by the HrSp FOM (**Tables 5.11** on page 122 & **Table 5.13** on page 124). These results agree with previous studies (Husien, 1995; Taplin et al., 2000), where double image reader interpretation resulted in an increase in sensitivity of 10%. However, there was a decrease in specificity of 1.8%. For my thesis, in the single observer data, there was a negative significant difference in the impact of motion blur on breast mass detection performance. A statistical difference in detection performance was found when motion blur was applied to the images at 0.7 mm for the combined observer data.

Many studies have discussed the advantages and disadvantages of double reporting. Firstly, double reporting can increase sensitivity through decreasing the chance of undetected lesions (Blanks et al., 1998; Dinnes et al., 2001; Harvey et al., 2003; Klompenhouwer et al., 2015). Accordingly, double reporting of mammographic images became normal practice in European breast screening programmes (Perry et al., 2008). However, there are some disadvantages of double reporting related to its cost-effectiveness. First, double reporting effectiveness can be less important when a high level of agreement between image readers is achieved (Taplin et al., 2000). Second, the benefit of double reporting might be restricted to specific situations when the detection of cancer is difficult, i.e. mammographic images of females in prevalent screening (first participation) when previous mammograms do not exist, females with small lesions that are difficult to detect, or when the image readers are less experienced (Dinnes et al., 2001; Sickles, 2010). Finally, double reporting increases staff costs and resources utilised in the interpretation procedure and takes longer time (Posso et al., 2016). However, others argued that in some contexts more advantages can be achieved from single reporting as it may decrease costs and FP without significantly decreasing the detection rate of breast cancer (Varela et al., 2005). Overall, double reporting in clinical practice remains controversial, with benefits and values being noted in the literature.

7.3.1 Microcalcifications Combined two Observers' Data

This part of the discussion will focus on the comparison between images which contain two levels of motion blur (0.7mm & 1.5mm) and images which have no blur (0.0mm). The purpose of this discussion is to determine whether the combination of two observers' data reduces the impact of simulated motion blur in FFDM images in microcalcifications or not. The results of

two combined observers' data for microcalcifications demonstrated that there is an improvement in detection performance. The p-values indicated a statistically significant difference between all three comparisons (0.0-0.7, 0.0-1.5 and 0.7-1.5mm) (see **Table 5.11** on page 122). Differences between FOM pairs of images without motion blur (0.0mm) was 0.923 (0.883, 0.964) and images with magnitudes of simulated motion blur (0.7mm and 1.5mm) were 0.876 (0.831, 0.921), 0.826 (0.771, 0.880) for (0.7mm and 1.5mm) respectively. The sensitivity of images without motion blur (0.0 mm) was 99.7, and the sensitivities for blurred images (0.7mm and 1.5mm) were 96.0 and 89.6, respectively. It can be noticed that the sensitivity of detected lesion decreases when levels of motion blur increase. In contrast, specificity decreased with the increasing levels of motion blur (0.0mm and 0.7mm was 72.0 and 70.9). This means there is an increase in FP in microcalcification cases between these two levels (0.0mm and 0.7mm). These findings suggest that there is some advantage of having a second observer for the detection of microcalcifications when motion blur is present. Given the method used to combine the free-response data, an expected increase in sensitivity and decrease in specificity when the data has been combined leads to decrease in specificity due to an increase in the false positive fraction.

7.3.2 Masses Combined Two Observers' Data

For combined two observers' masses data, a statistically significant difference was found for the detection of masses ($F(2,21)=6.01$, $P=0.0084$). A significant difference was observed between 0 mm and 0.7 mm, and between 0 mm and 1.5 mm of simulated motion blur . No significant difference was detected between 0.7 mm and 1.5 mm. Rjafroc was also used to calculate observer averaged sensitivity (FOM=HrSe) and specificity (FOM=HrSp) as the FOM for all comparisons between 0.0mm, 0.7mm and 1.5mm (**Table 5.13** on page 124). There was no significant difference in detection performance between images blurred with a magnitude of 0.7 mm and those with 1.5 mm, for cases containing masses for both single observer data and combined two observers' data methods. This was not the case for microcalcifications, where detection performance became statistically worse as the magnitude of motion blur was increased.

Summarising of combined observers' data for masses and microcalcification, this must be evaluated with some caution given the differences between an observer study of this type and a clinical evaluation. Since it was a retrospective decision (secondary analysis of data) to

combine the free-response data, there was no opportunity for arbitration to occur in cases in which they did not agree. Had this occurred, it is possible that the values of specificity could have been more favourable (i.e. a consensus decision may have reduced the number of non-lesion localisation marks). However, the converse could be true for sensitivity, where a consensus decision may result in a true lesion being downgraded. A study by (Tanaka et al., 2015) investigated the impact of combining data from a free-response study to simulate a dual-read. They found a general improvement in performance when combining the interpretation of a radiographer with a radiologist, demonstrated by an inflated FOM, but the overall significance of combined observations was not stated. The key finding, of Tanaka's study and the current thesis, is that a combined read is unlikely to be detrimental to patient outcomes.

7.4 Physical Measures:

7.4.1 Physical Measures of Microcalcifications

This part of the discussion focusses on the impact of motion blur on the physical characteristics of malignant microcalcifications, including a new experimental metric (dispersion index, DI), contrast, image noise and SNR. The DI of microcalcifications represents the number of calcifications within a specified area divided by the area. DI was measured within ImageJ software because the conspicuity index could not be applied to microcalcifications due to their small individual size and wide distribution pattern. No validation has been conducted on DI, but this could be a focus for post-doctoral work. A literature search conducted prior to this research did not reveal any validated method for achieving a physical measure of microcalcification clusters; this led to the development of the new DI metric. The result demonstrates that the DI decreases when the level of simulated motion blur increases (see **Table 6.8** on page 139). Simulated motion blur has a significant negative impact on the dispersion of calcifications image. **Figure (7.3)** demonstrates magnified mammographic images which contain clustered microcalcifications. The DI in the image without motion blur (0.0mm) was 0.608 per cm^2 , while the DI for images with motion blur (0.7 and 1.5mm) decreased to become 0.405 and 0.262 per cm^2, respectively. In general, the lesion background can have a negative impact on the search pattern. This is referred to as the crowding effect (Levi 2009). The contrast threshold represents the contrast essential for the visibility of a test object for a determined task of the image reader, e.g. for detecting an object. A mammographic image can contain anatomical noise and this can have an impact on the perception of structures (e.g. lesions). The results of this thesis show that the contrast of clustered microcalcifications

increases when in the level of simulated motion blur increases (**Table 6.10** page 141). In addition, the results demonstrate that there is no relationship between (DI. x contrast) and the detectability of lesions by the observers.

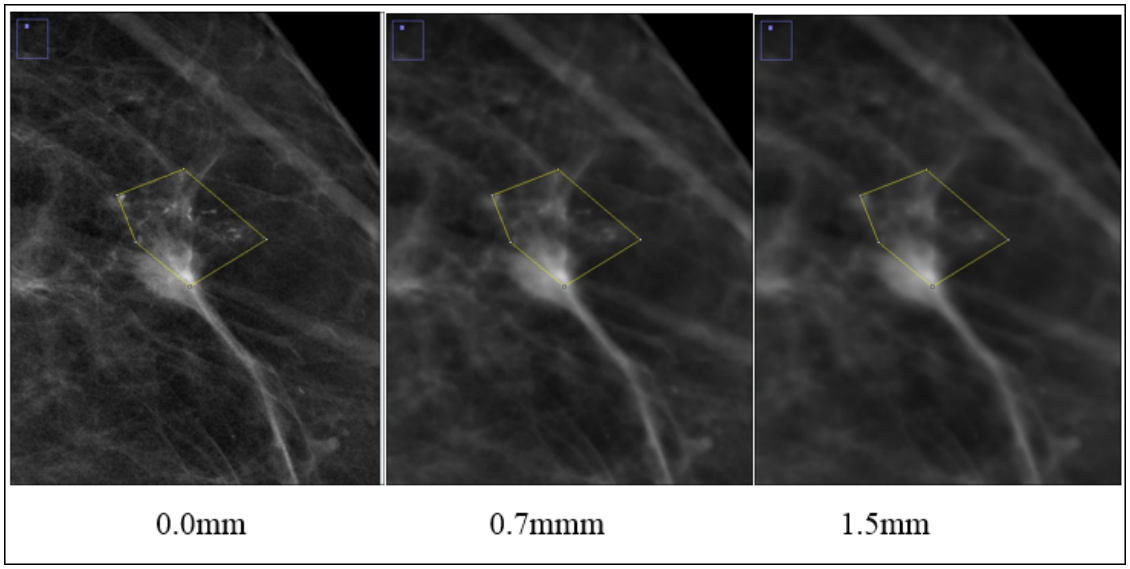

Figure 7.3 Magnified mammographic images contain clustered microcalcification. The DI in the image without motion blur (0.0mm) was 0.608 per cm^2, while the DI for images with motion blur (0.7 and 1.5mm) were 0.405 and 0.262 per cm2 respectively.

Many researchers define a cluster of microcalcifications or suspicious group as at least five calcifications in a breast volume of 1 cm^3 (e.g. Evans et al., 2002; Shetty, 2015). Small subtle microcalcifications with a size of less than 0.5 mm are a distinctive feature of malignancy, although this threshold will differ somewhat in the thickness and density of the breast. With the exception of motion blur, the key determinant for visibility of small calcifications is the magnitude of image noise relative to the calcification's signal (Ruschin, Timberg and Båth, 2007b). Since smaller calcifications will provide a signal sometimes as small as a single pixel, the pixel-to-pixel difference depends on the image noise and it will reduce the visibility of small calcifications to a much higher extent than the visibility of the mass due to mass being larger than the size of the individual calcifications. To ensure better visualisation of structures as small as 0.1 mm in size, the European guidelines for quality assurance in breast cancer screening determined acceptable threshold levels of contrast for objects ranging from 0.1 to 2.0 mm in size, which should be available in digital mammography at acceptable glandular dose levels (Perry et al., 2006). For optimal visualisation of microcalcifications at a given glandular dose, it is typically beneficial to enhance the SNR. The SNR difference between the two

magnitudes of simulated motion blur and no motion blur were statistically significant for all comparisons between 0.0mm, 0.7mm and 1.5mm (**Table 6.12** on page 144). A graphical representation of the means and adjusted 95% confidence intervals are displayed in (**Figure 6.8** page 144). The average of SNR was 26.97 for images without simulated motion blur and the average for blurred images (0.7 mm and 1.5mm motion blur) are 34.413 and 38.035, respectively. However, there is no relationship between the physical measures and the lesion detection performance of the observers (lesion detectability).

7.4.2 Physical Measures of Malignant Masses

The physical characteristics of malignant breast masses were determined by physical parameters including conspicuity index, edge angle, grey level change, and image noise. The physical measures of malignant masses have been analysed using conspicuity software (Szczepura and Manning, 2016), partly to demonstrate the behaviour of blurring software and partly to assess the impact of motion blur on the physical characteristics of breast mass images.

7.4.2.1 The Lesion Conspicuity and Edge Angle

The results demonstrated that the conspicuity index increases significantly when simulated motion blur increased from 0mm to 0.7mm and then to 1.5mm (See **Table 6.3** page 130). This change in the image lesion characteristics and may negatively impact on the differential diagnosis. It is reasonable to hypothesize that, when the conspicuity of lesions increase this does not necessarily mean that the detectability of the lesion should also increase. The observers may see the lesion but it is possible they might not be able to decide if the lesion is malignant or benign due to the influence of motion blur. It is hypothesised that the motion blur may cause a decision error rather than a detection error; in the other words, decision-making errors can happen when the lesion is obvious, but the assessment of its nature is made incorrectly. It should be noted that further studies are required in future work to evaluate decision error with eye-tracking. This result in a lesion being falsely dismissed as benign when it is actually malignant, false-negative (FN). Manning et al., 2004 concluded that most errors in image perception were failures of decision-making instead of detection errors (Manning, Ethell and Donovan, 2004b). According to (Zuley, 2010) the mistakes in perceiving mammographic images can be categorised into three types: search errors, recognition errors and decision-making errors. If a lesion is not identified by the observer this is considered a

search error. However, if the lesion catches the observer's eye but is then quickly dismissed it is considered a recognition error. This will lead to the lesion going undiagnosed. Manning et al., (2002) also demonstrated a poor relationship between conspicuity index and missed lesions in chest radiography and pointed out the decision errors were mainly related to detection (Manning and Ethell, 2002).

Perception errors can be considered as the main cause of missed cancers in mammography. Misdiagnosed breast cancers can be attributed to their subtle characteristics. A suboptimal technique related to technical factors and/or poor positioning can also lead to reduced lesion conspicuity leading to poor detection (Goergen et al., 1997). The average of conspicuity index for malignant masses in this thesis is 87.28 for images without simulated motion blur to 116.33 and 124.08 for images with simulated motion blur (0.7 mm and 1.5mm motion blur), (see **Figure 6.1** on page 130). The size of a focal lesion is a significant factor used to determine the conspicuity of the lesion. This thesis included a wide range of lesion sizes from approximately 5 mm to 30 mm (see tables of the collected data Appendix G). The cancer lesion sizes were similar to lesion sizes used in other observer based studies (Michaelson et al., 2003; Obuchowski et al., 2000). For example, a study by Michaelson et al., (2003) demonstrated that the size of lesions detected by screening mammography varies between 5 mm and 32 mm (Michaelson *et al.*, 2003). Some image characteristics of malignant masses can be difficult to interpret due to their small size due to their relatively low contrast with background tissue; this can have an impact on visual perception. The difference in edge angle between the two magnitudes of simulated motion blur and no motion blur were statistically significant for all comparisons between 0.0mm, 0.7mm and 1.5mm (**Table 6.4** on page 132). Edge angle magnitude decreased as simulated motion blur level increased. The results of edge angle correlated with the results of the free-response study. The detection performance of breast masses reduced with a reduction in edge angle, as the magnitude of simulated motion blur was increased. Simulated motion blur has an impact on edge angle of breast masses and this could therefore influence the image characteristics of lesions. This suggests that any impact on the image characteristics of breast masses appearance could negatively affect differentiation between malignant and benign masses. **Figure 6.2** (on page 132) demonstrates the means of edge angle (confidence interval 95%) of the two magnitudes of simulated motion blur and no motion blur. The average edge angle is 69.11 for images without simulated motion blur and

the range for blurred images (0.7 mm and 1.5mm motion blur) are 67.63 and 66.65, respectively (**Figure 6.2**).

7.4.2.2 Change in grey level (ΔGL) of masses

The results demonstrated that there was no difference in the change of grey level when the level of motion blur increases. The change of the grey level difference between the two magnitudes of simulated motion blur and no motion blur was not statistically significant for all comparisons (0.0mm, 0.7mm and 1.5mm) of simulated motion blur. A previous study by Rawashdeh et al., (2014) measured breast lesion ΔGL for global background regions as the mean grey level value of lesion minus the mean grey level value of the whole breast without pectoralis muscle. The aim was to establish the key morphological criteria of the global background (i.e. the breast that contains the lesion) that impacted on breast cancer detection. They suggested that there was a relationship between "rating of detectability" and breast density, lesion size, lesion edge and solidity. Some of these previous results agreed with the results that have been established in this thesis, however, there is no relationship between detectability and the change in grey level. This could be related to there being no impact of motion blur on ΔGL. An early study by (Aldrich & Desai, 1994) used grey level to evaluate the textual content of digitized mammography images. Statistics calculated from the GL were utilised to highlight image lesion characteristics. They reported that GL has an apparent capability to provide discrimination between normal and abnormal areas to enhance breast cancer diagnosis. A study by (Boher and Collomb-patton, 2012) used temporal measurements to characterise the motion blur of liquid-crystal display (LCD) displays. This calculation was conducted automatically for each grey level transition. The contrast sensitivity function of the human eye was introduced to assess perceived blur edge width and time for each grey level transition providing a powerful process for a full characterisation of motion blur in such displays (Boher and Collomb-patton, 2012). The results of my thesis demonstrated that there was no impact of motion blur on GL and there is no relationship between GL and detection performance.

7.4.2.3 Image Noise and Signal to Noise Ratio (SNR)

Both the noise and signal to noise ratio (SNR) of mass images were analysed to investigate the impact of simulated motion blur on the physical characteristics of the images. The difference in SNR between the two magnitudes of simulated motion blur and no motion blur were statistically significant for all comparisons between (0.0-0.7, 0.0-1.5 and 0.7-1.5mm) (**Table 6.6** on the page 136). Image noise decreased as the level of simulated motion blur increased; this is believed to be a consequence of the smoothing process induced by the motion blur software (Dougherty, 2009). The average of SNR (**Figure 6.4** on page 136) is 2.741 for images without simulated motion blur and the average for blurred images (0.7 mm and 1.5mm motion blur) are 4.394 and 5.653 , respectively. The results in my thesis showed noise had a statistically significant difference between 0.0–0.7mm $t(22)=22.95$ ($p<0.000$), 0.0–1.5mm $t(22)=24.66$ ($p<0.000$), and for 0.7–1.5mm $t(22)=18.11$ ($p<0.000$). Noise decreased as the magnitude of simulated motion blur increased, this finding is in line with the smoothing effect imposed by simulated motion blur. Saunders et al., (2007) have examined the impact of different noise levels and resolution on cancer detection performance in digital mammography. They used images at three different resolution levels and three different noise levels. For the detection of malignant masses and microcalcifications, reducing the display resolution demonstrated a small influence on overall accuracy and individual detection performance. They found noise changed the detection performance of microcalcification. It decreased from 89% to 67% and the discrimination performance of masses fell from 93% to 79%, while malignant mass detection performance remained relatively constant with values of 88% and 84%, respectively.

7.5 The Impact of Motion Blur on Mammographic Features of Microcalcifications

The distribution and shape of calcifications are considered a good indicator for the likelihood of malignancy. It is reasonable to hypothesise that when the distribution and/or shape is changed due to motion blur that this could affect the differential diagnosis of the lesion. For instance, there are several distributions of breast microcalcifications. **Tables 7.1** provide an overview of the findings from the microcalcifications cases.

Firstly, diffuse and scattered microcalcifications, which are commonly benign especially when bilateral. Such a distribution is predominantly seen with amorphous and punctate types of

microcalcifications, this type of distribution was frequently affected by motion blur in this study with a reduction in detection performance; this was characterized by a reduction in the dispersion index (DI). It should be noted that this understanding has been generated from cases in my thesis and this would need evaluating over a larger sample of each type of cluster/lesion feature. **Figure 7.4** shows an example of amorphous and punctuate microcalcifications, which were affected by motion blur.

Secondly, regional calcifications could comprise most of a quadrant or more than a single quadrant and do not conform to a ductal distribution. This type of distribution is also affected by motion blur that can lead to a change in shape and/or distribution. Consequently, the detection performance can be decreased.

Thirdly, clustered or grouped calcifications when five or more small calcifications are shown in a small area of breast tissue (see **Figure 7.4**).

Fourthly, linear distribution microcalcifications which are arranged in a line; such a distribution is highly suspicious of cancer and indicates that microcalcifications are intra-ductal.

Fifthly, segmental distribution of microcalcifications imply calcifications in ducts and their branches and could suggest multifocal or extensive breast cancer in a segment or lobe of the breast. The exception is in the incident of coarse rod-like microcalcifications in older females, where this is related to secretory microcalcifications. The granular calcifications showing an irregularity in density, size or shape and they are tiny with dot-like or elongated shapes and are innumerable. Motion blur has a negative impact on the detection of granular calcification, especially when they are located in a high density breast. The amorphous microcalcifications presentation is considered the most difficult lesion to identify due to its poor contrast and small size (Liu, 1999). **Figure (7.4)** shows a group of malignant microcalcifications, which were affected by simulated motion blur, whereas the **Figure (7.5)** demonstrates a group of malignant microcalcifications, which were not affected by simulated motion blur in this study.

Table 7.1 The types of clustered microcalcifications and the impact of motion blur on each type. It should be noted that this table generated from cases of current study and this would need evaluating over a larger sample of each type of cluster/lesion feature.

Types Calcification	**Size of individual Calcifications**	**Lesion features**	**Motion blur effect**
Cluster with ≤10 amorphous calcifications	Small size (heterogeneous)	clustered non-focal lesion	affected by motion blur
rod shaped	Large size of individuals calcifications (Homogeneous)	focal lesion with dense central area	Not affected by motion blur
Punctate	Small size (similar size of individual calcifications)	small cluster size with same density and shape of individual calcifications	affected by motion blur
Granular	granular calcifications which vary in size	showing irregularity in density, size or shape	affected by motion blur
Branching	Large size with irregularly shaped cluster (Heterogeneous)	showing irregularity in density	not affected by motion blur
ductal distribution	Large size with irregularly shaped	Similar in density & size	Not affected by motion blur

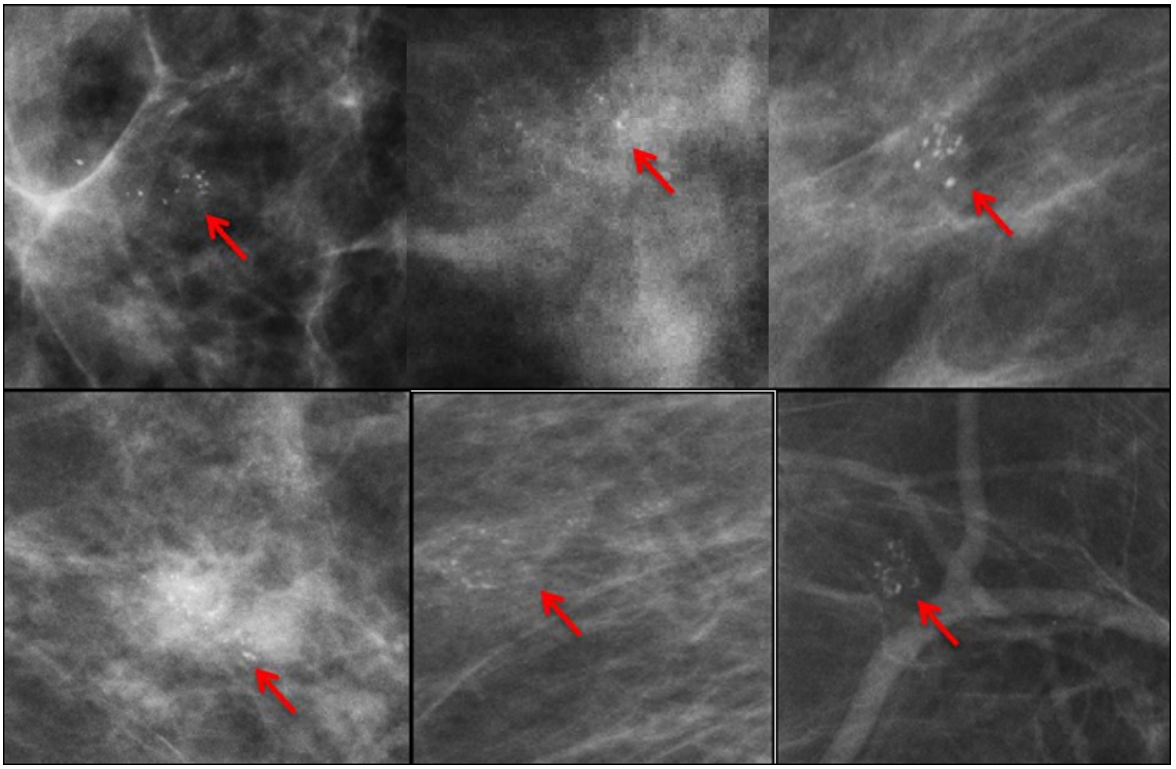

Figure 7.4 A group of malignant microcalcifications, which were affected by motion blur.

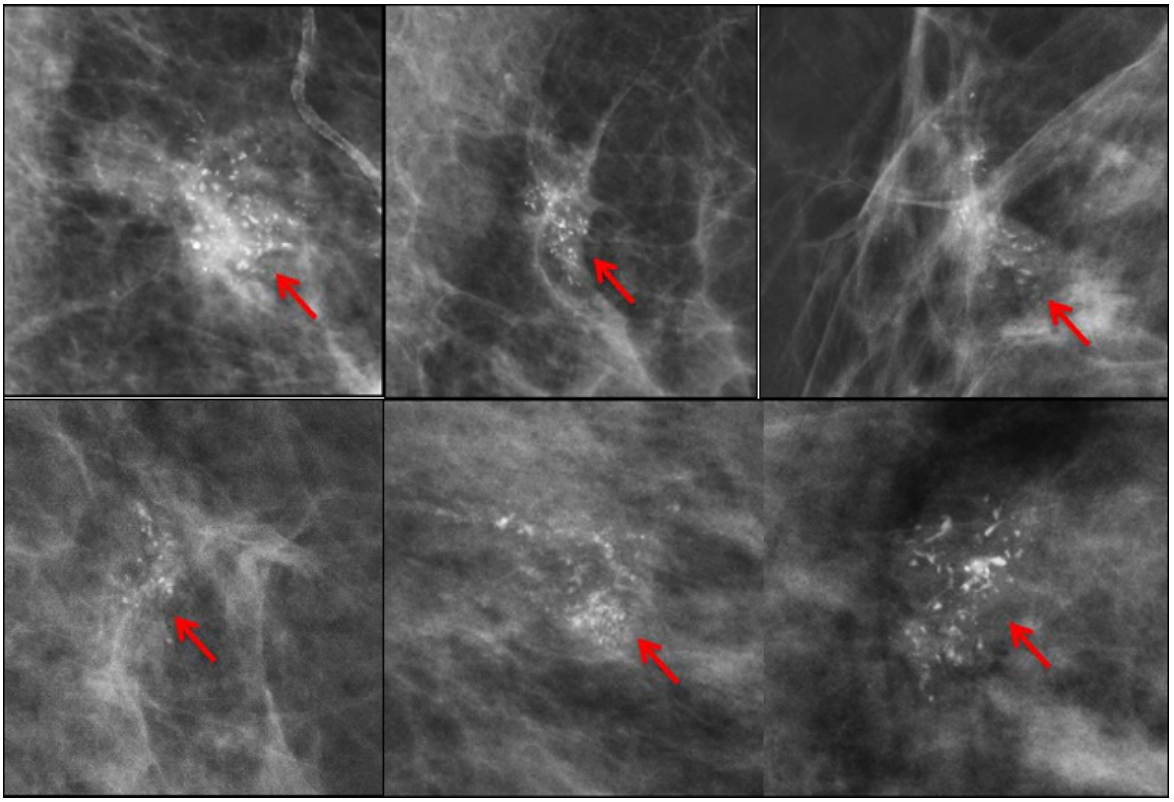

Figure 7.5 A group of malignant microcalcifications, which are not affected by motion blur.

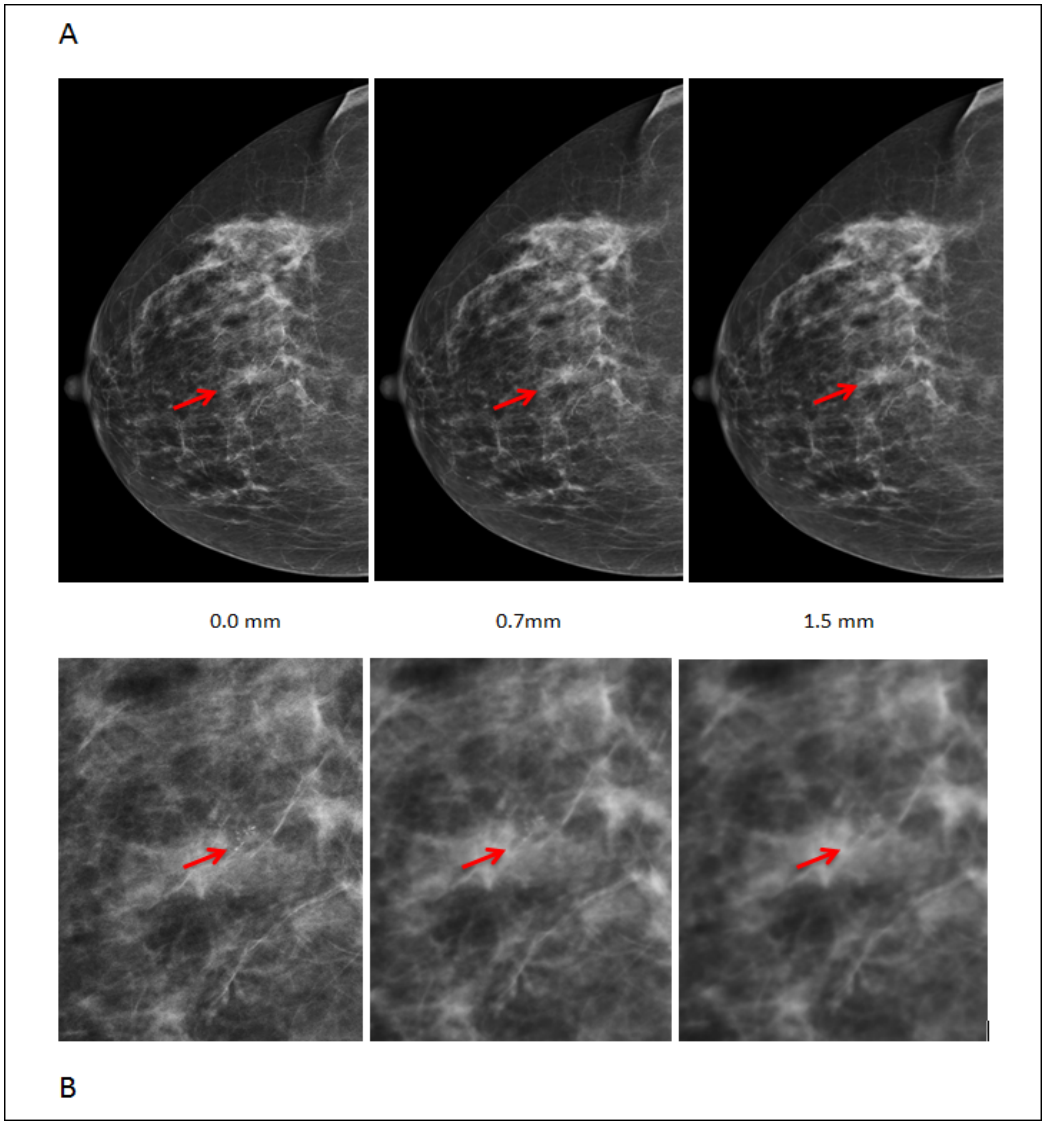

Figure 7.6 (A) Right CC projection demonstrates (B) Magnified areas of FFDM images at 0 mm, 0.7 mm, and 1.5 mm of simulated motion blur.

Particular image lesion characteristics in mammography images have different degrees of lesion detection difficulty. Microcalcifications may be missed due to the difficulty in identifying suspicious or normal appearance and we know that the visibility of microcalcifications is decreased with increasing magnitudes of simulated motion blur. **Figure 7.6** (A) shows an example of an image without motion blur (0.0mm) and blurred mammographic images (0.7 and 1.5mm). It contains a small cluster of calcifications of approximately (6.5 mm in size) in the right breast. The DI in the image without motion blur (0.0mm) was 0.519 cm^2, while the DI for images with motion blur (0.7 and 1.5mm) were 0.424 and 0.377 per cm^2 respectively. **Figure 7.6** (B) shows magnified views of the left image

without motion blur (0.0mm) and images with motion blur (0.7 and 1.5mm). The calcifications are less well seen on the 0.7mm and 1.5mm due to motion blur.

Microcalcification images: not affected by motion blur

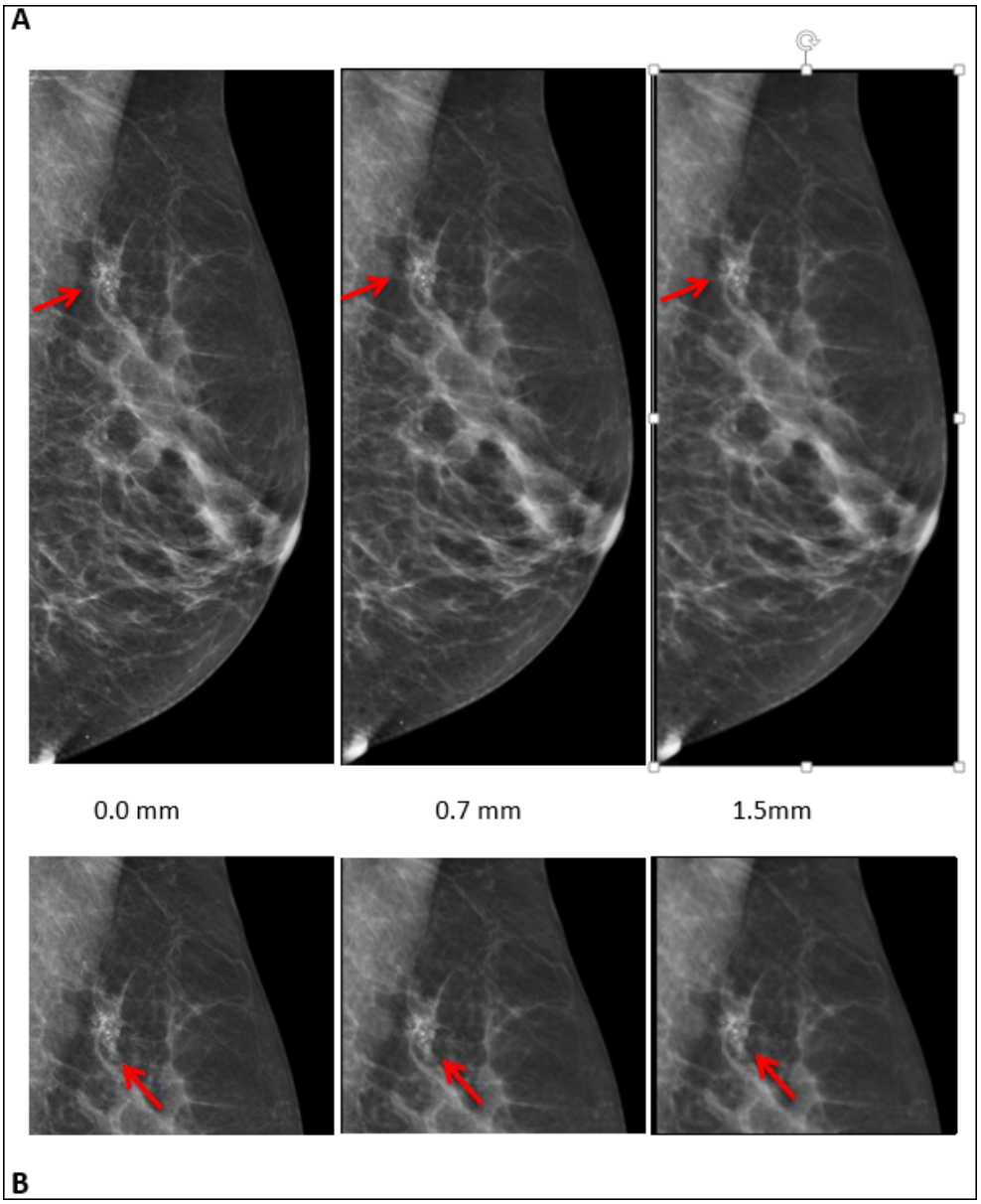

Figure 7.7 (A) left CC projection demonstrates (B) Magnified areas of FFDM images at 0 mm, 0.7 mm, and 1.5 mm of simulated motion blur.

Figure (7.7) shows a single cluster of granular microcalcifications of varying shapes and densities in the outer half of the left breast from ductal carcinoma in situ. This type of lesion was not affected by simulated motion blur at both levels (0.7 mm and 1.5mm). Observer

detectability remained the same when simulated motion blur increased. Almost 100% of the observers detected the lesion in all three comparisons (0.0-0.7mm, 0.0-1.5mm and 0.7-1.5mm). The calcifications appear as focal clusters with an irregular outline. The microcalcifications of similar shape, density and size of of individual calcifications within a focal cluster were not affected by simulated motion blur. A cluster of about 2.0 cm^2 was detected in the left breast. The DI in the image without motion blur (0.0mm) was 1.798 per cm^2 , while the DI for images with motion blur (0.7 and 1.5mm) were 1.498 and 1.199 per cm^2 respectively.

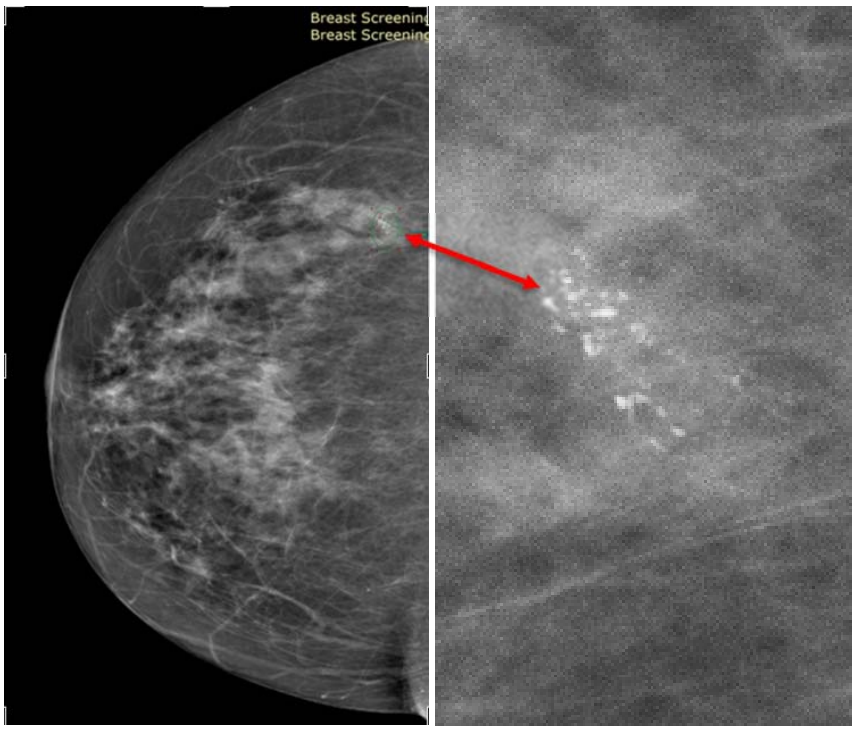

Figure 7.8 (A) Screening mammography image of right CC Projection. Magnified areas of a cluster of microcalcifications.

Calcifications can appear as a focal cluster **(Figure 7.8).** In this example the microcalcifications have similar shape, density and size of flecks. This type of calcification was not affected by simulated motion blur for the three conditions (0.0-0.7 mm, 0.0-1.5 mm and 0.7-1.5mm) due to the large size of the individual calcifications and also that the calcifications have high contrast with their background tissues. Observer detectability remained the same when simulated motion blur increased. A 100% of the observers detected the lesion in images without motion blur (0.0 mm) and in both levels of blurred images (0.7 mm and 1.5 mm). The DI in the image without motion blur (0.0 mm) was 0.863 per cm^2, while the DI for images with motion blur (0.7 and 1.5mm) were 0.648 and 0.504 per cm^2, respectively. It is reasonable to

suggest that the impact of motion blur does not necessarily mean that the lesion has been obscured completely by motion blur. The lesion may still appear, but it might not be determined whether it is malignant or benign.

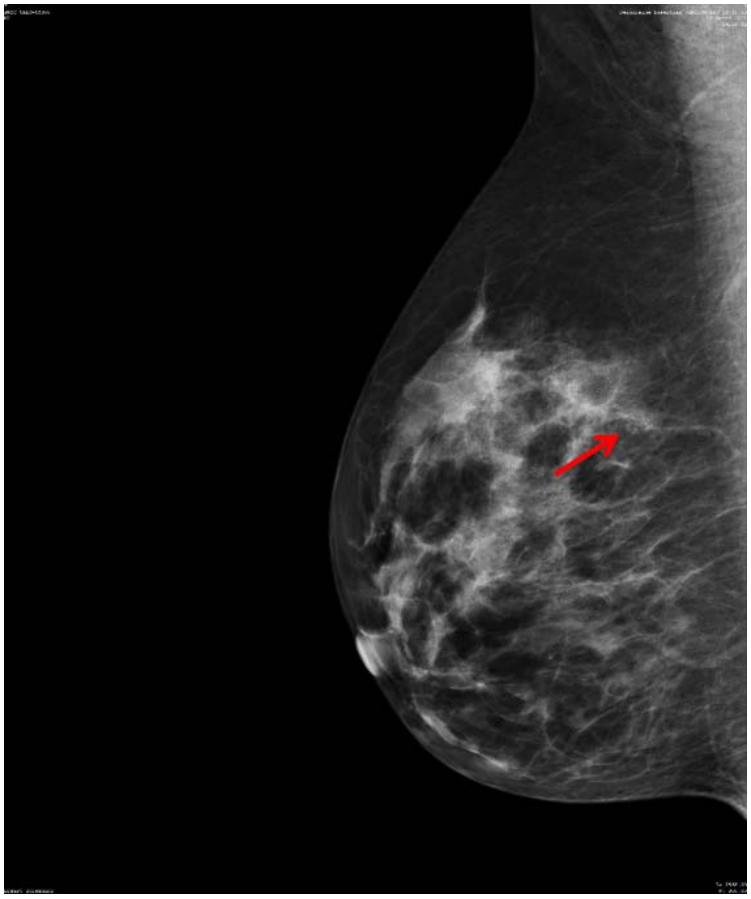

Figure 7.9 Screening mammography image of right cranio-caudal projection.

A cluster of microcalcifications that have a punctate shape is presented in **Figure 7.9**. For this case, the BIRADS breast density is low dense (category B). This type of microcalcification is considered difficult to see due to the small lesion size (less than 0.7 cm^2) and low contrast in relation to the background breast tissues. This type of lesion was affected by simulated motion blur at 1.5 mm and its detectability decreased with increasing levels of motion blur. The detectability at 0.0mm was 100%, while at 0.7 mm it decreased to 85%, but at a level of 1.5mm, it became 42%. The DI in the image without motion blur (0.0 mm) was 0.863 per cm^2, while the DI for images with motion blur (0.7 and 1.5 mm) was 0.648 and 0.504 per cm^2 respectively. High-density breast tissue can make breast lesions difficult to see. Burrell et al., (2001)

reviewed 28 females who had breast cancer identified in screening mammography. They found microcalcifications demonstrated high levels of FNs when compared with the other types of breast lesions. However, Tot et al. (2005) found that some microcalcifications were diagnosed with high accuracy. The results of by Debono (2012) found levels of sensitivity for diagnosis microcalcifications of 90.0%, confirm the results of Tot et al. (2005). Tot et al., (2005) also found that stellate lesions are diagnosed with high accuracy (Tot et al., 2005). However, the findings of a study by Debono (2012) indicated levels of sensitivity to be lower, at approximately 77.6% for the observers diagnosing stellate lesions (Debono, 2012b).

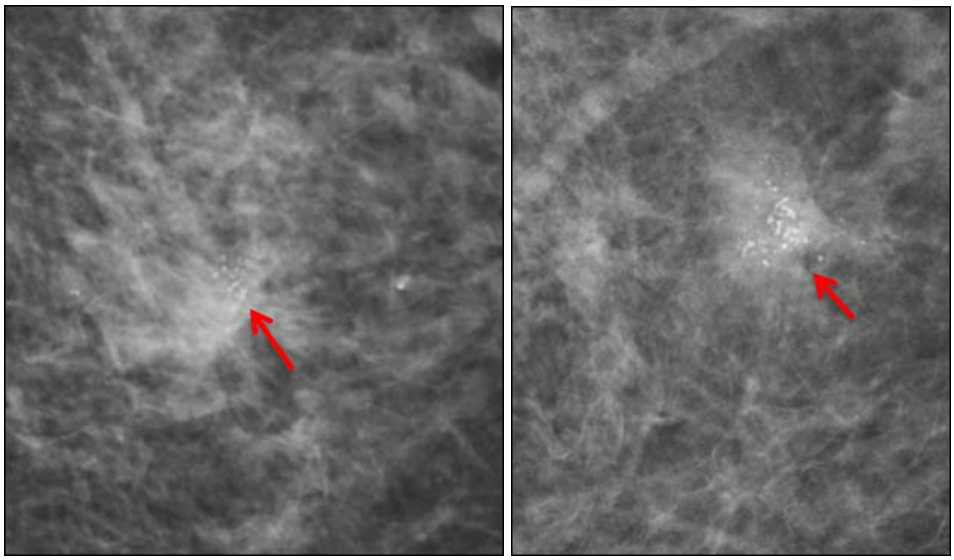

Figure 7.10 (A) a magnified mediolateral Projection demonstrates a small irregular mass with pleomorphic clustered microcalcifications. (B) Magnified cranio-caudal Projection demonstrates a small irregular mass with pleomorphic clustered microcalcifications.

During a clinical evaluation, regions of microcalcifications can be assessed with magnification views to help determine their morphologic appearances as well as their distribution and number of calcifications per cluster. Image blurring can obscure very small calcifications due to using the magnification zoom (e.g. see **Figure 7.10**). Rosen et al., (2002) demonstrated that in 62% of breast cancers that were identified as microcalcifications they were incorrectly followed up with imaging rather than biopsy; it was noted that image blurring on magnification views compromised image quality which compromised the follow up decision (Majid et al., 2003).

7.6 The Impact of Motion Blur on Mammographic Image Features of Breast Masses:

This part of the discussion focuses on the impact of motion blur on the image characteristics of breast lesions. **Tables 7.2** provides an overview of the findings from the FROC study, generalising to different types of malignant mass present in this study. It is worth remembering that the following 'evaluation of image appearances' in relation to cancer detection is based on a limited number of cases. Consequently, caution should be exercised, as the evaluation would need extending to a larger sample of each type of mass/lesion feature in order to have confidence in the results. A larger sample size of different lesion types would be required to make population based generalisations. Nevertheless, the following presents the first discussion ever about lesion features in relation to cancer detection performance in blurred and non-blurred mammographic images.

Table 7.2 Summary of the impact of motion blur on detection performance on each type of breast masses. It is worth mentioning that this table was generated from cases in the current study and this would need evaluating over a larger sample of each type of masses/lesion feature.

Types Mass	Lesion density	Size of mass	Motion blur effect
Spiculated	Low contrast ratio with its background	Small size	affected by motion blur
Irregular shape	low or equal density	Small size which vary in size	affected by motion blur
Obscured	Low contrast ratio with its background	vary in size	affected by motion blur
Oval or round/ Circumscribed	High contrast ratio with its background	Large size with regularly shaped	Not affected by motion blur
Microlobulated	High contrast ratio with its background	Large size with irregularly shaped	Not affected by motion blur
Indistinct	High contrast ratio with its background	small size with irregularly shaped	affected by motion blur

There are many factors related to the appearance of breast lesions within mammographic images that could have an effect on lesion detection performance, such as lesion location within the breast, lesion size, lesion shape and its contrast against background structures. Firstly, lesion location within the breast, when the lesion is located within the fibro-glandular region within an area of high breast density, or when the lesion has overlapping anatomical structures, this makes lesion visibility more challenging. Secondly, lesion size, small types of breast calcifications which have indefinite edges are considered the most difficult lesions to identify due to their poor contrast and small size. Thirdly, lesion shape this can affect whether the malignancy of a breast lesion is determined or not (Berlin, 2001; Fujihashi, 1994; Yankaskas et al. 2001). Fourth, lesion contrast this can be calculated for both local and global background areas (Rawashdeh et al., 2014; Mello-Thoms et al., 2005; Manning & Ethell, 2002); it represents the ratio of the signal intensity of the lesion to its background. **Figure (7.11)** shows examples of mammography images containing breast masses with different appearances due to location, size and tissue background. The lesions have low contrast against background tissues, thus making lesion visibility difficult, especially in the presence of simulate motion blur. Some lesion locations within the breast present additional difficulties in the detection of the lesion. For instance, when a breast lesion is located in the glandular area (appearing as 'white' in the image) this can be affected by motion blur. In contrast, a lesion located in the fatty area (appearing as 'dark' in the image) will have high contrast in relation to the background breast tissues, and this may not be greatly affected by motion blur. Generally, cancers in some locations, such as in the inframammary fold or the axillary tail, are predominantly perceived on only one mammographic image projection; this can lead to difficulties in detection because an alternative image is not available. Such a difficulty extends to when motion blur is present, as the diagnostic decision has to be made on a [potentially] deficient image. A study by Bird et al., (1992) found a significant proportion of undetected cancers in these difficult regions - approximately (25%) of cancers were in the retro-glandular area of the breast and the sensitivity was between 85% and 90% (Bird et al., 1992). However, Goergen et al., (1997) reported that no statistically significant differences exist between regions, in terms of detection efficiency.

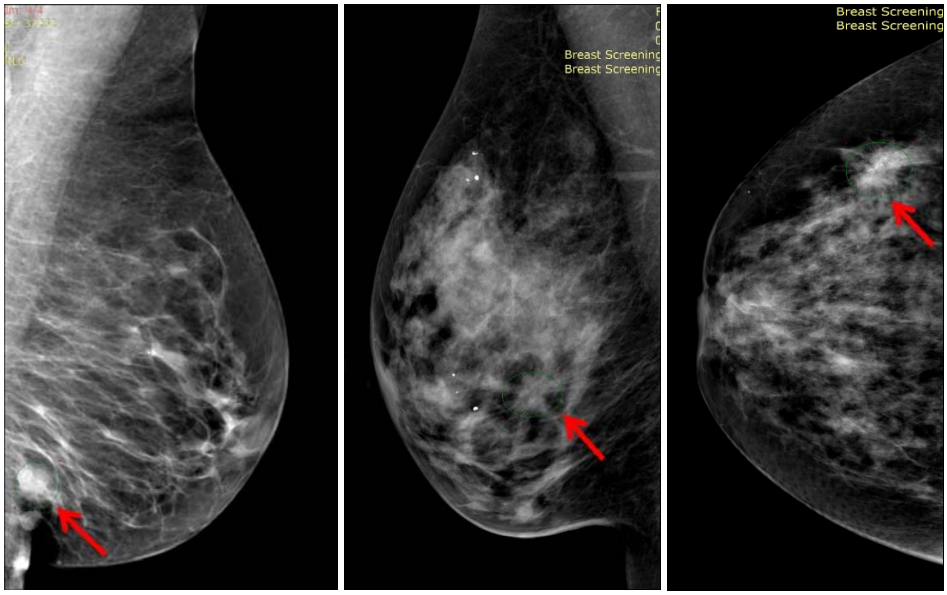

Figure 7.11 Demonstrates mammography images containing breast masses with different lesion appearance due to location, size and tissue background.

A clear finding from this thesis is that motion blur has a high impact on low-density and isodense masses. This thesis has assessed the combined influence of lesion density and motion blur on detection performance and it has been generally demonstrated that better lesion detection performance is associated with masses of higher density; this is in contrast to low-density masses, which tend to have a poorer detection performance in the presence of simulated motion blur. Previous studies have confirmed that mammographic density contributes to challenges in screen reading accuracy (American College of Radiology, 2013; The Radiology Assistant, 2013). It can be reasoned that small differences in contrast between the lesion density and density of breast tissues (density of normal and abnormal tissue) could create difficulties in the perception of important lesion characteristics, such as the edge angle of the lesion. The assessment of lesion density is important in the differential diagnosis of breast masses. The lesion density should be assessed in comparison with the surrounding parenchyma, or in relation to the nipple in the case of fatty involution. The breast mass, in relation to the surrounding parenchyma, is either low density radiopaque, high density radiopaque, radiolucent, radiolucent and radiopaque combined. **Figure (7.12)** shows a group of malignant breast masses, which were not affected by motion blur due to their having higher densities than the background breast tissue. When the relevant lesion density is assessed, the choices of lesion diagnosis will be restricted to the following probabilities; radiolucent circular/oval lesions such as galactocele, lipoma and oil cyst. Low density radiopaque is considered equivalent to the

density of the surrounding parenchyma. In this thesis, low-density masses were affected by motion blur, and they became more difficult to diagnose due to blurring. **Figure (7.13)** shows a group of malignant breast masses. In these cases lesion detection performance was affected by motion blur due to small differences in density between the lesions and background tissues.

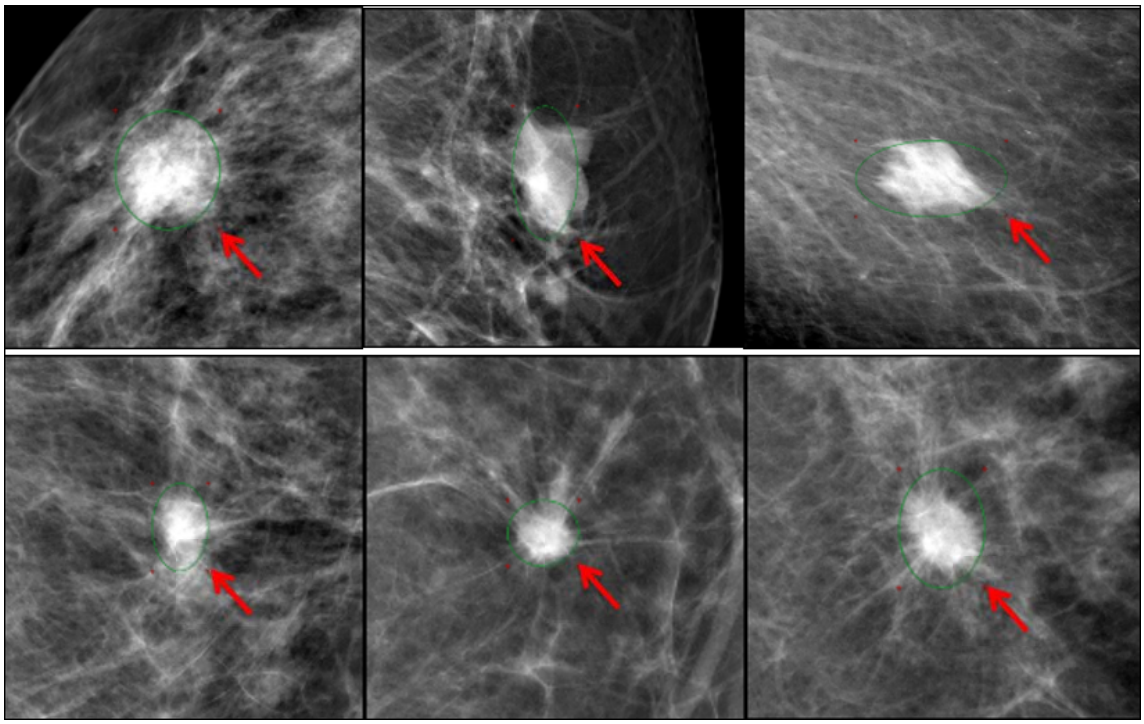

Figure 7.12 Demonstrates a group of malignant of breast masses, which are not affected by motion blur.

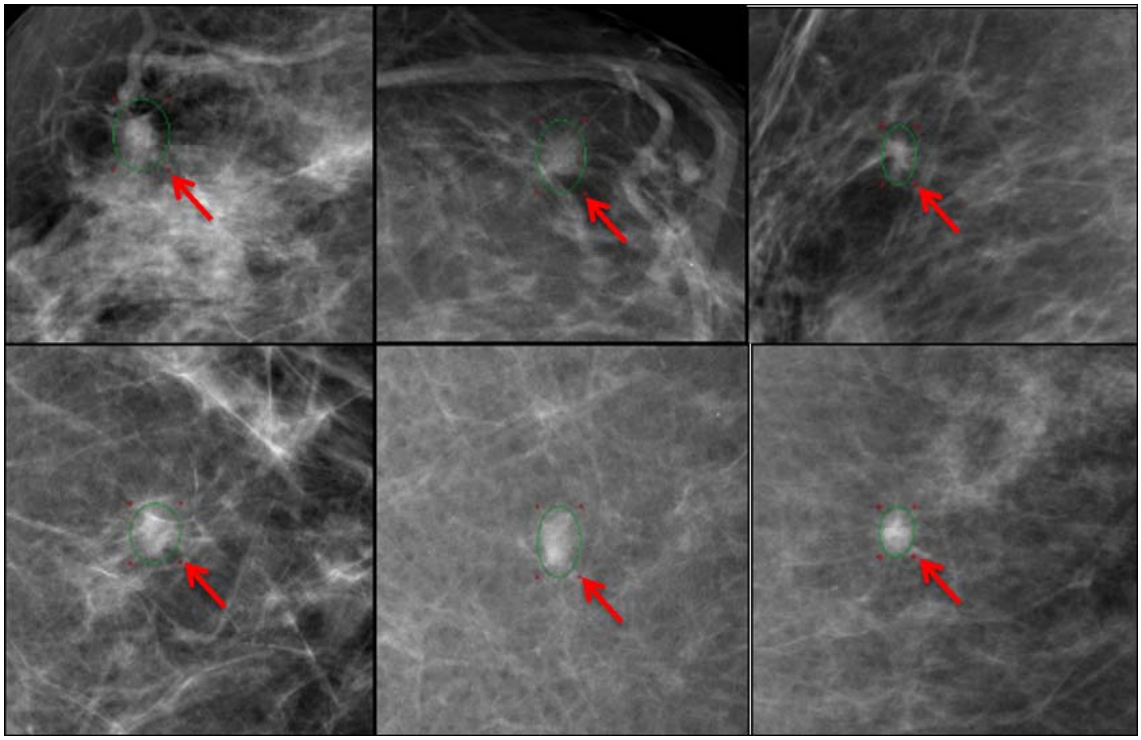

Figure 7.13 Demonstrates a group of malignant of breast masses, which are not affected by motion blur.

To simplify the analysis of lesion characteristics, breast masses can also be classified according to shape and edge features into one of the following types; spiculated or stellate shaped, obscured/indistinct, oval/round/circumscribed and microlobulated. Stellate/spiculated masses are radiating structures with ill-defined boundaries. The thesis demonstrated that stellate/spiculated mass detection performance was adversely affected by simulated motion blur. Circular/oval masses may have poorly or well outlined circular, lobulated or oval, multiple or solitary, for these lesions, detection performance was not adversely affected by simulated motion blur. However, any combination of two or more of these lesion characteristics such as irregular shape, obscured, microlobulated and indistinct, did adversely affect detection performance in the presence of simulated motion blur.

7.6.1 Examples of Masses Affected by Simulated Motion Blur

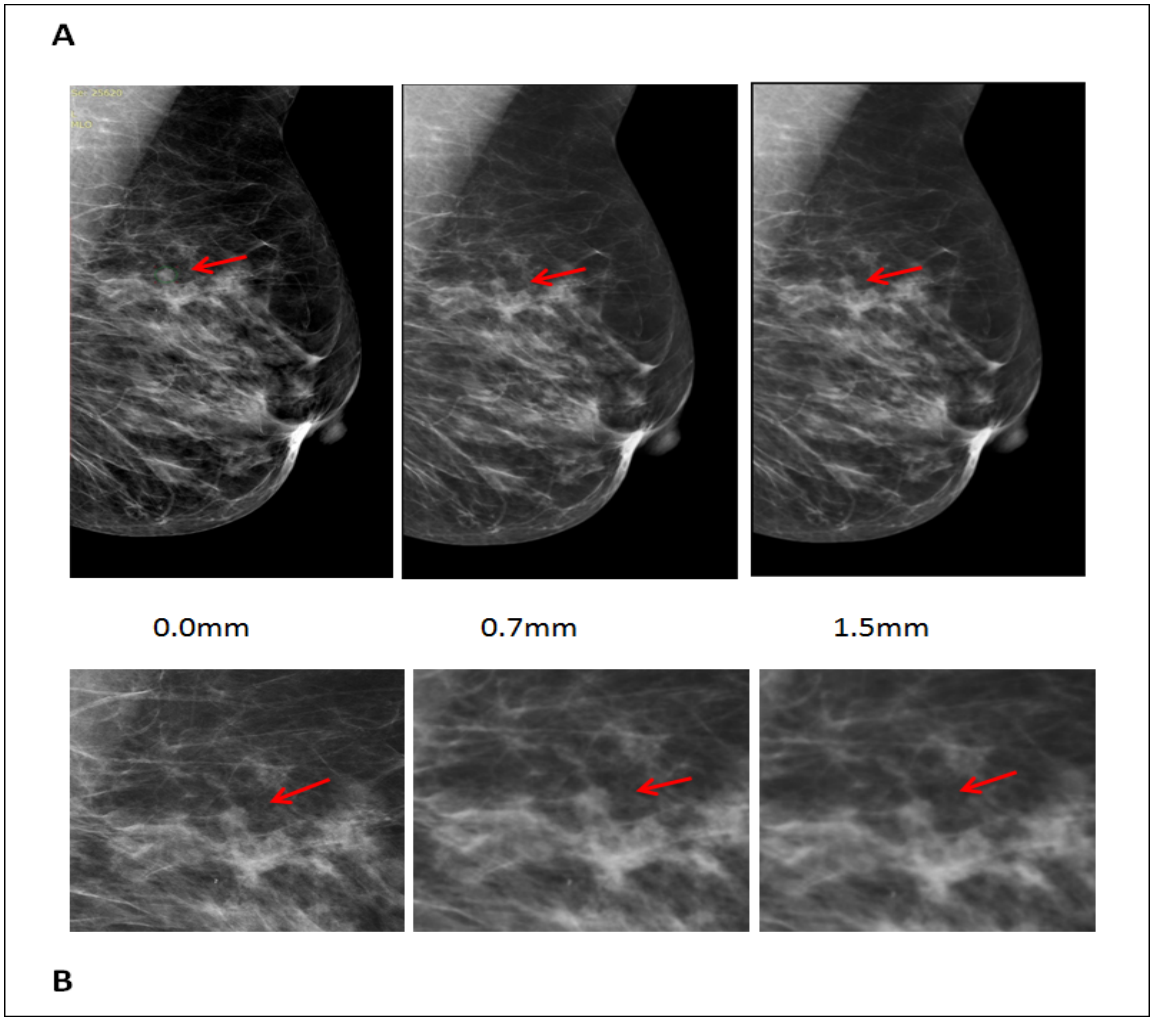

Figure 7.14 (A) mammography images with left MLO Projection, contains different magnitudes of motion blur (0.7 & 1.5 mm) and image without motion blur (0.0mm). (B) Magnified views show small malignant mass (signposted by red arrows).

Figure (7.14) demonstrates a small speculated malignant mass (measuring approximately 7.0 mm in diameter), indicated by the red arrow, in the upper half of the breast. This mass has an irregular outline with fuzzy edges and it is pressing on the tissues around it. It is difficult to see it. 29% of observers missed the mass even when no motion blur (0.0 mm) was present. The detection performance relating to this malignant mass was worse in the presence of simulated motion blur. Lesion detection performance decreased as the level of simulated motion blur increased. 71% (5/7) of the observers detected the lesion in 0.0 mm level, whereas this decreased to 43% (3/7) at 0.7mm and only 29% (2/7) at 1.5mm.

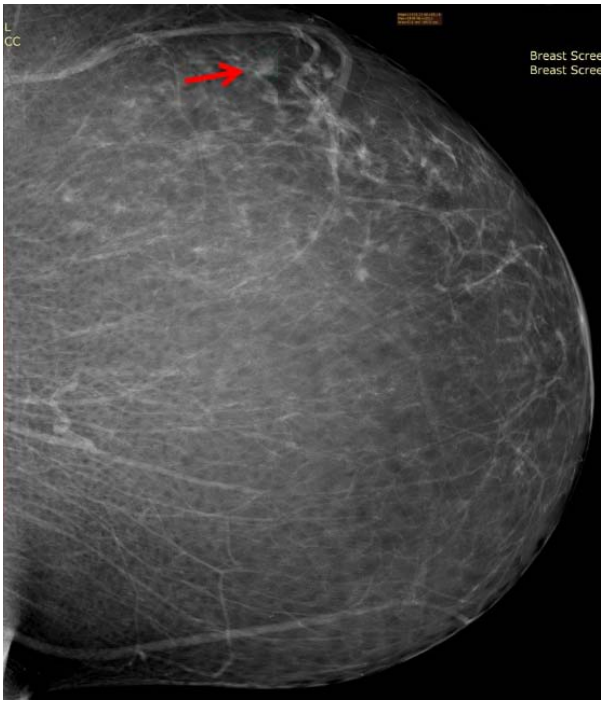

Figure 7.15 Left CC Projection, this mammography image shows a spiculated mass (arrow) that has an irregular shape with indefinite edges.

Figure (7.15) is a cancerous mass which appears as partially round with irregular / spiked outline (see arrows). Its BI-RADS breast density is category B. This mass is considered difficult to see because the lesion size is very small (approximate lesion area <0.8 cm^2) and it has a low contrast, compared with the surrounding background tissues. Detection performance was adversely affected by simulated motion blur and its detection performance decreased as simulated motion blur increased. 100% (7/7) of the observers detected the lesion with no motion blur (0.0 mm), whereas this decreased to 57% (4/7) at 0.7mm and only 29% (2/7) at 1.5mm of simulated motion blur.

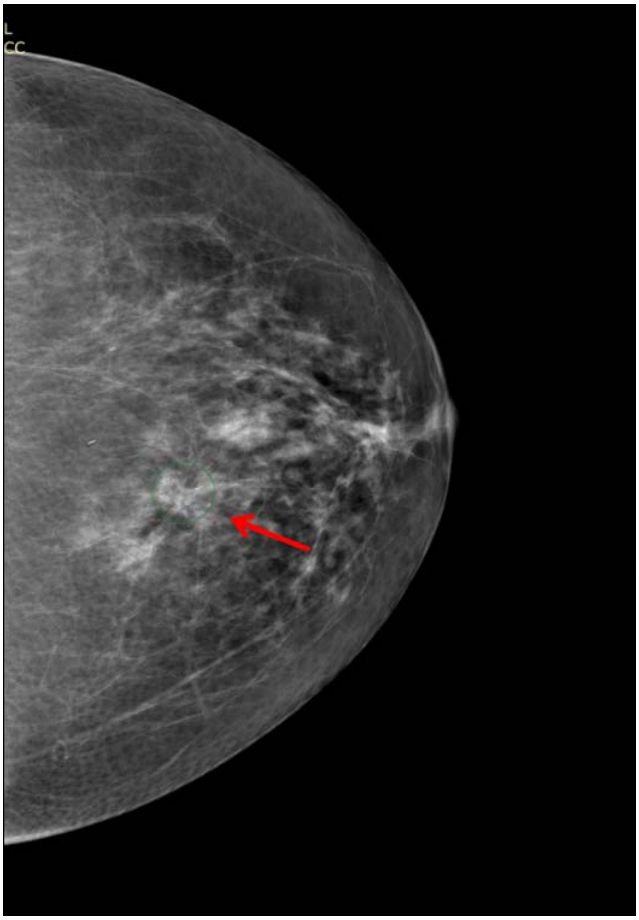

Figure 7.16 Left Cranio-Caudal Projection mammography image contains a stellate mass (arrow) that has an irregular outline (Lesion size 2.2 cm2).

Figure (7.16) shows a stellate mass (see arrow) with an irregular outline (approximate lesion area 2.2 cm^2); it has a BI-RADS breast density grade B. Although its density is higher than the surrounding breast tissue and its size is fairly large, its detection performance was adversely affected by simulated motion blur; detectability decreased as simulated motion blur increased. 71% (5/7) of the observers detected it with no motion blur (0.0mm); this decreased to 43% (3/7) at 0.7mm and only 57% (4/7) detected the lesion at 1.5mm of simulated motion blur . This thesis suggests that stellate masses are affected by simulated motion blur.

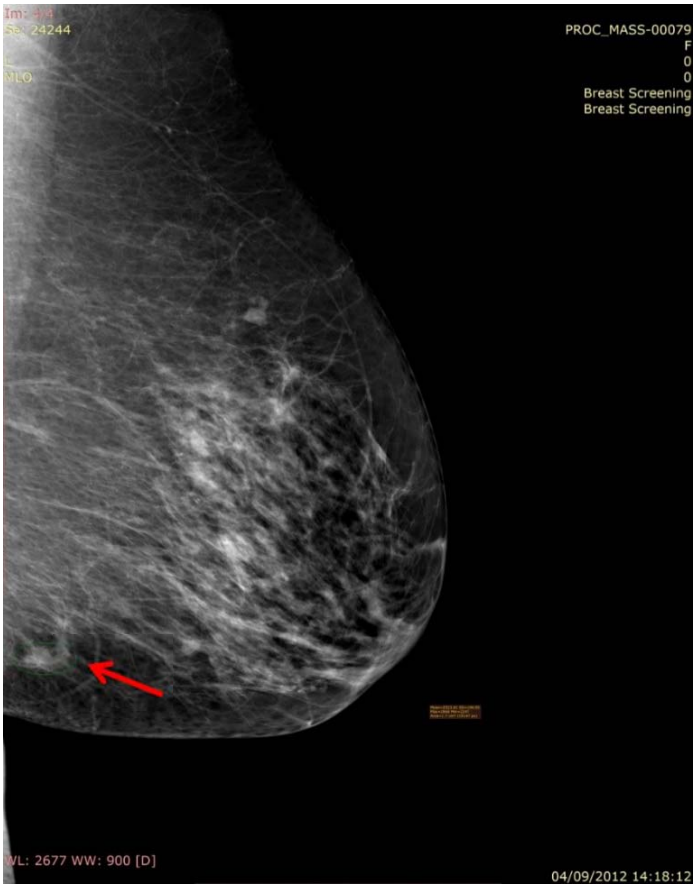

Figure 7.17 Mammography image left Medio-lateral oblique Projection shows indistinct breast mass (arrow) that has an irregular outline.

Figure (7.17) demonstrates an indistinct partially round mass (arrow). It has an irregular outline (approximate area of 1.7 cm^2); it has a BI-RADS breast density grade B, and is located in lower part of the breast (see red arrow). Its detection performance was adversely affected by simulated motion blur, meaning its detectability decreased as simulated motion blur increased. 71% (5/7) of observers detected the lesion with no blur (0.0mm), and this decreased to 57% at 0.7mm and only 43% (3/7) at 1.5mm of simulated motion blur.

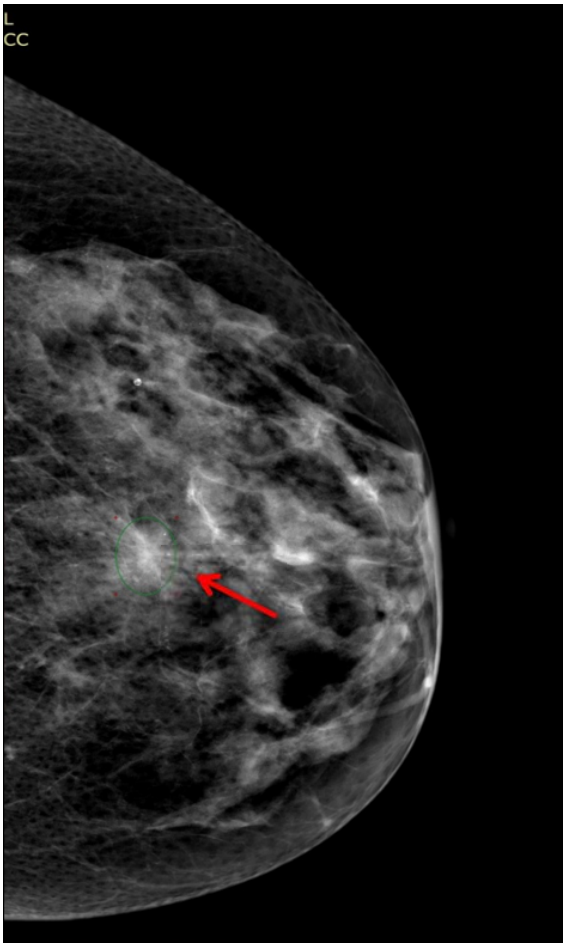

Figure 7.18 Mammography image with left Cranio-Caudal Projection demonstrates a stellate mass (arrow) that has an irregular outline.

Figure (7.18) shows a large stellate mass (approximate area of 1.4 cm^2) located in the middle part of the breast (see arrow), it has a BI-RADS breast density C. It was adversely affected by simulated motion blur. Its detectability decreased with increasing simulated motion blur. Approximately 86% (6/7) of observers detected the lesion with no motion blur (0.0mm). This decreased to 71% (5/7) at 0.7mm and only 57% (4/7) at 1.5mm of simulated motion blur. Stellate masses may be difficult to diagnose due to the surrounding tissue obscuring its spicules. Also, architectural distortion has subtle appearances and may present similarly to normal overlapping breast tissue, causing it to be a typically undetected cancer and FN presentation.

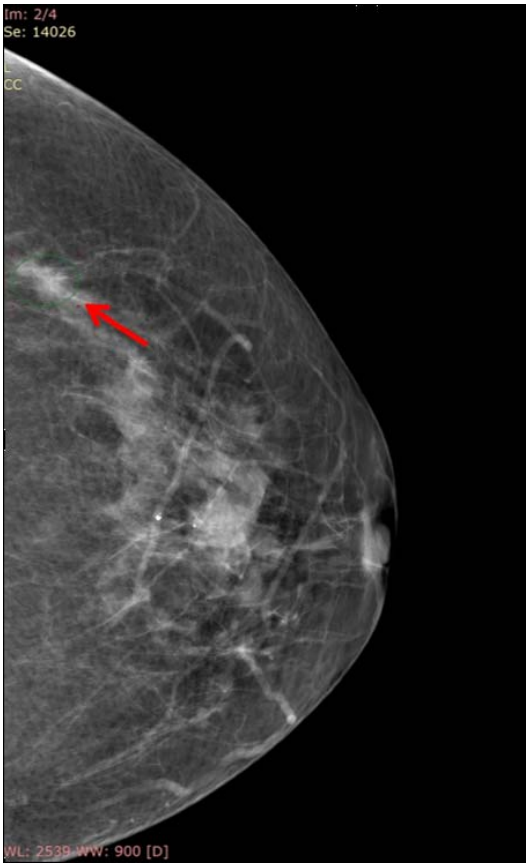

Figure 7.19 Mammography image with left mediolateral oblique Projection contains breast mass (arrow) that has an irregular outline (fuzzy edges).

Figure (7.19) shows a spiculated mass with a multi-pointed star-shaped outline. Its size is approximately 1.4 cm^2 and it is located in the upper part of the breast (see arrow). Its BI-RADS grade is C. Lesion detection performance was adversely affected by motion blur. This spiculated mass has a very small mass centre and a lace-like, fine reticular radiating structure which causes parenchymal distortion and/or asymmetry. Detectability decreased with increasing simulated motion blur. Approximately 86% (6/7) of the observers detected the lesion with no motion blur (0.0 mm). This decreased to 57% (4/7) at 0.7mm and 57% (4/7) at 1.5mm of simulated motion blur.

7.6.2 Masses Not Affected by Simulated Motion Blur

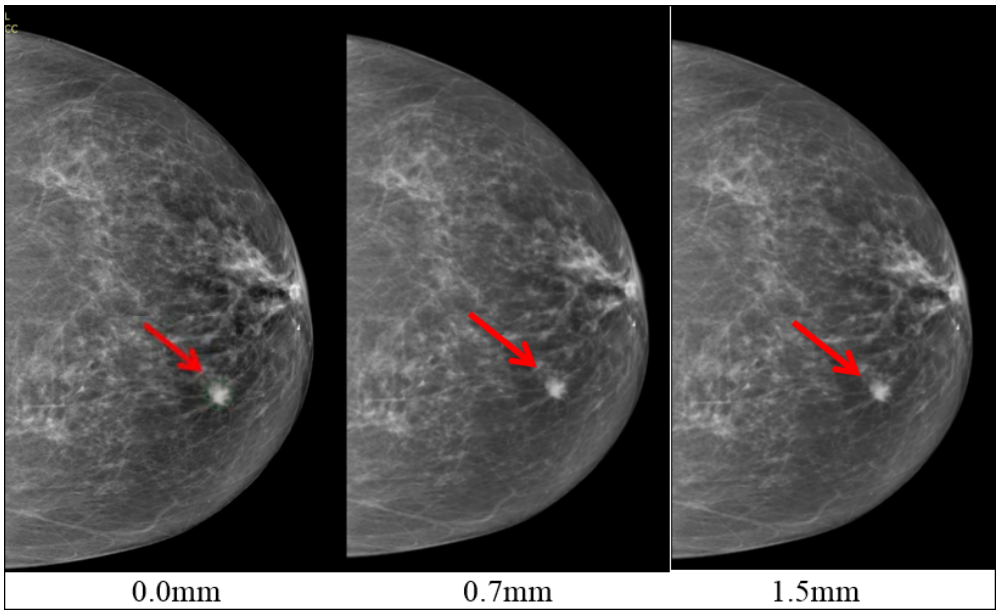

Figure 7.20 Mammography images of left CC projection contain focal breast mass (arrow) with the dense central area.

Figure (7.20) shows mammography images without motion blur (0.0 mm), and two simulated levels of motion blur (0.7 and 1.5 mm). The Figure shows a small malignant mass in the lower part of the breast (see arrows). These images demonstrate a malignant mass which is partially round and partially spiked / irregular shape with definite edges. This mass was not affected by motion blur; this is likely due to its high contrast against surrounding background tissues. Its BIRADS breast density is grade B. 100% (7/7) of the observers detected the mass at (0.0mm) and at both levels (0.7 and 1.5 mm) of simulated motion blur.

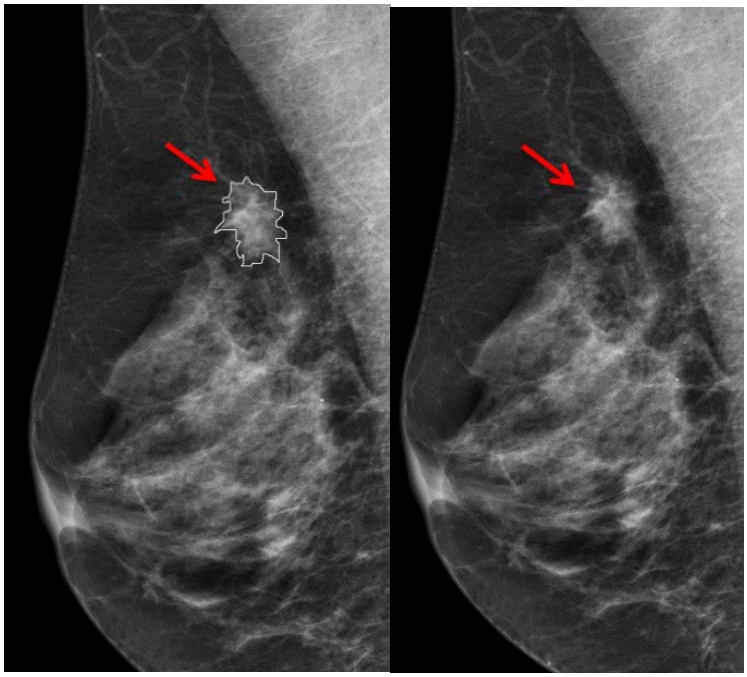

Figure 7. 21 Screening mammography image of right Medio-lateral Oblique projection.

Figure (7.21) demonstrates a microlobulated mass which has an irregular shape with definite edges. It is in the upper half of the breast (see arrow). Its density is higher than the surrounding background breast tissues and its BIRADS density grade is C. Its detection performance was not adversely affected by simulated motion blur. 100% (7/7) of the observers detected the mass at (0.0mm) and at both levels (0.7 and 1.5 mm) of simulated motion blur.

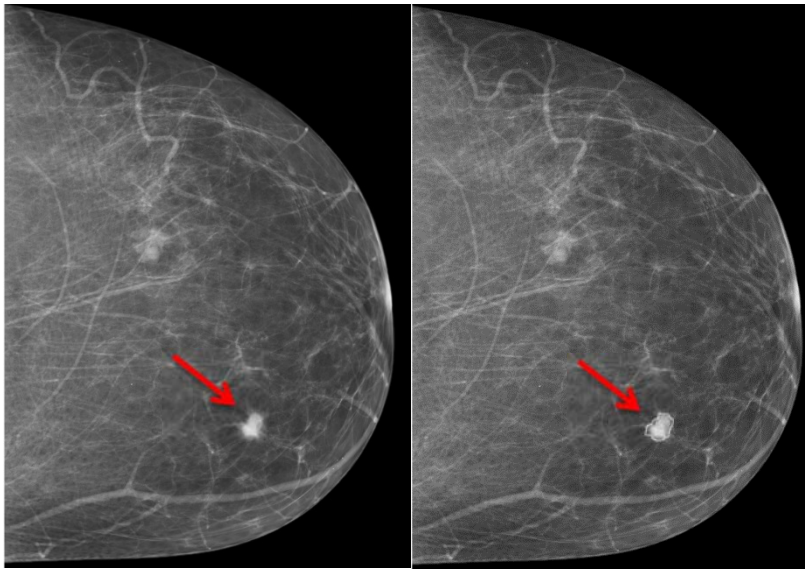

Figure 7.22 Screening mammography image of left CC projection.

Figure (7.22) demonstrates a well circumscribed microlobulated mass with definite edges. It has an approximate area of 12 mm^2; it is depicted by (arrow) and is located in the lower half of the breast. Its detection performance was not adversely affected by simulated motion blur. 100% (7/7) of the observers detected it with no blur (0.0mm) and at both levels of simulated motion blur (0.7 and 1.5 mm).

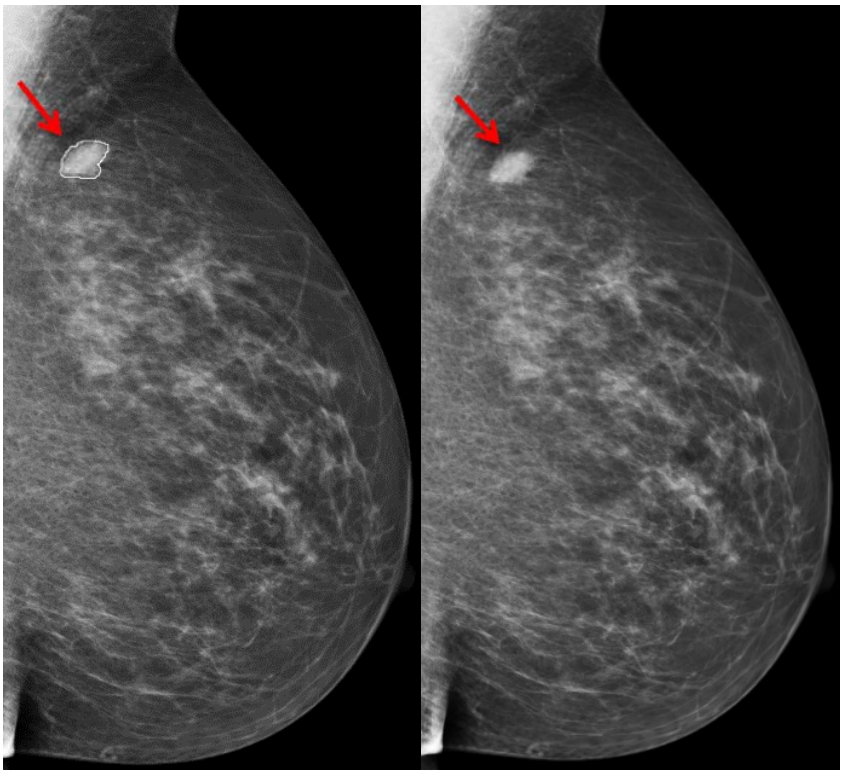

Figure 7.23 Left MLO projection, mammography images show malignant breast mass, with an oval or round shape and definite edges.

Figure (7.23) illustrates a large malignant mass (approximate area of 1.9 mm^2) in the upper half of the breast (see arrow). Its detection performance was not adversely affected by simulated motion blur. 100% (7/7) of the observers detected it with no motion blur (0.0 mm) and also at 0.7 and 1.5 mm levels of simulated motion blur.

7.7 Limitations of this Thesis:

While there is some promise in the results generated in this novel work, there are some limitations to the results achieved. In clinical mammography, the image reader does not know what magnitude of motion blur is present in an image, so it could be argued that it was superfluous to investigate two different magnitudes of motion blur. However, it is known from previous work (Ma et al., 2015) that motion blur is visible at around 0.7 mm of simulated motion blur , so it is of interest to understand if this caused a reduction in observer performance; if it didn't, it was necessary to understand whether a higher magnitude of motion blur did cause an effect. In this thesis the simulated motion blur had a global effect on the whole image and in reality this is not always the case, as 'real motion blur' may affect only one region, several regions or the whole mammographic image. Consequently, the results in this thesis are not able to predict the impact of regional blurring on lesion detection performance.

Further limitations are related to the process of introducing simulated motion blur into the image: It is possible that any image noise present in the original image may be blurred through the mathematical simulation, while in real motion blur this would not occur. For the mathematical simulation of blurring, as is the case in this thesis, the image would appear to be slightly smoother than the non-blurred image. To overcome this potential smoothing effect, it may be possible to adapt the mathematical simulation by adding noise back into the newly created blurred image. Despite this, the current method gives us a certain level of control on motion blur that could not be achieved with 'real' blurred images from a clinical setting.

The mathematical blurring process is enacted as a convolution mask that, in effect spreads each pixel, redistributing its intensity into the neighbouring pixels based on a function and mask size determined by the modelling of the pixel motion as a random vector path parameterised by the characteristics of breast tissue (generalised) elastic coefficient, required duration and required displacement. The latter two factors act as input to the simulation to determine the magnitude of the blur effect. This creates a controllable blur mask for convolution that has a distribution curve reflective of the intensity spread within a collimated light (energy) propagation system reflective of the X-ray system used. Without modelling actual motion within the breast it is not possible to determine the direction of motion at a specific locality within the breast, so this is an approximation to the blur effect that is uniform for the entire image region. Localisation is possible, but requires each source image to have a specific region of blur defined and in this

case motion is assumed to be radial, and the mask application adjusted accordingly on a per-pixel basis, from the centre of the defined region, with maximum motion at the centre, reducing to zero motion at the perimeter of the region. Given a large number of source images processed for this study and the requirement for a consistent blur effect on all the generated image sets, regional blurring was not used in this study. This is a limitation in that the blur effect is indicative of the blur that would be present within a 'real' patient image in terms of magnitude and effect, but does not replicate the directional nature of the blur that would occur for a 'real' image.

In respect of the power of the study, it should be noted that the prevalence of disease is much higher than would be expected in a screening population, but this is difficult to overcome in observer studies because the proportion of cancer cases to normal cases in clinical practice cannot be represented exactly in a small sample as in observer studies. However, all participants in observer studies have a heightened expectation of disease, since they are always aware that their detection performance is being assessed. There are also many differences between observer studies and clinical practice. For instance, in clinical practice, the observer can review many images for each client (e.g. right and left for CC & MLO) as well as previous screening mammograms. In addition, full patients' information, risk factors and clinical examination information is often available. With a free-response study of the type detailed in this thesis, the observer can only see one image for each case and no information about the client. Also they do not have available to them other clinical information which could help inform their decision making.

7.8 Chapter Summary:

In summary, free-response data were analysed for the detection of malignant microcalcifications and masses for three conditions; (i) no simulated motion blur (0.0 mm), and for two magnitudes of simulated motion blur (0.7 and 1.5 mm). A statistically significant difference was found for the detection of masses and microcalcifications. For both analyses, a significant difference was observed between 0 mm and 0.7 mm, and between 0 mm and 1.5 mm of simulated motion blur , and also between (0.7and 1.5 mm) for microcalcifications. No significant difference was detected between (0.7 and 1.5 mm) for masses. These trends were similar, but not exactly the same as those observed in the combined two observers' data analysis. Comparison between single observer free-response data and combined two observers' data demonstrates that the detection performance of microcalcifications improved, while there was no improvement in detection performance for malignant masses. Regarding, the impact of motion blur on physical characteristics, the results demonstrate that there were significant differences in the physical measures of both masses and microcalcifications for all three comparisons of simulated motion blur (0.0-0.7, 0.0-1.5 and 0.7-1.5 mm).

Chapter 8: Conclusion, Recommendations and Future work

This thesis used a novel mathematical algorithm to apply simulated motion blur to clinical FFDM images which were either normal or had proven breast cancer present. Using this blurring approach, this thesis represents the first study to investigate the impact of simulated motion blur on cancer detection performance in FFDM using observer performance methods and characterisation of lesion types.

For the single observer study, the results from this thesis are likely to have implications for clinical practice. It could mean that when blur is observed in an image, a repeat image should be considered as one would simply not know how much motion blur is present and what impact it is having, in terms of cancer detection performance. In view of this, a key outcome of the thesis is that caution should be exercised when making decisions about the acceptability of images that appear to contain motion blur. This may also have implications for the type of monitor used for the initial evaluation of technical quality of mammograms. For both masses and microcalcifications, the findings indicate that simulated motion blur has a significant detrimental effect on cancer detection performance.

When two observers' data were combined to simulate double reporting, as occurs in mammography screening, the key finding was that a combined read is likely to only have beneficial outcomes. While there was no statistically significant benefit for breast masses, for microcalcifications, there was a statistically significant difference between single and combined free-response data. Given that image readers do not have a prior expectation of masses or microcalcifications occurring in the image, the only recommendation can be that all images have to receive double reporting.

For the physical measures of malignant masses, simulated motion blur had a negative impact on edge angle and this appeared to have only a weak correlation with a reduction in detection performance. It is reasonable to hypothesise that when the conspicuity of the mass increases it does not necessarily mean that the detectability of mass would also increase. However, conspicuity index did get statistically as the magnitude of simulate motion blur increased. The edge angle was decreased with increasing the level of simulated motion blur. The change in grey level was not statistically significant between the different magnitudes of simulated

motion blur. Image noise was statistically worse with an increasing level of simulated motion blur.

For microcalcifications, the dispersion index was statistically worse with an increasing level of simulated motion blur. This negative impact on the dispersion index was due to some small calcifications/tight clusters becoming obscured. There are many factors related to the appearance of breast lesions within mammographic images that could have an impact on lesion detection performance, such as lesion location within the breast, lesion size, and lesion shape. The calculation of missed lesions was used to identify the detectability of different lesion types. The analysis of missed lesions should provide a less abstract concept which can be used to evaluate lesion types. In summary, microcalcification clusters of small size or individual calcifications are likely to be missed in the presence of simulated motion blur. For masses, large lesions and those with high lesion-to-background contrast were not affected by simulated motion blur. However, those with an irregular outline, with stellate shape, or those that have fuzzy edges, have multi-pointed star-shaped are difficult to detect with simulated motion blur present. Finally, high breast density was also a strong factor linked to poorer detection. Images readers and technical staff need to be aware of the impact of motion blur on the detection of cancer during the acquisition and reporting of FFDM images. For the benefit of clients, further work is required to ensure that motion is recognised at the earliest possible opportunity.

8.2 Statement of Novelty

The main novel contributions of this PhD are summarised as follows:

1. **Research problem:** This is the first study to evaluate the impact of motion blur on mammography lesion detection performance.

2. **Novel method:** This is the first study to use mathematical simulation for blur induction in order to assess its impact on mammography breast cancer detection performance.

3. **Novel method for physical measures:** This is the first study to assess the impact of simulated motion blur on the physical characteristics of microcalcification and masses in mammography images. The impact of simulated motion blur on the physical characteristics of malignant microcalcification images have been assessed using dispersion index, which is a novel measure.

4. **Novel analysis of data:** This is the first study to use free-response data assess the impact of mimic double reporting, using combined two observers' data on blurred FFDM images.

5. **New method:** This is the first study to conduct a missed lesions analysis to establish reasons why observers failed to detect lesions in the presence of simulated image blurring.

8.7 Recommendations and Future work

Future work

1. Evaluation of regional simulated motion blur

The simulated blur applied in this study was global in effect (i.e. the entire image). In clinical mammography, motion blur may be global or regional. This study is not able to predict the impact of regional blurring on lesion detection performance. In future work, it is important to study the impact of regional blurring on lesion detection performance.

2. Evaluation of 'real' motion blur

Further studies are required to investigate the impact of real motion blur on lesion detection performance. This will be a prospective study, collecting an appropriate number of real blurred mammograms and their repeated images (containing no motion blur). A free-response study will be used to measure detection performance.

3. Validation of Dispersion Index

The dispersion index was develeoped as a novel metric for this work since existing conspicuity software could not be applied to microcalcifications due to their small individual size and wide distribution pattern. No validation has been conducted on DI, but this could be a focus for post-doctoral work.

Recommendations

There are significant consequences to motion blur in clinical practice and consequently this thesis provides a number of recommendations to breast imaging professionals. Image readers should be aware of the impact of motion blur on cancer detection and they should evaluate images carefully for its presence prior to making an interpretation. In addition, staff should be aware of motion blur during quality assessment of images in the mammography imaging room. Within the UK, blurred images may need to be repeated, however due regard should be given to NHSBSP quality assurance recommendations in which a repeat threshold of 3% has been set. When motion blur is detected, this could lead to repeated images and increased recall rates, both of which will increase radiation dose and represent a negative physical and psychological experience for the client. If motion blur is not recognised, this could lead to misdiagnosis, late detection and even symptomatic presentation as an interval cancer. On the other hand, motion blur also has the potential to increase the number of lesion mimics (false positives), which may lead to unnecessary biopsy, with the consequence of an unnecessary invasive procedure and increased client anxiety.

Appendices:

Appendix A: Ethics Application HSCR 15-107

University of Salford MANCHESTER

Research, Innovation and Academic Engagement Ethical Approval Panel

Research Centres Support Team
G0.3 Joule House
University of Salford
M5 4WT

T +44(0)161 295 2280

www.salford.ac.uk/

6 November 2015

Dear Ahmed,

RE: ETHICS APPLICATION HSCR 15-107 – The impact of image blurring on lesion detection performance in full field digital mammography (FFDM)

Based on the information you provided, I am pleased to inform you that application HSCR15-107 has been approved.

If there are any changes to the project and/ or its methodology, please inform the Panel as soon as possible by contacting Health-ResearchEthics@salford.ac.uk

Yours sincerely,

Sue McAndrew
Chair of the Research Ethics Panel

Appendix B: Ethics Application HSCR 15-110

University of Salford MANCHESTER

Research, Innovation and Academic Engagement Ethical Approval Panel

Research Centres Support Team
G0.3 Joule House
University of Salford
M5 4WT

T +44(0)161 295 2280

www.salford.ac.uk/

30 November 2015

Dear Ahmed,

RE: ETHICS APPLICATION HSCR 15-110 – Assess the impact of image blurring on human visual performance during visual acuity and contrast sensitivity testing

Based on the information you provided, I am pleased to inform you that application HSCR15-110 has been approved.

If there are any changes to the project and/ or its methodology, please inform the Panel as soon as possible by contacting Health-ResearchEthics@salford.ac.uk

Yours sincerely,

Sue McAndrew
Chair of the Research Ethics Panel

Appendix C : Organisation Management Consent/ Agreement Letter

University Hospital of South Manchester NHS
NHS Foundation Trust

Wythenshawe Hospital
Southmoor Road
Wythenshawe
Manchester
M23 9LT
Tel: 0161 998 7070

26th August 2015

Dr Claire Mercer
School of Health Sciences
Allerton Building
University of Salford
Manchester
Salford, UK
M5 4WT

Ahmed Abdullah
School of Health Sciences
Allerton Building
University of Salford
Manchester
Salford, UK
M5 4WT

RE : Organisation Management Consent / Agreement Letter
Consent to use mammography images, as detailed below, for research studies at the University of Salford, U.K.

Dear Dr. Mercer and Mr. Abdullah,

I formally give my consent and agreement for the mammography images detailed below to be used for mammography research studies at the University of Salford under the principle investigators and postgraduate students of Dr Claire Mercer and/or Professor Peter Hogg.
In giving consent I understand that researchers from the University of Salford, College of Health and Social Care, will be copying anonymised images from the PROCAS data set under the supervision of Nightingale Centre professional colleagues.

These anonymised images will be stored on a password protected memory device and then transferred to the University of Salford's PACS. This will be carried out only in the presence of Dr Claire Mercer and/or Professor Peter Hogg with the PhD student Ahmed Abdullah.
I understand that by giving consent Dr Claire Mercer and/or Professor Peter Hogg and PhD student Ahmed Abdullah at the University of Salford, College of Health and Social Care will then:

- use the data for scientific study, ethics approved research and education
- be unable to trace back the identity of the participants
- store the data for as long as necessary for scientific research and education

UHSM
Your Hospital

University Hospital of South Manchester NHS
NHS Foundation Trust

Wythenshawe Hospital
Southmoor Road
Wythenshawe
Manchester
M23 9LT
Tel: 0161 998 7070

inform the Nightingale Centre of any publications arising from this data and acknowledge the contributions in all publications

The mammography images I consent to being anonymised from the PROCAS data set are:

150 mammogram images which have been classified as normal from each BI-RADS category (A-D)
150 mammography images which have been classified with malignant calcifications
150 mammography images which have been classified with malignant masses

Yours sincerely

Dr Mary Wilson
Clinical Director of Breast Screening

Appendix D: Participant Invitation Letter

Directorate of Radiograph,
Centre of Health Sciences Research,

University of Salford,
Allerton Building,
Salford, M6 6PU
31 May 2018

Dear Sir or Madam:

RE: Research Involvement: Image blurring and lesion detection in mammography

Research Governance and Ethics Committee Approval: RGEC

I am a PhD student under the supervision of Professor Peter Hogg, Dr John Thompson, Dr Claire Mercer, Mrs Judith Kelly and Dr Rob Aspin at the University of Salford. I am currently investigating the impact of image blurring caused by unwanted motion on an observers' ability to detect clinically significant lesions in full field digital mammography (FFDM) images. This research uses the latest and most advanced techniques in observer performance, namely free-response receiver operating characteristics (FROC) method and a statistically powerful jackknife alternative FROC (JAFROC) analysis. For this research I require expert observers to examine a series of images that are either normal (no lesions) or contain lesions with varying degrees of simulated image blurring. In this study an advanced computer algorithm developed at the University has been used to introduce the image blurring.

I am approaching you as an experienced professional and potential volunteer to take part in the observer study. If you are happy to take part in the research, please respond to the email address at the bottom of this letter and I will be happy to give you more information. Your contribution will be appreciated, though no financial reward or otherwise will be offered. It is expected that you will be required to make 3-4 visits to the University to complete image evaluations using our 5 megapixel monitors. Each evaluation is expected to last up to 90 minutes. This contract lays out the standards by which the observer group will adhere to and the conditions under which the evaluations will be completed, thereby ensuring respect is afforded to all who are directly involved in this study.

If you have any further questions about the study that will help you decide whether to volunteer for this research, or if you have any further queries, please get in touch via telephone or e-mail. Thank you for taking the time to read this letter and I hope to hear from you in the near future.

Sincerely

Student name------

Email ----------

Appendix E: Participant Information Sheet

University of Salford MANCHESTER

Participant information sheet for observers participants in observation study (FROC study)

Study title:	Determine the impact of image blurring on lesion detection performance in full field digital mammography images (FFDM)
Chief investigator	
Telephone number	

Study Sponsor: University of Salford

We would like to invite you to take part in our research study. Before you decide we would like you to understand why the research is being done and what it would involve for you. Talk to others about the study if you wish and please ask if there is anything that is not clear. This is a Student project, required for successful completion of a Doctoral programme.
I am currently investigating the impact of image blurring caused by unwanted motion on an observers' ability to detect clinically significant lesions in full field digital mammography (FFDM) images. The aim of the study is to determine the impact of image blurring on lesion detection performance in full field digital mammography images (FFDM) using free-response receiver operating characteristics (FROC) method

Participant name:

You will be given a copy of this information sheet to keep

1. What is the purpose of this study?

The purpose of this study to determine the impact of image blurring on lesion detection performance in full field digital mammography using the free-response receiver operating characteristics (FROC) method.

2. Why have I been invited?

This research uses the latest and most advanced techniques in observer performance, namely the Free-response Receiver Operating Characteristics (FROC) method and the statistically powerful jackknife alternative FROC (JAFROC) analysis. For this research I require expert observers to examine a series of full field digital mammographic (FFDM) images that are either normal (no lesions) or contain lesions with varying degrees of simulated image blurring. In this study an advanced computer algorithm developed at the University has been used to introduce image blurring to clinical images.
You have been invited because you are considered an expert observer in mammography.

3. Do I have to take part?

Your decision to take part in this study is entirely voluntary. You may refuse to participate or you can withdraw from the study at any time.

4. What will happen to me if I take part?

It is expected that you will need to make 3-4 visits to the University of Salford to complete image evaluations using our 5 megapixel monitors. Each evaluation is expected to last up to 90 minutes. You will be asked to assess and localise lesions in mammographic images .The information you provide will be kept confidential and will be used only towards achieving the aim of the research.

5. Expenses and payments

Your contribution will be appreciated, though no financial reward or otherwise will be offered.

6. What are the possible disadvantages and risks of taking

This research does not pose any risk to its participants.

7. What are the possible benefits of taking part?

Your participation may help improve understanding of the impact of image blurring on cancer detection performance. Better awareness of the impact of image blurring may result in better breast cancer detection rates at the early stage and overall result in to the reduction of the mortality rate due to breast cancer. Alternatively, it may reduce the number of repeated images, if blurring is found to have no significant impact.

8. What if there is a problem or I want to complain?

If you wishes to complain in the first instance this can be discussed with researcher:

If you have any queries or questions please contact:

Principal investigator: ----------

Email ----------

Phone number ----------

University of Salford, School of Health Sciences

Or if preferred with researcher's supervisor

Professor ----------

Email ----------

If you remain dissatisfied, please contact:

Research Centres Manager
Research and Enterprise
G-08, Joule House, Acton Square,
University of Salford,
U.K, M5 4WT

9. Will my taking part in this study be kept confidential?

The information you give during FROC study will be kept in a locked cabinet within the University. The documents will be destroyed in five year after the end of the study.

10. What will happen to the results of the research study?

The results of the study will be included in a research thesis, would be discussed at research conferences and published in peer reviewed research journals.

11. Who is sponsoring the study?

The sponsor of the study has the duty to ensure that it runs properly and that it is insured. In this study, the sponsor is the University of Salford.

12. Who has reviewed this study?

This research was reviewed by the University of Salford Research and Ethics Committee, to protect your safety, rights, wellbeing and dignity. This Committee is

run by University of Salford but its members are not connected to the research they examine. This study has been reviewed and given a favourable opinion.

13. Further information and contact details

If you have any queries or questions please contact:

Principal investigator: ----------

Email ----------

Phone number ----------

University of Salford,
School of Health Sciences

Alternatively, you can contact my supervisory team:

Appendix F: Poster to Invite the Participants

University of Salford MANCHESTER

Experts of diagnostic mammography field are invited to participate in a PhD study, to determine lesion detection performance FFDM images

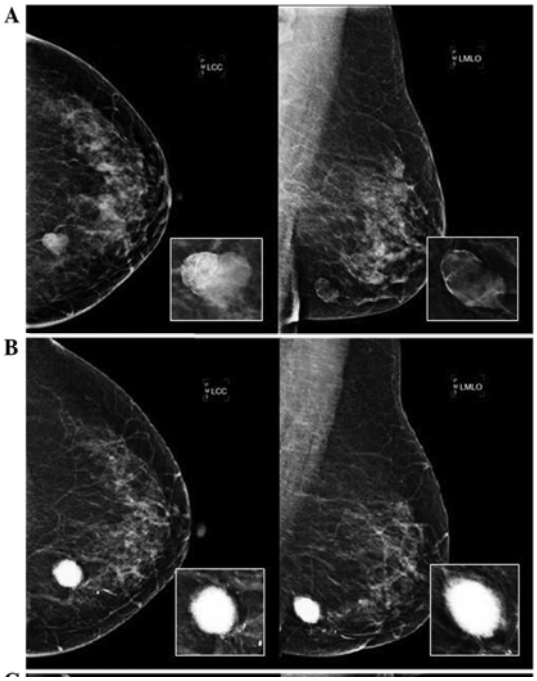

This research uses the latest and most advanced techniques in observer performance study, namely Free-response Receiver Operating Characteristics (FROC) method and a statistically powerful jackknife alternative FROC (JAFROC) analysis. For this research I require expert observers to examine a series of images that are either normal (no lesions) or contain lesions (malignant masses and calcifications) with varying degrees of simulated image blurring. In this study an advanced computer algorithm developed at the University of Salford has been used to introduce the image blurring.

As a participant in this study, it is expected that you will be required to make 3-4 visits to the University to complete image evaluations using our 5 megapixel monitors. Each evaluation is expected to last up to 90 minutes.

If you decide that you would like to take part in the study and for further information, please contact the researcher:

Mr. Ahmed Abdullah, PhD student

E-mail: (*a.k.abdullah@edu.salford.ac.uk*).

Appendix G: Tables of the Collected Data

Table (G-1) Demonstrates the features of mammographic images (Projection of image, breast density, and number of lesions per image). The characteristics of malignant breast masses with different shape of margin, lesions' BI-RADS and size of lesions are presented.

Image NO.	Projection of image & Side	Sharpness	Type of lesion	Number of lesion per image	Breast density	shape of margin	Lesion BI-RADS	Lesion size in mm
1	LCC	acceptable	Malignant	1	C	irregular	R5	16
2	RCC	acceptable	Malignant	1	D	irregular	R4	14
3	LCC	acceptable	Malignant	1	C	irregular	R5	10
4	RMLO	acceptable	Malignant	1	B	irregular	R5	16
5	RMLO	acceptable	Malignant	1	B	Spiculated	R5	14
6	LCC	acceptable	Malignant	1	C	irregular	R4	25
7	LMLO	acceptable	Malignant	1	B	irregular	R5	20
8	LCC	acceptable	Malignant	1	C	irregular	R4	25
9	LCC	acceptable	Malignant	1	B	irregular	R5	12.5
10	LMLO	acceptable	Malignant	1	C	irregular	R4	7
11	RMLO	acceptable	Malignant	1	C	Spiculated	R4	16
12	LCC	acceptable	Malignant	1	C	lobulated	R4	22.6
13	RMLO	acceptable	Malignant	1	B	Spiculated	R5	10
14	RCC	acceptable	Malignant	1	C	Irregular	R5	21
15	LCC	acceptable	Malignant	1	B	Spiculated	R5	9
16	LMLO	acceptable	Malignant	1	C	irregular	R5	8
17	LMLO	acceptable	Malignant	1	B	irregular	R5	15
18	LCC	acceptable	Malignant	1	B	irregular	R5	11
19	LMLO	acceptable	Malignant	1	B	irregular	R5	5
20	LCC	acceptable	Malignant	1	C	irregular	R4	8

Table (G-2) Demonstrates the features of mammographic images (Projection of image, breast density, and number of lesions per image). The characteristics of malignant breast masses with different shape of margin, lesions' BI-RADS and size of lesions are presented.

Image NO.	Projection of image & Side	Sharpness	Type of lesion	Number of lesion per image	Breast density	the shape of margin	Lesion BI-RADS	Lesion size in mm
21	RCC	acceptable	Malignant	1	C	Round	R3	9
22	RMLO	acceptable	Malignant	1	B	irregular	R4	14
23	RCC	acceptable	Malignant	1	C	irregular	R5	17
24	LMLO	acceptable	Malignant	1	B	lobulated	R4	23
25	LMLO	acceptable	Malignant	1	B	irregular	R5	25
26	LCC	acceptable	Malignant	1	B	irregular	R4	12
27	LCC	acceptable	Malignant	1	B	Spiculated	R5	10
28	RMLO	acceptable	Malignant	1	B	Spiculated	R4	12
29	LMLO	acceptable	Malignant	1	C	irregular	R4	16
30	LCC	acceptable	Malignant	1	C	Spiculated	R3	10
31	LCC	acceptable	Malignant	1	B	irregular	R4	14
32	RCC	acceptable	Malignant	1	D	irregular	R5	17
33	LMLO	acceptable	Malignant	1	D	irregular	R4	20
34	RMLO	acceptable	Malignant	1	D	irregular	R4	21
35	RCC	acceptable	Malignant	1	B	irregular	R4	9
36	LCC	acceptable	Malignant	1	C	Spiculated	R5	14
37	CC	acceptable	Malignant	1	B	irregular	R4	17
38	LCC	acceptable	Malignant	1	C	lobulated	R5	23
39	LCC	acceptable	Malignant	1	B	Spiculated	R4	14
40	LCC	acceptable	Malignant	1	D	Spiculated	R4	15

Table (G-3) Demonstrates the features of mammographic images (Projection of image, breast density, and number of lesions per image). The characteristics of malignant breast masses with different shape of margin, lesions' BI-RADS and size of lesions are presented.

No.	Projection of image	sharpness	Type of lesion	lesions per image	Breast density	Shape of margin	Lesion BIRADS	LESION SIZE in mm
41	LCC	acceptable	Malignant	1	B	Spiculated	R4	12
42	RCC	acceptable	Malignant	1	B	Spiculated	R4	8
43	RCC	acceptable	Malignant	1	C	Round	R4	7
44	RMLO	acceptable	Malignant	1	C	irregular	R5	15
45	RMLO	acceptable	Malignant	1	C	irregular	R5	20
46	LMLO	acceptable	Malignant	1	C	lobulated	R3	14
47	LCC	acceptable	Malignant	1	B	irregular	R4	10
48	LMLO	acceptable	Malignant	1	B	irregular	R4	8
49	LMLO	acceptable	Malignant	1	D	irregular	R5	18
50	LCC	acceptable	Malignant	1	C	Spiculated	R5	10
51	LCC	acceptable	Malignant	2	C	irregular	R3&R3	14&19
52	R	acceptable	Malignant	1	C	irregular	R5	15
53	RCC	acceptable	Malignant	1	B	irregular	R4	10
54	RMLO	acceptable	Malignant	1	C	Spiculated	R5	17
55	RMLO	acceptable	Malignant	1	B	irregular	R5	28
56	LMLO	acceptable	Malignant	1	C	irregular	R4	23
57	RCC	acceptable	Malignant	1	B	irregular	R4	11
58	LMLO	acceptable	Malignant	1	D	distortion	R4	27
59	LCC	acceptable	Malignant	1	B	irregular	R5	22
60	RCC	acceptable	Malignant	1	C	Spiculated	R4	13
61	RMLO	acceptable	Malignant	1	B	Spiculated	R4	8

Table (G-4) Demonstrates the features of mammographic images (Projection of image, breast density, and number of lesions per image), and the characteristics of malignant breast masses with different shape of margin, lesions' BI-RADS and size of lesions are presented.

Image No.	Projection of image	sharpness	Type of lesion	lesions per image	Breast density	Shape of margin	Lesion BIRADS	LESION SIZE in mm
62	LCC	acceptable	Malignant	1	B	Spiculated	R4	8
63	LCC	acceptable	Malignant	1	C	Spiculated	R4	5
64	LMLO	acceptable	Malignant	1	C	irregular	R4	13
65	RMLO	acceptable	Malignant	1	C	irregular	R4	14
66	LMLO	acceptable	Malignant	1	C	irregular	R4	17
67	RMLO	acceptable	Malignant	1	C	irregular	R5	22
68	RCC	acceptable	Malignant	1	A	Spiculated	R5	27
69	RCC	acceptable	Malignant	1	C	Spiculated	R4	15
70	RMLO	acceptable	Malignant	1	B	Spiculated	R4	6
71	LMLO	acceptable	Malignant	1	C	irregular	R4	15
72	LCC	acceptable	Malignant	1	D	irregular	R4	10
73	RCC	acceptable	Malignant	1	B	irregular	R4	10
74	RMLO	acceptable	Malignant	1	B	irregular	R5	17
75	LMLO	acceptable	Malignant	1	D	irregular	R5	13.5
76	LCC	acceptable	Malignant	1	C	Spiculated	R4	17
77	RMLO	acceptable	Malignant	1	B	irregular	R4	9
78	RCC	acceptable	Malignant	1	C	irregular	R5	16
79	LMLO	acceptable	Malignant	1	C	Spiculated	R5	12
80	LCC	acceptable	Malignant	1	A	irregular	R4	8

Table (G-5) Demonstrates the features of mammographic images (Projection of image, breast density, and number of lesions per image), and the characteristics of malignant breast masses with different shape of margin, lesions' BI-RADS and size of lesions are presented.

Image No.	Projection of image	sharpness	Type of lesion	lesions per image	Breast density	Shape of margin	Lesion BIRADS	Lesion Size in mm
81	RCC	acceptable	Malignant	1	C	irregular	R4	8
82	LCC	acceptable	Malignant	1	B	Spiculated	R4	9
83	LCC	acceptable	Malignant	1	B	irregular	R5	15
84	RCC	acceptable	Malignant	1	D	irregular	R4	22
85	LCC	acceptable	Malignant	1	C	irregular	R5	13
86	RCC	acceptable	Malignant	1	C	Spiculated	R5	10
87	LCC	acceptable	Malignant	1	B	Spiculated	R5	18
88	LCC	acceptable	Malignant	1	B	Lobulated	R4	10
89	LCC	acceptable	Malignant	1	A	irregular	R4	9
90	RCC	acceptable	Malignant	1	C	Spiculated	R5	11
91	RMLO	acceptable	Malignant	1	C	irregular	R4	17
92	RMLO	acceptable	Malignant	1	D	irregular	R4	10
93	RCC	acceptable	Malignant	1	B	irregular	R4	9
94	LCC	acceptable	Malignant	1	D	Spiculated	R5	23
95	RCC	acceptable	Malignant	1	D	Spiculated	R5	21
96	LMLO	acceptable	Malignant	1	D	irregular	R4	15
97	LCC	acceptable	Malignant	1	B	Spiculated	R5	16
98	LMLO	acceptable	Malignant	1	D	irregular	R4	12.5
99	RCC	acceptable	Malignant	1	B	irregular	R4	27
100	RCC	acceptable	Malignant	1	B	Spiculated	R4	13
101	RMLO	acceptable	Malignant	1	C	Spiculated	R4	20

Table (G-6) Demonstrates the features of mammographic images (Projection of image, breast density, and number of lesions per image), and the characteristics of malignant breast microcalcifications with different shape, distribution, lesions' BI-RADS and size of lesions are presented.

Image No.	Projection of image	Sharpness	Type of lesion	lesion per image	Breast density	Calci. Distribution	Lesion BI-RADS	Lesion size in mm
1	LMLO	acceptable	Malignant	1	B	Clustered	R4	5
2	RCC	acceptable	Malignant	1	B	Clustered	R4	8
3	RCC	acceptable	Malignant	1	D	Clustered	R5	7
4	RCC	acceptable	Malignant	3	D	Clustered	R3	Whole group=9.6
5	LMLO	acceptable	Malignant	2	C	Clustered	R5	30&13
6	RCC	acceptable	Malignant	1	B	Clustered	R5	12
7	RCC	acceptable	Malignant	1	C	Clustered	R5	10
8	RCC	acceptable	Malignant	2	C	Clustered	R5	16&11
9	RMLO	acceptable	Malignant	1	B	Clustered	R3	10
10	RMLO	acceptable	Malignant	1	C	Clustered	R5	17.5
11	LCC	acceptable	Malignant	1	B	Clustered	R3	6
12	RCC	acceptable	Malignant	1	C	Clustered	R4	9
13	LCC	acceptable	Malignant	1	C	Clustered	R4	7.5
14	RCC	acceptable	Malignant	1	C	Clustered	R4	7
15	RCC	acceptable	Malignant	2	D	Clustered	R5	26&26
16	LMLO	acceptable	Malignant	2	D	Clustered	R5	27&9
17	LMLO	acceptable	Malignant	1	D	Clustered	R3	12.5
18	RCC	acceptable	Malignant	1	B	Clustered	R4	11.6
19	RCC	acceptable	Malignant	1	B	Clustered	R4	5.4
20	RMLO	acceptable	Malignant	1	B	Clustered	R4	10

Table (G-7) Demonstrates the features of mammographic images (Projection of image, breast density, and number of lesions per image), and the characteristics of malignant breast microcalcifications with different shape, distribution, lesions' BI-RADS and size of lesions are presented.

Image No.	Projection of image	Sharpness	Type of lesion	lesion per image	Breast density	Calci. Distribution	Lesion BI-RADS	Lesion size in mm
21	LMLO	acceptable	Malignant	1	C	Clustered	R5	22
22	LCC	acceptable	Malignant	1	C	Clustered	R4	13
23	RMLO	acceptable	Malignant	1	B	Clustered	R4	15
24	LMLO	acceptable	Malignant	1	B	Clustered	R5	9
25	RCC	acceptable	Malignant	1	B	Clustered	R4	13.7
26	RCC	acceptable	Malignant	3	C	Clustered	R4	10
27	LMLO	acceptable	Malignant	2	B	Clustered	R5	5
28	LMLO	acceptable	Malignant	1	B	Clustered	R4	12
29	LCC	acceptable	Malignant	1	B	Clustered	R4	15
30	RCC	acceptable	Malignant	1	C	Clustered	R4	6
31	RCC	acceptable	Malignant	1	B	Clustered	R3	8
32	RMLO	acceptable	Malignant	1	C	Clustered	R4	18
33	RCC	acceptable	Malignant	1	D	Clustered	R5	7
34	RCC	acceptable	Malignant	1	B	Clustered	R4	7
35	LMLO	acceptable	Malignant	2	C	Clustered	R3	12, 5
36	RCC	acceptable	Malignant	1	B	Clustered	R5	12
37	RMLO	acceptable	Malignant	1	C	Clustered	R4	15.6
38	RCC	acceptable	Malignant	1	B	Clustered	R3	6.5
39	LMLO	acceptable	Malignant	1	C	Clustered	R4	19
40	RCC	acceptable	Malignant	1	B	Clustered	R5	8

Table (G-8) Demonstrates the features of mammographic images (Projection of image, breast density, and number of lesions per image), and the characteristics of malignant breast microcalcifications with different shape, distribution, lesions' BI-RADS and size of lesions are presented.

Image No.	Projection of image	Sharpness	Type of lesion	lesion per image	Breast density	Calci. Distribution	Lesion BI-RADS	Lesion size in mm
41	LMLO	acceptable	Malignant	1	D	Clustered	R5	16
42	LCC	acceptable	Malignant	1	D	Clustered	R4	6
43	RCC	acceptable	Malignant	1	C	Clustered	R4	24
44	LCC	acceptable	Malignant	1	D	Clustered	R4	8
45	RCC	acceptable	Malignant	3	D	Clustered	R3,R3,R4	7.5,5.5,14
46	LCC	acceptable	Malignant	2	B	Clustered	R4,R5	10.5,25
47	RCC	acceptable	Malignant	1	C	Clustered	R5	20
48	RCC	acceptable	Malignant	2	C	Clustered	R5,R4	6, 6
49	RCC	acceptable	Malignant	1	D	Clustered	R3	6
50	LCC	acceptable	Malignant	1	B	Clustered	R4	11
51	RCC	acceptable	Malignant	1	B	Clustered	R5	14
52	LCC	acceptable	Malignant	1	C	Clustered	R3	5
53	RCC	acceptable	Malignant	1	D	Clustered	R4	14
54	LCC	acceptable	Malignant	1	C	Clustered	R3	6.4
55	RMLO	acceptable	Malignant	2	B	Clustered	R4	13
56	LCC	acceptable	Malignant	1	B	Clustered	R4	18
57	RCC	acceptable	Malignant	1	D	Clustered	R4	18
58	LMLO	acceptable	Malignant	1	B	Clustered	R4	12.5
59	LMLO	acceptable	Malignant	1	D	Clustered	R4	15
60	RCC	acceptable	Malignant	1	C	Clustered	R4	12
61	RCC	acceptable	Malignant	1	C	Clustered	R4	14
62	LCC	acceptable	Malignant	1	C	Clustered	R4	11

Appendix H: ROCView Instructions

University of Salford MANCHESTER

The Impact of Motion blur on Lesion Detection Performance in FFDM

ROCView Instructions to implement Free-response study

Overview

University of Salford MANCHESTER

- Observer performance assessment
  - Short training to show the difference between mammographic report and FROC study
  - Free-response receiver operating characteristic (FROC) method
  - To localise any areas of the image that you think are suspicious of malignancy
  - Rate your suspicion of malignancy using a confidence scale

The purpose of the study

University of Salford MANCHESTER

- Determine the impact of image blurring on lesion detection performance in FFDM using FROC method.
- We will make a comparison for the detection performance and confidence level of the observer before and after applying image blurring

Training to use ROCView:

University of Salford MANCHESTER

- Short training to show how ROCView software works at the first visit.
- To demonstrate the difference between the mammographic report and the FROC study
- Only one view **CC** or **MLO** decision to be made on this images
- Each abnormal images contains 1 or more lesions
- This will allow you to:

  1. Localize up to 9 areas suspicious for malignancy
  2. Provide a rating (likelihood of malignancy) using a confidence scale

- A training dataset of 5 normal cases, 5 containing masses and 5 containing microcalcifications will be used to familiarize yourself with the task

The Images

University of Salford MANCHESTER

For each evaluation you will search for:

- Malignant Masses
- Malignant Microcalcifications

- Each data set contains 124 cases, 50:50 normal/abnormal

- Each case is a single image, either CC or MLO

How will we do this?

University of Salford MANCHESTER

- The research is to evaluate the impact on lesion detection performance on different amounts of image blurring.

1. Reviewing a set of FFDM images that are very blurred 1.5 mm motion blur
2. Reviewing a set of FFDM images that are not blurred 0.0 mm motion blur
3. Reviewing a set of images that are slightly blurred 0.7 mm motion blur

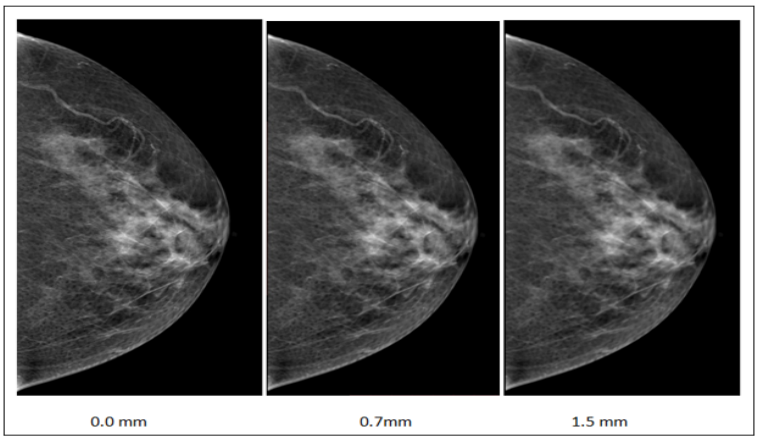

Figure demonstrate an example of FFDM images with and without simulated blur imposed.

ROCView

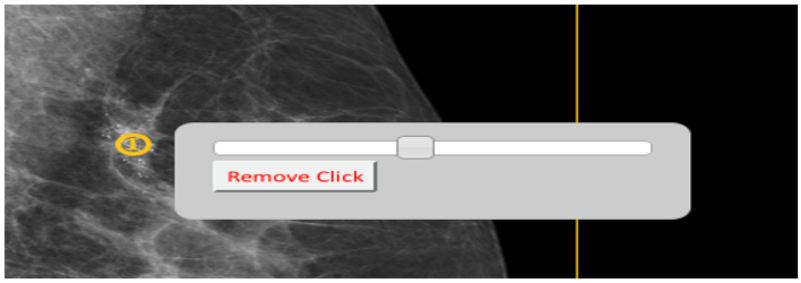

Figure demonstrate the confidence scale variant. A mouse click prompts the slider bar to appear. The slider starts at the left side of the bar (score 1.0/low confidence) and can be moved to any point along it to a maximum of 10.0 (high confidence)

Appendix I:

Table (I-1) **The results of observation session for one observer represent true positive cases (images contain malignant masses without image blurring).**

Reader _ID	Modality _ID	Case _ID	Lesion _ID	TP _rating
2	0	1	1	5
2	0	2	1	10
2	0	4	1	9
2	0	5	1	10
2	0	6	1	8
2	0	7	1	7
2	0	8	1	10
2	0	9	1	5
2	0	10	1	9
2	0	11	1	3
2	0	12	1	9
2	0	13	1	9
2	0	14	1	9
2	0	15	1	9
2	0	16	1	10
2	0	17	1	3
2	0	18	1	5
2	0	19	1	9
2	0	20	1	7
2	0	21	1	9
2	0	22	1	7
2	0	23	1	7
2	0	24	1	10
2	0	25	1	9
2	0	26	1	4
2	0	27	1	4
2	0	28	1	4
2	0	30	1	7
2	0	31	1	9
2	0	32	1	9
2	0	33	1	10
2	0	34	1	5
2	0	35	1	10
2	0	36	1	4
2	0	37	1	8
2	0	38	1	8
2	0	39	1	5
2	0	41	1	7
2	0	42	1	10
2	0	43	1	9
2	0	44	1	6
2	0	45	1	6

2	0	46	1	4
2	0	47	1	9
2	0	48	1	2
2	0	49	1	4
2	0	51	1	9
2	0	52	1	9
2	0	53	1	9
2	0	54	1	6
2	0	55	1	9
2	0	56	1	7
2	0	57	1	7
2	0	58	1	6
2	0	59	1	6
2	0	60	1	2
2	0	61	1	9
2	0	62	1	4

Table (I-2) **The results of observation session for one observer represent true positive cases (images contain malignant masses with image blurring 0.7 mm).**

Reader _ID	Modality _ID	Case _ID	Lesion _ID	TP _rating
2	0.7	1	1	5
2	0.7	2	1	4
2	0.7	4	1	6
2	0.7	5	1	6
2	0.7	6	1	7
2	0.7	7	1	7
2	0.7	8	1	4
2	0.7	9	1	3
2	0.7	12	1	8
2	0.7	13	1	7
2	0.7	14	1	2
2	0.7	15	1	8
2	0.7	16	1	8
2	0.7	17	1	4
2	0.7	18	1	4
2	0.7	19	1	8
2	0.7	20	1	7
2	0.7	21	1	6
2	0.7	22	1	4
2	0.7	23	1	7
2	0.7	24	1	9
2	0.7	25	1	6
2	0.7	26	1	5
2	0.7	27	1	4
2	0.7	30	1	1
2	0.7	31	1	6
2	0.7	32	1	9
2	0.7	33	1	6
2	0.7	35	1	8
2	0.7	36	1	6
2	0.7	37	1	5
2	0.7	38	1	3
2	0.7	39	1	6
2	0.7	41	1	5
2	0.7	42	1	6

2	0.7	43	1	6
2	0.7	45	1	3
2	0.7	46	1	4
2	0.7	47	1	6
2	0.7	48	1	2
2	0.7	49	1	6
2	0.7	50	1	3
2	0.7	51	1	5
2	0.7	52	1	6
2	0.7	53	1	6
2	0.7	54	1	2
2	0.7	55	1	5
2	0.7	56	1	5
2	0.7	57	1	6
2	0.7	58	1	2
2	0.7	59	1	3
2	0.7	60	1	4
2	0.7	61	1	6
2	0.7	62	1	4

Table (I-3) The results of observation session for one observer represent true **positive cases (images contain malignant masses with image blurring 1.5 mm).**

Reader _ID	Modality _ID	Case _ID	Lesion _ID	TP _rating
2	1.5	1	1	7
2	1.5	2	1	6
2	1.5	4	1	6
2	1.5	5	1	5
2	1.5	6	1	2
2	1.5	7	1	7
2	1.5	8	1	8
2	1.5	10	1	7
2	1.5	11	1	2
2	1.5	12	1	6
2	1.5	13	1	7
2	1.5	14	1	5
2	1.5	15	1	8
2	1.5	16	1	7
2	1.5	17	1	2
2	1.5	18	1	5
2	1.5	19	1	7
2	1.5	20	1	4
2	1.5	21	1	8
2	1.5	22	1	5
2	1.5	23	1	6
2	1.5	24	1	8
2	1.5	25	1	8
2	1.5	26	1	6
2	1.5	27	1	2
2	1.5	31	1	5
2	1.5	32	1	8
2	1.5	33	1	8
2	1.5	35	1	6
2	1.5	36	1	3
2	1.5	37	1	5
2	1.5	38	1	4
2	1.5	39	1	4
2	1.5	41	1	2
2	1.5	42	1	8
2	1.5	43	1	7
2	1.5	44	1	2
2	1.5	46	1	6
2	1.5	47	1	5
2	1.5	49	1	7
2	1.5	50	1	2
2	1.5	51	1	6

2	1.5	52	1	7
2	1.5	53	1	3
2	1.5	54	1	5
2	1.5	56	1	3
2	1.5	57	1	2
2	1.5	58	1	5
2	1.5	60	1	3
2	1.5	61	1	6
2	1.5	62	1	5

Table (I-4) The results of observation session for one observer represent false positive cases (images contain malignant masses with image blurring).

Reader _ID	Modality _ID	Case _ID	FP _rating
2	0	1	4
2	0	3	7
2	0	3	8
2	0	8	4
2	0	16	4
2	0	22	4
2	0	27	4
2	0	28	5
2	0	33	3
2	0	40	4
2	0	44	6
2	0	54	2
2	0	58	5
2	0	59	4
2	0	74	2
2	0	77	7
2	0	86	4
2	0	99	3
2	0	100	4
2	0	109	4
2	0	111	2
2	0	116	6
2	0	119	4
2	0.7	3	1
2	0.7	8	3
2	0.7	10	9
2	0.7	11	4
2	0.7	22	5
2	0.7	28	2
2	0.7	40	1
2	0.7	40	2
2	0.7	44	1
2	0.7	54	2
2	0.7	58	1
2	0.7	59	4
2	0.7	64	1
2	0.7	66	1
2	0.7	67	1
2	0.7	72	1

2	0.7	74	1
2	0.7	77	5
2	0.7	79	1
2	0.7	80	1
2	0.7	82	2
2	0.7	86	3
2	0.7	88	1
2	0.7	89	1
2	0.7	94	1
2	0.7	94	2
2	0.7	99	4
2	0.7	100	3
2	0.7	102	2
2	0.7	104	2
2	0.7	106	1
2	0.7	106	1
2	0.7	110	1
2	0.7	111	4
2	0.7	116	5
2	0.7	119	5
2	0.7	121	1
2	1.5	8	2
2	1.5	22	2
2	1.5	27	4
2	1.5	28	2
2	1.5	40	4
2	1.5	58	2
2	1.5	59	5
2	1.5	74	2
2	1.5	86	3
2	1.5	89	2
2	1.5	97	4
2	1.5	100	3
2	1.5	104	3
2	1.5	108	3
2	1.5	111	3
2	1.5	116	4

Appendix J: The Results of Combined Two Observers Data

Table M-1 Demonstrates the FOMs of the 21 pairs of combining two observers' data for three levels of motion blur for microcalcification cases.

Observers pairs	FOMs for three levels motion blur		
	0.0 mm	0.7 mm	1.5 mm
1	0.944	0.860	0.853
2	0.923	0.850	0.796
3	0.908	0.860	0.781
4	0.936	0.884	0.811
5	0.947	0.898	0.8487
6	0.901	0.853	0.730
7	0.946	0.857	0.888
8	0.914	0.892	0.855
9	0.947	0.882	0.871
10	0.950	0.874	0.882
11	0.896	0.869	0.815
12	0.907	0.923	0.792
13	0.948	0.878	0.859
14	0.942	0.886	0.846
15	0.923	0.870	0.763
16	0.907	0.901	0.855
17	0.903	0.867	0.837
18	0.887	0.877	0.800
19	0.950	0.902	0.847
20	0.916	0.872	0.818
21	0.909	0.893	0.799
Average across Observers	0.923	0.876	0.826

Table M-2 Demonstrates the FOMs of the 21 pairs of the observers for three levels of motion blur for masses.

Observers pairs	FOMs for three levels of motion blur		
	0.0 mm	0.7 mm	1.5 mm
1	0.958	0.905	0.917
2	0.906	0.880	0.836
3	0.958	0.912	0.918
4	0.966	0.940	0.923
5	0.957	0.934	0.907
6	0.941	0.870	0.836
7	0.929	0.926	0.959
8	0.962	0.928	0.962
9	0.971	0.925	0.939
10	0.951	0.938	0.940
11	0.948	0.890	0.866
12	0.941	0.905	0.944
13	0.951	0.950	0.948
14	0.934	0.933	0.923
15	0.931	0.881	0.882
16	0.974	0.947	0.920
17	0.958	0.897	0.959
18	0.920	0.905	0.877
19	0.965	0.931	0.949
20	0.960	0.862	0.905
21	0.938	0.928	0.907
Average across Observers	0.948	0.913	0.915

Appendix K: Conspicuity Index

Table: Measurement of conspicuity index of breast masses within mammographic images using conspicuity software. The physical parameters includes the maximum lesion diameter, the θ represents is the maximum slope angle to the edge of the lesion profile in degrees, σ_s = mean noise within the lesion, σ_n= mean background noise and SNR of lesions.

Blur Level mm	Conspicuity Index	d (max diameter)	θ (degrees)	ΔGL	σ (l)	σ (b)	μ Lesion	μ Background
	Case 1							
0.0	51.631	24.450	63.765	88.903	42.734	69.744	192.939	104.036
0.7	66.389	18.589	61.030	93.344	21.061	40.134	194.894	101.550
1.5	74.993	17.133	59.797	93.600	16.109	31.417	194.417	100.817
	Case 2							
0.0	71.577	42.183	69.151	69.483	60.864	82.009	178.011	108.528
0.7	101.672	39.644	67.259	70.189	34.217	51.973	178.272	108.083
1.5	110.622	38.578	66.415	69.886	27.714	45.491	178.044	108.158
	Case 3							
0.0	45.003	24.917	66.945	76.644	51.102	80.162	184.039	107.394
0.7	55.621	18.911	64.153	79.006	22.724	47.957	185.694	106.689
1.5	58.383	16.928	62.927	79.353	15.307	40.332	185.950	106.597
	Case 4							
0.0	108.879	44.567	73.240	84.333	73.301	79.006	174.361	90.028
0.7	153.361	43.294	72.357	84.797	46.650	53.463	174.311	89.514
1.5	169.432	42.367	71.568	84.600	38.306	46.135	174.033	89.433
	Case 5							
0.0	66.273	48.606	70.833	66.464	96.237	91.397	166.844	100.381
0.7	78.105	45.194	67.952	67.706	67.191	62.960	167.272	99.567
1.5	81.129	43.583	66.377	68.269	58.253	54.862	167.417	99.147
	Case 6							
0.0	40.113	32.456	65.036	59.036	56.479	80.202	172.139	113.103
0.7	43.759	20.461	58.806	63.083	16.520	43.842	175.272	112.189
1.5	47.462	19.394	57.771	63.042	12.358	37.331	175.161	112.119

Blur Level mm	Conspicuity Index	d (max diameter)	θ (degrees)	ΔGL	σ (l)	σ (b)	μ Lesion	μ Background
	Case 7							
0.0	170.73	51.667	70.653	133.19	69.05	83.929	206.483	73.29
0.7	252.59	51.306	70.526	133.54	50.13	52.581	206.556	73.01
1.5	272.5	50.544	70.256	133.61	45.48	47.03	206.622	73.00
	Case 8							
0.0	140.63	40.339	72.605	96.358	54.27	62.947	161.567	65.20
0.7	222.31	38.761	71.959	96.797	28.2	39.953	161.783	64.98
1.5	238.35	37.289	71.290	96.836	23.71	35.017	161.806	64.96
	Case 9							
0.0	113.44	36.4	72.974	99.35	63.11	74.922	186.967	87.61
0.7	150.18	34.85	71.939	99.558	41.68	52.282	186.678	87.11
1.5	162.84	34.039	71.200	98.869	34.17	46.13	185.956	87.08
	Case 10							
0.0	124.98	66.322	71.213	108.73	84.55	136.28	188.722	79.9
0.7	169.81	64.222	70.483	109.86	43.24	102.26	189.556	79.69
1.5	181.56	63.439	70.149	109.91	36.41	94.026	189.6	79.69
	Case 11							
0.0	116.22	31.567	73.520	115.36	65.99	74.468	179.561	64.2
0.7	155.95	30.883	72.929	114.86	44.59	53.584	178.733	63.87
1.5	168.74	30.144	72.239	114.26	36.81	47.5	177.933	63.6
	Case 12							
0.0	82.89	24.728	69.508	107.98	57.51	58.192	155.578	47.60
0.7	117.32	23.311	68.925	108.1	29.77	43.803	155.344	47.24
1.5	127.94	22.811	68.526	107.41	24.9	39.023	154.589	47.18
	Case 13							
0.0	123.43	46.761	71.087	86.517	62.41	65.514	171.939	85.42
0.7	179.01	44.483	69.64	87.256	38.04	40.341	172.022	84.76
1.5	192.82	43.056	68.755	87.494	33.39	34.163	171.972	84.47
	Case 14							
0.0	127.07	47.378	69.536	127.66	58.45	106.01	202.578	74.916
0.7	166.60	45.644	69.144	128.66	34.55	80.8	203.35	74.69
1.5	178.28	44.361	68.758	128.76	27.53	73.348	203.506	74.74
	Case 15							
0	212.32	8.11	87.472	89.713	6.6268	55.20	252.00	162.29
0.7	229.83	7.055	86.018	87.172	5.8137	30.145	250.90	163.73
1.5	211.05	6.577	84.963	84.161	5.8231	24.110	247.86	163.7

	Case 16							
0	145.51	4.694	87.822	70.497	26.845	30.94	218.9	148.40
0.7	165.40	4.105	85.892	53.644	8.6917	12.09	205.17	151.52
1.5	116.77	3.711	83.104	40.697	4.7621	8.018	192.83	152.1
	Case 17							
0	239.96	4.1	88.336	133.43	17.60	45.73	239.56	106.13
0.7	221.32	2.85	87.149	113.26	8.718	19.83	222.47	109.20
1.5	198.75	2.838	86.088	90.783	6.846	13.44	200.50	109.72
	Case 18							
0	246.51	21.916	86.026	129.00	107.6	76.10	229.96	100.9
0.7	344.10	22.361	84.444	140.12	63.27	47.69	229.87	89.75
1.5	351.86	22.438	83.122	143.65	56.6	34.25	226.48	82.836
	Case 19							
0	542.70	9.383	88.400	133.98	29.39	41.71	242.04	108.06
0.7	553.27	8.533	87.386	128.25	17.49	25.98	237.85	109.6
1.5	451.24	7.205	86.277	121.58	12.44	19.93	231.17	109.58
	Case 20							
0	199.30	5.53	87.823	94	14.73	44.65	233.1	139.1
0.7	191.61	4.677	86.252	80.68	8.919	21.97	220.51	139.83
1.5	131.28	3.366	83.692	71.23	4.024	13.66	209.28	138.04
	Case 21							
0	124.32	5.1	87.425	90.563	32.9	49.50	217.84	127.28
0.7	128.06	3.35	85.811	84.266	10.14	22.09	213.58	129.316
1.5	116.57	3.233	84.238	70.694	6.947	15.00	200.4	129.70
	Case 22							
0	466.85	11.866	88.764	121.24	52.78	58.70	234.53	113.34
0.7	552.188	10.72	87.862	119.13	24.32	34.48	234.42	115.28
1.5	472.39	9.6	86.963	112.48	17.95	26.96	229.25	116.77
	Case 23							
0	192.33	4.255	88.092	112.89	15.30	46.7	222.43	109.53
0.7	162.39	3.35	86.562	89.40	9.191	21.91	200.35	110.9
1.5	91.292	3.616	82.005	68.65	8.410	14.98	180.15	111.5

Appendix M: Dispersion Index Tables

Table 7 The physical measures of the microcalcification in image without blurring

	Area1	Mean 1	StdDev 1	Min1	Max1	Calc. NO.	D.I	contras t	DI x Con	SNR	Detect-ability
1	13.7	2610	62	2457	2933	11	0.801	0.890	0.713	41.94	1.00
2	23.5	2968	90	2702	3361	25	1.062	0.883	0.937	33.10	1.00
3	34.8	2965	93	2683	3361	29	0.832	0.882	0.734	31.98	1.00
4	40.4	2673	105	2381	3145	13	0.322	0.850	0.273	25.42	0.57
5	315.3	2889	170	2511	4095	61	0.193	0.705	0.274	16.99	1.00
5	58.7	2898	164	2520	3544	9	0.153	0.818	0.188	17.62	0.57
6	28.8	2704	101	2503	3298	24	0.834	0.820	0.684	26.73	1.00
7	13.9	2571	85	2361	2943	12	0.863	0.874	0.754	30.42	1.00
8	61.6	2520	111	2247	3017	15	0.243	0.835	0.291	22.64	0.86
8	79.2	2803	115	2335	3379	22	0.278	0.829	0.335	24.36	1.00
9	13.9	2571	85	2361	2943	9	0.648	0.874	0.566	30.42	1.00
10	66.7	2603	81	2368	3000	30	0.449	0.868	0.390	32.06	0.85
11	11.9	2787	108	2556	3236	9	0.755	0.861	0.651	25.83	1.00
12	18.2	2760	91	2572	3300	30	1.644	0.836	1.375	30.50	1.00
13	24.1	2765	140	2540	3385	25	1.039	0.817	0.849	19.74	1.00
14	3.9	2706	75	2549	3000	9	2.311	0.902	2.084	36.04	1.00
15	376.7	2809	161	2361	3722	27	0.072	0.755	0.095	17.48	0.57
16	159.3	2897	168	2278	3760	18	0.113	0.770	0.147	17.20	0.43
17	46.2	2720	143	2393	3342	9	0.195	0.814	0.158	19.09	1.00
18	21.2	2676	102	2453	3197	11	0.519	0.837	0.434	26.14	1.00
19	8.9	2906	109	2740	3433	10	1.123	0.847	0.951	26.72	0.72
20	15.2	2944	126	2732	3608	8	0.527	0.816	0.430	23.45	1.00
21	98.4	2613	136	2257	3528	60	0.610	0.741	0.452	19.16	1.00
22	15.2	2944	126	2732	3608	9	0.593	0.816	0.484	23.45	1.00
24	6.7	2624	87	2409	3085	10	1.498	0.851	1.274	30.09	1.00
25	32.5	2179	90	1911	2664	10	0.308	0.818	0.252	24.27	1.00
27	45.6	2393	81	2203	2740	23	0.504	0.873	0.441	29.44	1.00
28	7.6	2710	89	2515	3086	15	1.979	0.878	1.739	30.42	1.00
29	61.9	2670	91	2418	3037	13	0.210	0.879	0.185	29.41	1.00
30	11.1	2875	127	2595	3536	20	1.807	0.813	1.469	22.56	1.00
31	19.7	2663	63	2527	3008	8	0.407	0.885	0.360	42.16	1.00
32	63.9	2626	87	2397	3108	22	0.344	0.845	0.408	30.25	0.72
32	15.4	2654	67	2465	2915	5	0.325	0.910	0.357	39.52	1.00
33	13.9	2912	122	2646	3398	16	1.154	0.857	0.989	23.80	1.00
34	12.7	2857	66	2650	3113	8	0.629	0.918	0.578	43.32	1.00
35	23.8	2427	62	2256	2689	17	0.713	0.903	0.790	39.17	1.00
35	9.8	2539	68	2375	2835	9	0.914	0.896	1.021	37.35	0.72

36	37.1	2849	116	2411	3328	20	0.539	0.856	0.461	24.55	0.86
37	5.0	2744	96	2527	3128	8	1.596	0.877	1.401	28.57	1.00
38	14.1	2660	79	2490	3040	10	0.709	0.875	0.810	33.86	1.00
39	136.5	2276	143	1950	2881	42	0.308	0.790	0.390	15.87	0.86
40	29.5	2584	77	2408	2946	22	0.746	0.877	0.850	33.42	0.00
41	69.3	2579	121	2312	3314	40	0.577	0.778	0.449	21.30	1.00
42	12.4	2840	93	2659	3246	29	2.336	0.875	2.044	30.62	1.00
44	28.8	2719	90	2485	3200	20	0.695	0.850	0.591	30.13	1.00
45	22.2	2686	96	2465	3114	7	0.316	0.863	0.366	28.02	0.86
45	25.2	2738	73	2500	3099	9	0.357	0.883	0.404	37.72	0.72
46	92.1	2737	112	2447	3207	48	0.521	0.853	0.611	24.45	0.86
46	155.2	2545	116	2312	3104	35	0.225	0.820	0.275	21.93	0.72
47	201.2	2518	142	2194	3232	25	0.124	0.779	0.159	17.68	0.86
48	24.9	2728	85	2344	3223	35	1.404	0.847	1.659	32.14	1.00
48	9.2	2595	85	2425	3072	8	0.874	0.845	1.035	30.50	1.00
49	2.7	2612	61	2485	2799	8	3.002	0.933	2.801	42.56	1.00
50	19.2	2985	98	2719	3391	20	1.043	0.880	0.919	30.47	1.00
51	34.1	2889	109	2577	3340	13	0.382	0.865	0.330	26.42	0.57
52	9.5	2628	141	2369	3237	21	2.207	0.812	1.792	18.59	1.00
53	33.1	2349	117	2017	2770	18	0.544	0.848	0.462	20.02	0.86
54	13.6	2834	91	2596	3242	28	2.064	0.874	1.805	31.03	1.00
55	59.1	2472	65	2305	2914	15	0.254	0.848	0.215	38.22	1.00
56	83.9	2701	120	2431	3190	43	0.513	0.847	0.434	22.60	1.00
57	135.3	2637	211	2252	3686	54	0.399	0.715	0.286	12.50	0.00
58	55.1	2453	124	2267	3061	18	0.327	0.802	0.262	19.82	1.00
59	361.5	2319	172	1845	3269	60	0.166	0.709	0.118	13.46	0.72
60	20.5	2102	271	1775	3114	26	1.266	0.675	0.854	7.74	0.86
61	90.5	2532	119	2225	3154	32	0.354	0.803	0.284	21.33	1.00
62	115.7	2616	72	2366	2927	50	0.432	0.894	0.386	36.54	1.00

Table 7.7: The physical and clinical measures of the microcalcification cases in image with 0.7mm level of simulated blurring

	Area1	Mean1	StdDev1	Min1	Max1	Calc. NO.	DI	contrast	DI x Con	SNR	Detect-ability
1	13.731	2607	39.558	2544	2774	11	0.80	0.94	0.75	65.90	1.00
2	23.55	2966	73.434	2766	3191	25	1.06	0.93	0.99	40.39	1.00
3	34.85	2964	77.104	2758	3191	29	0.83	0.93	0.77	38.44	0.86
4	40.41	2672	93.39	2420	2870	13	0.32	0.93	0.30	28.61	0.43
5	315.28	2888	156.028	2576	3928	61	0.19	0.74	0.26	18.51	1.00
5	58.66	2896	153.375	2589	3343	9	0.15	0.87	0.18	18.88	0.43
6	28.77	2702	73.459	2568	2996	24	0.83	0.90	0.75	36.78	1.00
7	13.90	2569	71.498	2405	2733	12	0.86	0.94	0.81	35.93	1.00
8	61.63	2519	102.512	2298	2887	15	0.24	0.87	0.28	24.58	0.57
8	79.18	2801	105.569	2375	3056	22	0.28	0.92	0.30	26.54	0.86
9	13.90	2569	71.498	2405	2733	9	0.65	0.94	0.61	35.93	0.85
10	66.74	2602	67.821	2419	2835	30	0.45	0.92	0.41	38.37	0.72
11	11.92	2781	77.574	2617	2999	9	0.76	0.93	0.70	35.85	0.57
12	18.25	2757	60.373	2657	3028	30	1.64	0.91	1.50	45.66	1.00
13	24.06	2760	105.626	2598	3152	25	1.04	0.88	0.91	26.13	0.57
14	3.90	2702	43.168	2600	2838	9	2.31	0.95	2.20	62.58	0.43
15	376.66	2808	154.694	2407	3304	27	0.07	0.85	0.08	18.15	0.14
16	159.29	2896	163.738	2317	3579	18	0.11	0.81	0.14	17.69	0.29
17	46.24	2718	133.598	2463	3078	9	0.19	0.88	0.17	20.35	0.43
18	21.21	2674	91.463	2497	2958	11	0.52	0.90	0.47	29.24	0.43
19	8.91	2892	66.389	2765	3136	10	1.12	0.92	1.04	43.56	0.43
20	15.18	2941	88.99	2775	3297	8	0.53	0.89	0.47	33.04	1.00
21	98.37	2612	119.705	2315	3180	60	0.61	0.82	0.50	21.82	1.00
22	15.18	2941	88.99	2775	3297	9	0.59	0.89	0.53	33.04	0.72
24	6.68	2620	60.679	2479	2818	10	1.50	0.93	1.39	43.18	1.00
25	32.46	2178	80.464	1971	2439	10	0.31	0.89	0.28	27.07	0.14
27	7.58	2705	51.628	2592	2862	15	1.98	0.95	1.87	52.39	1.00
28	45.60	2392	72.971	2244	2581	23	0.50	0.93	0.47	32.79	0.29
29	61.94	2669	80.685	2464	2894	13	0.21	0.92	0.19	33.08	0.86
30	11.07	2871	93.864	2669	3195	20	1.81	0.90	1.62	30.59	1.00
31	19.66	2661	45.362	2574	2885	8	0.41	0.92	0.38	58.66	0.72
32	15.37	2651	52.472	2517	2794	5	0.33	0.95	0.34	50.53	0.43
33	13.86	2907	87.203	2710	3185	16	1.15	0.91	1.05	33.34	1.00
34	12.71	2855	48.317	2736	2977	8	0.63	0.96	0.60	59.09	1.00
35	23.83	2426	48.466	2286	2566	17	0.71	0.95	0.75	50.05	0.43
35	9.85	2537	50.029	2420	2667	9	0.91	0.95	0.96	50.70	0.14
36	37.12	2847	103.645	2465	3176	20	0.54	0.90	0.48	27.47	1.00
37	5.01	2736	65.585	2565	2932	8	1.60	0.93	1.49	41.71	1.00
38	14.11	2660	60.335	2534	2884	10	0.71	0.92	0.77	44.09	1.00
39	136.47	2275	135.88	1999	2704	42	0.31	0.84	0.37	16.74	0.86
40	29.49	2583	56.726	2448	2805	22	0.75	0.92	0.81	45.53	0.00
41	69.29	2578	98.026	2346	3054	40	0.58	0.84	0.49	26.30	1.00
42	12.41	2837	57.486	2711	3011	29	2.34	0.94	2.20	49.35	1.00
44	28.76	2718	66.485	2539	3005	20	0.70	0.90	0.63	40.87	1.00
45	22.16	2686	81.269	2543	2904	7	0.32	0.92	0.34	33.05	0.57
45	25.21	2737	57.389	2576	2915	9	0.36	0.94	0.38	47.68	0.29
46	92.06	2736	100.833	2499	3059	48	0.52	0.89	0.58	27.13	0.72
46	155.22	2544	108.818	2362	2965	35	0.23	0.86	0.26	23.38	0.29

47	201.23	2517	134.244	2241	3023	25	0.12	0.83	0.15	18.75	1.00
48	24.92	2727	66.746	2388	2966	35	1.40	0.92	1.53	40.85	1.00
48	9.15	2593	59.546	2481	2827	8	0.87	0.92	0.95	43.54	0.86
49	2.67	2609	39.09	2543	2695	8	3.00	0.97	2.91	66.74	0.43
50	19.17	2982	82.713	2774	3226	20	1.04	0.92	0.96	36.05	0.86
51	34.07	2888	99.713	2614	3157	13	0.38	0.91	0.35	28.96	0.14
52	9.52	2621	93.8	2405	2918	21	2.21	0.90	1.98	27.94	0.86
53	33.07	2348	108.941	2060	2635	18	0.54	0.89	0.49	21.55	1.00
54	13.56	2772	410.758	2596	3057	28	2.06	0.91	1.87	6.75	0.86
55	59.05	2470	48.297	2360	2748	15	0.25	0.90	0.23	51.15	1.00
56	83.90	2699	106.534	2485	2996	43	0.51	0.90	0.46	25.34	1.00
57	135.26	2636	199.71	2305	3396	54	0.40	0.78	0.31	13.20	0.00
58	55.11	2452	114.308	2296	2970	18	0.33	0.83	0.27	21.45	1.00
59	361.54	2318	158.994	1916	2921	60	0.17	0.79	0.13	14.58	0.29
60	20.54	2072	319.739	1775	2823	26	1.27	0.73	0.93	6.48	0.72
61	90.48	2531	108.622	2276	2960	32	0.35	0.86	0.30	23.30	0.72
62	115.70	2614	59.432	2413	2814	50	0.43	0.93	0.40	43.99	0.72

Table The physical measures of the microcalcification in image with 1.5mm level of simulated blurring

	Area 1	Mean1	StdDev 1	Min1	Max 1	Calc. NO.	DI	contrast	DI x Con	SNR	Detect-ability
1	13.7	2605	32	2555	2718	11	0.80	0.96	0.77	80.94	0.572
2	23.5	2966	70	2776	3137	25	1.06	0.95	1.00	42.61	0.850
3	34.8	2963	73	2769	3137	29	0.83	0.94	0.79	40.49	0.572
4	40.4	2672	88	2433	2838	13	0.32	0.94	0.30	30.24	0.000
5	315.3	2888	151	2590	3742	61	0.19	0.77	0.25	19.18	1.000
5	58.7	2896	148	2600	3260	9	0.15	0.89	0.17	19.51	0.143
6	28.8	2701	64	2585	2898	24	0.83	0.93	0.78	42.35	1.000
7	13.9	2568	69	2414	2697	12	0.86	0.95	0.82	37.32	1.000
8	61.6	2519	99	2316	2845	15	0.24	0.89	0.27	25.47	0.143
8	79.2	2801	103	2384	2990	22	0.28	0.94	0.30	27.24	0.430
9	13.9	2568	69	2414	2697	9	0.65	0.95	0.62	37.32	0.430
10	66.7	2602	64	2426	2777	30	0.45	0.94	0.42	40.66	0.430
11	11.9	2776	66	2634	2940	9	0.76	0.94	0.71	42.05	0.858
12	18.2	2754	52	2672	2946	30	1.64	0.93	1.54	52.84	1.000
13	24.1	2756	92	2605	3061	25	1.04	0.90	0.94	29.91	0.715
14	3.9	2698	35	2616	2803	9	2.31	0.96	2.22	76.60	0.286
15	376.7	2808	152	2430	3231	27	0.07	0.87	0.08	18.43	0.290
16	159.3	2895	162	2333	3475	18	0.11	0.83	0.14	17.86	0.000
17	46.2	2717	130	2474	2995	9	0.19	0.91	0.18	20.89	0.286
18	21.2	2673	90	2508	2901	11	0.52	0.92	0.48	29.86	0.572
19	8.9	2882	52	2771	3055	10	1.12	0.94	1.06	55.10	0.858
20	15.2	2938	73	2786	3199	8	0.53	0.92	0.48	40.38	1.000
21	98.4	2612	114	2323	3038	60	0.61	0.86	0.52	22.93	1.000
22	15.2	2938	73	2786	3199	9	0.59	0.92	0.54	40.38	0.286
24	6.7	2617	51	2498	2755	10	1.50	0.95	1.42	51.73	0.720
25	32.5	2177	77	1978	2395	10	0.31	0.91	0.28	28.23	0.430
27	7.6	2700	42	2601	2806	15	1.98	0.96	1.90	65.02	1.000
28	45.6	2392	70	2255	2555	23	0.50	0.94	0.47	34.21	0.000
29	61.9	2668	77	2474	2871	13	0.21	0.93	0.20	34.51	0.000
30	11.1	2869	83	2687	3079	20	1.81	0.93	1.68	34.51	0.715
31	19.7	2660	39	2590	2828	8	0.41	0.94	0.38	68.31	0.715
32	63.9	2625	71	2470	2814	22	0.34	0.93	0.37	36.83	0.290
32	15.4	2648	46	2530	2752	5	0.33	0.96	0.34	57.99	1.000
33	13.9	2902	72	2730	3085	16	1.15	0.94	1.09	40.41	1.000
34	12.7	2853	46	2744	2954	8	0.63	0.97	0.61	62.59	0.715
35	23.8	2425	44	2299	2530	17	0.71	0.96	0.74	55.12	0.143
35	9.8	2534	43	2431	2641	9	0.91	0.96	0.95	58.91	0.000

36	37.1	2845	99	2476	3123	20	0.54	0.91	0.49	28.69	0.715
37	5.0	2729	57	2564	2879	8	1.60	0.95	1.51	47.75	1.000
38	14.1	2661	55	2536	2815	10	0.71	0.95	0.75	48.15	0.860
39	136.5	2274	132	2017	2659	42	0.31	0.86	0.36	17.23	0.720
40	29.5	2582	49	2460	2745	22	0.75	0.94	0.79	53.15	0.000
41	69.3	2577	90	2355	2958	40	0.58	0.87	0.50	28.76	1.000
42	12.4	2834	48	2718	2954	29	2.34	0.96	2.24	59.00	1.000
44	28.8	2716	58	2557	2921	20	0.70	0.93	0.65	46.92	0.715
45	22.2	2685	77	2558	2869	7	0.32	0.94	0.34	34.80	0.143
45	25.2	2736	53	2594	2861	9	0.36	0.96	0.37	51.54	0.000
46	92.1	2736	97	2518	3018	48	0.52	0.91	0.58	28.19	0.720
46	155.2	2544	105	2374	2916	35	0.23	0.87	0.26	24.12	0.290
47	201.2	2517	131	2252	2939	25	0.12	0.86	0.15	19.20	0.860
48	24.9	2726	62	2398	2896	35	1.40	0.94	1.49	43.84	0.572
48	9.2	2591	51	2488	2762	8	0.87	0.94	0.93	50.34	0.290
49	2.7	2607	32	2555	2667	8	3.00	0.98	2.93	82.38	0.290
50	19.2	2979	79	2778	3175	20	1.04	0.94	0.98	37.85	0.585
52	9.5	2615	76	2424	2831	21	2.21	0.92	2.04	34.38	1.000
53	33.1	2347	107	2062	2601	18	0.54	0.90	0.49	21.84	0.572
54	13.6	2709	569	2596	2998	28	2.06	0.90	1.87	4.76	0.429
55	59.1	2469	42	2373	2669	15	0.25	0.93	0.24	58.31	1.000
56	83.9	2698	102	2498	2959	43	0.51	0.91	0.47	26.49	0.858
57	135.3	2636	196	2323	3280	54	0.40	0.80	0.32	13.46	0.000
58	55.1	2452	109	2301	2920	18	0.33	0.84	0.27	22.39	0.715
59	361.5	2318	155	1938	2763	60	0.17	0.84	0.14	14.99	0.286
60	20.5	1986	516	1775	2653	26	1.27	0.75	0.95	3.85	0.429
61	90.5	2531	104	2290	2878	32	0.35	0.88	0.31	24.23	1.000
62	115.7	2613	56	2425	2782	50	0.43	0.94	0.41	46.92	0.429

References

Akobeng, A. K. (2007) 'Understanding diagnostic tests 1: sensitivity, specificity and predictive values.', Acta paediatrica, 96(3), pp. 338–341. doi: 10.1111/j.1651-2227.2006.00180.x.

Al-osta, H. E. I. (2010) Detection of Breast Cancer Microcalcifications in Digitized Mammograms. University of Bradford. Available at: https://bradscholars.brad.ac.uk/bitstream/handle/20Al-Osta Thesis.pdf?

Al Mousa, D. S., Ryan, E. A., Mello-Thoms, C. and Brennan, P. C. (2014) 'What effect does mammographic breast density have on lesion detection in digital mammography?', Clinical Radiology. The Royal College of Radiologists, 69(4), pp. 333–341. doi: 10.1016/j.crad.2013.11.014.

Aldrich, B. and Desai, M. (1994) 'Application of Spatial Grey Level Dependence Methods to Digitized Mammograms'.

Ali, R. M., England, A., McEntee, M. F. and Hogg, P. (2015) 'A method for calculating effective lifetime risk of radiation-induced cancer from screening mammography', Radiography. Elsevier Ltd, 21(4), pp. 298–303. doi: 10.1016/j.radi.2015.07.008.

Allec, N., Abbaszadeh, S., Scott, C. C., Lewin, J. M. and Karim, K. S. (2012) 'Including the effect of motion artifacts in noise and performance analysis of dual-energy contrast-enhanced mammography', Physics in Medicine and Biology, 57(24), pp. 8405–8425. doi: 10.1088/0031-9155/57/24/8405.

Alonzo-Proulx, O., Jong, R. A., & Yaffe, M. J. (2012). Volumetric breast density characteristics as determined from digital mammograms. Physics in medicine and biology, 57(1), 7443–7457. doi: 10.1088/0031-9155/57/22/7443

Alonzo-Proulx, O., Packard, N., Boone, J. M., Al-Mayah, A., Brock, K. K., Shen, S. Z., & Yaffe, M. J. (2010). Validation of a method for measuring the volumetric breast density from digital mammograms. Phys Med Biol, 55(11), 3027-3044. doi: 10.1088/0031-9155/55/11/003

American Cancer Society [ACS]. (2011a). Breast cancer facts & figures 2011-2012. Atlanta: American Cancer Society, Inc.

American Cancer Society [ACS]. (2013a). Breast cancer facts & figures 2013-2014. Atlanta.

American Cancer Society [ACS]. (2013b). Mammograms and other breast imaging tests. from http://www.cancer.org/healthy/findcancerearly/examandtestdescriptions/mammogramsandotherbreastimagingprocedures/mammograms-and-other-breast-imaging-procedures-toc

American Cancer Society [ACS]. (2015). Global cancer facts & figures (3rd. ed.). Atlanta.

AR Custom Medical Products. (2007). Custom Compression Paddles. Retrieved July 24, 2014, from http://www.arcustommedical.com/: http://www.arcustommedical.com/products.htm

American College of Radiology (2013) American College of Radiology BI-RADS® ATLAS — Mammography.

Apelt, D. and Peitgen, H. (2008) 'Contrast Sensitivity in Mammographic Softcopy Reading – Determination with Psychophysical Procedures', in Krupinski, E. (ed.) Digital

Mammography. USA: Springer Berlin Heidelberg, pp. 756–763.

Apelt, D., Strasburger, H., Klein, J. and Preim, B. (2010) 'Impact of Adaptation Time on Contrast Sensitivity', in Abbey, D. J. M. C. K. (ed.) Medical Imaging 2010: Image Perception, Observer Performance, and Technology Assessment. San Diego, California, USA. doi: 10.1117/12.845241.

Apelt, D., Strasburger, H., Rascher-Friesenhausen, R., Klein, J., Preim, B. and Peitgen, H.-O. (2009) 'Contrast Senstivity in Mammographic Softcopy Reading'. Edited by B. Sahiner and D. J. Manning, 2(1), pp. 726318-726318–11. doi: 10.1117/12.810221.

Arden, G. B. (1978) 'The importance of measuring contrast sensitivity in cases of visual disturbance.', British Journal of Ophthalmology, 62(4), pp. 198–209. doi: 10.1136/bjo.62.4.198.

Aslund, M. (2007) 'Digital Mammography with a Photon Counting Detector in a Scanned Multislit Geometry'. Available at: http://www.diva-portal.org/smash/record.jsf?pid=diva2:11798 (Accessed: 28 April 2015).

Ayyala Rama S.,MaryAnn Chorlton,Richard H. BehrmanPhyllis J. Kornguth, P. J. S. (2008) 'Digital Mammographic Artifacts on Full-Field Systems : What Are They and How Do I Fix Them ?', 2215.

Badano, A. (2003) 'Optical blur and collection efficiency in columnar phosphors for X-ray imaging', Nuclear Instruments and Methods in Physics Research Section A: Accelerators, Spectrometers, Detectors and Associated Equipment, 508(3), pp. 467–479. doi: 10.1016/S0168-9002(03)01651-6.

Baldelli, P., Phelan, N. and Egan, G. (2010) 'Investigation of the effect of anode/filter materials on the dose and image quality of a digital mammography system based on an amorphous selenium flat panel detector', British Journal of Radiology, 83(988), pp. 290–295. doi: 10.1259/bjr/60404532.

Bass, J. and Chiles, C. (1990) 'Visual skill: Correlation with detection of solitary pulmonary nodules', Invest Radiol., 25(9), p. 994–8. Investigative Radiology. 1990;25(9):994–997. doi: 10.1097/00004424-199009000-00006.

Bator, M. and Chmielewski, L. J. (2008) 'Finding regions of interest for cancerous masses enhanced by elimination of linear structures and considerations on detection correctness measures in mammography', Pattern Analysis and Applications, 12(4), pp. 377–390. doi: 10.1007/s10044-008-0134-x.

Berlin, L. (2001a) 'Malpractice issues in radio: Defending the "missed" radiographic diagnosis', American Journal of Roentgenology, 176(2), pp. 317–322. Available at: http://www.ajronline.org/doi/pdf/10.2214/ajr.176.2.1760317.

Berry-Smith, J. and Lonsdale, C. (2000) 'Image blur: back to basics , Abstracts from Symposium Mammographicum 2000'. Available at: http://breast-cancer-research.com/supplements/2/S2 Abstracts.

Bick, U. (2010) 'Mammographic Signs of Malignancy: Impact of Digital Mammography on Visibility and Appearance', in Bick, U. and Diekmann, F. (eds) Digital Mammography. Springer Berlin Heidelberg, pp. 175–186.

Bick, U. and Diekmann, F. (2010) Digital Mammography, Journal of the Electrochemical Society.

Edited by U. Bick and F. Diekmann. Berlin, Heidelberg: Springer Berlin Heidelberg (Medical Radiology). doi: 10.1007/978-3-540-78450-0.

Broeders, M. J., Ten Voorde, M., Veldkamp, W. J., van Engen, R. E., van Landsveld – Verhoeven, C., 't Jong – Gunneman, M. N., et al. (2015). Comparison of a flexible versus a rigid breast compression paddle: pain experience, projected breast area, radiation dose and technical image quality. European Radiology, 25(3), 821–829.

Bushberg, J. T., Seibert, J. A., Leidholdt, E. M., & Boone, J. M. (2012). The Essential Physics of Medical Imaging (Third ed.). Philadelphia, PA. USA: Lippincot (Wolters Kluwer Health).

Biltawi, M., Al-Najdawi, N. and Tedmori, S. (2012) 'Mammogram enhancement and segmentation methods: classification, analysis, and evaluation', The 13th international Arab …, (1), pp. 477–485. Available at: http://www.acit2k.org/ACIT/2012Proceedings/7103.pdf (Accessed: 28 April 2015).

Bird, R. E., Wallace, T. W. and Yankaskas, B. C. (1992) 'Analysis of cancers missed at screening mammography.', Radiology, 184(3), pp. 613–617. doi: 10.1148/radiology.184.3.1509041.

Birdwell, R. L., Ikeda, D. M., O'Shaughnessy, K. F. and Sickles, E. a (2001) 'Mammographic characteristics of 115 missed cancers later detected with screening mammography and the potential utility of computer-aided detection.', Radiology, 219(1), pp. 192–202. doi: 10.1148/radiology.219.1.r01ap16192.

Bisset, L. (2014) 'Clinical audit of technical recall data for blur following the introduction of the breath hold technique in breast screening LE', Breast Cancer Research, 15(Suppl 1), pp. 1–15. Available at: http://www.ncbi.nlm.nih.gov.scd-rproxy.u-strasbg.fr/pmc/articles/PMC4243136/pdf/bcr3701.pdf.

Blanch, J., Sala, M., Román, M., Ederra, M., Salas, D., Zubizarreta, R., Sanchez, M., Rué, M. and Castells, X. (2013) 'Cumulative risk of cancer detection in breast cancer screening by protocol strategy', Breast Cancer Research and Treatment, 138(3), pp. 869–877. doi: 10.1007/s10549-013-2458-5.

Blanks, R. G., Wallis, M. G. and Moss, S. M. (1998) 'A comparison of cancer detection rates achieved by breast cancer screening programmes by number of readers , for one and two view mammography : results from the UK National Health Service breast screening programme', pp. 195–201.

Boher, P. and Collomb-patton, V. (2012) 'Full characterization of perceived motion-blur versus grey level transitions', (August). Available at: https://www.researchgate.net/profile/Pierre_Boher/publication/251881716.

Boyle, E. R., Pak, D. and Williams, J. B. (1999) 'Motion artifact seen on slot-scanning direct digital mammography', American Journal of Roentgenology, 172(3), pp. 697–701. Available at: http://www.ajronline.org/doi/abs/10.2214/ajr.172.3.10063863 (Accessed: 28 April 2015).

Brook, O. R., Gourtsoyianni, S., Brook, A., Siewert, B., Kent, T. and Raptopoulos, V. (2013) 'Split-bolus spectral multidetector CT of the pancreas: assessment of radiation dose and tumor conspicuity.', Radiology, 269(1), pp. 139–48. doi: 10.1148/radiol.13121409.

Buissink, C., Thompson, J. D., Voet, M., Sanderud, a., Kamping, L. V., Savary, L., Mughal, M., Rocha, C. S., Hart, G. E., Parreiral, R., Martin, G. and Hogg, P. (2014) 'The influence of

experience and training in a group of novice observers: A jackknife alternative free-response receiver operating characteristic analysis', Radiography. Elsevier Ltd, 20(4), pp. 300–305. doi: 10.1016/j.radi.2014.06.016.

Burgess, A. E. (2011) 'Visual perception studies and observer models in medical imaging.', Seminars in nuclear medicine. Elsevier Inc., 41(6), pp. 419–36. doi: 10.1053/j.semnuclmed.2011.06.005.

Burgess, E. (1994) 'Comparison of receiver operating characteristic and forced choice observer performance measurement methods'. Medical Physics, 22(5), pp.643–655. Available at: http://doi.wiley.com/10.1118/1.597576.

Byng, J., Boyd, N. and Fishell, E. (1994) 'The quantitative analysis of mammographic densities.', Physics in Medicine and Biology, 39, pp. 1629–1638. doi: 10.1088/0031-9155/39/10/008.

Cancer research UK (2016) Breast cancer mortality statistics. Available at: http://www.cancerresearchuk.org/health-professional/cancer-statistics/statistics-by-cancer-type/breast-cancer#heading-Two.

Cao, G., Zhao, Y. and Ni, R. (2010) 'Edge-based Blur Metric for Tamper Detection', Journal of Information Hiding and Multimedia Signal Processing, 1(1), pp. 20–27.

Carl J. D'Orsi, E. A. S. B. M. A. M. (2013) 'Summary for Policymakers', in Intergovernmental Panel on Climate Change (ed.) Climate Change 2013 - The Physical Science Basis. Cambridge: Cambridge University Press, pp. 1–30. doi: 10.1017/CBO9781107415324.004.

Carney, P. A., Miglioretti, D. L., Yankaskas, B. C., Kerlikowske, K., Rosenberg, R., Rutter, C. M., Geller, B. M., Abraham, L. A., Taplin, S. H., Dignan, M., Cutter, G. and Ballard-Barbash, R. (2003) 'Individual and combined effects of age, breast density, and hormone replacement therapy use on the accuracy of screening mammography', Annals of Internal Medicine, 138(3), pp. 168–175. doi: 200302040-00008 [pii].

Canadian Cancer Society. (2014). Mammography. Retrieved July 22, 2014, from http://www.cancer.ca: http://www.cancer.ca/en/cancer-information/diagnosis-and-treatment/tests-and-procedures/mammography

Chotas, H. G., Dobbins III, J. T., & Ravin, C. E. (1999). Principles of digital radiography with large-area, electronically readable detectors: a review of the basics. Radiology, 595-599.

Chakraborty, D. (2002) 'Statistical power in observer-performance studies: comparison of the receiver operating characteristic and free-response methods in tasks involving localization', Acad Radiol, 9(2), pp. 147–156. doi: 10.1016/S1076-6332(03)80164-2.

Chakraborty, D. P. (2010a) 'A Status report on free-response analysis', Radiation Protection Dosimetry, 139(1–3), pp. 20–25. doi: 10.1093/rpd/ncp305.

Chakraborty, D. P. (2010b) 'Clinical relevance of the ROC and free-response paradigms for comparing imaging system efficacies', Radiation Protection Dosimetry, 139(1–3), pp. 37–41. doi: 10.1093/rpd/ncq017.

Chakraborty, D. P. (2011) 'New developments in observer performance methodology in medical imaging.', Seminars in nuclear medicine. Elsevier Inc., 41(6), pp. 401–18. doi: 10.1053/j.semnuclmed.2011.07.001.

Chakraborty, D. P. and Berbaum, K. S. (2004) 'Observer studies involving detection and localization: Modeling, analysis, and validation', Medical Physics, 31(8), p. 2313. doi: 10.1118/1.1769352.

Chakraborty, D. P. and Yoon, H.-J. (2008) 'Investigation of methods for analyzing location specific observer performance data'. Edited by B. Sahiner and D. J. Manning, 6917, p. 69170C–69170C–12. doi: 10.1117/12.770531.

Chakraborty, D. P. and Zhai, X. (2015) 'Rjafroc'. Pittsburgh, PA. RJafroc software version 4.2; 2015. Available from: http://www.devchakra- borty.com/RJafroc.php32.

Chaloeykitti, L., Muttarak, M. and Ng, K. (2006) 'Artifacts in mammography: ways to identify and overcome them.', Singapore medical journal, 47(7)(66), p. 634. Available at: http://europepmc.org/abstract/med/16810441 (Accessed: 28 April 2015).

Chang, W., Lee, J. M., Lee, K., Yoon, J. H., Yu, M. H., Han, J. K. and Choi, B. I. (2013) 'Assessment of a model-based, iterative reconstruction algorithm (MBIR) regarding image quality and dose reduction in liver computed tomography.', Investigative radiology, 48(8), pp. 598–606. doi: 10.1097/RLI.0b013e3182899104.

Chesters, M. S. (1992) 'Human visual perception and ROC methodology in medical imaging.', Physics in medicine and biology, 37, pp. 1433–1476. doi: 10.1088/0031-9155/37/7/001.

Chevalier, M., Leyton, F., Tavares, M. N., Oliveira, M., Silva, T. A. and Peixoto, J. E. (2012) 'Image Quality Requirements for Digital Mammography in Breast Cancer Screening', Imaging of the Breast - Technical Aspects and Clinical Implication, (May 2014), pp. 115–132. doi: 10.5772/1230.

Chiu, S. Y. H., Duffy, S., Yen, A. M. F., Tab??r, L., Smith, R. A. and Chen, H. H. (2010) 'Effect of baseline breast density on breast cancer incidence, stage, mortality, and screening parameters: 25-Year follow-up of a Swedish mammographic screening', Cancer Epidemiology Biomarkers and Prevention, 19(5), pp. 1219–1228. doi: 10.1158/1055-9965.EPI-09-1028.

Choi, J. J., Kim, S. H., Kang, B. J., Choi, B. G., Song, B. and Jung, H. (2014) 'Mammographic artifacts on full-field digital mammography.', Journal of digital imaging, 27(2), pp. 231–6. doi: 10.1007/s10278-013-9641-4.

Cole, E., Pisano, E., Kistner, E. and Muller, K. (2003) 'Diagnostic accuracy of digital mammography in patients with dense breasts who underwent problem-solving mammography: Effects of image processing and lesion', Radiology, (2), pp. 153–160. Available at: http://pubs.rsna.org/doi/abs/10.1148/radiol.2261012024 (Accessed: 28 April 2015).

Colenbrander, A. (2001) 'Measuring Vision and Vision Loss', in Duane TD, Tasman W, E. A. (ed.) Duane's Clinical Ophthalmology. Vol 5. pp. 1–42. Available at: http://www.ergoftalmologie.nl/presentaties/6_Kooijman_ref_Colenbrander.pdf.

Cook, A. J., Elmore, J. G., Miglioretti, D. L., Sickles, E. A., Aiello Bowles, E. J., Cutter, G. R. and Carney, P. A. (2010) 'Decreased accuracy in interpretation of community-based screening mammography for women with multiple clinical risk factors', Journal of Clinical Epidemiology. Elsevier Inc, 63(4), pp. 441–451. doi: 10.1016/j.jclinepi.2009.06.008.

Darlington, A. J. (2015) 'Anatomy of the Breast', in Digital Mammography. First. Cham: Springer

International Publishing, pp. 3–10. doi: 10.1007/978-3-319-04831-4_1.

Data, P., Shiel, S., Perry, N., Isabel, M. and Silva, S. (2009) 'Full-Field Digital versus Screen- Film Mammography : Comparison within the UK Breast Screening Program and Systematic Review of Purpose : Methods : Results : Conclusion ':, 251(2).

Danziger, K., & Simonsen, J. (2011). What Are the Different Types of Breast Cancer. Retrieved August 13, 2012, from http://www.geneticheath.com/brov_types_of_breast_cancer.shtml

Debono, J. (2012a) 'Accuracy evaluation of radiographers screen reading mammograms'. Available at: http://hdl.handle.net/2123/10540.

Debono, J. C., Poulos, A. E., Houssami, N., Turner, R. M. and Boyages, J. (2015) 'Evaluation of radiographers' mammography screen-reading accuracy in Australia', Journal of Medical Radiation Sciences, 62(1), pp. 15–22. doi: 10.1002/jmrs.59.

Delrue, L., Gosselin, R. and Ilsen, B. (2011) 'Comparative Interpretation of CT and Standard Radiography of the Chest', Comparative Interpretation of CT and Standard Radiography of the Chest, pp. 27–49. doi: 10.1007/978-3-540-79942-9.

Desai, N., Singh, A. and Valentino, D. J. (2010) 'Practical evaluation of image quality in computed radiographic (CR) imaging systems'. Edited by E. Samei and N. J. Pelc, 1(c), p. 76224Q. doi: 10.1117/12.844640.

Dev Chakraborty Professor (no date) 'Using JAFROC software to analyze data acquired according to the ROI paradigm Analyzing two breasts per case data', (1), pp. 6–7.

Dewar, J. A. (2015) 'Mammography Screening: Philosophy – Evidence for and against', in Digital Mammography. Cham: Springer International Publishing, pp. 59–65. doi: 10.1007/978-3-319-04831-4_7.

Defreitas, K. F., Pellegrino, A., Farbizio, T. A., Janer, R., & Hitzke, G. (2008). Patent No. US 7319735 B2. US. Available at: http://www.scopus.com/inward/record.url?eid=2-s2.0-0242287170&partnerID=40&md5=c9745139d47a60bc4c190b9b0997acb8

Diekmann, F., Freyer, M., Diekmann, S., Fallenberg, E. M., Fischer, T., Bick, U. and Pöllinger, A. (2011) 'Evaluation of contrast-enhanced digital mammography', European Journal of Radiology. Elsevier Ireland Ltd, 78(1), pp. 112–121. doi: 10.1016/j.ejrad.2009.10.002.

Dinnes, J., Moss, S., Melia, J., Blanks, R., Song, F. and Kleijnen, J. (2001) 'Effectiveness and cost-effectiveness of double reading of mammograms in breast cancer screening: findings of a systematic review', The Breast, 10(6), pp. 455–463. doi: 10.1054/brst.2001.0350.

Drum, B., Calogero, D. and Rorer, E. (2007) 'Assessment of visual performance in the evaluation of new medical products.', Drug discovery today. Technologies, 4(2), pp. 55–61. doi: 10.1016/j.ddtec.2007.10.009.

Duijm, L. E. M., Louwman, M. W. J., Groenewoud, J. H., van de Poll-Franse, L. V, Fracheboud, J. and Coebergh, J. W. (2009) 'Inter-observer variability in mammography screening and effect of type and number of readers on screening outcome.', British journal of cancer, 100(6), pp. 901–907. doi: 10.1038/sj.bjc.6604954.

Dougherty, G., 2009. Digital image processing for medical applications CAMBRIDGE UNIVERSITY PRESS, ed., the United States of America by Cambridge University Press,

New York.

Donnelly, D. and JD Thompson (2017) 'The impact of simulated respiratory motion on nodule detection in low-resolution Computed Tomography (CT) for attenuation correction (AC): a phantom stu', in Poster Presentation, BNMS 2017, Birmingham, UK.

Duquenoy, P., George, C., & Solomonides, A. (2008). Considering something "ELSE": ethical, legal and socio-economic factors in medical imaging and medical informatics. Computer Methods and Programs in Biomedicine, 92(3), 227–37. doi:10.1016/j.cmpb.2008.06.001

Eckstein, M. P. and Whiting, J. S. (1995) 'Lesion detection in structured noise', Academic Radiology, 2(3), pp. 249–253. doi: 10.1016/S1076-6332(05)80174-6.

Elder, J. H. and Zucker, S. W. (1998) 'Local scale control for edge detection and blur estimation', IEEE Transactions on Pattern Analysis and Machine Intelligence, 20(7), pp. 699–716. doi: 10.1109/34.689301.

Evans, A., Ellis, I., Pinder, S. and Wilson, R. (2002) Breast Calcification A Diagnostic Manual. first Publ. London: Greenwich Medical Media. Available at: http://mariorad.com/books/breast/015 Breast Calcification A Diagnostic Manual.

Evans, a. . and Blanks, R. . (2002) 'Should Breast Screening Programmes Limit their Detection of Ductal Carcinoma In Situ?', Clinical Radiology, 57(12), pp. 1086–1089. doi: 10.1053/crad.2002.1097.

Fallis, A. . (2013) Digital Image Processing for Medical Applications, Journal of Chemical Information and Modeling. Cambridge University Press. doi: 10.1017/CBO9781107415324.004.

Farshid, G., Sullivan, T., Downey, P., Gill, P. G. and Pieterse, S. (2011) 'Independent predictors of breast malignancy in screen-detected microcalcifications : biopsy results in 2545 cases', British Journal of Cancer. Nature Publishing Group, 105(11), pp. 1669–1675. doi: 10.1038/bjc.2011.466.

Field, A., Miles, J. and Field, Z. (2013) Discovering Statistics Using SPSS, Sage. doi: 10.1111/insr.12011_21.

Fujihashi, C. (1994) 'Detection of decision error caused by the quantum noise in an optical signal system', Journal of Lightwave Technology, 12(6), pp. 1057–1061. doi: 10.1109/50.296200.

Freitas, A. G., Kemp, C., Louveira, M. H., Fujiwara, S. M., & Campos, L. F. (2006). Digital mammography: current view and future applications. Radiologia Brasileira, 39.

Gao, X., Lu, W., Tao, D. and Li, X. (2010) 'Image Quality Assessment and Human Visual System Xinbo', IEEE transactions on medical imaging. Edited by P. Frossard, H. Li, F. Wu, B. Girod, S. Li, and G. Wei, 7744, p. 77440Z–77440Z–10. doi: 10.1117/12.862431.

Garnett, S. E. (2015) 'Male Mammography', in Digital Mammography. Cham: Springer International Publishing, pp. 239–240. doi: 10.1007/978-3-319-04831-4_29.

Gathani, T., Bull, D., Green, J., Reeves, G. and Beral, V. (2005) 'Breast cancer histological classification: agreement between the Office for National Statistics and the National Health Service Breast Screening Programme.', Breast cancer research : BCR, 7(6), pp. R1090-6. doi: 10.1186/bcr1352.

Gedraite, E. and Hadad, M. (2011) 'Investigation on the effect of a Gaussian Blur in image filtering and segmentation', ELMAR, 2011 Proceedings, (September), pp. 14–16. Available at: http://ieeexplore.ieee.org/xpls/abs_all.jsp?arnumber=6044249 (Accessed: 28 April 2015).

Geerligs, M., Peters, G. W. M., Ackermans, P. A. J., Oomens, C. W. J. and Baaijens, F. P. T. (2010) 'Does subcutaneous adipose tissue behave as an (anti-)thixotropic material?', Journal of Biomechanics. Elsevier, 43(6), pp. 1153–1159. doi: 10.1016/j.jbiomech.2009.11.037.

Geiser, W. R., Haygood, T. M., Santiago, L., Stephens, T., Thames, D. and Whitman, G. J. (2011) 'Challenges in Mammography: Part 1, Artifacts in Digital Mammography', American Journal of Roentgenology, 197(6), pp. W1023–W1030. doi: 10.2214/AJR.10.7246.

Gennaro, G., Toledano, A., Di Maggio, C., Baldan, E., Bezzon, E., La Grassa, M., Pescarini, L., Polico, I., Proietti, A., Toffoli, A. and Muzzio, P. C. (2010) 'Digital breast tomosynthesis versus digital mammography: A clinical performance study', European Radiology, 20(7), pp. 1545–1553. doi: 10.1007/s00330-009-1699-5.

Geller, B., Barlow, W., Ballard-Barbash, R., Ernster, V., Yankaskas, B., Sickles, E., et al. (2002). Use of the American College of Radiology BI-RADS to Report on the Mammographic Evaluation of Women with Signs and Symptoms of Breast Disease. Radiology, 536-542.

Goergen, S. K., Evans, J., Cohen, G. P. and MacMillan, J. H. (1997) 'Characteristics of breast carcinomas missed by screening radiologists.', Radiology, 204(1), pp. 131–135. doi: 10.1148/radiology.204.1.9205234.

Goossens, B., Luong, H., Platiša, L. and Philips, W. (2013) 'Objectively measuring signal detectability, contrast, blur and noise in medical images using channelized joint observers', 8673, p. 86730J. doi: 10.1117/12.2007915.

Gram, I. T., Funkhouser, E. and Tabár, L. (1997) 'The Tabár classification of mammographic parenchymal patterns', European Journal of Radiology, 24(2), pp. 131–136. doi: 10.1016/S0720-048X(96)01138-2.

Gur, D. (2007) 'Objectively Measuring and Comparing Performance Levels of Diagnostic Imaging Systems and Practices', Academic Radiology, 14(6), pp. 641–642. doi: 10.1016/j.acra.2007.04.007.

Hackney, L. (2015) 'Aetiology and Epidemiology of Breast Cancer', in Digital Mammography. Cham: Springer International Publishing, pp. 17–25. doi: 10.1007/978-3-319-04831-4_3.

Haimo Liu, I. K. (2012) Task Specific Evaluation Methology for Clinical Full Field Digital Mammomgraphy. University of Maryland. Available at: https://drum.lib.umd.edu/bitstream/handle/1903/13812/Liu_umd_0117E_13640.pdf?sequence=1&isAllowed=y.

Hambly, N. M., McNicholas, M. M., Phelan, N., Hargaden, G. C., O'Doherty, A. and Flanagan, F. L. (2009) 'Comparison of digital mammography and screen-film mammography in breast cancer screening: A review in the Irish Breast Screening Program', American Journal of Roentgenology, 193(October), pp. 1010–1018. doi: 10.2214/AJR.08.2157.

Haneuse, S., Buist, D. S. M., Miglioretti, D. L., Anderson, M. L., Carney, P. A., Onega, T., Geller, B. M., Kerlikowske, K., Rosenberg, R. D., Yankaskas, B. C., Elmore, J. G., Taplin, S. H., Smith, R. A. and Sickles, E. A. (2012) 'Mammographic Interpretive Volume and Diagnostic

Mammogram Interpretation Performance in Community Practice', 262(1), pp. 69–79. doi: 10.1148/radiol.11111026/-/DC1.

Harvey, S. C., Geller, B., Oppenheimer, R. G., Pinet, M., Riddell, L. and Garra, B. (2003) 'Increase in cancer detection and recall rates with independent double interpretation of screening mammography', American Journal of Roentgenology, 180(5), pp. 1461–1467. doi: 10.2214/ajr.180.5.1801461.

Haygood, T. M., Ryan, J., Brennan, P. C., Li, S., Marom, E. M., McEntee, M., Itani, M., Evanoff, M. and Chakraborty, D. (2012) 'On the choice of acceptance radius in free-response observer performance studies', The British journal of radiology, pp. 1–6. doi: 10.1259/bjr/42313554.

Heddson, B., Rönnow, K., Olsson, M. and Miller, D. (2007) 'Digital versus screen-film mammography: a retrospective comparison in a population-based screening program.', European journal of radiology, 64(3), pp. 419–25. doi: 10.1016/j.ejrad.2007.02.030.

Health Protection Agency. (2011). Risk of solid cancers following radiation Exposure: estimates for the UK population. Oxfordshire: Health Protection Agency.

Hendrick, R. E. (2010). Radiation doses and cancer risks from breast imaging studies. Radiology, 257(1), 246-253.

Hizukuri, A., Nakayama, R., Kashikura, Y., Takase, H., Kawanaka, H., Ogawa, T. and Tsuruoka, S. (2013) 'Computerized determination scheme for histological classification of breast mass using objective features corresponding to clinicians' subjective impressions on ultrasonographic images.', Journal of digital imaging, 26(5), pp. 958–70. doi: 10.1007/s10278-013-9594-7.

Hofvind, S. S. H. and de Wolf, C. J. M. (2015) 'Screening Programmes for Breast Cancer in Europe', in Digital Mammography. Cham: Springer International Publishing, pp. 67–74. doi: 10.1007/978-3-319-04831-4_8.

Holladay, J. (2004) 'Visual acuity measurements', Journal of Cataract & Refractive Surgery, 3350(3). Available at: http://scholar.google.com/scholar?hl=en&btnG=Search&q=intitle:Visual+acuity+measurements#0 (Accessed: 8 May 2015).

Hogg p. Kelly J. and Mercer C. (2015) Digital Mammography. Edited by P. Hogg, J. Kelly, and C. Mercer. Cham: Springer International Publishing. doi: 10.1007/978-3-319-04831-4.

Husien, A. M. A. (1995) 'The efficacy of double reading mammograms in breast screening', Clinical Radiology, 50(1), p. 67. doi: 10.1016/S0009-9260(05)82972-1.

Huynh, P. T., Jarolimek, A. M. and Daye, S. (1998) 'The false-negative mammogram', Radiographics, 18(5), pp. 1137–1154. doi: 10.1148/radiographics.18.5.9747612.

Jackson, W. (1996) 'X-ray image system design using a human visual model' Available at: http://proceedings.spiedigitallibrary.org/proceeding.aspx?articleid=1016759 (Accessed: 28 April 2015).

Kaiser, P. (2009) 'Prospective evaluation of visual acuity assessment: a comparison of Snellen versus ETDRS charts in clinical practice (An AOS Thesis)', Transactions of the American Ophthalmological Society, (107), pp. 311–324. Available at: http://www.ncbi.nlm.nih.gov/pmc/articles/PMC2814576/ (Accessed: 28 April 2015).

Kallenberg, M. G. J. and Karssemeijer, N. (2012) 'Compression paddle tilt correction in full-field digital mammograms.', Physics in medicine and biology, 57(3), pp. 703–15. doi: 10.1088/0031-9155/57/3/703.

Kanal, K. M., Krupinski, E., Berns, E. a, Geiser, W. R., Karellas, A., Mainiero, M. B., Martin, M. C., Patel, S. B., Rubin, D. L., Shepard, J. D., Siegel, E. L., Wolfman, J. a, Mian, T. a and Mahoney, M. C. (2013) 'ACR-AAPM-SIIM practice guideline for determinants of image quality in digital mammography.', Journal of digital imaging, 26(1), pp. 10–25. doi: 10.1007/s10278-012-9521-3.

Kelly J, Hogg P, Millington S, Sanderud A, Willcock C, M. G. et al. (2012) 'Paddle motion analysis – preliminary research', in UK: University of Salford, 2011. In United Kingdom Radiological Congress (UKRC). Manchester, pp. 25–27. doi: 10.1111/j.1365-2990.2011.01241.x.

Kerlikowske, K., Grady, D., Barclay, J., Sickles, E. A. and Ernster, V. (1996) 'Effect of age, breast density, and family history on the sensitivity of first screening mammography.', JAMA : the journal of the American Medical Association, 276(1), pp. 33–38. doi: 10.1001/jama.276.1.33.

Klompenhouwer, E. G., Voogd, A. C., Den Heeten, G. J., Strobbe, L. J. A., De Haan, A. F. J., Wauters, C. A., Broeders, M. J. M. and Duijm, L. E. M. (2015) 'Blinded double reading yields a higher programme sensitivity than non-blinded double reading at digital screening mammography: A prospected population based study in the south of the Netherlands', European Journal of Cancer. Elsevier Ltd, 51(3), pp. 391–399. doi: 10.1016/j.ejca.2014.12.008.

Knox, M., O'Brien, A., Szabó, E., Smith, C. S., Fenlon, H. M., McNicholas, M. M. and Flanagan, F. L. (2015) 'Impact of full field digital mammography on the classification and mammographic characteristics of interval breast cancers', European Journal of Radiology. Elsevier Ireland Ltd, 84(6), pp. 1056–1061. doi: 10.1016/j.ejrad.2015.03.007.

Kolb, T. M., Lichy, J. and Newhouse, J. H. (2002) 'Comparison of the performance of screening mammography, physical examination, and breast US and evaluation of factors that influence them: an analysis of 27,825 patient evaluations.', Radiology, 225(1), pp. 165–75. doi: 10.1148/radiol.2251011667.

Kopans, D. B. (2007). Breast imaging (Third ed.). Philadelphia: Lippincott Williams & Wilkin.

Kriege, M., Brekelmans, C. T. M., Obdeijn, I. M., Boetes, C., Zonderland, H. M., Muller, S. H., Kok, T., Manoliu, R. A., Besnard, A. P. E., Tilanus-Linthorst, M. M. A., Seynaeve, C., Bartels, C. C. M., Kaas, R., Meijer, S., Oosterwijk, J. C., Hoogerbrugge, N., Tollenaar, R. A. E. M., Rutgers, E. J. T., De Koning, H. J. and Klijn, J. G. M. (2006) 'Factors affecting sensitivity and specificity of screening mammography and MRI in women with an inherited risk for breast cancer', Breast Cancer Research and Treatment, 100(1), pp. 109–119. doi: 10.1007/s10549-006-9230-z.

Krupinski, E. a (2011) 'The role of perception in imaging: past and future.', Seminars in nuclear medicine. Elsevier Inc., 41(6), pp. 392–400. doi: 10.1053/j.semnuclmed.2011.05.002.

Kulama, E. (2009) 'Commissioning and Routine Testing of Full Field Digital Mammography Systems', (April). Available at: https://assets.publishing.service.gov.uk/government/uploads/system/uploads/attachment_data/file/441857/nhsbsp-equipment-report-0604.pdf

Kundel, Harold and Revesz, G. (1976) 'Lesion Conspicuity, Structured Noise , and Film Reader Error', AJR. American journal of roentgenology, (126), pp. 1233–1238. Available at: http://www.ajronline.org/doi/abs/10.2214/ajr.126.6.1233.

Kundel, H. (1995) 'Medical image perception', Academic radiology. Cambridge. Available at: http://www.sciencedirect.com/science/article/pii/S1076633212800444 (Accessed: 28 April 2015).

Lança, C., Thompson, J. D. and Lança, L. (2015) 'Visual Function Assessment in Medical Imaging Research', 87(2), pp. 129–138.

Lanca, C., Thompson, J., Lanca, L. and Hogg, P. (2014) 'A method to assess visual function prior to conducting medical imaging research using perceptual methodologies', Radiologic Technology. Available at: http://usir.salford.ac.uk/34113/ (Accessed: 8 May 2015).

Lehman, W., Peacock, S., Drucker, M. J. and Urban, N. (1999) 'Effect of age and breast density on screening mammograms with false-positive findings', Cancer Research, (December), pp. 1651–1655.

Lewin, J. M., D'Orsi, C. J. and Hendrick, R. E. (2004) 'Digital mammography', Radiologic Clinics of North America, 42(5), pp. 871–884. doi: 10.1016/j.rcl.2004.06.004.

Legislation.gov.uk. (1998). Data Protection Act 1998. Retrieved from http://www.legislation.gov.uk/ukpga/1998/29/contents

Li, Y., Poulos, A., McLean, D. and Rickard, M. (2010) 'A review of methods of clinical image quality evaluation in mammography.', European journal of radiology. Elsevier Ireland Ltd, 74(3), pp. e122-31. doi: 10.1016/j.ejrad.2009.04.069.

Linder-Ganz, E., Shabshin, N., Itzchak, Y. and Gefen, A. (2007) 'Assessment of mechanical conditions in sub-dermal tissues during sitting: A combined experimental-MRI and finite element approach', Journal of Biomechanics, 40(7), pp. 1443–1454. doi: 10.1016/j.jbiomech.2006.06.020.

Lip, G., Zakharova, N., Duffy, S., Gillan, M. and Gilbert, F. (2010) 'Breast density as a predictor of breast cancer risk', 12(Suppl 3), p. P1. doi: 10.1186/bcr2654.

Liu, S. (1999) 'The analysis of digital mammograms: spiculated tumor detection and normal mammogram characterization', (May). Available at: ftp://ftp.ecn.purdue.edu/ace/delp/sheng-thesis/thesis.ps.Z.

Lu, W., Parikh, P. J., Hubenschmidt, J. P., Politte, D. G., Whiting, B. R., Bradley, J. D., Mutic, S. and Low, D. a. (2005) 'Reduction of motion blurring artifacts using respiratory gated CT in sinogram space: A quantitative evaluation', Medical Physics, 32(11), p. 3295. doi: 10.1118/1.2074187.

Ma, W., Hilton, B., Borgen, R., Kelly, J. and Hogg, P. (2016) 'Comparative analysis of visual blurring detection in mammography images - clinical room monitor versus reporting grade monitor: initial results', European Congress of Radiology, pp. 1–14. doi: 10.1594/ecr2016/C-0316.

Ma, W. K., Aspin, R., Kelly, J., Millington, S. and Hogg, P. (2015) 'What is the minimum amount of simulated breast movement required for visual detection of blurring? An exploratory investigation', The British Journal of Radiology, 88(1052), p. 20150126. doi: 10.1259/bjr.20150126.

Ma, W. K., Borgen, R., Kelly, J., Millington, S., Hilton, B., Aspin, R., Lança, C. and Hogg, P. (2017) 'Blurred digital mammography images: an analysis of technical recall and observer detection performance', The British Journal of Radiology, 90(1071), p. 20160271. doi: 10.1259/bjr.20160271.

Ma, W. K., Brettle, D., Howard, D., Kelly, J., Millington, S. and Hogg, P. (2014) 'Extra patient movement during mammographic imaging: an experimental study.', The British journal of radiology, 87(1044), p. 20140241. doi: 10.1259/bjr.20140241.

Ma, W. K., Hogg, P., Kelly, J. and Millington, S. (2014) 'A method to investigate image blurring due to mammography machine compression paddle movement', Radiography. Elsevier Ltd, pp. 4–9. doi: 10.1016/j.radi.2014.06.004.

Ma, W. Ke., McEntee, M. F., Mercer, C., Kelly, J., Millington, S. and Hogg, P. (2016) 'Analysis of motion during the breast clamping phase of mammography', The British Journal of Radiology, 89(1059), p. 20150715. doi: 10.1259/bjr.20150715.

Majid, A. S., de Paredes, E. S., Doherty, R. D., Sharma, N. R. and Salvador, X. (2003) 'Missed Breast Carcinoma: Pitfalls and Pearls', RadioGraphics, 23(4), pp. 881–895. doi: 10.1148/rg.234025083.

Manning, D. and Ethell, S. C. (2002) 'Lesion conspicuity and AFROC performance in pulmonary nodule detection', Radiography, (October), pp. 300–311. doi: 10.1117/12.462691.

Manning, D., Ethell, S., Donovan, T. and Crawford, T. (2006) 'How do radiologists do it? The influence of experience and training on searching for chest nodules', Radiography, 12(2), pp. 134–142. doi: 10.1016/j.radi.2005.02.003.

Manning, D. J. (1998) 'Evaluation of diagnostic performance in radiography', Radiography, 4(1), pp. 49–60. doi: 10.1016/S1078-8174(98)80030-8.

Manning, D. J., Ethell, S. C. and Donovan, T. (2004a) 'Detection or decision errors? Missed lung cancer from the posteroanterior chest radiograph', The British Journal of Radiology, 77(915), pp. 231–235. doi: 10.1259/bjr/28883951.

Marin, D., Choudhury, K. R., Gupta, R. T., Ho, L. M., Allen, B. C., Schindera, S. T., Colsher, J. G., Samei, E. and Nelson, R. C. (2013) 'Clinical impact of an adaptive statistical iterative reconstruction algorithm for detection of hypervascular liver tumours using a low tube voltage, high tube current MDCT technique', European Radiology, 23(12), pp. 3325–3335. doi: 10.1007/s00330-013-2964-1.

Masotti, M. (2005) Optimal image representations for mass detection in digital mammography. Available at: http://amsacta.unibo.it/1090/ (Accessed: 28 April 2015).

Massanes, F. and Brankov, J. G. (2011) 'Motion perception in medical imaging', SPIE Medical Imaging, 7966, pp. 1–10. doi: 10.1117/12.878417.

McDonald, D. M. (2015) 'Breast Density and Influencing Factors', in Digital Mammography. Cham: Springer International Publishing, pp. 11–16. doi: 10.1007/978-3-319-04831-4_2.

Medicine, A. A. of P. in (2005) 'Assessment of display performance for medical imaging systems', Med Phys, 4095. Available at: http://scholar.google.com/scholar?hl=en&btnG=Search&q=intitle:Assessment+of+Display (Accessed: 28 April 2015).

Mello-Thoms, C. (2006) 'How does the perception of a lesion influence visual search strategy in mammogram reading?', Academic radiology, 13(3), pp. 275–88. doi: 10.1016/j.acra.2005.11.034.

Mello-Thoms, C., Hardesty, L., Sumkin, J., Ganott, M., Hakim, C., Britton, C., Stalder, J. and Maitz, G. (2005) 'Effects of lesion conspicuity on visual search in mammogram reading', Academic Radiology, 12(9), pp. 830–840. doi: 10.1016/j.acra.2005.03.068.

Metz, C. E. (2008) 'ROC analysis in medical imaging: a tutorial review of the literature', Radiological physics and technology, 1(1), pp. 2–12. doi: 10.1007/s12194-007-0002-1.

Miglioretti, D. L., Smith-bindman, R., Abraham, L., Brenner, R. J., Patricia, A., Bowles, E. J. A., Buist, D. S. M. and Elmore, J. G. (2011) 'Radiologist Characteristics Associated With Interpretive Performance of Diagnostic Mammography', 99(24), pp. 1854–1863. doi: 10.1093/jnci/djm238.Radiologist.

Mucci, B., Lawson, S., Athey, G. and Scarisbrick, G. (1997) 'Radiographers as readers in breast screening: Experience with a "red dot" method', Breast, 6(4), pp. 183–185. doi: 10.1016/S0960-9776(97)90570-1.

Muller, S. (1999) 'Full-field digital mammography designed as a complete system', European journal of radiology, 31(1997), pp. 25–34. Available at: http://www.sciencedirect.com/science/article/pii/S0720048X99000662 (Accessed: 28 April 2015).

Murphy, F., Nightingale, J., Hogg, P., Robinson, L., Seddon, D. and Mackay, S. (2014) 'Compression force behaviours: An exploration of the beliefs and values influencing the application of breast compression during screening mammography', Radiography. Elsevier Ltd, pp. 1–6. doi: 10.1016/j.radi.2014.05.009.

Michaelson , J., Satija S., Moore, R. et al., "Estimates of the Sizes at Which Breast Cancers Become Detectable on Mammographic and Clinical Grounds," Journal of Women's Imaging, 5(1), 3-10 (2003).

Nadenau, M., Winkler, S., Alleysson, D. and Kunt, M. (2000) 'Human vision models for perceptually optimized image processing–a review', Proceedings of the IEEE, pp. 1–15. Available at: ftp://ftp.c-tt.ru/Symmetricom/V-Factor/V-Factor-Support-Docs/HVS_Review_Final.pdf (Accessed: 28 April 2015).

NHSBSP Publication No 60 (2005) Consolidated Guidance on Standards For The NHS Breast screening Programme, NHS cancer Screening Programmes. Sheffield.

NHSBSP Publication No 63 (2006) Quality assurance guidelines for mammography including radiographic quality control, NHS cancer Screening Programmes. Available at: http://capitadiscovery.co.uk/bcu/items/1175568%5Cnhttp://www.cancerscreening.nhs.uk/breastscreen/publications/nhsbsp63.pdf.

Nicholson, B. T., LoRusso, A. P., Smolkin, M., Bovbjerg, V. E., Petroni, G. R. and Harvey, J. A. (2006) 'Accuracy of Assigned BI-RADS Breast Density Category Definitions', Academic Radiology, 13(9), pp. 1143–1149. doi: 10.1016/j.acra.2006.06.005.

Nodine, F. and Kundel, L. (1987) 'Using eye movements to study visual search and to improve tumor detection', (November), pp. 1241–1250.

Obuchowski, Nancy A., Michael L. Lieber, and K. A. P. (2000) 'Data analysis for detection and localization of multiple abnormalities with application to mammography.', Academic radiology, 7(7), pp. 516–525. doi: 10.1016/S1076-6332(00)80324-4.

Obuchowski, N. (2000) 'Sample size tables for receiver operating characteristic studies', American Journal of Roentgenology, (September), pp. 603–608. Available at: http://www.ajronline.org/doi/abs/10.2214/ajr.175.3.1750603 (Accessed: 24 August 2015).

Obuchowski, N. (2005) 'Fundamentals of clinical research for radiologists', Am. J. Roentgenol, (February), pp. 364–372. Available at: http://66.199.228.237/boundary/complex_decision_making_and_ethics/ROC_Analysis.pdf (Accessed: 28 April 2015).

Obuchowski, N. a, Beiden, S. V, Berbaum, K. S., Hillis, S. L., Ishwaran, H., Song, H. H. and Wagner, R. F. (2004) 'Multireader, multicase receiver operating characteristic analysis: an empirical comparison of five methods.', Academic radiology, 11(9), pp. 980–95. doi: 10.1016/j.acra.2004.04.014.

Ortiz-Perez, T. and Watson, A. B. (2015) 'Mammography Techniques, Positioning, and Optimizing Image Quality', in Breast Cancer Screening and Diagnosis. New York, NY: Springer New York, pp. 37–63. doi: 10.1007/978-1-4939-1267-4_3.

Osberger, W. (1999) Perceptual Vision Models for Picture Quality Assessmnet and Compression Applications. Available at: http://www.cis.rit.edu/people/faculty/pelz/lab/papers/eyetracking_methods/Osberger_thesis.pdf (Accessed: 28 April 2015).

Ossati, M. S. (2015) 'Design , development and use of a deformable breast phantom to assess the relationship between thickness and lesion visibility in full field digital mammography Design , development and use of a deformable breast phantom to assess the relationship between', (July).

Office for National Statistics[ONS]. (2012). Breast cancer: incidence, mortality and survival, 2010. Retrieved from www.ons.gov.uk.

Patel, P. N., Smith, C. K. and Patrick, C. W. (2005) 'Rheological and recovery properties of poly(ethylene glycol) diacrylate hydrogels and human adipose tissue', Journal of Biomedical Materials Research - Part A, 73(3), pp. 313–319. doi: 10.1002/jbm.a.30291.

Pathmanathan, P. (2006) Predicting Tumour Location by Simulating the Deformation of the Breast using Nonlinear Elasticity and the Finite Element Method. University of Oxford.

Perry, N., Broeders, M., de Wolf, C., Törnberg, S., Holland, R. and von Karsa, L. (2008) European guidelines for quality assurance in breast cancer screening and diagnosis., Annals of oncology : official journal of the European Society for Medical Oncology / ESMO. doi: 10.1093/annonc/mdm481.

Peters, C. O. and G. (2010) 'Mechanical Behavior and Properties of Adipose Tissue', in Biomaterials As Stem Cell Niche, pp. 153–171. doi: 10.1007/8415.

Pisano, E. D. and Yaffe, M. J. (2005) 'Digital Mammography', Radiology, Published (234), pp. 353–362.

Plöckinger, U. (2012) 'Diagnosis and treatment of gastrinomas in multiple endocrine neoplasia type 1

(MEN-1)', Cancers, 4(1), pp. 39–54. doi: 10.3390/cancers4010039.

Posso, M. C., Puig, T., Quintana, M. J., Sol??-Roca, J. and Bonfill, X. (2016) 'Double versus single reading of mammograms in a breast cancer screening programme: a cost-consequence analysis', European Radiology. European Radiology, 26(9), pp. 3262–3271. doi: 10.1007/s00330-015-4175-4.

Public Health England and NHS Screening Programme (2017) 'NHS Breast Screening Programme: Consolidated standards', (April), p. 28.

Polit, D. , & Beck, C. (2003). Nursing research: principles and methods (7 ed.): Lippincott Williams & Wilkins

Quinn B. Carroll, M.ED., R.T., (2011). Radiography in the Digital Age, physics, exposure, radiation biology, LTD.

Rafferty, E. a (2007) 'Digital mammography: novel applications.', Radiologic clinics of North America, 45(5), p. 831–43, vii. doi: 10.1016/j.rcl.2007.06.005.

Rawashdeh, M. A., Mello-thoms, C., Bourne, R. and Brennan, P. C. (2014) 'Mammography : Radiologist and Image Characteristics That Determine the Accuracy of Breast Cancer Diagnosis', pp. 731–736.

Ranger, N. T., Lo, J. Y., & Samei, E. (2010). A technique optimization protocol and the potential for dose reduction in digital mammography. Medical Physics, 37(3), 962–969.

Reed, W. (2005) 'Mammography interpretation: factors influencing the assessment of accuracy and the perception of abnormality', Journal of Medical Radiation Sciences, 52(2), pp. 23–25. doi: 10.1002/j.2051-3909.2005.tb00033.x.

Richard, S. and Siewerdsen, J. H. (2008) 'Comparison of model and human observer performance for detection and discrimination tasks using dual-energy x-ray images.', Medical physics, 35(11), pp. 5043–5053. doi: 10.1118/1.2988161.

Rourke, J. O., Mercer, C. E. and Starr, L. (2016) 'Programme Evaluation : Technical recall and image blur within a breast screening service', (January), pp. 3–4.

Ruschin, M., Timberg, P. and Båth, M. (2007b) 'Dose dependence of mass and microcalcification detection in digital mammography: free response human observer studies', Medical …, 34(2), pp. 400–407. Available at: http://scitation.aip.org/content/aapm/journal/medphys/34/2/10.1118/1.2405324 (Accessed: 21 May 2015).

Sabih, D.-E.-, Sabih, A., Sabih, Q. and Khan, A. N. (2011) 'Image perception and interpretation of abnormalities; can we believe our eyes? Can we do something about it?', Insights into imaging, 2(1), pp. 47–55. doi: 10.1007/s13244-010-0048-1.

Safdar, N. M., Siddiqui, K. M., Qureshi, F., Mirza, M. K., Knight, N., Nagy, P. and Siegel, E. (2009) 'Vision and quality in the digital imaging environment: how much does the visual acuity of radiologists vary at an intermediate distance?', AJR. American journal of roentgenology, 192(6), pp. W335-40. doi: 10.2214/AJR.07.3515.

Samani, A., Zubovits, J. and Plewes, D. (2007) 'Elastic moduli of normal and pathological human breast tissues: an inversion-technique-based investigation of 169 samples', Phys. Med. Biol,

52, pp. 1565–1576. doi: 10.1088/0031-9155/52/6/002.

Samei, E. (2003) 'Performance of digital radiographic detectors: quantification and assessment methods', Advances in digital radiography: RSNA, 27710, pp. 37–47. Available at: http://www.aapm.org/meetings/amos2/pdf/29-7979-41789-512.pdf (Accessed: 25 August 2015).

Samei, E., Flynn, M. J., Peterson, E. and Eyler, W. R. (2003) 'Subtle lung nodules: influence of local anatomic variations on detection.', Radiology, 228(1), pp. 76–84. doi: 10.1148/radiol.2273020509.

Saunders, R. S., Baker, J. a, Delong, D. M., Johnson, J. P. and Samei, E. (2007) 'Does image quality matter? Impact of resolution and noise on mammographic task performance.', Medical physics, 34(10), pp. 3971–3981. doi: 10.1118/1.2776253.

Saunders, R. S. and Samei, E. (2008) 'The effect of breast compression on mass conspicuity in digital mammography.', Medical physics, 35(10), pp. 4464–4473. doi: 10.1118/1.2977600.

Schindelin, J., Arganda-Carreras, I., Frise, E., Kaynig, V., Longair, M., Pietzsch, T., Preibisch, S., Rueden, C., Saalfeld, S., Schmid, B., Tinevez, J.-Y., White, D. J., Hartenstein, V., Eliceiri, K., Tomancak, P. and Cardona, A. (2012) 'Fiji: an open-source platform for biological-image analysis', Nature Methods, 9(7), pp. 676–682. doi: 10.1038/nmeth.2019.

Schueller, G., Riedl, C. C., Mallek, R., Eibenberger, K., Langenberger, H., Kaindl, E., Kulinna-Cosentini, C., Rudas, M. and Helbich, T. H. (2008) 'Image quality, lesion detection, and diagnostic efficacy in digital mammography: full-field digital mammography versus computed radiography-based mammography using digital storage phosphor plates.', European journal of radiology, 67(3), pp. 487–96. doi: 10.1016/j.ejrad.2007.08.016.

Schulz-Wendtland, R., Fuchsjäger, M., Wacker, T. and Hermann, K.-P. (2009) 'Digital mammography: An update', European Journal of Radiology, 72(2), pp. 258–265. doi: 10.1016/j.ejrad.2009.05.052.

Shannon, K. M. and Chittenden, A. (2015) 'Breast Cancer Genetics and Risk Assessment', in Breast Cancer Screening and Diagnosis. New York, NY: Springer New York, pp. 1–21. doi: 10.1007/978-1-4939-1267-4_1.

Shao, Y.-Z., Liu, L.-Z., Bie, M.-J., Li, C., Wu, Y., Xie, X. and Li, L. (2011) 'Characterizing the clustered microcalcifications on mammograms to predict the pathological classification and grading: a mathematical modeling approach.', Journal of digital imaging, 24(5), pp. 764–71. doi: 10.1007/s10278-011-9381-2.

Shetty, M. K. (2015a) Breast Cancer Screening and Diagnosis. Edited by M. K. Shetty. New York, NY: Springer New York. doi: 10.1007/978-1-4939-1267-4.

Shetty, M. K. (2015b) 'Mammographic Signs of Breast Cancer', in Breast Cancer Screening and Diagnosis. New York, NY: Springer New York, pp. 93–117. doi: 10.1007/978-1-4939-1267-4_5.

Sickles, E. A. (2010) 'Screening-detected breast cancers: Discordant independent double reading in a population-based screening program', Breast Diseases, 21(4), pp. 329–330. doi: 10.1016/j.breastdis.2010.10.023.

Souza, F. H., Wendland, E. M., Rosa, M. I. and Polanczyk, C. a (2013) 'Is full-field digital

mammography more accurate than screen-film mammography in overall population screening? A systematic review and meta-analysis.', Breast (Edinburgh, Scotland). Elsevier Ltd, 22(3), pp. 217–24. doi: 10.1016/j.breast.2013.02.013.

Spear, S. L., Bulan, E. J. and Venturi, M. L. (2009) Breast Augmentation, Plastic and Reconstructive Surgery. Edited by M. A. Shiffman. Berlin, Heidelberg: Springer Berlin Heidelberg. doi: 10.1007/978-3-540-78948-2.

Spuur, K., Hung, W. T., Poulos, A. and Rickard, M. (2011) 'Mammography image quality: model for predicting compliance with posterior nipple line criterion.', European journal of radiology. Elsevier Ireland Ltd, 80(3), pp. 713–8. doi: 10.1016/j.ejrad.2010.06.026.

Saha, G. B. (2013). Physics and Radiobiology of Nuclear Medicine. Springer.

Sprawls, P. (1995). http://www.sprawls.org. Retrieved from Mammography Physics and Technology for effective clinical imaging: http://www.sprawls.org/resources/MAMMO/module.htm#12

Sprawls, P. (1995). Image Noise. Retrieved 7 23, 2014, from http://www.sprawls.org: http://www.sprawls.org/ppmi2/NOISE/

Sprawls, P. (1995). Iodine and Barium Contrast Media. Retrieved September 22, 2014, from http://www.sprawls.org/: http://www.sprawls.org/ppmi2/XRAYCON/#Iodine and Barium Contrast Media

Svahn, T. and Tingberg, A. (2005) Optimisation of direct digital mammography with the Jackknife FROC method. Malmö University Hospital. Available at: http://lup.lub.lu.se/student-papers/record/.pdf.

Szczepura, K. & D. J. Manning (2016) 'Validated novel software to measure the conspicuity index of lesions in DICOM images', pp. 1–12. Available at: papers://7a3983cb-07ee-455d-beaa-365bbcdf065f/Paper/p969.

Säbel, M., & Aichinger, H. (1996). Recent development in breast imaging. Physics in medicine and biology, 41(3), 315–368.

Tanaka, R., Takamori, M., Uchiyama, Y., Nishikawa, R. M. and Shiraishi, J. (2015) 'Using breast radiographers' reports as a second opinion for radiologists' readings of microcalcifications in digital mammography', British Journal of Radiology, 88(1047). doi: 10.1259/bjr.20140565.

Taplin, S. H., Rutter, C. M., Elmore, J. G., Seger, D., White, D. and Brenner, R. J. (2000) 'Accuracy of screening mammography using single versus independent double interpretation', American Journal of Roentgenology, 174(5), pp. 1257–1262. doi: 10.2214/ajr.174.5.1741257.

Taplin, S. H., Rutter, C. M., Finder, C., Mandelson, M. T., Houn, F. and White, E. (2002) 'Screening Mammography : Clinical Image Quality and the Risk of Interval', (April), pp. 797–803.

The American College of Radiology (2014) 'ACR – AAPM – SIIM Practice Parameter For Determinats of Image Quality in Digital Mammography', Digital Mammography, 1076(Revised 2008), pp. 1–20.

The Radiology Assistant (2013) The Radiology Assistant _ BI-RADS for Mammography and Ultrasound 2013. Available at: http://www.radiologyassistant.nl/en/p4793bfde0ed53/breast-

calcifications-differential-diagnosis.html (Accessed: 13 May 2015).

Thompson, J. D., Lança, C., Lança, L. and Hogg, P. (2017) 'A method to determine the impact of reduced visual function on nodule detection performance', Radiography. Elsevier Ltd, 23(1), pp. 19–24. doi: 10.1016/j.radi.2016.07.002.

Thompson, J. D., Manning, D. J. and Hogg, P. (2013) 'The value of observer performance studies in dose optimization: a focus on free-response receiver operating characteristic methods.', Journal of nuclear medicine technology, 41(2), pp. 57–64. doi: 10.2967/jnmt.112.116566.

Thompson, J., Hogg, P., Thompson, S., Manning, D. and Szczepura, K. (2012) 'ROCView: prototype software for data collection in jackknife alternative free-response receiver operating characteristic analysis.', The British journal of radiology, 85(1017), pp. 1320–6. doi: 10.1259/bjr/99497945.

Tobergte, D. R. and Curtis, S. (2013) Digital Image Processing for Medical Applications, Journal of Chemical Information and Modeling. doi: 10.1017/CBO9781107415324.004.

Toennies, K. D. (2012) Guide to Medical Image Analysis. London: Springer London. doi: 10.1007/978-1-4471-2751-2.

Tot, T. (2005) 'Correlating the ground truth of mammographic histology with the success or failure of imaging.', Technology in cancer research & treatment, 4(1), pp. 23–28. Available at: http://ovidsp.ovid.com/ovidweb.cgi?T=JS&PAGE=reference&D=med4&NEWS=N&AN=15649084.

Uchiyama, Nachiko& Zanchetta, M. (2012) Mammography-Recent Advance. 1st edn. Edited by T. Smiljanic.

Varela, C., Karssemeijer, N., Hendriks, J. H. C. L. and Holland, R. (2005) 'Use of prior mammograms in the classification of benign and malignant masses', European Journal of Radiology, 56(2), pp. 248–255. doi: 10.1016/j.ejrad.2005.04.007.

Van Overveld, I. M. C. J. (1995) 'Contrast, noise, and blur affect performance and appreciation of digital radiographs', Journal of Digital Imaging, 8(4), pp. 168–179. doi: 10.1007/BF03168716.

Van den Biggelaar, F. J. H. M., Nelemans, P. J. and Flobbe, K. (2008) 'Performance of radiographers in mammogram interpretation: A systematic review', The Breast, 17(1), pp. 85–90. doi: 10.1016/j.breast.2007.07.035.

Van Ravesteijn, V. F., Boellaard, T. N., Van Der Paardt, M. P., Serlie, I. W. O., De Haan, M. C., Stoker, J., Van Vliet, L. J. and Vos, F. M. (2013) 'Electronic cleansing for 24-H limited bowel preparation CT colonography using principal curvature flow', IEEE Transactions on Biomedical Engineering, 60(11), pp. 3036–3045. doi: 10.1109/TBME.2013.2262046.

Veitch, D., Burford, K., Dench, P., Dean, N., & Griffin, P. (2012). Measurement of breast volume using body scan technology(computer-aided anthropometry). Work, 41 Suppl 1, 4038-4045. doi: 10.3233/WOR-2012-0068-4038

Waltz, F. and Miller, J. (1998) 'An efficient algorithm for Gaussian blur using finite-state machines', SPIE Conf. on Machine Vision…, (July), pp. 1–8. Available at: http://reviews.spiedigitallibrary.org/data/Conferences/SPIEP/47435/334_1.pdf (Accessed: 28 March 2015).

Wang Kei Ma, Rob Aspin, P. H. (2015) ‘What is the minimum amount of simulated breast movement required for visual detection of blurring: an exploratory investigation’.

Wang, F.-L., Chen, F., Yin, H., Xu, N., Wu, X., Ma, Lu, C. (2013). Effects of Age, Breast Density and Volume on Breast Cancer Diagnosis: A Retrospective Comparison of Sensitivity of Mammography and Ultrasonography in China's Rural Areas. Asian Pacific Journal of Cancer Prevention, 14(4), 2277-2282. doi: 10.7314/apjcp.2013.14.4.2277

Watson, A. and Null, C. (1997a) ‘Digital images and human vision’, A Bradford Book. Available at: http://ntrs.nasa.gov/search.jsp?R=20020041928 (Accessed: 28 April 2015).

Watson, A. and Null, C. (1997b) ‘Digital images and human vision’, MIT Press, 26, pp. 929–930. Available at: http://ntrs.nasa.gov/search.jsp?R=20020041928 (Accessed: 28 April 2015).

Wolfe, J. (1976) ‘Breast patterns as an index of risk for developing breast cancer’, American Journal of Roentgenology, 126(6), pp. 1130–1137. doi: 10.2214/ajr.126.6.1130.

Wee, C.-Y., Paramesran, R. and Mukundan, R. (2007) ‘Quality Assessment of Gaussian Blurred Images Using Symmetric Geometric Moments’, 14th International Conference on Image Analysis and Processing (ICIAP 2007). Ieee, pp. 807–812. doi: 10.1109/ICIAP.2007.4362875.

Wellman, P. S., Howe, R. D., Dalton, E. and Kern, K. a (1999) ‘Breast Tissue Stiffness in Compression is Correlated to Histological Diagnosis’, Technical Report. Harvard BioRobotics Laboratory, pp. 1–15.

Wellings, S. R., Jensen, H. M. and Marcum, R. G. (1975) ‘An Atlas of Subgross Pathology of the Human Breast With Special Reference to Possible Precancerous Lesions’, JNCI: Journal of the National Cancer Institute, 55(2), pp. 231–273. doi: 10.1093/jnci/55.2.231.

Whitman, G. J. and Haygood, T. M. (2012) Digital Mammography. Edited by G. J. Whitman and T. M. Haygood. Cambridge: Cambridge University Press. doi: 10.1017/CBO9781139049337.

Wilson, R., Liston, J., Thomas, K. G., Hopkins, C., Sellars, S. and Thompson, W. (2011) Quality assurance Guidelines for Breast cancer screening radioloyy Second edition editors, Radiology.

Wivell, G., Denton, E. R. E., Eve, C. B., Inglis, J. C. and Harvey, I. (2003) ‘Can radiographers read screening mammograms?’, Clinical Radiology, 58(1), pp. 63–67. doi: 10.1053/crad.2002.1087.

Winchester, D. P., & Winchester, D. J. (2006). Breast Cancer (Second ed.). Hamilton, Ontario: BC Decker.

Williams, P. L. (1995). Gray's Anatomy (38th ed.). New York: Churchill Livingston.

Wu, X., Gingold, E. L., Barnes, G. T., & Tucker, D. M. (1994). Normalized average glandular dose in molybdenum target-rhodium filter and rhodium target-rhodium filter mammography. Radiology, 193(1), 83-89.

Woudenberg, S. Van, Thijssen, M. and Young, K. (2001) ‘European protocol for the quality control of the physical and technical aspects of mammography screening’, European Communiti, pp. 57–166. Available at: http://scholar.google.com/scholar?hl=en&btnG=Search&q=intitle:European+protocol+for

(Accessed: 28 April 2015).

Weiner, I. B. and W. E. C. (2010) 'The Corsini encyclopedia of psychology'. Available at: http://www.emeraldinsight.com/doi/10.1108/09504121011066941.

Yaffe, M. J. (2010) 'Basic Physics of Digital Mammography', in Bick, U. and Diekmann, F. (eds) Digital Mammography. Springer Berlin Heidelberg.

Yaffe, M. J. and Mainprize, J. G. (2011) 'Risk of Radiation-induced Breast Cancer from Mammographic Screening', Radiology, 258(1), pp. 98–105. doi: 10.1148/radiol.10100655.

Yaffe, M. J. (2010). Detectors for Digital Mammography. In U. Bick, & F. Diekmann, Digital Mammography. Springer

Yankaskas, B. C., Schell, M. J., Bird, R. E. and Desrochers, D. A. (2001) 'Reassessment of Breast Cancers Missed During Routine Screening Mammography: A Community-Based Study', (September), pp. 535–541.

Yap, M., Bister, M. and Ewe, H. (2003) 'Gaussian Blurring-Deblurring for Improved Image Compression', Digital Image Computing: …, pp. 10–12. Available at: http://books.google.com/books?hl=en&lr=&id=ozSinxlj08C&oi=fnd&pg (Accessed: 28 March 2015).

Young, S. Susan Ronald G. Driggers & Jacobs, E. L. (2008) Signal Processing and Performance Analysis for Imaging Systems.

Zanca, F., Hillis, S. L., Claus, F., Van Ongeval, C., Celis, V., Provoost, V., Yoon, H.-J. and Bosmans, H. (2012) 'Correlation of free-response and receiver-operating-characteristic area-under-the-curve estimates: results from independently conducted FROC/ROC studies in mammography.', Medical physics, 39(10), pp. 5917–29. doi: 10.1118/1.4747262.

Zanca, F., Van Ongeval, C., Claus, F., Jacobs, J., Oyen, R. and Bosmans, H. (2012) 'Comparison of visual grading and free-response ROC analyses for assessment of image-processing algorithms in digital mammography.', The British journal of radiology, 85(1020), pp. e1233-41. doi: 10.1259/bjr/22608279.

Zhang, D., Li, X. and Liu, B. (2012) 'X-ray spectral measurements for tungsten-anode from 20 to 49 kVp on a digital breast tomosynthesis system', Medical Physics, 39(6Part1), pp. 3493–3500. doi: 10.1118/1.4719958.

Zwiggelaar, R., Schumm, J. E. and Taylor, C. J. (1997) 'The Detection of Abnormal Masses in Mammograms', Medical Image Understanding Analysis, 7–8(Oxford 1979).

Zuley, M. L. (2010). Perceptual issues in reading mammograms. In E. K. Ehsan Samei, The Handbook of Medical Image Perception and Techniques (pp. 364-379). Cambridge: Cambridge University Press.

Zuley, M. L., Willison, K. M., Bonaccio, E., Miller, D. P., Leong, D. L., Seifert, P. J., et al. (2006). Full-Field Digital Mammography on LCD Versus CRT Monitors. American Journal of Roentgenology, 1492-1498.